UNIVERSITY OF CALIFORNIA
Los Angeles

Safer Polymer Formulations for Stabilizing Protein Therapeutics

A dissertation submitted in partial satisfaction of the
requirements for the degree Doctor of Philosophy
in Chemistry

by

Madeline Bea Gelb

2022

ABSTRACT OF THE DISSERTATION

Safer Polymer Formulations for Stabilizing Protein Therapeutics

by

Madeline Bea Gelb
Doctor of Philosophy in Chemistry
University of California, Los Angeles 2022
Professor Heather D. Maynard, Chair

Biologically derived pharmaceuticals are increasingly useful therapeutics because their complexity and specificity make them effective and selective drugs. This same complexity, however, can render the biologics unstable and highly sensitive to environmental stressors. There are a variety of approaches to stabilizing proteins ranging from small molecule additives such as sugars or salts and covalent conjugation of polymers. Polymers offer suitably versatile scaffolds for biologics as they can be functionalized with stabilizing groups – in particular the sugar trehalose and a zwitterionic group, carboxybetaine. Chapter One provides an overview of the different trehalose based polymers that have been synthesized with a focus on those bearing trehalose as a pendent side chain. The different synthetic strategies are detailed along with a discussion of the advantages, limitations, and challenges of each. This is followed by a description of the various applications the polymers have been employed for including trehalose polymers as excipients for and conjugates of biologics.

Chapter Two details the mechanism by which poly(trehalose methacrylate) stabilizes insulin against environmental stresses as well as the safety of the polymer. The polymer was found to inhibit both aggregation and degradation through deamidation with insulin exposed to heat without shifting insulin from the less stable monomer and dimer states to the more stable hexamer. Over 46 weeks at 4 °C, while the percent of intact insulin alone dropped significantly, the trehalose polymer maintained the majority of the insulin intact. The adaptive and innate mouse immune response to the polymer are explored with immunogenicity assays alone and in the presence of an immunogenic protein ovalbumin. To better understand the polymer's safety and, in particular, the biodistribution and excretion, the synthesis of the trehalose methacrylate monomer and polymer was modified to incorporate the copper chelating tetraaza macrocycle DOTA for μPET and μCT imaging. It was found that the majority of the polymer was excreted in 24 h, with only residual amounts present at the final time point, 5 days post-injection.

Chapter Three continues the exploration of poly(trehalose methacrylate) as an excipient for insulin but with a focus on fluid characterization and optimizing the formulation as a function of polymer molecular weight and molecular equivalents relative to insulin. A library of trehalose polymers with molecular weights ranging from 2.4 kDa to 29.3 kDa were readily synthesized, and, interestingly, up to 100 mg/mL these polymers displayed Newtonian fluid behavior and low viscosities, unlike many macromolecules. The formulation was optimized by mixing insulin with increasing relative concentrations of each polymer molecular weight, exposing the formulation to both heating and agitation stress, and then measuring the amount of intact insulin remaining. Of the best performing molecular weights and concentrations, the viscosities of the lowest weight per volume formulations were found to be above that of insulin alone, but manageable and tolerable.

Chapter Four parallels the prior chapter by applying the same polymer, poly(trehalose methacrylate), as an excipient for the antibody Herceptin (generic name trastuzumab). Antibodies are another important class of biologics, and antibody formulations are known to have issues with high viscosities in addition to the instability against environmental stresses common to all biologics. In this chapter, the viscosity of the antibody alone, in market formulation, and formulated with the trehalose glycopolymer at high concentrations was measured. Additionally, the three formulations were evaluated for stabilization against mild heat stress.

Chapter Five describes the synthesis of a zwitterionic, degradable polymer, poly(caprolactone-zwitterion), with a reactive endgroup. The polymer was designed to be conjugated with an alkyne containing protein, incorporated by an alkyne linker or non-canonical amino acid, for a degradable protein-polymer conjugate that could safely improve the half-life of the protein. The polymer was studied alone for adaptive immune response. Copper-catalyzed alkyne-azide click chemistry was used to install the polymer onto a growth hormone receptor antagonist (B2036) that had previously had a propargyl tyrosine installed at site of tyrosine 35. The bioactivity and pharmacokinetics of the site-selective protein-polymer conjugate were explored. Challenges towards synthesizing both polymers and conjugates are discussed.

The dissertation of Madeline Bea Gelb is approved.

Timothy J. Deming

Margot E. Quinlan

Yi Tang

Heather D. Maynard, Committee Chair

University of California, Los Angeles

2022

TABLE OF CONTENTS

LIST OF FIGURES, TABLES AND SCHEMES

Chapter 1

Chapter 2

Chapter 3

Chapter 4

Chapter 5

LIST OF ABBREVIATIONS

AA	Ascorbic acid
AIBN	2,2′-Azobis(2-methylpropionitrile)
AGET	Activators generated by electron transfer
ACN	Acetonitrile
ATRP	Atom transfer radical polymerization
AUC	Area under the curve
BMDO	5,6-benzo-2-methylene-1,3-dioxepane
BSA	Bovine serum albumin
CT	Computer tomography
CTA	Chain transfer agent
CuAAC	Copper-catalyzed azide-alkyne cycloaddition
$CuBr_2$	Copper(II) bromide
DBCO	Dibenzocyclooctyl
DCM	Dichloromethane
DI	Deionized
DIPEA	*N,N*- Diisopropylethylamine
DLS	Dynamic light scattering
DMAP	4-Dimethylaminopyridine
DMF	*N,N*-dimethylformamide
DMSO	Dimethylsulfoxide
DNA	Deoxyribonucleic acid
DOTA	Dodecane tetraacetic acid
DPBS	Dulbecco's phosphate buffered saline
DTT	Dithiothreitol
EDC	1-Ethyl-3-(3-dimethylaminopropyl)carbodiimide
ELISA	Enzyme-linked immunosorbent assay

Eq.	Equivalents
ESI	Electron spray ionization
Ether	Diethyl ether
Fab	Antigen-binding fragment
FPLC	Fast protein liquid chromatography
FRP	Free radical polymerization
FT-IR	Fourier transform-infrared
GCSF	Granulocyte colony stimulating factor
GHRA	Growth hormone receptor antagonist
GPC	Gel-permeation chromatography
HEBIB	2-hydroxyethyl 2-bromoisobutyrate
HCl	hydrochloric acid
hGH	Human growth hormone
HMPA	Hexamethylphosphoramide
HPLC	High performance liquid chromatography
HRP	Horse radish peroxidase
IL	Interleukin
i.m.	Intramuscular
i.p.	Intraperitoneal
i.v.	Intravenous
ITT	Insulin tolerance test
LiHMDS	Lithium hexamethyldisilazide
n-BuLi	n-Butyl lithium
MALDI-ToF	Matrix assisted laser desorption/ionization time-of-flight
MeOH	Methanol
MD	Molecular dynamics
Mol.	molecular
MW	Molecular weight

MWCO	Molecular weight cut off
NMR	Nuclear magnetic resonance
NHS	*N*-hydroxysuccinimide
OVA	Ovalbumin
PAGE	Poly(acrylamide) gel electrophoresis
PBS	Phosphate buffered saline
PEG	Poly(ethylene glycol)
pCL	Poly(caprolactone)
pCL-allyl	Poly(allyl caprolactone)
pCLZ	Poly(zwitterion caprolactone)
PEG	Poly(ethylene glycol)
PET	Positon emission tomography
PDS	Pyridyl disulfide
PDSMA	Pyridyl disulfide methacrylate
PPI	Protein-protein interaction
pTrMA	Poly(trehalose methacrylate)
RAFT	Reversible addition-fragmentation chain-transfer polymerization
ROMP	Ring opening metathesis polymerization
ROP	Ring opening polymerization
s.c.	Subcutaneous
SDS	Sodium dodecyl sulfate
SEC-MALS	Size exclusion chromatography multi-angle light scattering
SST	Serum separator tube
RAFT	Reversible addition-fragmentation chain transfer
RDRO	Reversible-deactivation radical polymerization
TCEP	Tris(2-carboxyethyl)phosphine
TEA	Triethylamine
TFA	Trifluoroacetic acid

THF	Tetrahydrofuran
TLC	Thin layer chromatography
TMB	3,3',5,5'-Tetramethylbenzidine
TrMA	Trehalose methacrylate
UV	Ultraviolet
UV-Vis	Ultraviolet-visible
vol.	Volume
VRA	Viscosity reducing agent
wt	Weight

ACKNOWLEDGEMENTS

I am so grateful for my parents and sister for the support, care, and love that helped me get to and through my graduate studies. Thank you for taking me to the mountains or ocean when I got lost in the fog and needed to see the light of day. Many thanks also to my greater family, blood related and not, for always encouraging me and showering me with love. You have all helped me along my path in achieving this goal and becoming the person and scientist I am today. Thank you to my silliest cheerleaders, Dan and Moe, for suffering through the stress of graduate school alongside me purely out of love for me. You did not have to take this journey with me, and I will be forever grateful that you did.

I have been very fortunate to be mentored and championed by my advisor, Professor Heather Maynard, throughout the last five years. Thank you for guiding me in how to be both creative and precise in breaking apart scientific challenges. The opportunities I had to grow as a scientist were uncountable, and, when at times overwhelming, I always received encouragement from you. Thank you also to my committee members: Yi Tang, Margot Quinlan, and Tim Deming.Thank you to the many Maynard lab members, past and present, who not only taught and trained me but also laughed and toiled alongside me. I have enjoyed learning from you both inside and outside of the lab. Thank you also to my Case Macro family for sharing the graduate school experience across time zones.

Finally, thank you to the UCLA Biotechnology Training Program, UCLA Technology Development Group, UCLA Department of Chemistry & Biochemistry, and the UCLA Graduate Division for funding during my graduate studies.

Chapter 1 was reproduced with permission from: Gelb, M.B.; Maynard, H.D. “Effect of Poly(trehalose methacrylate) Molecular Weight and Concentration on the Stability and Viscosity of Insulin.” *Macromol. Mater. Eng.* **2021**, 306 (9), 2100197. Copyright 2021 WILEY-VCH Verlag GmbH & Co. KGaA, Weinheim.

Vita

Education

University of California Los Angeles (UCLA)

- Master of Science in Chemistry — Mar 2018

Case Western Reserve University (CWRU)

- Bachelor of Science and Engineering in Polymer Science & Engineering — May 2016
- *Summa cum laude*
- Minor in Chemistry

Research Experience and Internships

Scientist, Janssen Inc. of Johnson & Johnson — Dec 2021 – present

- Drug Product Development

Graduate Researcher, UCLA — Sep 2016 – Dec 2021

- Department of Chemistry & Biochemistry
- Advisor: Heather D. Maynard
- Safer polymer formulations for stabilizing protein therapeutics

Specialty Dosage Formulations Intern, Merck & Co. — May – Aug 2018

- Department of Biopharmaceutics and Specialty Dosage Formulations
- Controlled delivery of APIs through electrospun polymer nanofiber mats

Undergraduate Researcher, CWRU — Jan 2013 – May 2016

- Department of Macromolecular Science and Engineering
- Advisor: Jonathan K. Pokorski
- Therapeutic polymer-protein bio-hybrid nanoparticles

Research Experience for Undergraduates, Cornell University — May – Aug 2015

- Cornell Center for Materials Research
- Advisor: Christopher Ober
- Antifouling and high fouling-release polymer coatings

Research & Development Engineering Intern, The Procter & Gamble Co. — May – Aug 2014

- Global Baby Care (Pampers) – Product Research and Product Development
- Modeling consumer sensory signals in diapers derived from non-woven textiles

Research & Development Engineering Intern, The Procter & Gamble Co. May – Aug 2013

- Global Baby Care (Pampers) – Global Materials Development and Supply Organization
- Modeling diaper and non-woven textile structure-property relationships

Publications

Madeline B. Gelb, Kathryn M. M. Messina, Daniele Vinciguerra, Jeong Hoon Ko, Jeffrey Collins, Mikayla Tamboline, Shili Xu, F. Javier Ibarrondo, and Heather D. Maynard. "Poly(trehalose methacrylate) as an excipient for insulin stabilization: Mechanism and safety" *In preparation*.

Jane Yang[†], Madeline B. Gelb[†], Kyle Tamshen, Kathryn M. M. Messina, Emma M. Pelegri-O'Day, and Heather D. Maynard. "Degradable poly(caprolactone-carboxybetaine) conjugated to a growth hormone receptor antagonist" *In preparation*. ([†]Equal contribution).

Jeong Hoon Ko, Neil L. Forsythe, Madeline B. Gelb, Kathryn M. M. Messina, Uland Y. Lau, Arvind Bhattacharya, Tove Olafsen, Jason T. Lee, Kathleen A. Kelly, and Heather D. Maynard. "Immunological and biodistribution evaluation reveals that trehalose styrenyl glycopolymer is promising as a PEG alternative for use with protein drugs" *In preparation*.

Madeline B. Gelb, Ashish Punia*, Shari Sellers, Parul Kadakia, James Ormes, Nazia N. Khawaja, Jen Wylie, and Matthew S. Lamm. "Effect of drug incorporation and polymer properties on the characteristics of electrospun nanofibers for drug delivery." *J. Drug Deliv. Sci.Technol.,* **2022,** *68,* 103112. *Corresponding author: ashish.punia@merck.com

Madeline B. Gelb and Heather D. Maynard. "Effect of poly(trehalose methacrylate) molecular weight and concentration on the stability and viscosity of insulin." *Macromol. Mater. Eng.* **2021**, 306 (9), 2100197.

Awards and Honors

UCLA

- NIH Biotechnology Training in Biomedical Sciences and Engineering Fellowship
- Dorothy Radcliffe Dee Fellowship Award
- Michael E. Jung Excellence in Teaching Award

CWRU

- Macromolecular Senior Leadership Award
- John L. Fuller '36 Prize
- Tau Beta Pi, Engineering Honors Society
- Mortar Board, National Senior Honors Society
- University Scholarship Recipient

Chapter 1

Synthesis and Applications of Trehalose-Based Polymers and Nanomaterials

1.1 Introduction

Trehalose is a naturally occurring, non-reducing disaccharide formed by the α,α-1,1 glycosidic linkage of two glucose units (α-D-glucopyranosyl-α-D-glucopyranoside). This specific bond bends trehalose into a rigid clamshell structure.[1-2] Trehalose has the highest glass transition (T_g) of disaccharides at 114 °C[3] and an anhydrous melting temperature ($T_{m)}$ of 203 °C.[4] The exact stereochemical arrangement of trehalose's many hydroxyl groups is important in the formation of specific hydrogen bonds.[1-2, 5-6] Similarly to other osmolytes, trehalose can act as a bioprotective agent against various environmental stresses such as freezing and drying and is produced by some microorganisms in response to stress. Trehalose is often more effective than other sugars at maintaining cellular integrity by protecting the native three dimensional structure of cell bilayers and proteins, inhibiting their denaturation, degradation and aggregation.[3, 5, 7-11] Relative to other sugars, trehalose has a higher affinity for water and when hydrated it occupies a larger volume, thereby accounting for the size disparities between mono- and di- saccharides.[10-11] This property, however, is also likely responsible for the relatively high solution viscosity measured with trehalose solutions.[10] This drawback is often accepted in favor of the better stabilization properties and for the relative inertness of trehalose, which lacks the free aldehyde groups susceptible to unwanted Maillard reactions, common with other sugars.[9, 12] Furthermore, as the glycosidic bond is highly stable, trehalose is less susceptible to hydrolysis, thereby making it more inert than sucrose, the other common non-reducing sugar.

Trehalose is a highly versatile stabilizer that has already been implemented in the biomedical field in a wide variety of formulations used for a broad range of applications. Despite its widespread use, the precise stabilization mechanism is still disputed and most likely depends in part on the environmental conditions[4] and the type of molecule being stabilized.[7] The multiple,

non-exclusive theories to explain trehalose stabilization include water entrapment or preferential exclusion, water replacement, and vitrification.[4] Generally, these three mechanisms rely on trehalose decreasing the local mobility of biomacromolecules by forming many hydrogen bonds, directly or indirectly, and by resisting solvent crystallization through the formation of a glassy matrix around unstable biomolecules, respectively.[6, 8, 10-11] The difference between the water entrapment and replacement theories lies in whether a solvation layer around the protein is present or if trehalose is directly interacting with the protein surface. Vitrification requires trehalose to form an amorphous or glassy matrix to prevent formation of ice crystals that cause "freeze concentration" – that is the concentration of solute in the remaining liquid which can result in protein denaturation.[12]

Despite early research seeking a single answer to the stabilization mechanism question, it is now more accepted that multiple mechanisms can work simultaneously and/or are influenced by the specific macromolecule. Repeated lyophilization studies indicated that trehalose must continue to maintain direct or indirect hydrogen bonds with the polar residues to maintain native conformation of the molecule once dried.[3-4, 12] One of the earliest molecular dynamics (MD) studies on trehalose, and a prime example of early efforts to find a simple answer, concluded that trehalose did not affect the structure of water in sufficiently dilute conditions and therefore trehalose must stabilize proteins by water replacement.[5] Only a few years later, further MD exploration contradicted this theory, finding that trehalose has significant water interactions and disrupts the natural tetrahedral network of water, attributing the high degree of order in part to the conformational rigidity of trehalose.[1-2, 13] These later MD studies concluded that, while trehalose clearly had kosmotropic effects and could cause water entrapment, the ability to structure water does not exclude water replacement or vitrification as mechanisms by which trehalose stabilizes

biomolecules. Again, this more inclusive view on the role of mechanisms has been borne out experimentally with spectroscopic experiments reporting the importance of water entrapment,[13-15] water replacement,[8, 16] and formation of a glassy matrix by trehalose.[3, 12, 16-17] Non-spectroscopic evidence has also indicated multiple mechanisms with experiments involving lyophilizing proteins from organic solvents,[18] studying the thermodynamics of protein stability,[9, 19] and even measuring trehalose water matrix viscosity.[20] These studies confirmed that no one mechanism can exclusively explain the stabilizing properties of trehalose. From all of the mechanistic studies, Cordone et al. came to the conclusion that trehalose stabilizes proteins primarily by water entrapment whereas lipids are stabilized by water replacement, although this is disputed in the literature.[7] More generally, researchers agree that these mechanisms can and do act in combination to prevent the unfolding, misfolding, and aggregation of biomacromolecules.[1, 4, 16] Throughout the study of the mechanism by which trehalose stabilizes biomolecules, researchers repeatedly showed trehalose to be more effective than other sugars.[3, 10, 16] For instance, in stabilizing pyrophosphatase and glucose 6-phosphate dehydrogenase against heat, trehalose was 4x more effective than the same mole concentration of sucrose and maltose or double the mole concentration of glucose or fructose.[10] Comparatively, trehalose resulted in a better liposome protectant than sucrose against lyophilization followed by storage or heating conditions.[3]

As a small molecule, trehalose is a highly effective stabilizer, and trehalose has been incorporated into polymers for even more dramatic stabilization results.[21-24] As our group has previously shown, in heat and lyophilization stability assays, proteins retain greater bioactivity in the presence of trehalose polymers (excipient, conjugate, hydrogel, or nanogel) than alone or with the same weight concentration of trehalose.[21-22, 25-26] In the same vein, trehalose nanoparticles were better than trehalose alone at preventing proteins from undergoing fibrillation.[23] Cryopreservation

assays of different mammalian cells in the presence of increasing amounts of trehalose polymer similarly showed improved cell growth after freezing with trehalose polymer rather than trehalose alone.[24] These trehalose polymers and nanoparticles have also been shown to reduce the relative amount of trehalose molecules required to stabilize biomolecules and cells.[23-24, 27] Unexpectedly, amidst this improved stabilization work, linear trehalose polymers did not show similarly high viscosities as the small molecule or more complex fluid flow properties.[27]

Taken altogether, these characteristics firmly demonstrate the utility of trehalose polymers in the rapidly growing biopharmaceutical market. In this chapter, different polymerization strategies to prepare trehalose-based polymers will first be discussed. Afterwards, various applications in the biomedical field, such as protein stabilization, gene delivery and amyloid aggregate prevention, will be presented and discussed.

1.2 Polymerization Strategies

Many strategies have been employed over the years to synthesize poly(trehalose) polymers with various architectures. Linear polymers can be prepared following two different approaches: (i) step-growth polymerization where trehalose is incorporated by polyaddition or polycondensation directly into the backbone of the polymer, or (ii) chain-growth polymerization where trehalose is linked to unsaturated monomers as side chains and, typically, radical polymerization affords linear chains with trehalose pendant on the side chains. Crosslinked materials can be prepared by (iii) curing of trehalose containing multiple olefins to afford insoluble thermoset resins or crosslinking of poly(trehalose) in aqueous conditions to give hydrogels (**Figure 1.1**).

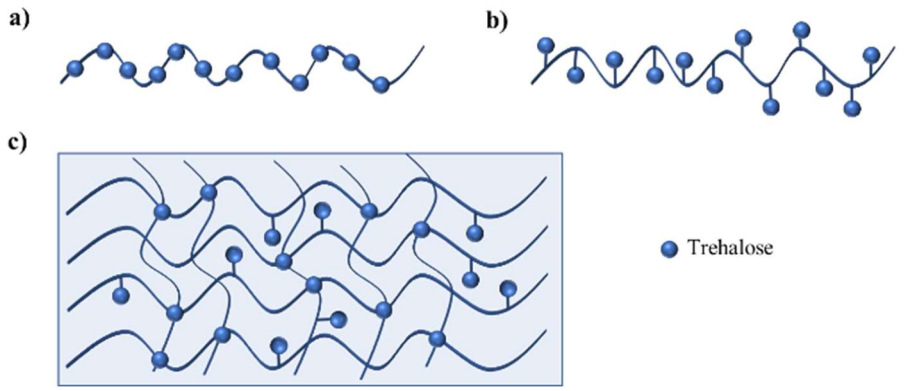

Figure 1.1 Schematic representation of a) polymer with trehalose in the backbone, b) polymer carrying trehalose in the side chains, c) thermoset or hydrogel network with trehalose as crosslinker or in the side chain.

1.2.1 Backbone-Trehalose

A selection of polymers with trehalose in the backbone are summarized in **Figure 1.2**. The first attempt to prepare linear trehalose polymers was reported in 1979 by Kurita et al., when the authors employed direct addition polymerization to copolymerize trehalose with diisocyanates yielding polyurethanes, although likely producing branched polymers as a side product.[28] They later resolved this issue by synthesizing diaminotrehalose using sequential protection-deprotection steps to selectively modify the C-6,6' hydroxyl groups. The modified trehalose was then reacted with various diisocyanates, such as diphenylmethane diisocyanate, to afford polyureas by polyaddition using various polar solvents at temperatures ranging from 5 to 20 °C. The resulting polymers could be biodegraded using trehalase or α-amylase.[29] Similarly, trehalose hydroxyls could be reacted with aldehydes or derived acetals to afford polyacetals by polycondensation.[30-31] This strategy presents the advantage of being regioselective for C-6,6’ hydroxyls with no protection steps required. However, this methodology presented some clear disadvantages such as harsh polymerization conditions, low (8.5 kDa) maximum molecular weight (MW) obtained, no

glass transition temperature (Tg) found up to the decomposition temperature (Td) of 325 °C,[30] and formation of a mixture of polymers with different end groups or even cyclization.[31] To overcome these drawbacks, Teramoto et al. designed a different strategy to regioselectively modify trehalose with 4-allyl-oxybenzaldehyde and then polymerize by hydrosilylation with SiH-terminated dimethylsiloxane oligomers.[32] Polymers with a MW up to 50 kDa were obtained when the mixture was heated at 80 °C for 72 h. Yields were generally high (~80%), but molecular weight polydispersity was also very high, averaging 3.5. The polymers presented two T_g peaks: one (~-110 °C) independent of and one (96-152 °C) dependent on siloxane oligomer segment length.[32] In parallel, they developed a synthetic strategy to afford degradable linear poly(trehalose) by exploiting the Diels-Alder reaction between trehalose bearing difurfurylidene and bismaleimides. At high temperature (140 °C), the polymer undergoes a retro Diels-Alder and degrades into its monomers.[33] In a follow up study, the two strategies were combined by using difurfurylidene trehalose and maleimide bearing dimethylsiloxanes oligomers. The degradable and flexible poly(trehalose-siloxanes) presented similar advantageous thermal properties to the previous siloxane copolymer, while retaining degradability from the Diels-Alder reversibility.[34] Finally, trehalose was derivatized to afford a diepoxide and polymerized following the addition of aliphatic diamines in the presence of a base catalyst. While the trehalose diepoxide had low solubility in various organic solvents, requiring the polymerization be conducted in 1-methyl-2-pyrrolidone (NMP) at 200 °C, the resulting polymer was soluble in a range of organic solvents and showed a T_g of 100 °C and a T_d of 320 °C.[35]

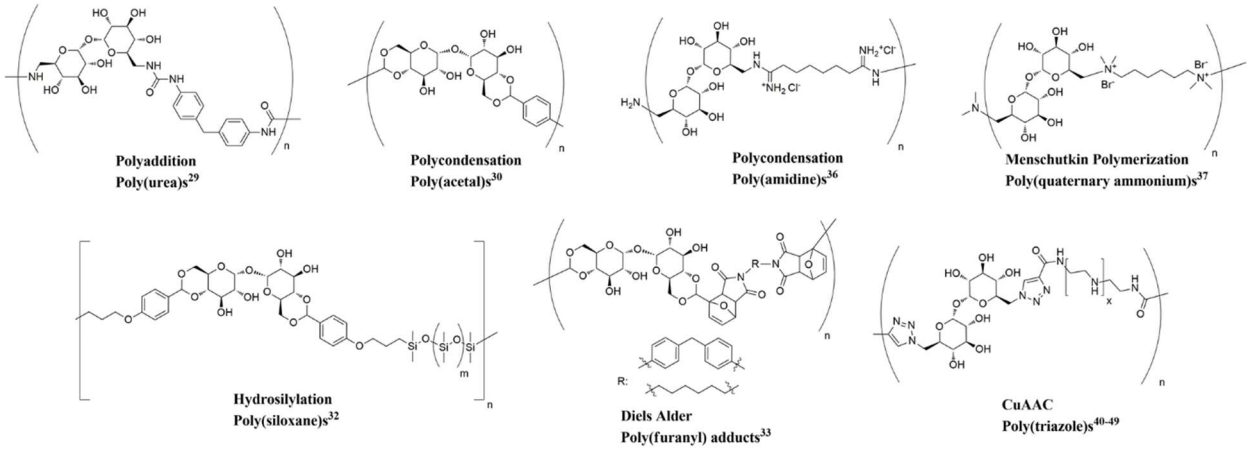

Figure 1.2 Representative selection of polymers and reaction classes with trehalose in the backbone.

Another early development in the polycondensation approach involves reacting monomers containing amine-reactive imidoester groups with diaminotrehalose in the presence of sodium carbonate to afford cationic polyamidines. The polymerization only took 16 h, but yields were limited (23-45%).[36] As part of the development of a family of sugar-containing polycations, trehalose was functionalized in 6 and 6' positions with dimethylamine, that proceeded through a diiodide intermediate. The tertiary amines were then reacted with 1,6-dibromohexane via Menschutkin reaction yielding polycations bearing quaternary amines. The polymerization was conducted at 40 °C for 3 days, but yields were similarly modest (32-38 %).[37]

Arguably, CuI-catalyzed azide–alkyne cycloaddition (CuAAC) has been the most successful reaction employed to synthesize polymers with trehalose in the backbone. CuAAC is widely applied both in polymer[38] and carbohydrate[39] syntheses. The strategy was popularized by Reineke and coworkers, in their effort to synthesize cationic trehalose copolymers for gene delivery.[40-49] Trehalose bearing two azido groups in the 6 and 6' positions was prepared by iodination of the respective hydroxyl group, followed by substitution with sodium azide, and finally protection of the remaining hydroxyls with acetyl groups. The diazidotrehalose monomer

was polymerized by a reaction with dialkyne-oligoamine monomers. Specifically, an equimolar mixture of the monomers was heated at 50 °C in a 1:1 cosolvent system of tert-butyl alcohol and water in the presence of CuII and sodium ascorbate and stirred for 4-24 h depending on the amine. Finally, the hydroxyls and the amines were deprotected following conventional methods to afford the desired water-soluble copolymer. In addition to the milder polymerization conditions than previously discussed strategies, these reactions could easily obtain polymers with higher MW, up to 40 kDa, dispersity as low as 1.2, and higher degree of polymerization (56-61).[40] This synthetic strategy and these conditions allow facile customization of many characteristics of the final polymer including polymer length,[41, 44] amine number,[42, 44] and end group chemistry, by introducing a capping monomer at the end of the polymerization.[43-44] Additionally, a third comonomer could be added, for instance to add a lanthanide chelating moiety for theranostic purposes.[47]

Other applications involving polymer prepared by CuAAC include a thermoresponsive glycopolymer in physiological temperature range[50] and an asymmetric trehalose bearing both an alkyne and azide for copper free topochemical azide–alkyne cycloaddition.[51] In the first case, trehalose primary and secondary alcohols were selectively tosylated and acetylated, respectively. After the initial protection, the tosyl groups were displaced with azides. Dialkyne terminated PEGs with MWs of 200, 600, and 1000 Da were prepared by reaction with propargyl bromide, and the comonomers were polymerized at 60 °C for 24 h with copper wire as a catalyst. Acetal-protected glycopolymers containing 600 Da PEG showed a cloud point at 2 mg/ml of 39 °C, but acetyl deprotection led to water soluble polymers that did not present thermoresponsive behavior. Interestingly, the analogous polymers of 200 Da and 1000 Da PEG were either insoluble in water or presented a phase transition at 90 °C, respectively.[50] In the last example, an asymmetric

acetylated trehalose monomer bearing either an azide or an alkyne at the primary alcohols was synthesized in five steps, with most yields above 80%. To avoid challenges from conventional glycopolymer synthesis, topochemical click chemistry was used. The monomer was crystalized from a 2:1 mixture of either ethyl acetate or chloroform and n-hexane. The crystals were heated at 90 °C and the polymer was visible by ^{1}H NMR after 24 h, reaching full conversion within 96 h, with the highest attained MW ~7 kDa.[51] This innovative approach requires more exploration in the future as it solves issues related to purification and metal removal related to conventional CuAAC chemistry. However, the final product is still acetylated and would require a final deprotection step to be useful as stabilizer, and the obtained MW is relatively low. Additionally, preparing copolymers might be more difficult than polymerization in solution phase, due to the possibly incompatible crystal structures and alignment, or the inability to prepare crystals from an eventual comonomer.

1.2.2 Side Chain-Trehalose

Figure 1.3 illustrates some examples of polymers bearing trehalose on the side chains. The earliest reports of side-chain trehalose polymers employed enzymes, such as protease or lipase, to regioselectively modify trehalose at the C6 position with vinyl esters that could subsequently be polymerized by free radical polymerization (FRP) to afford poly(vinyl esters) bearing trehalose on their side chains.[52-53] The polymers were explored only in terms of lectin recognition and enzyme inhibition.[53]

A decade later, our group became interested in the field of trehalose polymers with numerous contributions to the pendant trehalose design.[21-22, 25-27, 54-63] An innovative approach taking advantage of the benefits of reversible-deactivation radical polymerization (RDRP) was initially designed. A styrenyl monomer bearing monodiethyl acetal in the para position was reacted

selectively in 4,6 positions by acetalization to afford the styrenyltrehalose monomer in 41% yield. Using a pyridyl disulfide (PDS) functionalized chain transfer agent (CTA), polymers were synthesized via reversible addition-fragmentation chain transfer (RAFT) polymerization. As is common for controlled polymerization techniques, this method presents many advantages such as low dispersity, possibility to target a specific molecular weight, compatibility with multiple architectures, and high end group retention.[64] The last advantage is especially important in this case because the PDS group was installed for a post-polymerization reaction with proteins to create polymer-protein conjugates. Inclusion of a short PEG spacer between the PDS and the CTA improved conjugation yields with the protein as visualized by SDS-PAGE. Polymerizations proceeded in controlled fashion for 6 h with high conversion, affording a series of polymers with MW in the 4-50 kDa range and dispersity as low as 1.05.[21] Shortly after, the trehalose monomer library was expanded to include methacrylate acetal, styrenyl ether and methacrylate, each prepared in a few steps with moderate yields. Free radical polymerization (FRP) with azobisisobutyronitrile (AIBN) at 80 and 65 °C, for the styrenyl and methacrylate monomers, respectively, successfully yielded polymers of 10.8-23.4 kDa.[54] The monomer synthesis was designed without any protection step, thus it results in a mixture of various regioisomers that can be easily isolated by preparative HPLC, as was done in the case of styrenyl ether trehalose.[55] Four isomers were isolated, with styrenyl group in position 2, 3, 4 or 6. Regioselectivity could be controlled through careful choice of base metal counterion for the etherification reaction, with sodium and potassium hydroxide favoring 4 or 6 position, respectively, and higher reaction temperature or use of water as a solvent raising O6 relative yields. Quantum mechanical calculations confirmed that each isomer maintained the clam shell conformation, important for the stabilizing properties of trehalose.[55]

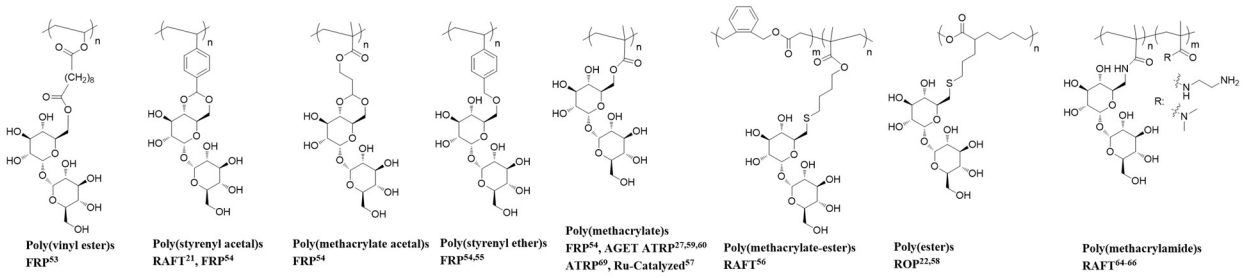

Figure 1.3 Representative selection of polymers with trehalose in the side chains and polymerization strategies.

Our group has made several efforts to incorporate biodegradable moieties into poly(trehalose) structures. One strategy used RAFT to copolymerize 5,6-benzo-2-methylene-1,3-dioxepane (BMDO), a cyclic ketene acetal (CKA) which ring opens during polymerization to form degradable esters, with but-3-enyl methacrylate (bMA), an alkene containing monomer. No cross reactivity of the alkene unit was noticed during polymerization, but the final dispersity was relatively high (1.76), which was attributed to mismatch reactivity between the monomers. Thiol-ene chemistry was then used to add thiol-trehalose to the alkenes, and the polymer was degraded in 24 h under basic conditions.[56] Alternatively, biodegradable units can be introduced in the polymer chain via ring opening polymerization (ROP) of cyclic esters. Polycaprolactone, polyvalerolactone, polycarbonate and polylactide with reactive alkene side chains were polymerized with different organocatalyst and co-catalyst systems at room temperature with fast kinetics and low dispersity. Thiol-trehalose was again added in post-polymerization, by photoinitiation.[22, 58] While the trehalose polycaprolactone backbone esters began to undergo hydrolytic cleavage within 24 h in accelerated basic conditions.[22] The same physiological conditions with trehalose polymers made of polyvalerolactone, polylactide, and polycarbonate backbones indicated no degradation up to 30 days, complete degradation within a few days, and complete degradation over the course of a month, respectively.[58]

Among the other advantages of RDRP, the ability to generate well defined block copolymers has been employed extensively by Reineke and coworkers. A trehalose-methacrylamide monomer could be polymerized by RAFT into a poly(trehalose) macroCTA from which the chain was then extended with a cationic block and used for gene delivery and stabilization.[65] Similarly, diblock terpolymers were easily prepared by polymerizing trehalose-methacrylamide with a variety of comonomers for usage in micelle formulation or pH-responsive drug delivery.[66-67]

Moving beyond RAFT, atom transfer radical polymerization (ATRP), and specifically activators generated by electron transfer (AGET) ATRP, has been employed by our group and others to prepare poly(trehalose) polymers. An insulin-poly(trehalose) conjugate was synthesized by installing a nitrophenyl carbonate-activated ATRP initiator to a lysine residue (LysB29), HPLC purifying the singly modified insulin, and using AGET ATRP to "graft from" the protein.[59] By growing the poly(trehalose) directly from insulin, both purification and characterization of the conjugate were streamlined when compared to "grafting to" insulin.[68-69]. AGET ATRP was chosen to polymerize the trehalose monomer because of the mild, aqueous, and room temperature conditions required. A sacrificial resin was added so that the polymerization would occur.[59] Recently, we used AGET ATRP to graft poly(trehalose) to the antibody Herceptin (trastuzumab) and Herceptin Fab via a bis-sulfone alkyl bromide initiator, which was chosen as a specific, stable, and irreversible reduction-conjugation handle for disulfide bridging. It was hypothesized that the bis-sulfone might undergo ligand-assisted elimination, giving an alkene that may potentially lead to side reactions and loss of polymerization control. Through careful optimization of polymerization conditions, such as TPMA ligand equimolar concentration relative to Cu salts or more dilute monomer concentration, the reaction occurred in a satisfactory controlled fashion, with

dispersity below 1.1. The resulting polymer was then conjugated to Herceptin and Herceptin Fab, and mass spectrometry experiments revealed that single modification was achieved as expected.[60] ATRP was also used to synthesize poly(trehalose) not as protein conjugates. Madeira do O et al. prepared linear and 4-arm star poly(propargyl methacrylate) polymers via classic ATRP, and azido-trehalose and other sugars were added in a post-polymerization CuAAC reaction.[70] Morelli et al. used a similar CuAAC post-polymerization modification approach to functionalize azido-bearing poly(disulfide)s with alkyne-trehalose and other sugars. The polymers were prepared by ring-opening disulfide exchange polymerization and underwent the post-polymerization modification with high yield. Both strategies employed post-modification to allow direct biological comparison of the various glycopolymers without concern for possible different polymer physicochemical characteristics.[71]

In addition to RAFT and ATRP, our group in collaboration with Sawamoto also utilized ruthenium-catalyzed living radical polymerization to copolymerize acetylated trehalose methacrylate (AcTrMA) with PEGMA and 1H,1H,2H,2H-perfluorooctyl methacrylate (13FOMA) to obtain amphiphilic macromolecules capable of self-assembly in water and organic solvents.[57] Solvent choice was critical in controlling the polymerization, achieving low dispersity and equimolar monomer incorporation. Initial AcTrMA and 13FOMA polymerizations carried out in toluene yielded polymers with relatively high dispersities (~1.55). Whereas switching to 1,2-dichloroethane (DCE) reduced dispersity to 1.27, polymerization time greatly increased, up to 96 h, and resulted in different relative monomer rates of consumption. Ultimately, a 6:4 mixture of toluene:DCE produced low dispersity (1.35) polymers in reasonable reaction times. The addition of PEGMA as a comonomer lowered the dispersity even more (1.26), as the monomer has intermediate polarity that mediates the interaction of the other two comonomers. The polymers

were deacetylated using hydrazine hydrate, and self-assembly monitored by dynamic light scattering (DLS) showed a bimodal distribution of smaller peaks of 10 nm coming from single-chain species and larger peaks at 100-200 nm resulting from interchain assemblies.[57]

Compared to the backbone strategy, the side chain approach presents some advantages. The ability to use controlled polymerization techniques opens the door for fine-tuning of MW and dispersity, facile chain-end control, and the ability to form well defined random, gradient or block copolymers along with larger (co)monomer scope and orthogonality. Moreover, modification of the side chains allows for the easy introduction of different functionalities.

1.2.3 Thermoset Resin

Other than producing linear polymers, trehalose monomers can be crosslinked to form thermoset resins of insoluble polymer networks with outstanding thermomechanical properties (**Figure 1.4**). Out of concern for the environment, a focus on producing thermosets from renewable resources has led multiple scientists to replace petroleum based polymers with bio-renewable stocks, such as polysaccharides.[72-73]

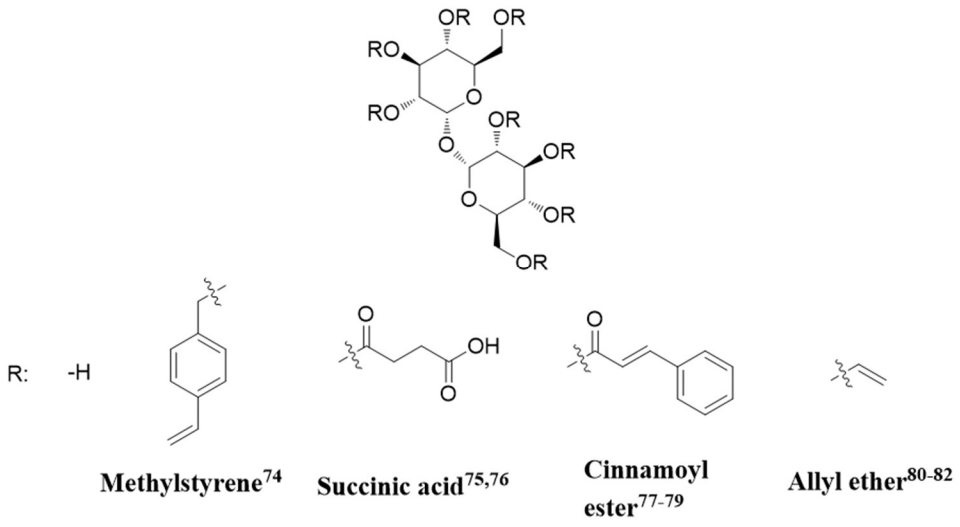

Figure 1.4 Representative trehalose monomers with different degree of substitution for curing and preparation of thermoset resins.

Teramoto and Shibata provided the first example of a thermoset polymer based on trehalose.[74] Styrenyl moieties were installed on the sugar by reaction with p-chloromethylstyrene, with a maximum degree of substitution (DS) of 3.2. The monomer was then cured by applying heat and pressure (200 °C, 29 bar, 30 min) and the thermal properties were analyzed. A correlation between T_g and DS was found, showing lower T_g (ranging 118-143 °C) with higher DS. Only 5% of the resin degraded over 50 days, and no further degradation was observed up to 90 days. This was attributed to the stability of the styrenyl backbone.[74] Instead of continuing research exclusively with trehalose monomers, the Reineke group functionalized trehalose with succinic anhydride to be used as a crosslinking hardener for their epoxy-containing trimethylolpropane triglycidyl ether (TTE)[75] or epoxidized soy bean oil (ESO)[7676] based thermosets. The properties of the cured thermosets varied greatly, with T_g's of 63 °C and 3 °C and tensile strengths up to 47 MPa and 1.3 MPa for the TTE and ESO based trehalose thermosets, respectively. In particular, the trehalose/TTE resin showed high adhesion strength of 3600 psi. The TTE resins were degradable

in both basic and acidic conditions, reaching full degradation in a few hours or 1-2 months, respectively, but remained stable at neutral pH. On the other hand, trehalose-containing ESO resins were instead stable in both neutral and acidic conditions, but quickly degraded in basic media. The different behavior in acidic media was attributed to the higher hydrophobicity of the ESO moiety compared to TTE.[76] The authors noticed that the ESO resins prevented cell adhesion and growth and attributed this to the low elastic modulus, thus proposing the material as a potential fouling-resistant coating material.[76] In a different study, trehalose cinnamoyl esters (TCs) smooth thin films promoted fibroblast cell proliferation, with better results than a standard polystyrene culture plate.[77] TCs were prepared by esterification between trehalose and cinnamoyl chloride, and thin films were prepared by photocuring of the monomer solution, as cinnamoyl undergoes dimerization to form a cyclobutane ring under UV irradiation. The polymerization is favored with a DS of 4 compared to a DS of 8, due to larger steric hindrance from the extra cinnamoyl groups in the latter. Photocured TCs showed a T_g of 91.6 °C.[78] In a follow up study, unreacted hydroxyl groups of the TCs were further functionalized with 4-(4-hexyloxybenzoyloxy)phenoxy-6-oxohexanoic acid (HBPHA) as a mesogenic unit, yielding a material with liquid-crystal morphology from 150 °C to 180 °C. The resulting thin film was found to be biocompatible, and plates coated with the film allowed fibroblast attachment and had properties comparable to a polystyrene culture plate. Due to the material's mesogenic characteristics, some of the cells were found to align the spindle shaped cells in controlled fashion.[79]

An alternative photocuring strategy employs thiol-ene photopolymerization of allyl-etherified trehalose (AT) with various thiols, such as pentaerythritol-based tetrathiol (S4P)[80] or isocyanurate-based trithiol (S3I).[80-81] The films were transparent to visible light and presented a T_g approx. 27-28 °C for most cases.[80] Interestingly, the S4P based film showed higher tensile

strength and modulus but lower elongation at break than the S3I based film.[80] To improve the thermomechanical properties, polysilsesquioxanes were included as a co-crosslinkers in the production of the S3I based film, affording organic/inorganic hybrid nanocomposites. The resulting films were transparent and uniform even at the microscopic level. Additionally, both T_g, tensile strength and modulus were higher than the organic analogues, increasing with inorganic content.[81] In a recent report, AT was functionalized with cysteamine hydrochloride to afford aminated trehalose. The monomer was cured with sorbitol polyglycidyl ether (SPE) in the presence or absence of cellulose nanofibers (CNFs). The surface of films without CNFs was smooth, and, while addition of CNFs rendered surfaces more uneven, they also had the expected effect of increasing tensile strength and modulus. In the case of trehalose polymers with high amine content and crosslinking, the T_g was ~43.6 °C regardless of the presence of CNFs. At lower amine content and crosslinking, the T_g decreased from 62 to ~50 °C in the presence of CNFs.[82]

1.2.4 Hydrogel

Hydrogels are highly crosslinked polymer networks able to trap and retain large amounts of water that have many applications in biomedicine and biotechnology.[83] Our group proposed a simple two-step synthesis to prepare trehalose-based hydrogels.[25, 61] Trehalose was modified by etherification with 4-vinylbenzyl chloride and after precipitation in DCM, a mixture of mono, di and tri-substituted monomer was obtained. The crude mixture could be polymerized directly in water at room temperature using ammonium persulfate (APS) and tetramethylethylenediamine (TEMED) as a co-initiator pair, with the multi-substituted monomer acting as a chemical crosslinker. The purified hydrogel was obtained as a colorless powder, although this first attempt yielded only a modest 17% product.[61] By increasing the 4-vinylbenzyl chloride to trehalose ratio, greater trehalose modification was achieved, with a preference for mono-substituted monomer

(**Figure 1.5a**). The scaled up multi-gram reaction gave an impressive 76% yield, suitable for industrial applications. Many solvent systems were screened to find a greener alternative to the precipitation step that previously used toxic DCM and hexane. Eventually, ethyl acetate:toluene (2:3) was selected as the greener choice that afforded the highest yield of 64% after radical gelation, which occurred within 10 min.[25]

The examples discussed above employed chemical crosslinking, but trehalose polymers can also be physically crosslinked to form hydrogels. When well-engineered, these hydrogels can be reversible and even stimuli responsive. For instance, our group synthesized a glucose-responsive trehalose polymer hydrogel for insulin stabilization and delivery, taking advantage of the dynamic covalent bond formed between phenyl boronic acids (PBA) and diols containing molecules, in this case trehalose. A styrenyl trehalose polymer was prepared by FRP and mixed in PBS with an 8-arm PEG bearing PBA at every end group. A gel formed within 5 min, and it was hypothesized that the multivalency of the trehalose polymer favors gelation since trehalose itself has almost no affinity for PBA's. Due to the higher binding affinity of PBA for glucose compared to trehalose, in the presence of glucose the polymer is displaced, crosslinking is broken, and the hydrogel dissolves in a concentration dependent manner. [62]

Related to hydrogels in composition and applications, nanogels and microgels are defined as highly cross-linked hydrophilic polymers that form particles in the nanometer or micrometer scale, respectively. Our group synthesized trehalose-based nanogels for the stabilization and delivery of glucagon, an unstable peptide used in the treatment of hypoglycemia.[26] Briefly, a PDS containing trehalose copolymer (PDSMA-co-TrMA) was prepared by FRP from methacrylate-derived trehalose and pyridyl disulfide methacrylate. Crosslinking with a 1 kDa PEG-dithiol yielded nanogels of about 9 nm regardless of the amount of crosslinker, although size could be

controlled by tuning the polymer concentration. By installing two thiols on glucagon using dimethyl-3,3′-dithio-bis(propionimidate), the peptide itself could be used as crosslinker to form nanogels in less than 2 h, with a 60-70% yield. A higher PDSMA content, polymer concentration of 1-0.5 mg mL-1, and a 5:1 thiol ratio of polymer to glucagon resulted in more defined and uniform particles (**Figure 1.5b**).[26]

Burek et al. designed a series of thermoresponsive and acid degradable hydrogels using modified trehalose as a crosslinker and NIPAM as a monomer.[84-89] Trehalose was functionalized with 2, 3 or 4-allyloxybenzaldehyde to form diacetals regioselectively at the C4 and C6 positions. These trehalose crosslinkers were insoluble in water, thus water:DMF mixtures were employed for the polymerization, with 1:1 and 2:1 ratios. The TEMED/APS co-initiator pair was used to generate the initial radicals, with TEMED maintaining a basic pH to avoid acetal hydrolysis throughout the 2 h polymerizations at room temperature. The effects of solvent system, crosslinker identity, and mol. % on LCST and volume phase transition temperature (VPTT) of the hydrogels were studied. Due to the low mol. % of trehalose crosslinker, VPTTs were similar to NIPAM homopolymer hydrogels with a range of 31.5-34.5 °C until the mol. % was increased to 4%, when VPTT unexpectedly decreased to 29 °C. The authors hypothesized that water preferentially interacts with trehalose moieties, resulting in weakened hydrogen bonds with the NIPAM amide groups. The same characteristics also influenced swelling abilities, with low crosslinking, 2-isomer and higher water content in the solvent system leading to higher swelling capacity. Due to the presence of acetals in the crosslinker, the hydrogel degraded within hours in acidic solution at room temperature, although no degradation occurred at acidic pH above the VPTT, due to shrinkage of the hydrogel and masking of the acetals (**Figure 1.5c**).[84]

To obtain a hydrogel able to degrade at physiological temperature, hydrophilic comonomers, such as acrylamide (AAm), N-(2-hydroxyethyl)acrylamide (DMAAm) and N,N-dimethylacrylamide (HEAAm) were added in the polymerization feed. Using a 13-25 mol. % of these comonomers, hydrogels with VPTTs of 37-42 °C were obtained, with HEAAm and AAm containing hydrogels showing the highest VPTT values. With increased hydrophilic comonomer content, swelling capacities and degradation rates also increased, making degradation possible at physiological temperature.[85] Among other parameters that were altered to tune and modify thermomechanical and degradations properties, a different trehalose comonomer, 4,6-O-acrylidene-α,α-D-trehalose, was prepared and found to be water soluble, eliminating the need for DMF during the polymerization. Moreover, it enabled higher overall trehalose content for protein stabilization, although real incorporation was much lower than theoretical feed content (up to a 75% difference).[88] The acrylidene monomer and its diacrylidene version, as a crosslinker, were copolymerized with NIPAM to form thermoresponsive microgels by surfactant-free precipitation copolymerization. The microgels had diameters in the 200-400 nm range, dispersities <0.1, and shrinking abilities above their VPTT (~29 °C). However, when dispersed in solutions with ionic strengths of 0.165 M, such as in DMEM cell culture media, the microgels aggregated into a macroscopic hydrogel above their VPTT.[90] These hydrogels could be used as soft matrices for 3D cell culture[90] or in microfluidic microchambers.[91]

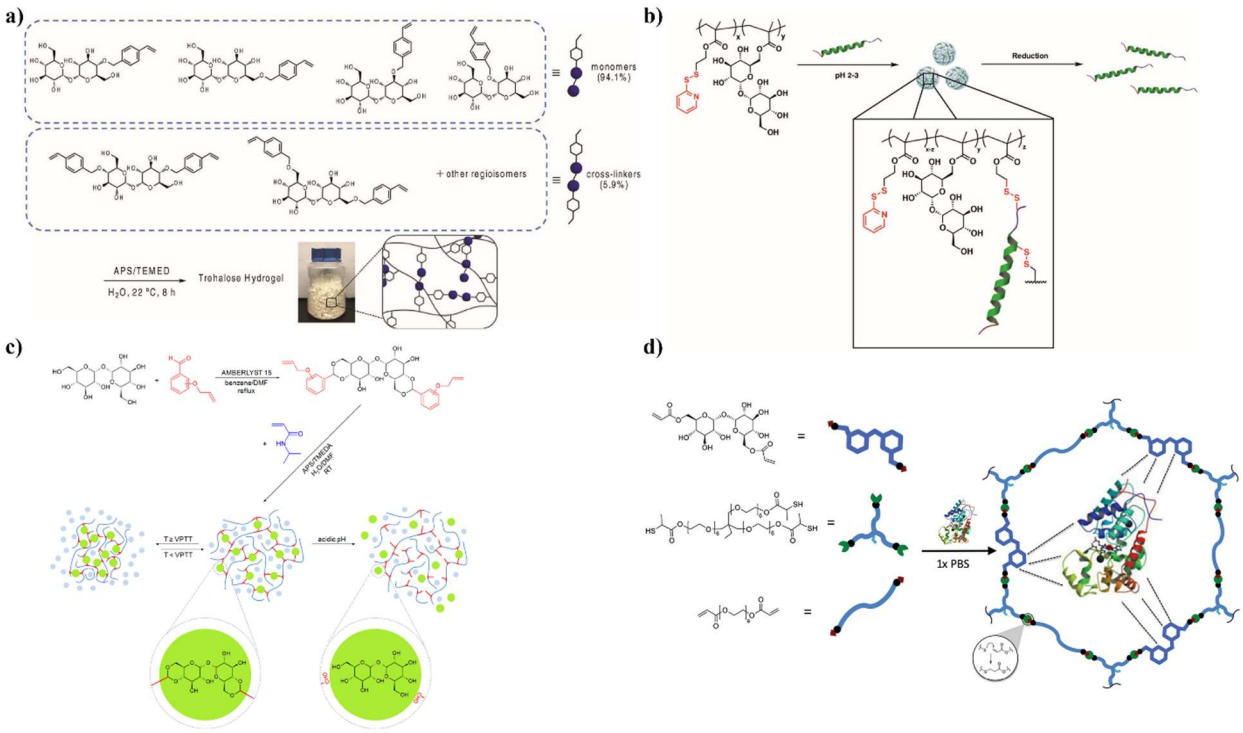

Figure 1.5 Representative hydrogel formation: a) Large scale hydrogel synthesis using styrenyl ether trehalose monomer and crosslinker; b) Glucagon-crosslinked trehalose nanogels for the treatment of hypoglycemia; c) Thermoresponsive, acid-cleavable acetal trehalose hydrogel; d) Trehalose hydrogel prepared by thiol-ene reaction for protein delivery. Reprinted and adapted with permissions from Ref. 25, 26, 84, and 93.

Alternatively, hydrogels with even higher trehalose content, up to 51.7 wt. %, were prepared to treat neurodegenerative diseases, with trehalose as the drug being delivered.[89] To ensure these hydrogels would also be degradable at basic pH, an ester moiety was added to the trehalose crosslinker.[86, 89] The degradation characteristics could additionally be controlled by the nature of the linker in para and meta position of the acetals and the hydrophilicity of comonomers used.[86-87] A final set of degradable chitosan hydrogels were prepared using a diiodo-trehalose derivative as the chemical crosslinker, and could be fully biodegraded in 96 h by trehalase.[92]

Recent examples of trehalose-based hydrogels have shown expanded uses to protein stabilization and controlled released,[93] hydrogels for skin burn treatment[94] and trehalose-epichlorohydrin hydrogels for cryopreservation and to act as a cell scaffold.[24] For instance, O'Shea et al. developed tri-composite hydrogels by thiol-ene reaction using enzyme derived diacrylate trehalose, PEG diacrylate and trimethylolpropane ethoxylate thiolactate as a thiol-bearing crosslinker (**Figure 1.5d**). Within a few minutes of mixing, hydrogels with varied trehalose contents were prepared and their rate of degradation increased proportionally with trehalose amount. Using attenuated total reflection Fourier transform infrared spectroscopy (ATR-FTIR), they found that the signal strength of the hydroxyl hydrogen bond was linearly dependent on trehalose content. Moreover, hydrogels in the semi-dry state were found to possess more robust mechanical properties, such as stiffness and tensile strength, compared to fully hydrated gels, and complete dehydration led to materials with properties comparable to analogous gels not containing trehalose, confirming the importance of the carbohydrate in hydrogen bond formation and organization.[93]

1.3 Applications

1.3.1 Protein and Peptide Stabilization and Delivery

Based on the stabilization, hydrophilic, and biocompatible properties of trehalose as a small molecule, it was hypothesized by many groups that incorporating trehalose into a polymer would aid in drug solubility and prevent aggregation, denaturation, and degradation of proteins. In the following section, the ability of trehalose polymers to stabilize proteins and peptides as excipients, conjugates, or hydrogels will be discussed.

1.3.1.1 Excipients

Linear or star, homopolymers and copolymers of trehalose have been studied as excipients for different protein drugs, although all have utilized pendant trehalose monomers rather than incorporating trehalose into the backbone.

The earliest published use of trehalose polymers specifically to stabilize proteins as an excipient and as a protein polymer conjugate came from our group in 2012.[21] RAFT of styrenyl trehalose yielded polymers that stabilize hen egg white lysozyme (HEWL) against heat (90 °C for 1 h, 100 mol. eq.) and lyophilization (10 cycles, 1 or 100 mol. eq.). The remaining HEWL activity was vastly improved with polymer, 55-100% activity as compared to less than 20% activity alone or 20-30% activity with a comparable amount of small molecule trehalose (1 or 100 wt. eq) (**Figure 1.6a**). It was hypothesized that, by covalently joining trehalose molecules into a single chain, the entropic barrier would be lowered.[21] This chemistry was rapidly expanded to include another trehalose styrene monomer and trehalose methacrylate monomers.[54] The derived polymers, as well as small molecule trehalose, were applied in 1-80 weight equivalents (wt. eq.) to horseradish peroxidase (HRP), β-galactosidase (β-gal), and glucose oxidase (GOx). The percent original activity of β-gal after three lyophilization cycles or of HRP (**Figure 1.6b**) and GOx after heating (70 °C for 30 min) clearly showed that all of the polymer excipient formulations, except for 1 wt. eq. of poly(trehalose methacrylate) (pTrMA) with β-gal, significantly increased the remaining enzyme activity (60-100% HRP, 50-100% β-gal, and 80-95% GOx activity) relative to no excipient or trehalose.[54]

Counterintuitively, initial experiments with trehalose polymers did not appear to have improved stabilization with increasing molecular weight (MW)[21] even though concentration clearly played a critical role in stabilizing proteins.[21, 54-55] Eventually the stabilization effect was

confirmed to be MW dependent.[22] Furthermore, Pelegri-O'Day et al. found that, keeping the total amount of polymer or trehalose in solution constant, increasing the MW of trehalose-based polymer excipients resulted in more stable protein formulations.[22] This effect, known as polyvalency or multivalency, has also been observed in entirely different classes of polymers including a sialic acid containing polyacrylamide copolymer that prevents agglutination of erythrocytes by an influenza virus.[95] Due to the polymer backbone connecting individual trehalose molecules, the likelihood of more trehalose molecules in the polymer interacting with the protein surface is increased. Taking the effect of both MW and concentration into account, trehalose polymer formulations were optimized to reduce the total amount of polymer needed to stabilize proteins.[27]

After exploring the initial range of model enzymes, researchers began employing trehalose polymers to improve the formulation properties and stability of therapeutically relevant drugs: insulin,[27, 55, 58-59] granulocyte colony stimulating factor (GCSF),[22, 56] and probucal,[67] as well as antibodies.[70] Our trehalose polystyrene,[55] polymethacrylate,[27, 59] polycaprolactone, polyvalerolactone, polycarbonate, and polylactide polymers[58] were all able to maintain fully intact insulin (97-100%) despite heat and agitation (37 °C and 250 rpm for 3-4 h). Although these polymers have yet to be compared in a single experiment, Pelegri-O'Day et al. found that, with 10 wt. eq. of the ROP degradable polymers, there was no difference in insulin stabilization, indicating that the side chain trehalose was more important to the stabilizing properties than the polymer backbone. Additionally, Messina et al. found that all of the different regioisomers of poly(trehalose styrenyl ether) fully stabilized insulin to mechanical agitation. As indicated by computational modeling, this is most likely due to the maintenance of the rigid clamshell structure of trehalose regardless of how trehalose is affixed to the polymer backbone.[55]

An additional therapeutic that has been studied with a range of different trehalose polymers is granulocyte colony-stimulating factor (GCSF), a particularly unstable protein. The degradable poly(trehalose caprolactone) maintained GCSF activity even after both mild (4 °C for 1.5 h) and aggressive (60 °C for 30 min) temperature changes with 100 wt. eq. as measured by cell proliferation, 168% and 179%, respectively, which hold comparison with fresh GCSF, showing 150-180% proliferation (**Figure 1.6c**).[22] In a similar heating assay (40 °C for 30 min), a RAFT copolymerized BMDO-trehalose copolymer maintained GCSF activity at 66% with 10 wt. eq. and 51% with 500 wt. eq.[56] While this was better than no excipient (~30% activity), the degradable copolymer's results did not hold up against the poly(trehalose styrenyl acetal) polymer with over 75% and full activity at 10 and 500 wt. eq., respectively, or even 77% activity with small molecule trehalose.[56] While all three polymers were found to be non-cytotoxic up to 1 mg/mL (primary human umbilical vein endothelial cells (HUVECs)[22] or human dermal fibroblasts (HDFs) and murine myeloblasts NFS-60),[56] the degradation products of the BMDO-trehalose copolymer reduced cell viability to 74%. Similarly to how the BMDO-trehalose copolymer better stabilized GCSF at 10 wt. eq. than at 500 wt. eq., linear and four-arm methacrylate-based trehalose polymers were found to better stabilize a highly concentrated model monoclonal antibody (mAb1, 50 mg/mL) against heat (25 °C and 40 °C for 7 weeks) with lower mol. eq. of polymer (1 and 100 vs 200 and 300).[70]

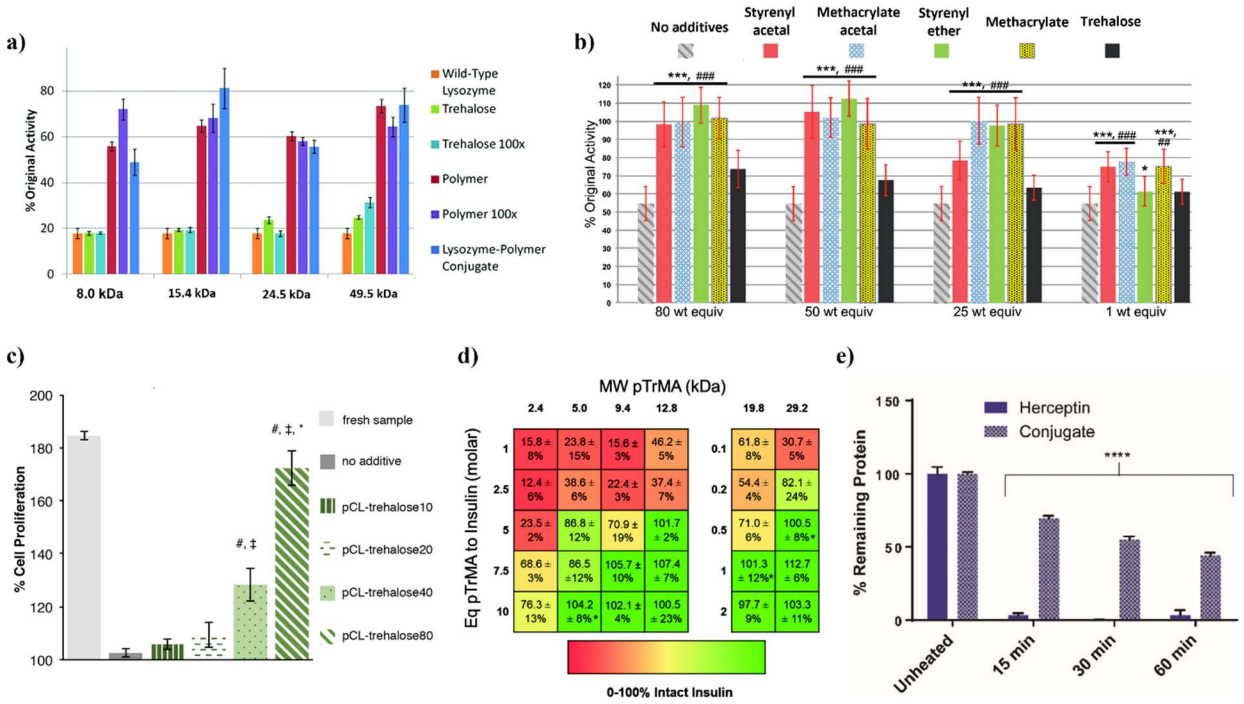

Figure 1.6 Protein stabilization by trehalose polymers. a) Activity of stabilized HEWL incubated at 90 °C for 1 h.; b) Activity of stabilized HRP incubated at 70 °C for 30 min; c) Activity of GCSF stabilized with 100 wt. eq. of polymers with increasing MW incubated at 60 °C for 30 min; d) Percentage of intact insulin stabilized with trehalose methacrylate with different MWs and concentrations incubated at 37 °C for 3 h; e) Percentage of intact Herceptin conjugated to trehalose methacrylate incubated at 75 °C for 1 h. Reprinted and adapted with permissions from Ref 21, 54, 22, 27, 60; copyrights for Ref 21, 54, and 22 in 2012, 2013, and 2017 with American Chemical Society, respectively.

The wide variety of pendant-trehalose polymers that are well suited for use as excipients emphasizes the utility of trehalose polymers in formulating drugs for solubility and stability. A recent exploration, **Chapter 3**, of the poly(trehalose methacrylate) examined the effect of polymer concentration and MW on stabilization of insulin. This study confirmed the hypothesized trend that increasing MW or concentration led to greater insulin stability against environmental stresses

(**Figure 1.6d**).[27] Based on the similarities in stabilization properties across polymer backbones, it seems likely that excipient formulations of the other trehalose polymers could be similarly optimized to reduce the amount of polymer in solution.

1.3.1.2 Conjugates

Excipient-based chemistry was further expanded by our group by incorporating protein reactive moieties to the polymer or initiator to synthesize protein-polymer conjugates. We hypothesized that conjugation of trehalose polymers to proteins would improve the stability of biomacromolecules against environmental stressors. Additionally, we expected that conjugating the polymer directly to the protein could further improve the stabilization provided by trehalose polymers by bringing the polymer closer to the protein. Another potential benefit that could come from conjugation was to extend the half-life of the biomolecules in vivo. Conjugation of poly(ethylene glycol) (PEG), or PEGylation, has been extensively shown to lengthen the half-life of proteins, including some already on the market such as Somavert, PEGasys, and Neulasta.[96-97] Beyond PEG, poly(oxazoline), poly(N-(2-hydroxypropyl)methacrylamide), and other polymers have also been used to improve the pharmacokinetics of biologics, so it was anticipated that trehalose polymers would have a similar effect.[98]

Thus far, the only protein conjugates made with trehalose polymers have come from the Maynard lab, using diverse conjugation methods, proteins, and trehalose monomers. The earliest published protein conjugation began with modification of amines on the surface of HEWL to which free thiols were nonspecifically added via N-succinimidyl-S-acetylthiopropionate.[21] Singly modified protein was purified before forming a disulfide bond via "grafting to" with a RAFT synthesized styrenyl trehalose polymers (MW: 8.0-49.5 kDa). Conjugation provided stability against both heat (1 h at 90 °C) and lyophilization (10 cycles) with up to 100% or 81% conjugate

stability relative to 17% and 18% of protein alone. The MW of the conjugated polymers led to no apparent trends in stabilization, and all of the conjugates performed significantly better than 1 or 100 eq. of excipient polymer (relative to HEWL) and 1 or 100 eq. of free trehalose (relative to conjugated polymer trehalose units).

This work was expanded to incorporate one of the most widely used therapeutic proteins, insulin, both as a non-specific "grafted to" conjugate[63] and as a site-specific "grafted from" conjugate.[59] The conjugation approaches relied on reductive amination or addition-elimination, respectively. In the second case, the greater nucleophilicity of lysine B29 was exploited by increasing the reaction pH from 8.0 to 9.5 in order to favor single modification of insulin using a nitrophenyl carbonate-activated ATRP initiator. Like with the HEWL conjugate, the insulin macroinitiator was purified by semipreparative HPLC to yield the singly modified insulin at 40%. AGET ATRP of trehalose methacrylate monomer in aqueous conditions and at room temperature yielded the site-specific protein polymer conjugate with a MW comparable to the grafted to conjugate (8.7 kDa and 1.2 Đ grafted from, 9.9 kDa and 1.1 Đ grafted to). While the dose of insulin required for each conjugate was higher than native insulin, the site-specifically modified insulin required only a three-fold dose as compared to the five-fold dosage of the original conjugate (16 μg/kg vs 48 μg/kg vs 80 μg/kg). However, both insulin conjugates stabilized insulin against environmental heat stress (90 °C for 30 min) better than unmodified insulin by HPLC analysis, and insulin tolerance tests (ITT) of the original conjugate and insulin after heat stress showed that the conjugate retained its activity. Furthermore, both conjugates prolonged the effect of glucose reduction measured by ITT, and pharmacokinetics of the "grafted to" conjugate confirmed that the insulin trehalose polymer had a longer circulation time in blood, comparable to that of a comparable sized insulin PEG conjugate.

Disulfide bonds were utilized to non-specifically or site-selectively conjugate trehalose polymers onto an antibody and antigen-binding fragment (Fab), respectively.[60] A bis-sulfone alkyl bromide ATRP initiator was used to polymerize trehalose methacrylate, and the bis-sulfone alkyl bromide could insert directly into one of the four disulfides of the full IgG Herceptin (trastuzumab) and into the single disulfide of Herceptin Fab for multiple and singly modified polymer conjugates. Conjugation of multiple 16 kDa trehalose polymers to Herceptin and the single 23 kDa trehalose polymer to Herceptin Fab did decrease bioactivity by ELISA. As expected, due to polymer steric hindrance, conjugates had higher EC_{50}'s relative to the unmodified antibody and Fab, 0.90 nM vs 0.26 nM and 2.74 nM vs 0.56 nM, respectively. However, conjugation of the trehalose polymer significantly increased the stability of both the antibody and Fab against heat stress (75 °C for 1 h) with around 50% soluble antibody or Fab conjugate rather than 0% soluble unmodified (**Figure 1.6e**).

All five of these protein-polymer conjugates provided the greater protein stability that is expected from trehalose polymers. Additionally, comparing the stability of conjugates to trehalose polymer and trehalose small molecule excipient formulations has shown some improvements in stabilization.[21, 59] For insulin, polymer conjugation also enhanced the circulation time of the biomolecule and prolonged the effect of treatment.[59, 63] Similar results are anticipated for other proteins. As expected, decreased bioactivity was the main drawback observed from conjugation.[59-60, 63] but site-selectivity provided some improvement. It is likely that more conscious selection of conjugation sites could further reduce the loss in bioactivity, as thus far conjugation sites have been chosen for their accessibility as site-selective points of modification without considering the effects on the biomolecule activity.

1.3.1.3 Hydrogels

With the success of trehalose polymers as excipients and conjugates for stabilizing proteins and the many functional hydroxyl groups on trehalose, a logical extension of previous work led researchers to create trehalose hydrogels to entrap and stabilize proteins. Hydrogels allow both the immobilization of proteins as well as controlled release through passive diffusion or through network degradation and dissolution. Additionally, it was expected that incorporating trehalose into hydrogels would provide the same protein stabilization observed with linear trehalose polymers.

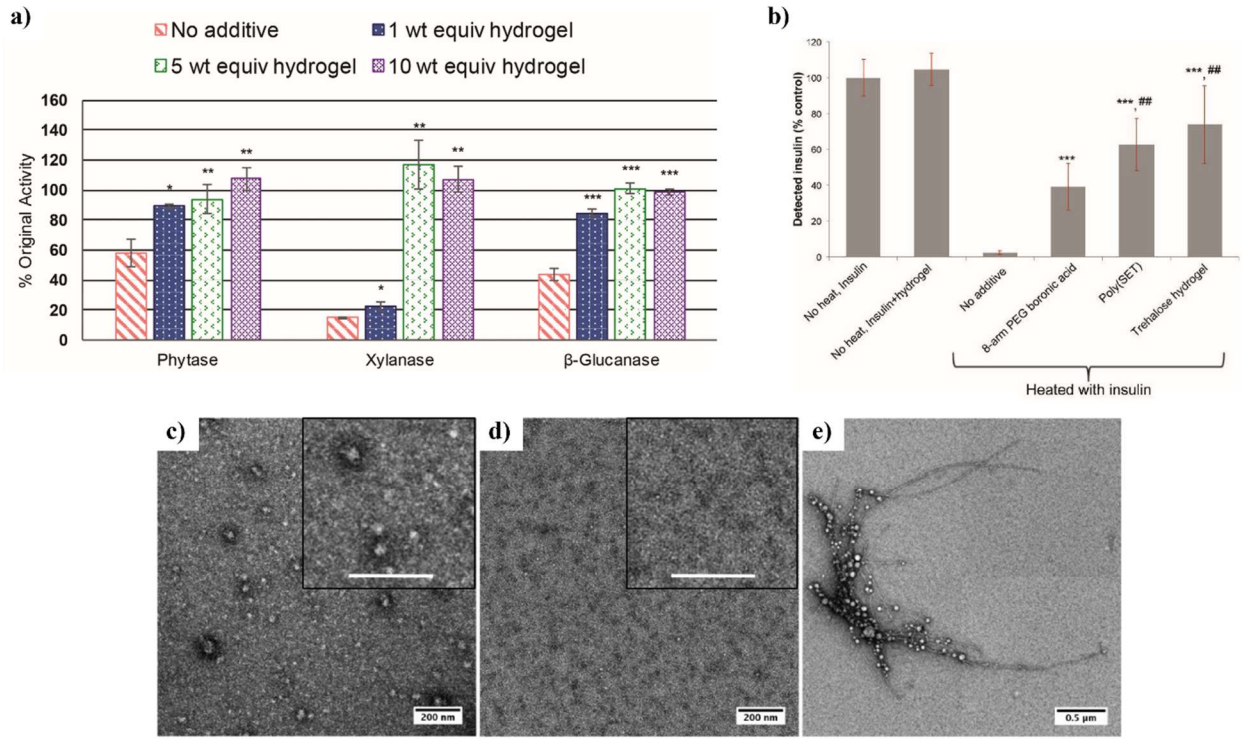

Figure 1.7 Protein or peptide stabilization by trehalose hydrogel/nanogel. a) Activity of phytase, xylanase, and β-glucanase loaded in trehalose hydrogels at various wt % after incubation for 1 min at 90 °C; b) Percentage intact insulin in the presence of trehalose hydrogel, linear trehalose polymer (Poly(SET)), 8-arm PEG-boronic acid, or no additives after incubation at 90 °C for 30 min; TEM images of c) glucagon nanogels in solution, d) immediately after reduction, e) 24 h after

reduction and release (note the presence of glucagon fibrils). Reprinted and adapted with permissions from Ref. 25, 62, and 26.

Our and the Langer groups simultaneously published two different routes for creating enzyme stabilizing trehalose hydrogels – the first based on mono- and multi- styrene functionalized trehalose and more focused on the protein stabilization,[61] and the second including trehalose diacrylate as part of a three-component system with PEG and TMPE with greater focus on the release kinetics.[93] After our group synthesized the styrenyl trehalose hydrogel, phytase (an enzyme important to agriculture feed stocks) was entrapped within the network structure in a 1, 10, and 40 wt. eq. of hydrogel to protein. The trehalose hydrogel was able to protect phytase during exposure to feedstock production-like conditions (90 °C, 1 min, 53 wt. % water), maintaining 80-100% activity as compared to 39% activity of phytase alone. The best performing hydrogel (10 wt. eq.) was used to study release kinetics, and ~80% of the phytase was released in 6 h from the hydrogels by passive diffusion with no agitation. An expansion of our styrenyl trehalose work was published more recently tested more feedstock relevant enzymes (phytase, β-glucanase, and xylanase).[25] As with the original work, the enzymes were encapsulated in the trehalose hydrogel, exposed to 90 °C for 1 min with 50 wt. % water, and then tested for activity. Based on the finding that 10 wt. eq. performed best, now 1, 5, and 10 wt. eq. were tested. At 10 wt. eq., >98% activity was maintained with all enzymes, great improvements over the 15-58% enzyme activities when alone. Notably, phytase and xylanase activity were increased above 100% possibly due to the gel network and/or trehalose scaffold stabilization enhancing substrate binding or stabilizing the proteins to the activity assay conditions (**Figure 1.7a**). These results were also compared to the stability of the enzymes in the presence of the same amount of molecular trehalose (0.54, 2.7, and 5.4 wt. eq), and only the highest concentration consistently retained any significant amount of activity (65-100%)

relative to the enzymes alone; all concentrations of hydrogel outperformed the equivalent concentration of free trehalose. Importantly, similar to the original work, quantitative release of phytase was achieved within 4 h at 37 °C.[25] The three-component trehalose/PEG/TMPE hydrogels with varying amounts (6.25-100% diacrylate component) of trehalose incorporation were found to have faster protein release with increasing trehalose content for both OVA and IgG proteins, despite the large difference in size.[93] This, along with a triphasic release profile, suggested that the initial diffusion release gives way to network degradation based release and that the higher amount of trehalose component the faster this degradation occurs. Furthermore, HRP encapsulated in the hydrogel, then exposed to heat (37 °C for up to 12 days), and subsequently recovered to test activity showed that higher trehalose content results in higher recovered activity (100% compared to <10% with protein alone) and activity within the gels (100% activity after up to 6 days at 37 °C, ~50% activity after 1 h at 70 °C, ~10% activity after 1 h at 80 °C). Conversely, the hydrogels with less trehalose content could destabilize the protein as hydrolysis of the network exposes carboxylate groups.[93]

In an effort to expand the functionality of trehalose based hydrogels, Burek et al. incorporated NIPAM, mono- and bis- functionalized trehalose, and other hydrophilic comonomers into thermoresponsive diacetal trehalose hydrogels.[88] By modifying the solvent system and concentration of different components, these hydrogels could be tuned for specific LCST, VPTT, and degradation rates. From swollen hydrogels, BSA was released in PBS pH 7.4 at 37 °C in a burst fashion nearly quantitatively within 2-6 h due to phase transition shrinkage and regardless of the hydrogel components. However, if the gels were dried first, release was delayed with higher trehalose content hydrogels, only reaching complete release in 5-8 h. Lower trehalose content hydrogels began to have near-linear release profiles over 10 h. The hydrogels at different

concentrations were also shown to stabilize β-galactosidase (β-Gal) against acidic pH (pH 3.0) and 37 °C for 1.5-6 h with 65-95% (10 wt. %) or 56-88% (5 wt. %) activity as compared to 42-82% activity for the β-gal alone.[88] The authors further explored the tunability of this hydrogel's degradability and subsequent protein release by using different trehalose diacetal crosslinkers that could be cleaved to yield soluble polymer chains and free trehalose.[87] With this design, the release profile of BSA in PBS pH 5.0 at 37 °C was initially linear and sustained until degradation of the hydrogel and enlarging pore size resulted in a burst of BSA, typically after 40-50% had already been released. The onset of this degradation-based burst release of BSA at pH 5.0 began at 21-72 h with complete release in 30-100 h, but this burst was suppressed at higher, more physiologically relevant, pHs.[87]

Our group further explored the possibilities of responsive trehalose hydrogels by incorporating boronic acid into networks to confer glucose responsiveness and treat diabetes.[62] By mixing pendant trehalose polymers with 8-arm PEGs end-capped with boronic acid groups, insulin was encapsulated within a hydrogel formed by the dynamic covalent bonds between boronic acid and trehalose. In a hyperglycemic event, the network is dissolved by glucose displacing trehalose in the boronic acid interaction, due to the 5.4x higher binding affinity of glucose with boronic acid, and the insulin released. In accordance with previous reports, the trehalose hydrogel stabilized insulin against accelerated heating conditions (90 °C, 30 min) with 74% intact insulin relative to 63% with just the linear trehalose polymer, 39% with the 8-arm PEG, or only 2% with insulin alone (**Figure 1.7b**). Furthermore, insulin was completely released from the hydrogel in 1 h at 1000 mg/dL glucose or 2 h at 500 mg/dL glucose, whereas at 0 mg/dL glucose only 60% of insulin was released in 2 h.[62] In a similar vein, glucagon, a highly unstable peptide used in hypoglycemia treatment, was entrapped within a trehalose network matrix in a non-responsive system to improve

stabilization.[26] Glucagon is a peptide notorious for its isoelectric point around physiological pH, making it very difficult to store in solution. Glucagon was modified to have two free thiol groups and then used to crosslink trehalose-PDSMA copolymer. The resulting nanogels increased the solution stability of glucagon from less than 24 h at physiological pH to at least 3 weeks (**Figure 1.7c-7e**). The in vitro activity of the thiolated glucagon was found to be similar to native glucagon. More surprisingly, glucagon in nanogels showed comparable activity to glucagon released under mild reducing conditions.[26]

As with other hydrogel drug delivery systems, these trehalose-containing hydrogels and nanogels offer tunable release and degradation delivery matrices. Even the multi-functionalized trehalose used as monomers and crosslinkers still provides stabilization for the encapsulated proteins. Similar to other hydrogel delivery systems, avoiding burst release is an ongoing issue, but the tunability on display already indicates that optimization is possible to match a specific system's need. Additionally, both thermoresponsive and chemically responsive trehalose hydrogels have already shown great promise for stabilization and controlled delivery of proteins.

1.3.2 Gene Delivery

Gene therapy recently witnessed a surge in translation to clinic with the approval and widespread use of mRNA-based COVID-19 vaccines, and many more nanoparticle gene formulations for a range of diseases are currently in clinical trials.[99] Polymeric materials play an important role in these non-viral gene delivery strategies.[100]

Poly(trehalose) was selected early on to prepare cationic copolymers carrying amidines[36] or quaternary amines[37] for plasmid DNA (pDNA) stabilization and delivery. The influence of sugar size, charge spacing and charge type of the trehalose polymer polyplexes on transfection, toxicity, and pDNA stabilization were investigated. Amidine-based polyplexes demonstrated

higher transfection ability than quaternary amines while achieving comparable toxicity.[37] Presence of trehalose significantly lowered the cytotoxicity.[36] This work was expanded by the Reineke group using a new click-chemistry based synthetic strategy to prepare trehalose cationic glycopolymers.[40-49] While trehalose promotes stability and prevents aggregation, the cationic units interact with DNA phosphate groups and amido-triazole units promote DNA binding via hydrogen bonding and hydrophobic interactions. As such, triazole containing polymers complexed pDNA at lower N/P ratios than analogues without triazoles. Moreover, increasing the number of amine repeating units (1-6, polymers labeled Tr1-Tr6) results in higher pDNA affinity, polyplexes stability in cell media, pDNA transfection, and gene expression in HeLa cells.[40] Nonetheless, although cellular uptake was higher than Jet-PEI, a common polymer used for gene delivery, gene expression was lower possibly indicating low endosomal escape. Higher amine content yielded higher cell toxicity, but trehalose copolymers were still much less toxic than Jet-PEI (70% vs 25% at N/P =15).[40] While Tr1 was found to interact with pDNA through an electrostatic mechanism, Tr3 and especially Tr4 were more dependent on base pair interactions through hydrogen bonding, probably due to the longer spacer between amine groups.[42]

Although the amine number did initially have a significant effect on polyplex formation, transfection, and stability, the effect tailed off at higher numbers (Tr5, Tr6), evidenced by reduced transfection of polyplexed pDNA into rat mesenchymal stem cells (RMSC) (20% Tr4 vs 10% Tr5 vs 8% Tr6).[44] To investigate chain length effect on biological properties, Tr4 was prepared at different DP (35, 53, 75, and 100). Interestingly, while chain length had no apparent impact on pDNA binding, heparin displacement, ITC, pDNA degradation, or gene uptake, increasing DP resulted in higher polyplex stability in complete media and higher gene expression, but with an unfortunate increase of toxicity in HeLa cells.[41] Moreover, higher DP Tr4 showed an impressive

40% transfection of pDNA in RMSC,[44] demonstrating this feature might be dependent on cell type. Further, exploring different polymer end groups of Tr4 polymers led to the discovery that carboxyl, octyl and oligoethyleneamine groups caused higher pDNA uptake and gene expression than other end groups, including adamantane, alkynyl-oligoethyleneamine and azido trehalose in HeLa cells.[43] The azido-trehalose end-capped Tr4 was also found to have reduced efficacy compared to PEGs and triphenylacetamide end groups in RMSC.[44] Additionally, 4D spatiotemporal cellular imaging was used to demonstrate that decreasing nanoparticle size allows for faster advancement to the perinuclear zone. In particular, Tr4 was internalized via caveolae/Rab-5 dependent pathway and reached the area within 4 h of cellular internalization.[45]

Importantly, RAFT trehalose-cation block copolymers stabilized pDNA polyplexes against one cycle of lyophilization and reconstitution; both colloidal stability and gene delivery ability were retained after the physical process (**Figure 1.8**).[101] Other than pDNA, Tr4[46-47] and RAFT[65] copolymers were used to deliver siRNA, demonstrating theragnostic abilities[47] and colloidal and freeze/drying stabilization properties.[65]

Finally, additives to increase transfection efficiencies and protein expression have been explored for delivering pDNA with trehalose-based polymers. Increasing heparin concentration was found to linearly increase GFP expression in primary fibroblasts (PFB), human liver carcinoma HepG2, and human glioblastoma U87 cells (4-fold), despite only increasing cellular internalization in HepG2 cells. It is possible this discrepancy is due to heparin-coated Tr4 polyplexes being taken up by a different endocytic pathway (clathrin-mediated endocytosis and micropinocytosis) or to enhanced nuclear delivery.[48] The effect of plasmid size on gene delivery was studied with heparin-coated polyplexes, and, predictably, larger plasmids (10 kbp) had reduced gene expression in primary human dermal fibroblasts (HDFs) and induced pluripotent

stem cells (iPSCs). An alternative additive, dexamethasone, was used to destabilize the nuclear barrier and increase trafficking enhancing transfection and expression.[49]

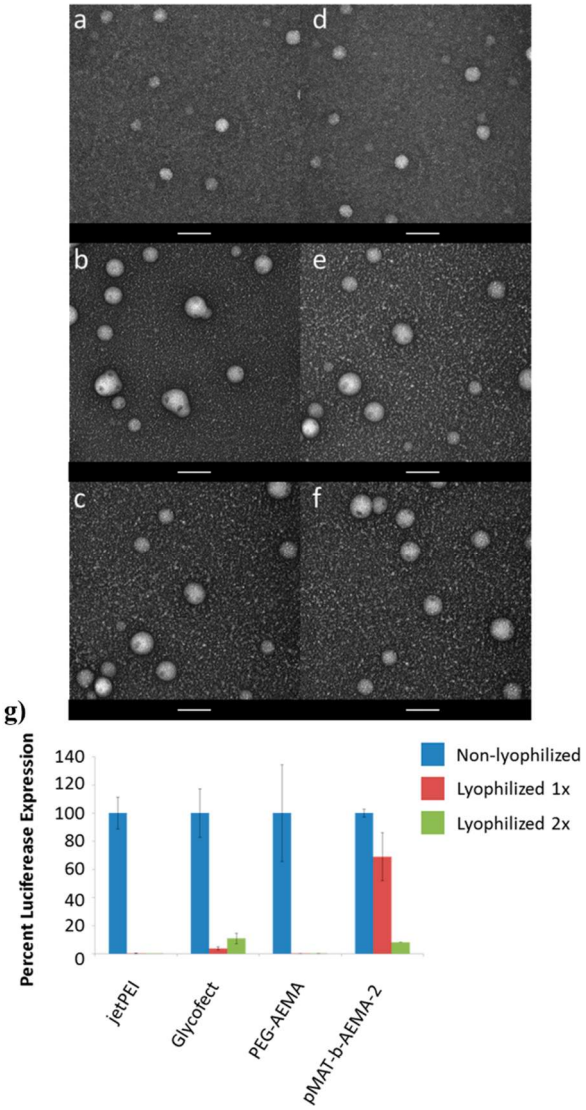

Figure 1.8 a-f) TEM images of p(trehalose-b-cation) with increasing cation block MW (a,d: DP = 21, b,e: DP = 44, c,f: DP = 57), a-c) fresh polyplexes and d-f) after lyophilization and reconstitution. Scale bar: 100 nm; g) Luciferase expression in U87 cells following transfection with lyophilized polyplexes (AEMA: cationic block, pMAT: trehalose block). Reprinted with permission from Ref. 101; copyright 2016 American Chemical Society. Ref 101

1.3.3 Aggregate Prevention for Amyloid Disorders

Trehalose has been found to be effective in the treatment of different neurodegenerative pathologies including Alzheimer, Parkinson and Huntington's diseases.[102-103] Although the exact mechanism is not clear yet, it likely includes anti-aggregation, anti-inflammation and, in particular, pro-autophagy.[104] Trehalose glycoclusters were more efficient in delaying fibril formation and protecting neurons than small molecule trehalose, indicating that the multivalency seen in stabilizing proteins with trehalose polymers is also in effect.[105] Recently, poly(trehalose) was also found effective in preventing amyloid β (Aβ) peptide aggregation, part of the progression of Alzheimer's disease. In two instances, Miura et al. prepared poly(trehalose)s by FRP and studied their effect on Aβ aggregation inhibition.[106-107] The polymer with a short adipoyl trehalose spacer showed greater aggregation inhibition than molecular trehalose or peptide alone, 20% vs 60% aggregation, respectively, protecting HeLa cells from Aβ cytotoxicity. However, a longer alkyl side spacer, sebacoyl, was found to induce aggregation.[106] To eliminate spacer contribution, acrylamide-trehalose copolymers were prepared and found to better prevent Aβ aggregation than small molecule trehalose and maltose and lactose based polymers, again decreasing Aβ aggregate cytotoxicity (**Figure 1.9**). Surprisingly, polymers with higher trehalose content were not more efficient at preventing aggregation, possibly due to higher steric hindrance and difficulties generating hydrogen bonds.[107]

Notably, Jana and Jana and coworkers prepared poly(trehalose) zwitterionic nanoparticles with an iron oxide core that were able to bind and completely disintegrate mature Aβ peptide or HEWL fibrils in 10 days or 20 hours, respectively.[108] These rates were three to four orders of magnitude more effective than molecular trehalose in preventing aggregation and aggregation-derived cytotoxicity in a Huntington's disease cell or mouse model.[108] The same group found

similar results for other neurodegenerative diseases using different trehalose nanoparticles: with a gold core,[109] dendrimer-based,[110] poly(lactide)-based to confer degradability and biocompatibility,[111] or prepared by heating/carbonization of trehalose.[23] In every case, the nanoparticles were more effective than molecular trehalose, again indicating that trehalose is more effective in a multivalent system than in small molecule form.

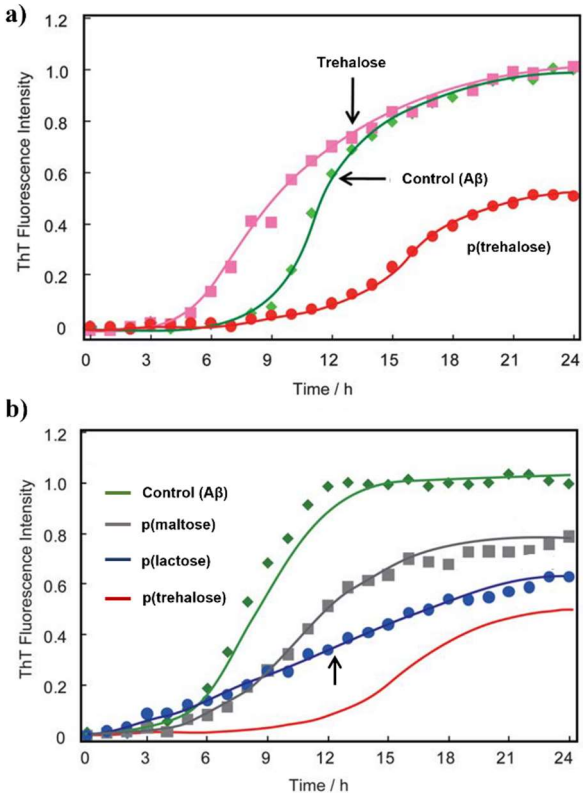

Figure 1.9 Thioflavin T assay for Aβ fibril detection over time at pH 7.4, 37 °C. a) green: no additives, pink: molecular trehalose, red: p(trehalose); b) green: no additives, grey: p(maltose), blue: p(lactose), red: p(trehalose). Reprinted with permission from Ref. 107.

1.3.4 Others

Beyond the applications discussed thus far, there have been assorted forays into the realms of photolithographic printing of proteins and metal-incorporated nanoparticles for the detection of bacteria and infection prevention. Trehalose polymers have enabled the direct-write electron-beam

lithography of multiple proteins into nanometric and submicron width lines and patterns. Photolithography requires electron beam irradiation and vacuum. By spin coating proteins with a styrenyl ether trehalose polymer, many proteins were able to withstand multiple iterations of these harsh conditions. The original experiments patterning HRP, GOx, IgG (chicken, human, mouse), streptavidin (SAv), vascular endothelial growth factor (VEGF), and basic fibroblast growth factor (bFGF) found that there was more active protein with the trehalose polymer than with trehalose, PEG, or nothing.[112] This protein patterning method was applied as the basis for a sandwich immunoassay measuring inflammatory cytokine production by localized surface plasmon resonance (LSPR).[113] Antibodies for two common cytokines, interleukin-6 (IL-6) and tumor necrosis factor-α (TNF-α) could be sequentially lithographically patterned using the trehalose polymer and still capture their respective cytokine from LPS-stimulated cell media.

In the pursuit of detecting and treating bacterial infections, trehalose polymers have been incorporated into nanoparticles encapsulating iron oxide[114] or poly(trehalose acrylate) coated gold.[115] As trehalose is a key component of the cell wall and glycolipids of some organisms, some bacteria, including *Mycobacteria* (*M.*), have lectins that will specifically bind to trehalose. Based on an earlier iteration of an iron oxide NP directly incorporating trehalose that interacted strongly with *M. smegmatis*,[116] researchers synthesized an iron oxide encapsulated pendant-trehalose poly(lactic acid) polymer micelle NP.[114] This NP not only specifically detects *M. smegmatis* over *Staphylococcus* (*S.*) *epidermidis* and *Escherichia* (*E.*) *coli* (gram-positive and –negative, respectively), but the NP could also facilitate removal by magnetically dragging the trehalose-lectin bound bacteria by the magnetic NPs. Using similar trehalose-lectin interactions, it was possible to reduce bacterial infection by grafting a RAFT polymerized poly(trehalose acrylate) to gold NPs by thiol-gold interaction.[115] The trehalose-gold NPs prevented HUVECs from being

infected with *S. aureus* by preferentially binding with HUVEC lectins, thereby avoiding the first step in bacterial infection i.e., adhesion via lectin-glycan bonding. These NPs were also found to be non-cytotoxic up to 0.75 mg/mL in either mouse macrophage RAW 264.7 or HUVEC cells.

1.4 Conclusion

In this introduction chapter, recent advances in the preparation and utilization of trehalose-based linear polymers, resins, gels, and nanoparticles were presented and discussed. Due to the impressive stabilization properties of trehalose, it has been widely used in the biopharmaceutical field. Moreover, the biocompatibility of trehalose makes it an ideal candidate for other fields, including plastic manufacturing and agriculture. Many synthetic strategies have proven successful in synthesizing trehalose polymers, with click chemistry and controlled radical polymerization becoming the most popular preparation methods for backbone or side chain trehalose molecules, respectively. Every form of trehalose polymer has shown increased efficacy in stabilizing and preventing biomacromolecules aggregation compared to molecular trehalose and other sugars both in vitro and in vivo, making trehalose polymers an ideal candidate for the biopharmaceutical industry.

Nonetheless, few studies on the safety and in vivo fate of these polymers can be found. Comprehensive studies regarding poly(trehalose) biodistribution, accumulation, pharmacokinetics, immunogenicity, and toxicity in general are needed to advance this polymer with great potential to being routinely utilized in everyday life. Herein this thesis, **Chapter 2** will explore the safety and mechanism by which the trehalose methacrylate polymer stabilizes insulin,[27] while **Chapter 3** investigates the effect of molecular weight and molar concentration on stabilizing insulin and characterizes the viscosity both of the polymer and optimized insulin formulations. Subsequently, **Chapter 4** studies how the trehalose methacrylate polymer prevents aggregation of

the antibody trastuzumab as well as the effect of the polymer on ultra-highly concentrated formulations. Finally, **Chapter 5** investigates the conjugation of a related stabilizing polymer that was previously studied as an excipient for GCSF and insulin, poly(caprolactone-carboxybetaine),[22, 58] site-specifically conjugated to the therapeutic protein growth hormone receptor antagonist (GHRA, B2036-yne).

References

1. Liu, Q.; Schmidt, R. K.; Teo, B.; Karplus, P. A.; Brady, J. W., Molecular Dynamics Studies of the Hydration of α,α-Trehalose. *J. Am. Chem. Soc.* **1997,** *119* (33), 7851-7862.

2. Choi, Y.; Cho, K. W.; Jeong, K.; Jung, S., Molecular dynamics simulations of trehalose as a 'dynamic reducer' for solvent water molecules in the hydration shell. *Carbohydr. Res.* **2006,** *341* (8), 1020-1028.

3. Crowe, L. M.; Reid, D. S.; Crowe, J. H., Is trehalose special for preserving dry biomaterials? *Biophys. J.* **1996,** *71* (4), 2087-2093.

4. Jain, N. K.; Roy, I., Effect of trehalose on protein structure. *Protein Sci.* **2009,** *18* (1), 24-36.

5. Donnamaria, M. C.; Howard, E. I.; Grigera, J. R., Interaction of water with α,α-trehalose in solution: molecular dynamics simulation approach. *J. Chem. Soc. Faraday Trans.* **1994,** *90* (18), 2731-2735.

6. Mensink, M. A.; Frijlink, H. W.; van der Voort Maarschalk, K.; Hinrichs, W. L. J., How sugars protect proteins in the solid state and during drying (review): Mechanisms of stabilization in relation to stress conditions. *Eur. J. Pharm. Biopharm.* **2017,** *114*, 288-295.

7. Cordone, L.; Cottone, G.; Giuffrida, S., Role of residual water hydrogen bonding in sugar/water/biomolecule systems: a possible explanation fortrehalose peculiarity. *J. Phys. Condens. Matter* **2007,** *19* (20), 205110.

8. Crowe, J. H.; Crowe, L. M.; Chapman, D., Preservation of Membranes in Anhydrobiotic Organisms: The Role of Trehalose. *Science* **1984,** *223* (4637), 701-703.

9. Kim, N. A.; Thapa, R.; Jeong, S. H., Preferential exclusion mechanism by carbohydrates on protein stabilization using thermodynamic evaluation. *Int. J. Biol. Macromol.* **2018,** *109*, 311-322.

10. Sola-Penna, M.; Meyer-Fernandes, J. R., Stabilization against thermal inactivation promoted by sugars on enzyme structure and function: why is trehalose more effective than other sugars? *Arch. Biochem. Biophys.* **1998,** *360* (1), 10-4.

11. Starciuc, T.; Malfait, B.; Danede, F.; Paccou, L.; Guinet, Y.; Correia, N. T.; Hedoux, A., Trehalose or Sucrose: Which of the Two Should be Used for Stabilizing Proteins in the Solid State? A Dilemma Investigated by In Situ Micro-Raman and Dielectric Relaxation Spectroscopies During and After Freeze-Drying. *J. Pharm. Sci.* **2020,** *109* (1), 496-504.

12. Horn, J.; Mahler, H. C.; Friess, W., Drying for Stabilization of Protein Formulations. In *Drying Technologies for Biotechnology and Pharmaceutical Applications*, Ohtake, S.; Izutsu, K. i.; Lechuga-Ballesteros, D., Eds. 2020; pp 91-119.

13. Lerbret, A.; Bordat, P.; Affouard, F.; Guinet, Y.; Hédoux, A.; Paccou, L.; Prévost, D.; Descamps, M., Influence of homologous disaccharides on the hydrogen-bond network of water: complementary Raman scattering experiments and molecular dynamics simulations. *Carbohydr. Res.* **2005,** *340* (5), 881-887.

14. Branca, C.; Maccarrone, S.; Magazù, S.; Maisano, G.; Bennington, S. M.; Taylor, J., Tetrahedral order in homologous disaccharide-water mixtures. *J. Chem. Phys.* **2005,** *122* (17), 174513.

15. Belton, P. S.; Gil, A. M., IR and Raman spectroscopic studies of the interaction of trehalose with hen egg white lysozyme. *Biopolymers* **1994,** *34* (7), 957-61.

16. Allison, S. D.; Chang, B.; Randolph, T. W.; Carpenter, J. F., Hydrogen Bonding between Sugar and Protein Is Responsible for Inhibition of Dehydration-Induced Protein Unfolding. *Arch. Biochem. Biophys.* **1999,** *365* (2), 289-298.

17. Jena, S.; Suryanarayanan, R.; Aksan, A., Mutual Influence of Mannitol and Trehalose on Crystallization Behavior in Frozen Solutions. *Pharm. Res.* **2016,** *33* (6), 1413-1425.

18. Roy, I.; Sharma, A.; Gupta, M. N., Obtaining higher transesterification rates with subtilisin Carlsberg in nonaqueous media. *Bioorganic Med. Chem. Lett.* **2004,** *14* (4), 887-889.

19. Xie, G.; Timasheff, S. N., The thermodynamic mechanism of protein stabilization by trehalose. *Biophys. Chem.* **1997,** *64* (1), 25-43.

20. Olsson, C.; Jansson, H.; Swenson, J., The Role of Trehalose for the Stabilization of Proteins. *J. Phys. Chem. B* **2016,** *120* (20), 4723-4731.

21. Mancini, R. J.; Lee, J.; Maynard, H. D., Trehalose Glycopolymers for Stabilization of Protein Conjugates to Environmental Stressors. *J. Am. Chem. Soc.* **2012,** *134* (20), 8474-8479.

22. Pelegri-O'Day, E. M.; Paluck, S. J.; Maynard, H. D., Substituted Polyesters by Thiol-Ene Modification: Rapid Diversification for Therapeutic Protein Stabilization. *J. Am. Chem. Soc.* **2017,** *139* (3), 1145-1154.

23. Pradhan, N.; Shekhar, S.; Jana, N. R.; Jana, N. R., Sugar-Terminated Nanoparticle Chaperones Are 102–105 Times Better Than Molecular Sugars in Inhibiting Protein Aggregation and Reducing Amyloidogenic Cytotoxicity. *ACS Appl. Mater. Interfaces* **2017,** *9* (12), 10554-10566.

24. Diaz-Dussan, D.; Peng, Y.-Y.; Sengupta, J.; Zabludowski, R.; Adam, M. K.; Acker, J. P.; Ben, R. N.; Kumar, P.; Narain, R., Trehalose-Based Polyethers for Cryopreservation and Three-Dimensional Cell Scaffolds. *Biomacromolecules* **2020,** *21* (3), 1264-1273.

25. Panescu, P. H.; Ko, J. H.; Maynard, H. D., Scalable Trehalose-Functionalized Hydrogel Synthesis for High-Temperature Protection of Enzymes. *Macromol. Mater. Eng.* **2019,** *304* (6), 1800782.

26. Boehnke, N.; Kammeyer, J. K.; Damoiseaux, R.; Maynard, H. D., Stabilization of Glucagon by Trehalose Glycopolymer Nanogels. *Adv. Funct. Mater.* **2018,** *28* (10), 1705475.

27. Gelb, M. B.; Maynard, H. D., Effect of Poly(trehalose methacrylate) Molecular Weight and Concentration on the Stability and Viscosity of Insulin. *Macromol. Mater. Eng.* **2021,** *306* (9), 2100197.

28. Kurita, K.; Hirakawa, N.; Morinaga, H.; Iwakura, Y., Synthetic polymers containing sugar residues, 6. Novel polyurethanes by direct addition polymerization of α, α-trehalose with diisocyanates. *Makromol. Chem.* **1979,** *180* (11), 2769-2773.

29. Kurita, K.; Masuda, N.; Aibe, S.; Murakami, K.; Ishii, S.; Nishimura, S.-I., Synthetic carbohydrate polymers containing trehalose residues in the main chain: preparation and characteristic properties. *Macromolecules* **1994,** *27* (26), 7544-7549.

30. Teramoto, N.; Arai, Y.; Shibasaki, Y.; Shibata, M., A facile synthesis of a novel polyacetal containing trehalose residue in the main chain. *Carbohydr. Polym.* **2004,** *56* (1), 1-6.

31. Kukowka, S.; Maślińska-Solich, J., α,α-Trehalose-based polyacetals and macrocyclic acetals. *Carbohydr. Polym.* **2010,** *80* (3), 711-719.

32. Teramoto, N.; Unosawa, M.; Matsushima, S.; Shibata, M., Synthesis and Properties of Thermoplastic Alternating Copolymers Containing Trehalose and Siloxane Units by Hydrosilylation Reaction. *Polym. J.* **2007,** *39* (9), 975-981.

33. Teramoto, N.; Arai, Y.; Shibata, M., Thermo-reversible Diels–Alder polymerization of difurfurylidene trehalose and bismaleimides. *Carbohydr. Polym.* **2006,** *64* (1), 78-84.

34. Teramoto, N.; Niwa, M.; Shibata, M., Synthesis and Properties of Trehalose-Based Flexible Polymers Prepared from Difurfurylidene Trehalose and Maleimide- Terminated Oligo(dimethylsiloxane) by Diels-Alder Reactions. *Materials* **2010,** *3* (1).

35. Teramoto, N.; Abe, Y.; Enomoto, A.; Watanabe, D.; Shibata, M., Novel synthetic route of a trehalose-based linear polymer by ring opening of two epoxy groups with aliphatic diamine. *Carbohydr. Polym.* **2005,** *59* (2), 217-224.

36. Reineke, T. M.; Davis, M. E., Structural Effects of Carbohydrate-Containing Polycations on Gene Delivery. 1. Carbohydrate Size and Its Distance from Charge Centers. *Bioconjugate Chem.* **2003,** *14* (1), 247-254.

37. Reineke, T. M.; Davis, M. E., Structural Effects of Carbohydrate-Containing Polycations on Gene Delivery. 2. Charge Center Type. *Bioconjugate Chem.* **2003,** *14* (1), 255-261.

38. Golas, P. L.; Matyjaszewski, K., Marrying click chemistry with polymerization: expanding the scope of polymeric materials. *Chem. Soc. Rev.* **2010,** *39* (4), 1338-1354.

39. Agrahari, A. K.; Bose, P.; Jaiswal, M. K.; Rajkhowa, S.; Singh, A. S.; Hotha, S.; Mishra, N.; Tiwari, V. K., Cu (I)-catalyzed click chemistry in glycoscience and their diverse applications. *Chem. Rev.* **2021,** *121* (13), 7638-7956.

40. Srinivasachari, S.; Liu, Y.; Zhang, G.; Prevette, L.; Reineke, T. M., Trehalose Click Polymers Inhibit Nanoparticle Aggregation and Promote pDNA Delivery in Serum. *J. Am. Chem. Soc.* **2006,** *128* (25), 8176-8184.

41. Srinivasachari, S.; Liu, Y.; Prevette, L. E.; Reineke, T. M., Effects of trehalose click polymer length on pDNA complex stability and delivery efficacy. *Biomaterials* **2007,** *28* (18), 2885-2898.

42. Prevette, L. E.; Lynch, M. L.; Kizjakina, K.; Reineke, T. M., Correlation of amine number and pDNA binding mechanism for trehalose-based polycations. *Langmuir* **2008,** *24* (15), 8090-8101.

43. Anderson, K.; Sizovs, A.; Cortez, M.; Waldron, C.; Haddleton, D. M.; Reineke, T. M., Effects of trehalose polycation end-group functionalization on plasmid DNA uptake and transfection. *Biomacromolecules* **2012,** *13* (8), 2229-2239.

44. Kizjakina, K.; Bryson, J. M.; Grandinetti, G.; Reineke, T. M., Cationic glycopolymers for the delivery of pDNA to human dermal fibroblasts and rat mesenchymal stem cells. *Biomaterials* **2012,** *33* (6), 1851-1862.

45. Ingle, N. P.; Xue, L.; Reineke, T. M., Spatiotemporal Cellular Imaging of Polymer–pDNA Nanocomplexes Affords in Situ Morphology and Trafficking Trends. *Mol. Pharm.* **2013,** *10* (11), 4120-4135.

46. Xue, L.; Ingle, N. P.; Reineke, T. M., Highlighting the Role of Polymer Length, Carbohydrate Size, and Nucleic Acid Type in Potency of Glycopolycation Agents for pDNA and siRNA Delivery. *Biomacromolecules* **2013,** *14* (11), 3903-3915.

47. Xue, L.; Kelkar, S. S.; Wang, X.; Ma, J.; Madsen, L. A.; Reineke, T. M., A theranostic polycation containing trehalose and lanthanide chelate domains for siRNA delivery and monitoring. *RSC Adv.* **2015,** *5* (90), 74102-74106.

48. Boyle, W. S.; Senger, K.; Tolar, J.; Reineke, T. M., Heparin Enhances Transfection in Concert with a Trehalose-Based Polycation with Challenging Cell Types. *Biomacromolecules* **2017,** *18* (1), 56-67.

49. Boyle, W. S.; Twaroski, K.; Woska, E. C.; Tolar, J.; Reineke, T. M., Molecular Additives Significantly Enhance Glycopolymer-Mediated Transfection of Large Plasmids and Functional

CRISPR-Cas9 Transcription Activation Ex Vivo in Primary Human Fibroblasts and Induced Pluripotent Stem Cells. *Bioconjugate Chem.* **2019,** *30* (2), 418-431.

50. Eissa, A. M.; Khosravi, E., Synthesis of a new smart temperature responsive glycopolymer via click-polymerisation. *Eur. Polym. J.* **2011,** *47* (1), 61-69.

51. Hema, K.; Gonnade, R. G.; Sureshan, K. M., Crystal-to-Crystal Synthesis of Helically Ordered Polymers of Trehalose by Topochemical Polymerization. *Angew. Chem. Int. Ed.* **2020,** *59* (7), 2897-2903.

52. Kitagawa, M.; Chalermisrachai, P.; Fan, H.; Tokiwa, Y. In *Chemoenzymatic synthesis of biodegradable polymers containing glucobiose branches*, 1999; Wiley Online Library: 1999; pp 247-256.

53. Miura, Y.; Wada, N.; Nishida, Y.; Mori, H.; Kobayashi, K., Chemoenzymatic synthesis of glycoconjugate polymers starting from nonreducing disaccharides. *J. Polym. Sci. A Polym. Chem.* **2004,** *42* (18), 4598-4606.

54. Lee, J.; Lin, E. W.; Lau, U. Y.; Hedrick, J. L.; Bat, E.; Maynard, H. D., Trehalose Glycopolymers as Excipients for Protein Stabilization. *Biomacromolecules* **2013,** *14* (8), 2561-2569.

55. Messina, M. S.; Ko, J. H.; Yang, Z. Y.; Strouse, M. J.; Houk, K. N.; Maynard, H. D., Effect of trehalose polymer regioisomers on protein stabilization. *Polym. Chem.* **2017,** *8* (33), 4781-4788.

56. Lau, U. Y.; Pelegri-O'Day, E. M.; Maynard, H. D., Synthesis and Biological Evaluation of a Degradable Trehalose Glycopolymer Prepared by RAFT Polymerization. *Macromol. Rapid Commun.* **2018,** *39* (5), 1700652.

57. Ko, J. H.; Bhattacharya, A.; Terashima, T.; Sawamoto, M.; Maynard, H. D., Amphiphilic fluorous random copolymer self-assembly for encapsulation of a fluorinated agrochemical. *J. Polym. Sci. A Polym. Chem.* **2019,** *57* (3), 352-359.

58. Pelegri-O'Day, E. M.; Bhattacharya, A.; Theopold, N.; Ko, J. H.; Maynard, H. D., Synthesis of Zwitterionic and Trehalose Polymers with Variable Degradation Rates and Stabilization of Insulin. *Biomacromolecules* **2020,** *21* (6), 2147-2154.

59. Mansfield, K. M.; Maynard, H. D., Site-Specific Insulin-Trehalose Glycopolymer Conjugate by Grafting from Strategy Improves Bioactivity. *ACS Macro Lett.* **2018**, 324-329.

60. Forsythe, N. L.; Maynard, H. D., Synthesis of disulfide-bridging trehalose polymers for antibody and Fab conjugation using a bis-sulfone ATRP initiator. *Polym. Chem.* **2021,** *12* (9), 1217-1223.

61. Lee, J.; Ko, J. H.; Lin, E. W.; Wallace, P.; Ruch, F.; Maynard, H. D., Trehalose hydrogels for stabilization of enzymes to heat. *Polym. Chem.* **2015,** *6* (18), 3443-3448.

62. Lee, J.; Ko, J. H.; Mansfield, K. M.; Nauka, P. C.; Bat, E.; Maynard, H. D., Glucose-Responsive Trehalose Hydrogel for Insulin Stabilization and Delivery. *Macromol. Biosci.* **2018,** *18* (5), 1700372.

63. Liu, Y.; Lee, J.; Mansfield, K. M.; Ko, J. H.; Sallam, S.; Wesderniotis, C.; Maynard, H. D., Trehalose Glycopolymer Enhances Both Solution Stability and Pharmacokinetics of a Therapeutic Protein. *Bioconjugate Chem.* **2017,** *28* (3), 836-845.

64. Perrier, S., 50th Anniversary Perspective: RAFT Polymerization A User Guide. *Macromolecules* **2017,** *50* (19), 7433-7447.

65. Sizovs, A.; Xue, L.; Tolstyka, Z. P.; Ingle, N. P.; Wu, Y.; Cortez, M.; Reineke, T. M., Poly(trehalose): Sugar-Coated Nanocomplexes Promote Stabilization and Effective Polyplex-Mediated siRNA Delivery. *J. Am. Chem. Soc.* **2013,** *135* (41), 15417-15424.

66. Tale, S. R.; Yin, L.; Reineke, T. M., Trehalose-functionalized block copolymers form serum-stable micelles. *Polym. Chem.* **2014,** *5* (17), 5160-5167.

67. Tale, S.; Purchel, A. A.; Dalsin, M. C.; Reineke, T. M., Diblock Terpolymers Are Tunable and pH Responsive Vehicles To Increase Hydrophobic Drug Solubility for Oral Administration. *Mol. Pharm.* **2017,** *14* (11), 4121-4127.

68. Bontempo, D.; Maynard, H. D., Streptavidin as a Macroinitiator for Polymerization: In Situ Protein−Polymer Conjugate Formation. *J. Am. Chem. Soc.* **2005,** *127* (18), 6508-6509.

69. Messina, M. S.; Messina, K. M. M.; Bhattacharya, A.; Montgomery, H. R.; Maynard, H. D., Preparation of biomolecule-polymer conjugates by grafting-from using ATRP, RAFT, or ROMP. *Prog. Polym. Sci.* **2020,** *100*, 101186.

70. Madeira do O, J.; Mastrotto, F.; Francini, N.; Allen, S.; van der Walle, C. F.; Stolnik, S.; Mantovani, G., Synthetic glycopolymers as modulators of protein aggregation: influences of chemical composition, topology and concentration. *J. Mater. Chem. B* **2018,** *6* (7), 1044-1054.

71. Morelli, P.; Bartolami, E.; Sakai, N.; Matile, S., Glycosylated Cell-Penetrating Poly(disulfide)s: Multifunctional Cellular Uptake at High Solubility. *Helvetica Chimica Acta* **2018,** *101* (1), e1700266.

72. Raquez, J. M.; Deléglise, M.; Lacrampe, M. F.; Krawczak, P., Thermosetting (bio) materials derived from renewable resources: A critical review. *Prog. Polym. Sci.* **2010,** *35* (4), 487-509.

73. Bobade, S. K.; Paluvai, N. R.; Mohanty, S.; Nayak, S. K., Bio-based thermosetting resins for future generation: a review. *Polym. Plast. Technol. Eng.* **2016,** *55* (17), 1863-1896.

74. Teramoto, N.; Shibata, M., Trehalose-based thermosetting resins. I. Synthesis and thermal properties of trehalose vinylbenzyl ether. *J. Appl. Polym. Sci.* **2004,** *91* (1), 46-51.

75. Zhang, Q.; Molenda, M.; Reineke, T. M., Epoxy Resin Thermosets Derived from Trehalose and β-Cyclodextrin. *Macromolecules* **2016,** *49* (22), 8397-8406.

76. Zhang, Q.; Phillips, H. R.; Purchel, A.; Hexum, J. K.; Reineke, T. M., Sustainable and Degradable Epoxy Resins from Trehalose, Cyclodextrin, and Soybean Oil Yield Tunable Mechanical Performance and Cell Adhesion. *ACS Sustainable Chem. Eng.* **2018,** *6* (11), 14967-14978.

77. Yano, S.; Teramoto, N.; Miyamoto, R.; Nakajima, E.; Hashimoto, K.; Shibata, M., Fibroblast cell proliferation on photo-cured trehalose cinnamoyl ester thin films. *J. Bioact. Compat. Polym.* **2015,** *30* (1), 87-98.

78. Teramoto, N.; Shibata, M., Synthesis and photocuring of cinnamoyl trehalose esters. *Polym. Adv. Technol.* **2007,** *18* (12), 971-977.

79. Yano, S.; Teramoto, N.; Shimasaki, T.; Shibata, M., Photocrosslinkable Trehalose Derivatives Carrying Mesogenic Groups: Synthesis, Characterization, and in Vitro Evaluation for Fibroblast Attachment. *J. Funct. Biomater.* **2016,** *7* (3), 24.

80. Nagashima, S.; Shimasaki, T.; Teramoto, N.; Shibata, M., Trehalose-incorporated polymer network by thiol-ene photopolymerization. *Polym. J.* **2014,** *46* (10), 728-735.

81. Shibata, M.; Nagashima, S., Trehalose-incorporated organic–inorganic hybrid nanocomposites produced by thiol-ene photopolymerization. *Polym. J.* **2016,** *48* (1), 111-116.

82. Sugai, K.; Sugane, K.; Teramoto, N.; Shibata, M., All carbohydrate-based nanocomposites composed of sorbitol polyglycidyl ether, aminated trehalose and cellulose nanofiber. *Carbohydr. Polym.* **2020,** *232*, 115779.

83. Hoffman, A. S., Hydrogels for biomedical applications. *MOST CITED PAPERS IN THE HISTORY OF ADVANCED DRUG DELIVERY REVIEWS: A TRIBUTE TO THE 25TH ANNIVERSARY OF THE JOURNAL* **2012,** *64*, 18-23.

84. Burek, M.; Czuba, Z. P.; Waskiewicz, S., Novel acid-degradable and thermo-sensitive poly(N-isopropylacrylamide) hydrogels cross-linked by α,α-trehalose diacetals. *Polymer* **2014,** *55* (25), 6460-6470.

85. Burek, M.; Kowalczyk, M.; Czuba, Z. P.; Krol, W.; Pilawka, R.; Waskiewicz, S., Poly(N-isopropylacrylamide) hydrogels cross-linked by α,α-trehalose diacetals as thermo-responsive and acid-degradable carriers for drug delivery. *Polym. Degrad. Stab.* **2016,** *129*, 296-305.

86. Burek, M.; Waśkiewicz, S.; Lalik, A.; Wandzik, I., Hydrogels with novel hydrolytically labile trehalose-based crosslinks: small changes – big differences in degradation behavior. *Polym. Chem.* **2018,** *9* (27), 3721-3726.

87. Burek, M.; Kubic, K.; Nabiałczyk, I.; Waśkiewicz, S.; Wandzik, I., Study on protein release from hydrolytically degradable hydrogels governed by substituent effects in trehalose-based crosslinker and network properties. *Eur. Polym. J.* **2019,** *111*, 123-133.

88. Burek, M.; Waśkiewicz, S.; Awietjan, S.; Wandzik, I., Thermoresponsive hydrogels with covalently incorporated trehalose as protein carriers. *React. Funct. Polym.* **2017,** *119*, 105-115.

89. Burek, M.; Wandzik, I., Trehalose-Rich, Degradable Hydrogels Designed for Trehalose Release under Physiologically Relevant Conditions. *Polymers* **2019,** *11* (12).

90. Burek, M.; Waśkiewicz, S.; Lalik, A.; Student, S.; Bieg, T.; Wandzik, I., Thermoresponsive microgels containing trehalose as soft matrices for 3D cell culture. *Biomater. Sci.* **2017,** *5* (2), 234-246.

91. Student, S.; Milewska, M.; Ostrowski, Z.; Gut, K.; Wandzik, I., Microchamber microfluidics combined with thermogellable glycomicrogels – Platform for single cells study in an artificial cellular microenvironment. *Mater. Sci. Eng. C* **2021,** *119*, 111647.

92. Iglesias, N.; Galbis, E.; Valencia, C.; Díaz-Blanco, M. J.; Lacroix, B.; de-Paz, M. V., Biodegradable double cross-linked chitosan hydrogels for drug delivery: Impact of chemistry on rheological and pharmacological performance. *Int. J. Biol. Macromol.* **2020,** *165*, 2205-2218.

93. O'Shea, T. M.; Webber, M. J.; Aimetti, A. A.; Langer, R., Covalent Incorporation of Trehalose within Hydrogels for Enhanced Long-Term Functional Stability and Controlled Release of Biomacromolecules. *Adv. Healthc. Mater.* **2015,** *4* (12), 1802-1812.

94. Cassano, R.; Trombino, S., Trehalose-based hydrogel potentially useful for the skin burn treatment. *J. Appl. Polym. Sci.* **2017,** *134* (17).

95. Lees, W. J.; Spaltenstein, A.; Kingery-Wood, J. E.; Whitesides, G. M., Polyacrylamides Bearing Pendant .alpha.-Sialoside Groups Strongly Inhibit Agglutination of Erythrocytes by Influenza A Virus: Multivalency and Steric Stabilization of Particulate Biological Systems. *J. Med. Chem.* **1994,** *37* (20), 3419-3433.

96. Alconcel, S. N. S.; Baas, A. S.; Maynard, H. D., FDA-approved poly(ethylene glycol)-protein conjugate drugs. *Polym. Chem.* **2011,** *2* (7), 1442-1448.

97. Veronese, F. M.; Mero, A., The impact of PEGylation on biological therapies. *Biodrugs* **2008,** *22* (5), 315-329.

98. Pelegri-O'Day, E. M.; Lin, E.-W.; Maynard, H. D., Therapeutic Protein–Polymer Conjugates: Advancing Beyond PEGylation. *J. Am. Chem. Soc.* **2014,** *136* (41), 14323-14332.

99. Lim, S. A.; Cox, A.; Tung, M.; Chung, E. J., Clinical progress of nanomedicine-based RNA therapies. *Bioact. Mater.* **2021**.

100. Kumar, R.; Santa Chalarca, C. F.; Bockman, M. R.; Bruggen, C. V.; Grimme, C. J.; Dalal, R. J.; Hanson, M. G.; Hexum, J. K.; Reineke, T. M., Polymeric Delivery of Therapeutic Nucleic Acids. *Chem. Rev.* **2021,** *121* (18), 11527-11652.

101. Tolstyka, Z. P.; Phillips, H.; Cortez, M.; Wu, Y.; Ingle, N.; Bell, J. B.; Hackett, P. B.; Reineke, T. M., Trehalose-Based Block Copolycations Promote Polyplex Stabilization for Lyophilization and in Vivo pDNA Delivery. *ACS Biomater. Sci. Eng.* **2016,** *2* (1), 43-55.

102. Tanaka, M.; Machida, Y.; Niu, S.; Ikeda, T.; Jana, N. R.; Doi, H.; Kurosawa, M.; Nekooki, M.; Nukina, N., Trehalose alleviates polyglutamine-mediated pathology in a mouse model of Huntington disease. *Nat. Med.* **2004,** *10* (2), 148-154.

103. Sarkar, S.; Davies, J. E.; Huang, Z.; Tunnacliffe, A.; Rubinsztein, D. C., Trehalose, a novel mTOR-independent autophagy enhancer, accelerates the clearance of mutant huntingtin and α-synuclein. *J. Biol. Chem.* **2007,** *282* (8), 5641-5652.

104. Khalifeh, M.; Read, M. I.; Barreto, G. E.; Sahebkar, A., Trehalose against Alzheimer's Disease: Insights into a Potential Therapy. *BioEssays* **2020,** *42* (8), 1900195.

105. Rajaram, H.; Palanivelu, M. K.; Arumugam, T. V.; Rao, V. M.; Shaw, P. N.; McGeary, R. P.; Ross, B. P., 'Click'assembly of glycoclusters and discovery of a trehalose analogue that retards Aβ40 aggregation and inhibits Aβ40-induced neurotoxicity. *Bioorganic Med. Chem. Lett.* **2014,** *24* (18), 4523-4528.

106. Miura, Y.; You, C.; Ohnishi, R., Inhibition of Alzheimer amyloid β aggregation by polyvalent trehalose. *Sci. Technol. Adv. Mater.* **2008,** *9* (2), 024407.

107. Wada, M.; Miyazawa, Y.; Miura, Y., A specific inhibitory effect of multivalent trehalose toward Aβ(1-40) aggregation. *Polym. Chem.* **2011,** *2* (8), 1822-1829.

108. Debnath, K.; Pradhan, N.; Singh, B. K.; Jana, N. R.; Jana, N. R., Poly(trehalose) Nanoparticles Prevent Amyloid Aggregation and Suppress Polyglutamine Aggregation in a Huntington's Disease Model Mouse. *ACS Appl. Mater. Interfaces* **2017,** *9* (28), 24126-24139.

109. Mandal, S.; Debnath, K.; Jana, N. R.; Jana, N. R., Trehalose-Functionalized Gold Nanoparticle for Inhibiting Intracellular Protein Aggregation. *Langmuir* **2017,** *33* (49), 13996-14003.

110. Mandal, S.; Panja, P.; Debnath, K.; Jana, N. R.; Jana, N. R., Small-Molecule-Functionalized Hyperbranched Polyglycerol Dendrimers for Inhibiting Protein Aggregation. *Biomacromolecules* **2020**.

111. Mandal, S.; Debnath, K.; Jana, N. R.; Jana, N. R., Trehalose-Conjugated, Catechin-Loaded Polylactide Nanoparticles for Improved Neuroprotection against Intracellular Polyglutamine Aggregates. *Biomacromolecules* **2020,** *21* (4), 1578-1586.

112. Bat, E.; Lee, J.; Lau, U. Y.; Maynard, H. D., Trehalose glycopolymer resists allow direct writing of protein patterns by electron-beam lithography. *Nat. Commun.* **2015,** *6*.

113. Lau, U. Y.; Saxer, S. S.; Lee, J.; Bat, E.; Maynard, H. D., Direct Write Protein Patterns for Multiplexed Cytokine Detection from Live Cells Using Electron Beam Lithography. *ACS Nano* **2016,** *10* (1), 723-729.

114. Chen, X.; Wu, B.; Jayawardana, K. W.; Hao, N.; Jayawardena, H. S. N.; Langer, R.; Jaklenec, A.; Yan, M., Magnetic Multivalent Trehalose Glycopolymer Nanoparticles for the Detection of Mycobacteria. *Adv. Healthc. Mater.* **2016,** *5* (16), 2007-2012.

115. Li, Y.; Ariotti, N.; Aghaei, B.; Pandzic, E.; Ganda, S.; Willcox, M.; Sanchez-Felix, M.; Stenzel, M., Inhibition of S. aureus Infection of Human Umbilical Vein Endothelial Cells (HUVECs) by Trehalose- and Glucose-Functionalized Gold Nanoparticles. *Angew. Chem. Int. Ed.* **2021,** *60* (42), 22652-22658.

116. Jayawardana, K. W.; Jayawardena, H. S. N.; Wijesundera, S. A.; De Zoysa, T.; Sundhoro, M.; Yan, M., Selective targeting of Mycobacterium smegmatis with trehalose-functionalized nanoparticles. *Chem. Commun.* **2015,** *51* (60), 12028-12031.

Chapter 2

Poly(Trehalose Methacrylate) as an Excipient for Insulin Stabilization: Mechanism and Safety

2.1 Introduction

Diabetes is a chronic metabolic disease that affects around 422 million people globally, making it one of the most pressing global health issues according to the World Health Organization (WHO) and Center for Disease Control.[1-2] The large number of diabetic patients that rely on injections of insulin to prevent permanent damage caused by hyperglycemia including impaired kidney function and retinal damage has brought insulin onto the WHO Model List of Essential Medicines.[3] While insulin is effective for managing diabetes in many patients, there are still challenges in stabilizing insulin to environmental stressors that are encountered in manufacture, storage, and transportation, particularly because it is a worldwide disease. Insulin requires a cold chain before and after being delivered to patients, so increasing the stability of insulin formulations would minimize the costs of insulin lost due to poor storage and short expiration dates and allow delivery to places where the cold chain is limited.[4]

Insulin undergoes two main mechanisms of degradation through either physical or chemical means. Insulin degrades chemically through deamidation at Asn A21 under acidic conditions and at Asn B3 under neutral to basic conditions.[5] Interestingly, deamidation does not appear to alter the activity of insulin *in vivo*. Physical degradation of insulin through aggregation and fibrillation is the major challenge associated with insulin instability and loss of activity. Insulin rapidly forms large fibrils upon exposure to heat and/or mechanical agitation.[6-7] These aggregates can lead to a multitude of issues including occlusion of needles and pumps, immunogenicity, and inadequate dosing.[7-8] While there are many insulin analogs on the market that alter pharmacokinetics, these modifications are not intended to improve the storage stability.

Our group has developed polymers based on the natural stabilizer trehalose, and we have shown that these polymers stabilize antibodies, enzymes, growth factors, and hormones against

environmental stressors.[9-18] The trehalose-based glycopolymers provide better stabilization than trehalose alone and showed no signs of cytotoxicity up to 8 mg/mL polymer *in vitro* with NIH 3T3 mouse embryonic fibroblast cells.[9] Studying insulin stabilization with a styrenyl ether-based trehalose polymer, we found that different regioisomers of the monomer all stabilized insulin against heat and agitation, indicating that the trehalose itself is more important in stabilizing insulin than the site by which trehalose is attached to the backbone.[13] Additionally, a clear dependency of insulin stability on polymer concentration was detected. At the same time, we found that conjugating the methacrylate trehalose polymer (pTrMA) to insulin both prolonged the half-life *in vivo* and stabilized insulin against heat and mechanical agitation.[14-15] Given that insulin is stabilized equally by pTrMA excipient and conjugate, we opted to study the excipient pTrMA so that the results are more easily translated to other biologics. Moreover, this choice removes the concern that the reaction conditions or modification site of a conjugate may cause loss of insulin bioactivity or increased susceptibility to degradation or aggregation.

We successfully optimized pTrMA concentration and molecular weight (MW) for complete insulin stabilization against heat and agitation, in order to reduce the amount of pTrMA in formulation for cost, safety, and improved fluid properties.[18] Further, while the pTrMA did increase the formulation viscosity from insulin alone, formulations were well-below a known threshold for tolerable injections.[19] This work provided formulations of insulin, but no understanding of the polymer safety or the mechanism by which pTrMA stabilizes insulin. Given the promising results we have obtained with the pTrMA regarding insulin stabilization, this chapter describes investigations of not only the mechanism by which the polymer stabilizes insulin, but also the safety profile of the pTrMA glycopolymer through immune and biodistribution studies. In addition,

the long term stability of insulin with and without polymer and the effect of the polymer excipient on the pharmacokinetics of insulin are explored in this chapter.

2.1 Results & Discussion

2.1.1 Immunogenicity of pTrMA

To study the adaptive immune response in the form of antibody production, mice were challenged at weeks 0 and 2 with the model immunogenic protein ovalbumin (OVA, 2 mg/kg) as a positive control, pTrMA (10 wt% or 100 mg/mL), or both OVA + pTrMA (2 mg/kg OVA, 10 wt% pTrMA) via intraperitoneal (i.p.) injection. Serum was collected each week and the immunoglobulins IgG and IgM antibodies specific to the OVA or pTrMA were measured by ELISA. For the ELISA, OVA or bovine serum albumin (BSA) conjugated with pTrMA (**Figure A1**) are adsorbed for 16 – 18 h on microplate wells to capture any antibodies in the serum. Serum from challenged mice and naïve mice as a negative control was measured for antibodies against the challenge antigen, OVA, or the BSA-pTrMA conjugate. Serum from the mice treated with OVA and pTrMA was tested against both OVA and the BSA-pTrMA conjugate. Testing against both antigens measures if the polymer increases the immunogenicity of OVA and, conversely, if the presence of an immunogenic protein, OVA, elicits an immunogenic response to the polymer (**Figure A2**). The resulting data indicates that only the OVA elicited an IgG response which, for OVA alone, increased in both weeks 2 and 3 and for OVA with trehalose polymer, increased from week 1 to week 2 but was not significantly different from naïve serum by week 3 (**Figure 2.1a)Error! Reference source not found.**. While OVA did also elicit an IgM immune response, it tailed off quickly; with OVA alone, IgM was only elevated in the first week, whereas for OVA with the trehalose polymer, IgM was only elevated in the second week (**Figure 2.1b**). pTrMA did

not induce any significant generation of polymer-specific IgG or IgM antibodies even in the presence of OVA.

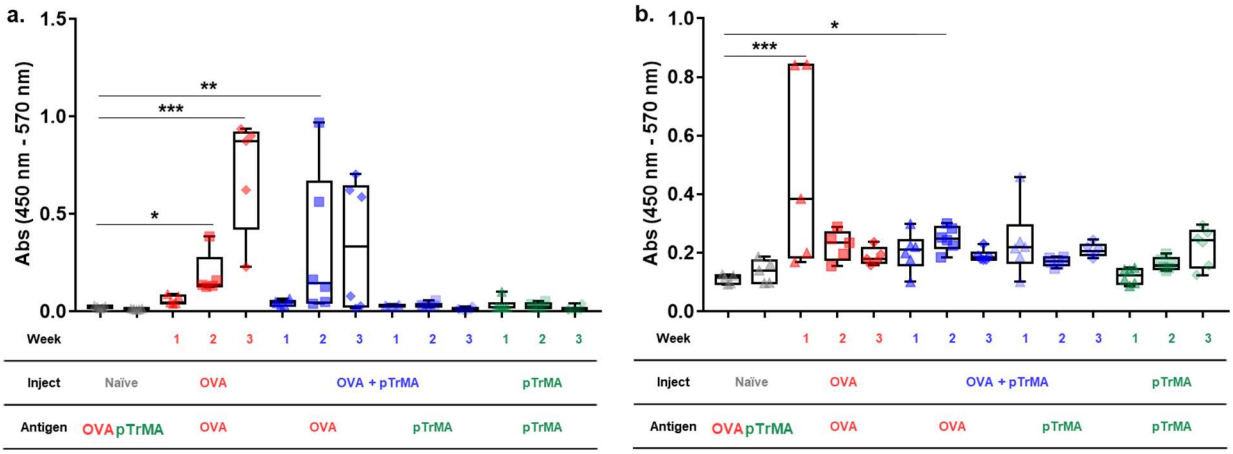

Figure 2.1 Antibody levels in mice specific to OVA or pTrMA (BSA-pTrMA conjugate) antigens over 3 weeks after i.p. injection of OVA (2 mg/kg), OVA + pTrMA (2 mg/kg, 10 wt%), or pTrMA (10 wt%) at weeks 0 and 2 (n = 5 – 6). Levels measured by immune ELISA for a. IgG and b. IgM specific antibody responses and compared to non-specific baseline antibody recognition in naïve mice (*: $p < 0.05$, **: $p < 0.01$, ***: $p < 0.001$, with horizontal lines indicating the conditions corresponding to the significant difference from the naïve control for the respective antigen).

For a full picture of immune response to pTrMA, the innate response was evaluated by measuring cytokine levels in mice (work done by Jeong Hoon Ko). A library of pro-inflammatory (interleukin (IL)-1b, IL-2, IL-6, IL-8 IL-12 KC (IL-8 analog in mice), TNF-α, and IFN-γ) and anti-inflammatory (IL-10 and IL-4) cytokines were detected by Luminex's xMAP® immunoassay, a multiplexed ELISA that measures multiple analytes at once. Cytokine levels were measured at 1 h, 6 h, and 24 h after i.p. injection of phosphate-buffered saline (PBS) or pTrMA (10 mg/kg). As expected from the negative control, PBS, there was minimal production of any of the tested cytokines over the study (**Figure 2.2**). Cytokine levels in the mice exposed to pTrMA were comparable to the negative control group indicating little innate response to the polymer. These

cytokine measurements together with the antibody response results show pTrMA to not be immunogenic or inflammatory alone or in the presence of an immunogenic protein.

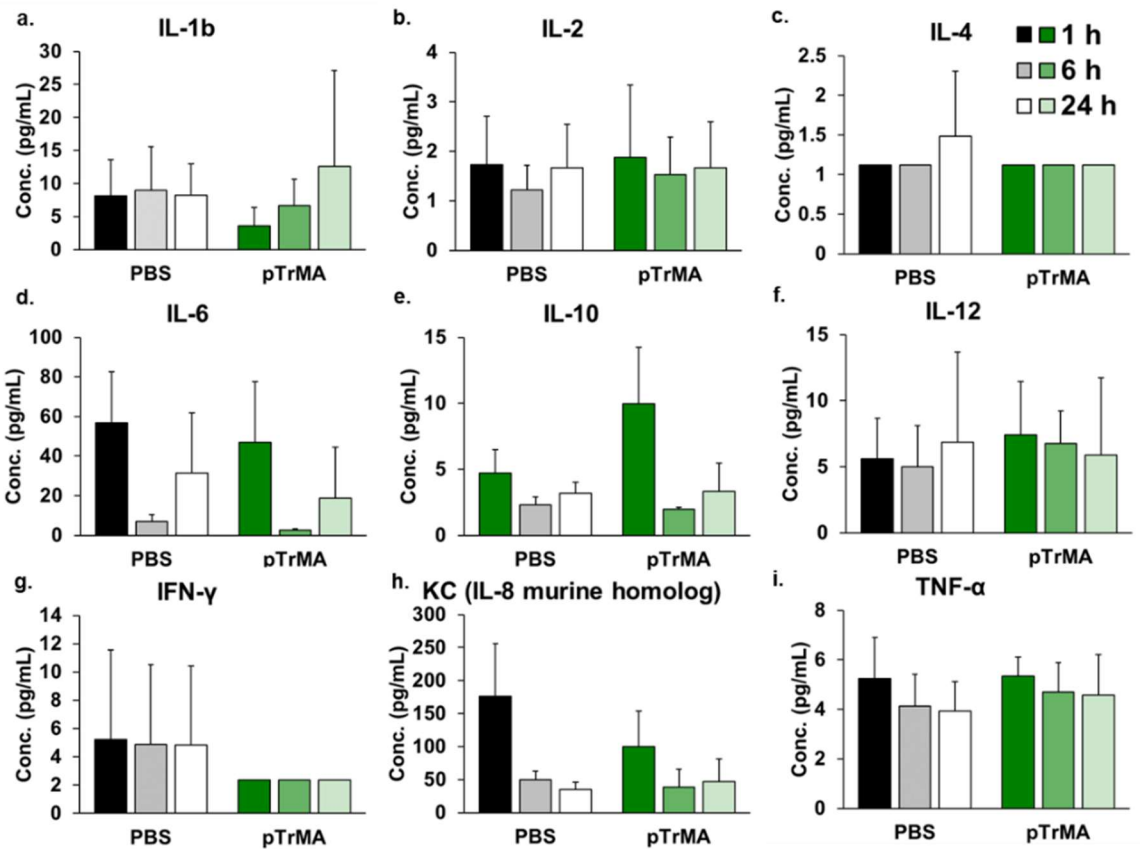

Figure 2.2 Plasma cytokine levels of a. IL-1b, b. IL-2, c. IL-4, d. IL-6, e. IL-10, f. IL-12, g. interferon-γ, h. KC (IL-8 murine homolog), i. tumor necrosis factor-α fin mice (n = 5) at 1 h, 6 h, and 24 h post i.p. injection of PBS or pTrMA (10 mg/kg) measured by Luminex xMAP immunoassay.

2.1.2 Biodistribution, Excretion, and Inflammation with pTrMA-*co*-DOTA by Micro Positron Emission Tomography (μPET) and Micro Computer Tomography (μCT)

pTrMA was synthesized as a random copolymer with a single unit of PDSMA on average per polymer chain (pTrMA-*co*-PDSMA) via free radical polymerization (**Scheme 2.1**). After the polymerization, the disulfide was reduced and reacted with the tetraaza 12-membered chelating

ring DOTA via thiol-maleimide chemistry, forming pTrMA-*co*-DOTA. This modification successfully removed all PDSMA from the polymer, but, despite attempts to improve modification, DOTA incorporation did not exceed 85%. Given there was an average of a single PDSMA unit per polymer chain, 85% of the pTrMA polymers bore a single DOTA as a pendant side chain. This pTrMA-*co*-DOTA polymer could then chelate ^{64}Cu with >99% efficiency by HPLC (radioactive work conducted by Crump Imaging Facility members: Jeffrey Collins JC, Mikayla Tamboline MT, and Shili Xu SX). Although the cytokine production studies showed that pTrMA does not cause a systemic inflammatory response, to further examine the possibility of pTrMA causing localized inflammation in specifically inflamed organs, JC, MT, and SX conducted an experiment using ^{18}F-fludeoxyglucose (FDG). Mice (female n = 4, male n = 4) were i.v. injected with ^{18}F-FDG as a baseline before injecting mice with pTrMA (1 mg/kg i.v.) or LPS (1 mg/kg i.p.), a positive control to cause inflammation, and repeating the ^{18}F-FDG i.v. injection 24 h later. While LPS did cause inflammation that resulted in 2 – 4 fold increases in signal intensity for the liver, intestine, spleen, and bone arrow, there was no significant change in FDG signal compared to the baseline in any organ with measurable signal from the mice injected with pTrMA (**Figures A3** – **5**).

Scheme 2.1 Two-step synthesis of pTrMA-*co*-DOTA by first a polymerization of pTrMA-*co*-PDSMA according to previous literature[20] followed by a post-polymerization disulfide reduction and thiol-ene addition of thiol-DOTA.

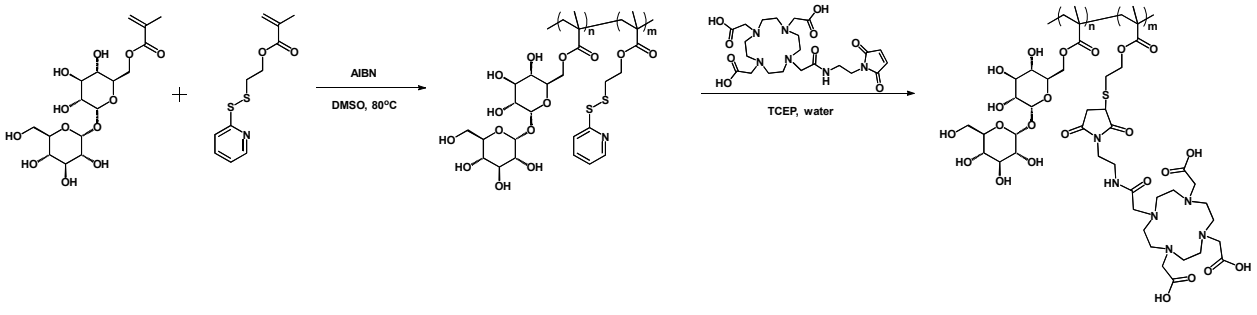

The time-course biodistribution and excretion of the trehalose polymer was aso studied *in vivo* with μPET co-registered with μCT images for the anatomical information and attenuation correction (again radiolabeling performed by JC and μPET/μCT by MT and SX). Mice (female n = 4, male n = 4) were injected intravenously (i.v.) with the ^{64}Cu-labeled pTrMA-*co*-DOTA (200 μCi) and underwent a series of μPET/μCT scans beginning with a 1 h dynamic scan followed by static scans at 4 h, 24 h, 48 h, 72 h, and 120 h post-injection (**Figure 2.3**, **Figures A6 – 13**). Radioactivity was measured as a percent of injected dose per cubic centimeter (% ID/cc) showed that pTrMA-*co*-DOTA was 77.5 ± 0.4% and 79.6 ± 2.0% excreted from female and male mice after 24 h, respectively. Dynamic scans over the first hour clearly show renal clearance of the majority of the ^{64}Cu-signal from labeled pTrMA-*co*-DOTA. The signal from the radiolabeled material moved through the kidneys, accumulated temporarily in the bladder, before being excreted from the animal. The pTrMA-*co*-DOTA was distributed symmetrically in paired organs. Final μPET and μCT time point of the mice indicated minimal signal of 8.3 ± 1.4% and 6.0 ± 1.2% in the liver and 3.0 ± 0.4% and 2.0 ± 0.3% in the kidneys of female and male mice, respectively, indicating incomplete clearance of the polymer with some accumulation in the liver (**Figure 2.4**).

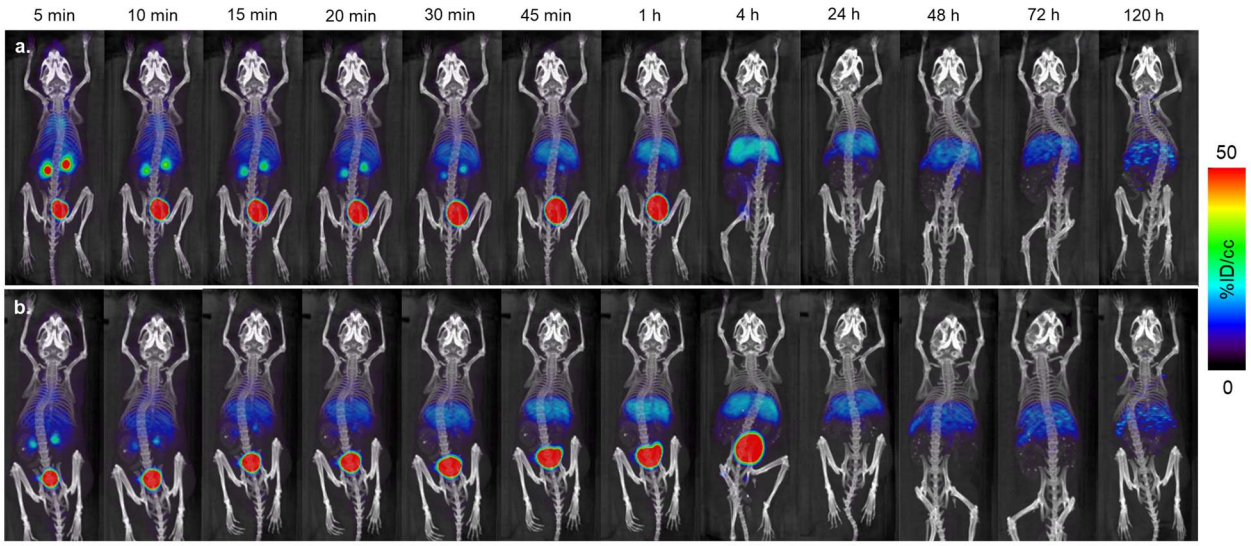

Figure 2.3 Representative maximum-intensity projection (MIP) μPET/ μCT images from 5 min to 120 h post-injection of ^{64}Cu-labeled pTrMA-*co*-DOTA (200 μCi) into b. female (n = 4) and c. male (n = 4) mice (dynamic scans 0-60 h, static scans for later time points).

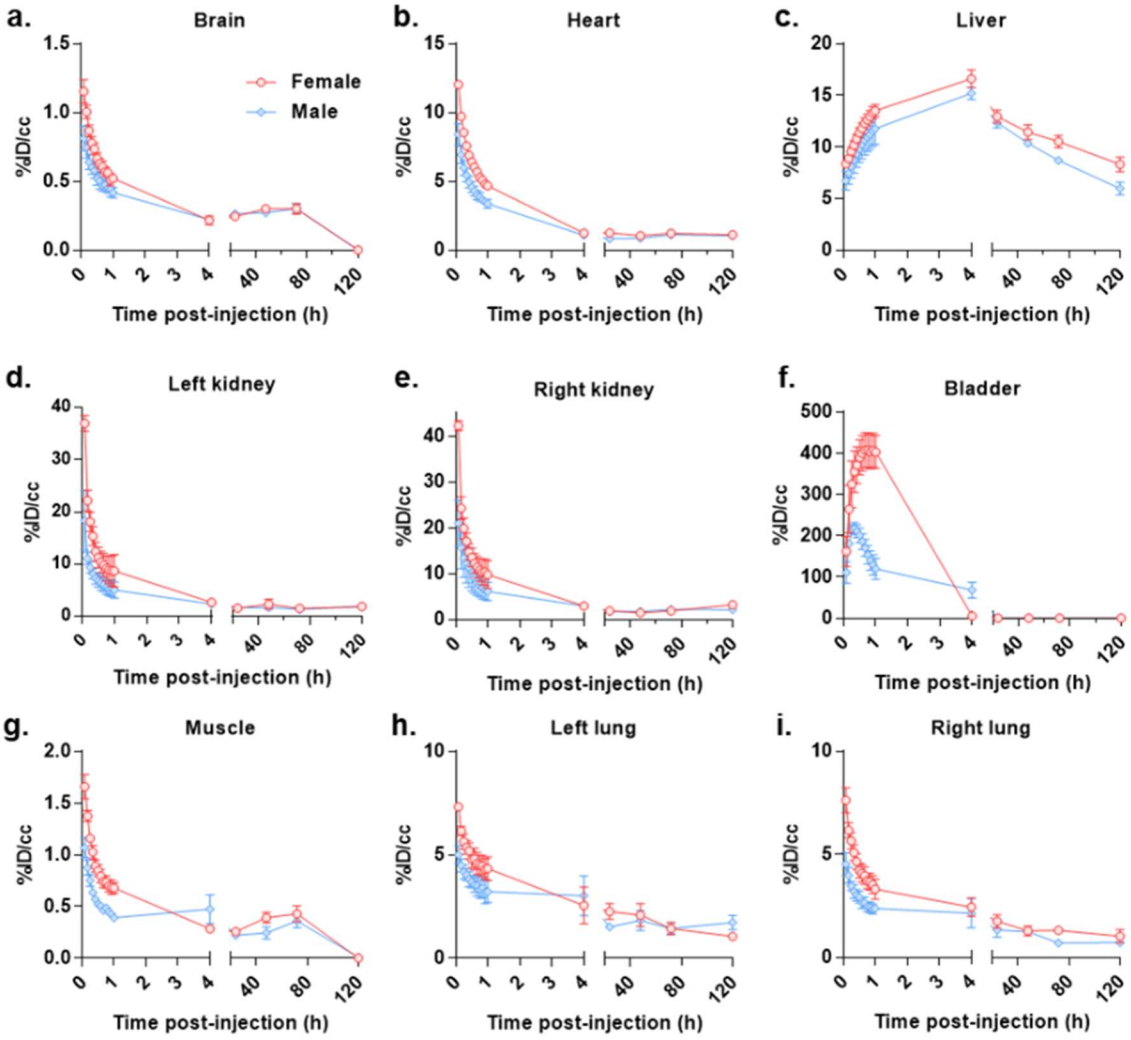

Figure 2.4 Time-course biodistribution and excretion of ^{64}Cu-labeled pTrMA-*co*-DOTA (200 μCi) from the organs a. brain, b. heart, c. liver, d. left kidney, e. right kidney, f. bladder, g. muscle, h. left lung, and i. right lung of female (red, n = 4) and male (blue, n = 4) mice. Data were quantified from μPET images.

To determine if organ signal attenuation was occurring because ^{64}Cu was released from pTrMA-co-DOTA *in vivo* due to insufficiently strong DOTA chelation, we explored the stability of the radiolabeled polymer as well as the biodistribution and excretion of free ^{64}Cu by further μPET/μCT imaging. Mice (female, n = 4) were i.v. injected with the fresh ^{64}Cu-labeled pTrMA-*co*-DOTA (200 μCi), ^{64}Cu-pTrMA-*co*-DOTA after incubating in plasma at 37 °C for 24 h (100 μCi), and free $^{64}CuCl_2$ (100 μCi). Post-injection, the mice were immediately scanned for 1 h with dynamic μPET followed by a μCT scan; subsequently they were scanned statically at 4 h (10 min) and 24 h (20 min) (**Figure 2.5**, **Figures A14 – 16**). We are able to conclude that the ^{64}Cu-pTrMA-*co*-DOTA is largely stable in the plasma, as the biodistribution patterns between the two groups exposed to the ^{64}Cu-pTrMA-*co*-DOTA is similar especially when compared to $^{64}CuCl_2$. If ^{64}Cu was readily leached from the DOTA group when incubated in plasma, the shifting biodistribution in the organs with time would have been the same as with the mice exposed to free $^{64}CuCl_2$. However, intensity from 24 h time point showed that, while 64.4 ± 5.7% of ^{64}Cu-pTrMA-*co*-DOTA had been cleared, only 49.7 ± 2.9% and 43.7 ± 19.7% signal had been cleared from the plasma incubated ^{64}Cu-pTrMA-*co*-DOTA and $^{64}CuCl_2$, respectively (**Figure 2.5l**). Additionally, as the fresh and plasma incubated ^{64}Cu-pTrMA-*co*-DOTA are quite similar, it cannot be determined from this if the attenuated liver signal is due to radiolabeled polymer or released ^{64}Cu. Additionally, there is an interesting accumulation of signal in the spleen from mice injected with the plasma incubated ^{64}Cu-pTrMA-co-DOTA that is not apparent in the other groups. While immunoglobulins are known to accumulate in the spleen, given the immunogenicity results and that the polymer was incubated *ex vivo* in naïve serum, attributing this accumulation to immunoglobulins binding would only be valid in the unlikely case of non-specific binding.[21] While this result was curious, further

exploration did not seem warranted as plasma incubation would not be a normal part of pTrMA use.

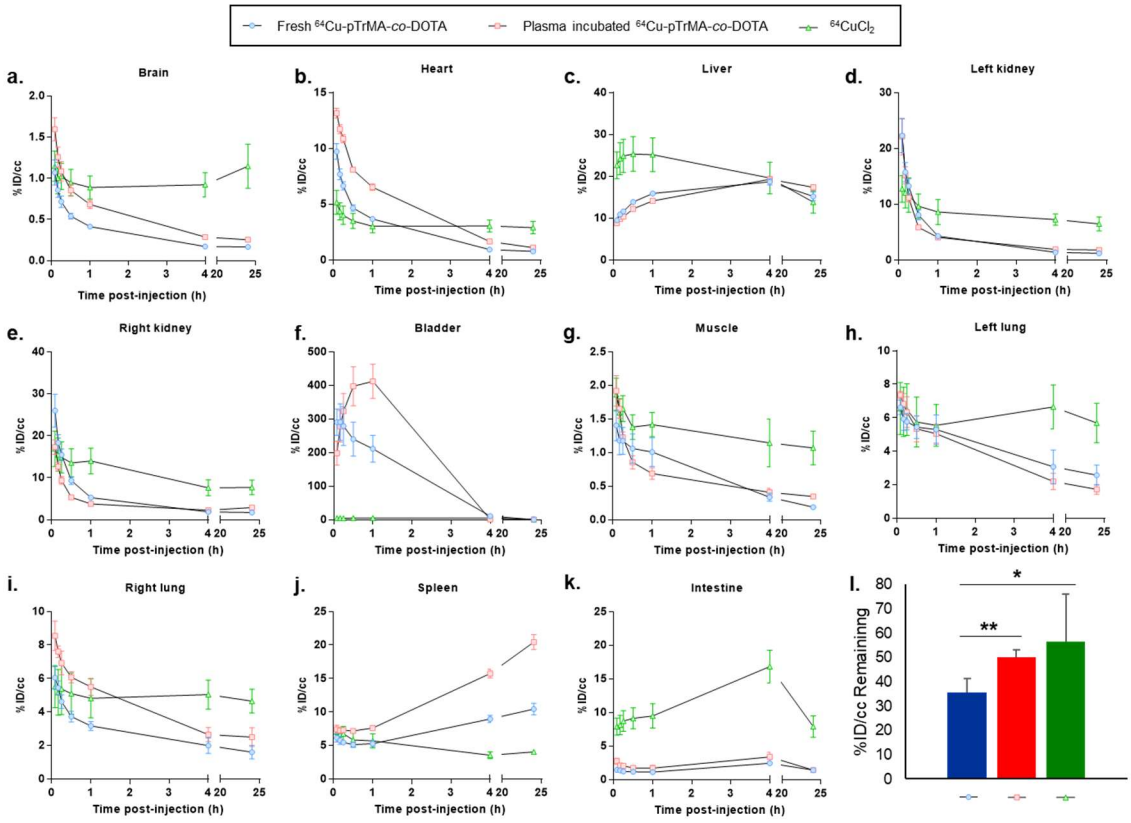

Figure 2.5 Time-course biodistribution and excretion of fresh ^{64}Cu-labeled pTrMA-*co*-DOTA (blue), plasma incubated ^{64}Cu-labeled pTrMA-*co*-DOTA (red), and free $^{64}CuCl_2$ (green) from the organs a. brain, b. heart, c. liver, d. left kidney, e. right kidney, f. bladder, g. muscle, h. left lung, i. right lung, j. spleen, and k. intestine of female (n = 4) mice. l. The total signal remaining for each condition after 24 h (*: $p < 0.05$, **: $p < 0.01$, with horizontal lines indicating the significantly different conditions). Data were quantified from μPET images.

2.1.3 Insulin Pharmacokinetics with pTrMA

Next Kathryn M. M. Messina (KMMM) looked at whether pTrMA affects the pharmacokinetics (PK) of a biologic it is formulating. Insulin was chosen to study PK since it is widely used and we have previously shown that pTrMA stabilizes this protein to elevated

temperatures and agitation.[13, 17] Insulin levels *in vivo* (n = 4) over time were determined by ELISA for mice injected with insulin alone or insulin with two molar equivalents of pTrMA, the amount known to stabilize insulin (**Figure 2.6**). PK of insulin was not significantly changed by the excipient pTrMA at any time point, further proving the benign nature of employing pTrMA as a stabilizing excipient in that alteration of the PK does not occur.

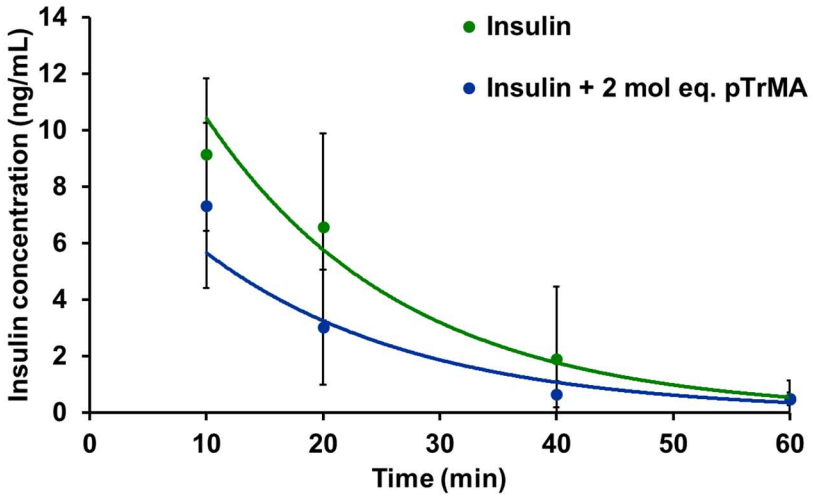

Figure 2.6 Pharmacokinetics of insulin (120 µg/kg) injected i.v. in mice (n = 4) alone and with 2 mol. eq. of pTrMA measured by insulin ELISA. No significant difference between the two conditions was detected at any time points (10 min, 20 min, 40 min, and 60 min).

2.1.4 Mechanism of Insulin Stabilization to Simulated Accelerated Storage and Standard Storage Conditions with pTrMA

Previous stabilization studies within the Maynard lab have found that the trehalose polymers stabilize insulin to both heat-only stress conditions as well as heat with mechanical agitation conditions.[13-18] An accelerated heating assay was applied herein to insulin and insulin with 2 mol. eq. of pTrMA to elucidate what mechanisms of degradation or aggregation pTrMA was inhibiting. The formulations were heated to 90 °C for 30 min. Samples were then analyzed by KMMM for degradation specifically by deamidation with high pressure liquid chromatography

(HPLC) using conditions that separate degraded insulin from the intact species as reported previously.[5] After heating, insulin alone degraded extensively at the AsnB3 site resulting in Asp and isoAsp insulin derivatives with very little intact insulin remaining (**Figure 2.7**Error! Reference source not found.**a**). Just the 2 mol. eq. of pTrMA prevented most degradation at AsnB3 with no Asp insulin present and only minimal isoAsp insulin formation. The heated samples were also investigated by native polyacrylate gel electrophoresis (PAGE) for changes to molecular weight or isoelectric point (pI) for evidence of chemical changes or aggregate formation (**Figure 2.7b**). PAGE gel confirmed the HPLC analysis that both insulin chemical degradation products form with heat, and that 2 mol. eq. of pTrMA is sufficient to inhibit such degradation. Additionally, native PAGE gel indicated aggregates had formed by the higher MW species in the gel (**Figure 2.7c**). However, changes to the insulin heated alone indicate the formation of the Asp and isoAsp insulin derivatives along with insulin aggregate.

KMMM next evaluated the fibrillation and aggregation of insulin by thioflavin T (ThT) assay whereby the ThT molecule binds to available amyloids or misfolded proteins causing a shift in its emission spectrum to strongly fluoresce. Heated insulin produced significantly higher ($p < 0.01$) fluorescence signal than fresh insulin or insulin heated with pTrMA indicative of the unfolded insulin forming fibrils that the ThT could bind (**Figure 2.7d**). Notably, the insulin heated with pTrMA was not significantly different from the fresh insulin with pTrMA although both pTrMA solutions were higher than fresh insulin alone (fresh $p < 0.05$, heated $p < 0.01$). SEC-MALS analysis of the insulin alone and with pTrMA was performed to investigate the oligomerization state of insulin.[22-23] Monomeric and dimeric insulin were not resolved by SEC and co-eluted in an overlapping peak (**Figure A17**), However, no hexameric insulin was present with insulin alone or when pTrMA was added, and, interestingly, the remaining soluble insulin after

heating was still monomeric or dimeric in apparently the same relative concentrations for insulin with and without pTrMA (all aggregated insulin was filtered out).

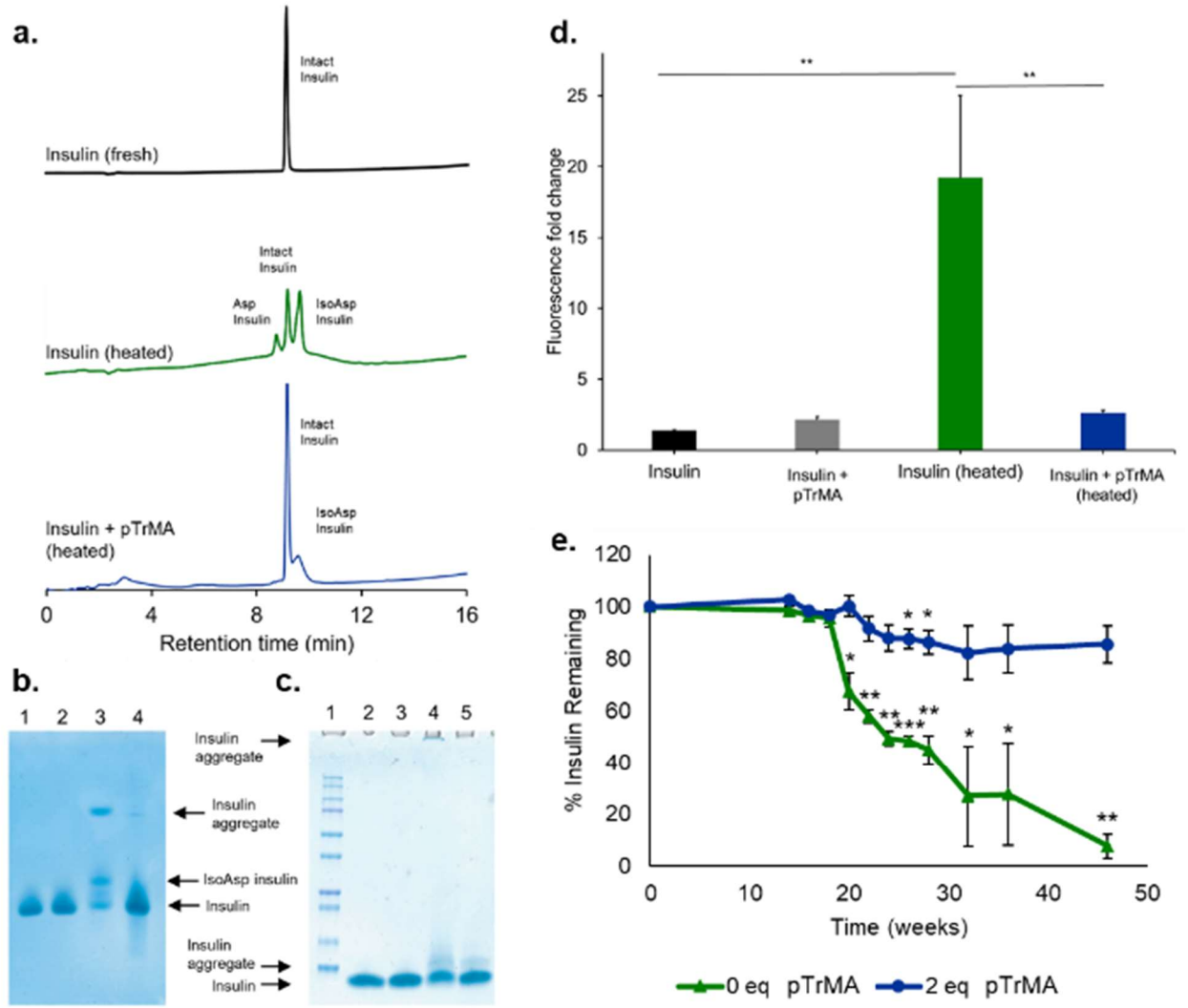

Figure 2.7 Characterization of insulin alone or in the presence of 2 mol. eq. of pTrMA after exposure to extreme heat (90 °C) for 30 min by a. HPLC, b. native PAGE gel [1. Insulin (fresh), 2. Insulin + 2 mol. eq. of pTrMA (fresh), 3. Insulin (heated), 4. Insulin + 2 mol. eq. of pTrMA (heated)], and c. SDS PAGE [0. Protein Dual Color Ladder (10, 15, 20, 25, 37, 50, 75, 100, 150, and 250 kDa standard bands), 1-4. same as b. native PAGE gel], and d. ThT assay (n = 3). e. Quantification of remaining intact insulin alone or in the presence of 2 mol. eq. of pTrMA (n = 3)

after mild storage conditions (4 °C) for 46 weeks by HPLC (difference compared to the original time point). For all *: $p < 0.05$, **: $p < 0.01$, ***: $p < 0.001$.

In the same manner, an extended storage assay was applied to insulin alone and insulin with 2 mol. eq. of pTrMA to measure and correlate the effects of realistic storage conditions for comparison with accelerated aging. Under the accelerated aging conditions, pTrMA inhibited both aggregation and degradation, leaving the majority of the insulin entirely intact. To study relevant storage, the formulations were stored at 4 °C (refrigeration temperature) for 46 weeks. After 14 weeks, samples were analyzed for the intact insulin with HPLC conditions to separate out the degraded insulin (**Figure 2.7e**).[5] After 20 weeks, insulin incubated alone significantly degraded to 67.4 ± 7.0% of original level ($p = 0.023$ compared to the original time point), while insulin with pTrMA did not significantly differ from the original time point (100.3 ± 4.0%). Over the subsequent 26 weeks, as the percent intact insulin alone dropped, the solutions became visually cloudy and noticeably more difficult to filter before HPLC indicating aggregation. At the final time point, only 7.8 ± 4.6% of the insulin alone was intact. However, the level of insulin formulated with pTrMA only decreased by 13.0 ± 7.1% over the whole 46 weeks at 4 °C.

pTrMA is shown in these studies to be a safe excipient for stabilizing insulin. While the immunogenic protein OVA elicited a clear IgG and IgM antibody response alone and in the presence of pTrMA, no significant immune response to the polymer was found for the polymer with or without OVA. Also, no significant cytokine response to pTrMA was detected. The expanded inflammation study by ^{18}F-FDG corroborated the ELISA-based immunogenicity results by showing that pTrMA did not cause inflammation, and it does not appear to localize in inflamed organs. Based on these observations, we do not expect that pTrMA would trigger antibody production as a host immune response or elicit increased inflammatory cytokine production due to

the generally safe nature of trehalose combined with a benign methyl methacrylate backbone. Additionally, earlier studies from within our group demonstrated that conjugation of pTrMA conjugated to insulin prolonged its half-life, indicating that no anti-pTrMA antibodies formed as they would have rapidly cleared the conjugate.[14-15]

A total of 77.5 ± 0.4% and 79.6 ± 2.0% of the radioactivity was cleared primarily via renal excretion within 24 h from female and male mice, respectively. ^{64}Cu has been shown to stably accumulate in the liver (13% ID/cc) of C57HL/6 mice with concurrent accumulation in the kidneys (10% ID/cc) at 72 h.[24] μPET/μCT of the Cu^{64} radiolabeled pTrMA revealed some signal attenuation in the liver even at the final time point, 8.3 ± 1.4% and 6.0 ± 1.2%, respectively, similar to the retention of signal in the liver and kidneys from $^{64}CuCl_2$ alone. In the final time points of the extended μPET/μCT experiment, signal in the liver still appeared to be going down; while the study could not be extended due to the nature of radioactive decay, it is possible that pTrMA was still being excreted. These results are similar to results with DOTA conjugated PEG-based star and linear polymers from the Wooley, Hawker, and Welch labs with some accumulation in the liver and kidneys across a range of polymer chemistries and architectural designs.[25-29] Like our 10 kDa linear copolymer, nanoparticles formed from poly(methyl methacrylate) and poly(ethylene glycol) comb copolymers (1 – 5 kDa) showed attenuation in the liver, spleen, and kidneys even at 50 h.[26] Alone, our data could not reveal whether the DOTA chelating ligand was leaching ^{64}Cu *in vivo*, but additional experiments by μPET/μCT could be used to explore this possibility in the future including using an alternative metal and chelators. Finally, the addition of trehalose polymer as excipient did not alter the *in vivo* pharmacokinetics of insulin, indicating it would not cause a delay in bioactivity. The lack of anti-pTrMA IgG or IgM antibodies combined with majority clearance

of pTrMA and no significant impact on the PK of insulin indicate reasonably benign behavior *in vivo*.

While *in vivo* safety is critical, the main purpose of pTrMA is to provide stabilization to the therapeutic protein or peptide. Insulin was stabilized against heat-induced chemical degradation and aggregation by the pTrMA according to HPLC, ThT assay, and native PAGE gel. All three assays indicated that the trehalose polymer decreased the aggregation of insulin. Furthermore, HPLC and native PAGE gel analysis demonstrated that the deamidation of insulin was inhibited, and gel indicated intact insulin to be present. Fibrillation of insulin is accelerated when the conformational stability is decreased, such as through exposure to heat, low pH, or the air-water interface during mechanical agitation.[5-6] SEC-MALS of fresh insulin indicated that the addition of pTrMA did not shift the monomeric and dimeric insulin into the more complexed hexameric assembly, and the relative concentrations did not appear to be affected by exposure to heat stress. These results indicate that the pTrMA is maintaining the stability of monomeric and dimeric insulin, the less stable conformations. By stabilizing insulin without complexing into the hexameric state, pTrMA would most likely not increase any delay in onset of insulin activity due to the time required for insulin to disassemble from greater oligomeric states into the active monomeric state.

While we did not detect any insulin complexation with pTrMA as indicated by SEC-MALs in this study, it is unknown at this time how pTrMA stabilizes insulin without complexing with it. SEC-MALS is additionally limited in resolution and any aggregate is removed by filtration. Better understanding of this protein-polymer relationship would likely come from NMR spectroscopy analysis to identify binding interfaces by their chemical shift perturbations. Studying different polymer chain lengths as well as polymer concentrations could also elucidate the importance of

polyvalence for the trehalose polymer. Further analysis should include thermal shift (differential scanning calorimetry or fluorimetry) to track protein unfolding when stabilized by the trehalose polymer. Other forms of particle characterization and sizing (including dynamic light scattering and micro-flow imaging) could also be used to further understand how pTrMA prevents insulin from undergoing the aggregation and fibrillation pathway that leads to loss in activity. In previous work using horseradish peroxidase, we reported that a similar methacrylate trehalose polymer made with an ether linkage acted as a chaperone and helped the protein refold after heating.[9] It is possible that pTrMA may improve the conformational stability of insulin, and of insulin monomer in particular, to prevent aggregation by a similar mechanism. Inhibition of heat-induced deamidation by pTrMA may also be related to conformational stability of the protein, as solvent accessibility/flexibility around relevant residues is related to the rate of deamidation in proteins.[30] Further investigation into the mechanism of stabilization of pTrMA is ongoing.

Thus far we have shown that the pTrMA successfully stabilizes insulin as a conjugate or excipient, and as an excipient can be optimized to reduce the total amount of polymer for cost and fluid flow purposes while maintaining insulin stability against heat and mechanical agitation. This work shows that pTrMA stabilizes insulin from heat and mechanical agitation by inhibiting both chemical degradation and aggregation into fibrils. We also find pTrMA to be promising from a safety standpoint with no innate or adaptive immune response, and majority excretion of the polymer in 24 h with continued clearance over the subsequent 4 days. Future work will explore further immune studies and extensive toxicity in higher-order animals. Key among these still-necessary studies will be more detailed understanding of the polymer excretion.

Overall, the pTrMA formulated insulin is highly promising especially for use in insulin pumps where formulations are exposed to body and elevated temperatures for prolonged periods

at the skin surface, and strenuous activity can cause mechanical agitation for the insulin within the pump reservoir. Further, the safety and stabilization capabilities of pTrMA as an excipient with insulin suggest it could be expanded to other therapeutic biologics, making it promising for formulation application in the pharmaceutical industry.

2.3 Conclusions

As insulin continues to be major therapeutic for treating diabetes, the need for stabilizing excipients becomes greater. Insulin needs to not only be stabilized against environmental stressors, but also be available in its active, less-stable, monomeric state to reduce delays in onset of activity post-administration. Biodistribution of the trehalose-based glycopolymer pTrMA by PET and immunogenicity by ELISA and multiplexed ELISA indicated that pTrMA resides only minimally in the liver, similarly to other polymers, and does not cause immunogenic clearance responses (innate or adaptive). Insulin injected with pTrMA had the same PK profile as free insulin further indicating that pTrMA does not affect insulin's *in vivo* properties. Stability studies into the mechanism by which insulin is stabilized demonstrated inhibition of the known chemical degradation pathways as well as prevention of aggregation pathways. Investigation of the oligomeric state of insulin showed that pTrMA did not shift the insulin to the slower onset of activity hexameric state even after heat stress. Long term stability studies at 4 °C showed that with just pTrMA, insulin was stabilized for 46 weeks at pH 7.4. This work clearly illustrates the safety and utility of pTrMA for the stabilization of insulin as an excipient, and should be further explored for use in the clinic.

2.4 Experimental Details

2.4.1 Materials

All chemicals purchased from Sigma Aldrich or Fisher Scientific were used without further purification unless mentioned otherwise. Azobis(isobutyronitrile) (AIBN) was recrystallized from acetone before use. Trehalose purchased from BulkSupplements.com (Henderson, NV) was repeatedly dried azeotropically from ethanol and stored under vacuum. Spectra/Por3® regenerated cellulose membrane (MWCO 3.5 kDa or 1.0 kDa) used for polymer dialysis was purchased from Spectrum Chemical (New Brunswick, NJ). Maleimide-DOTA (2,2′,2”-(10-(2-((2-(2,5-dioxo-2,5-dihydro-1H-pyrrol-1-yl)ethyl)amino)-2-oxoethyl)-1,4,7,10-tetraazacyclododecane-1,4,7-triyl)triacetic acid) was purchased from CheMatech and used as-is. Sterile, endotoxin-free, chicken egg white ovalbumin (OVA) containing <1 EU/mg was purchased from InvivoGen (EndoFit, Version 17E10-MM, EFP-41-02) and reconstituted with EU-free, sterile, saline solution according to manufacturer's protocol. Recombinant human insulin was purchased from Sigma-Aldrich (Lot no. 17N331). Bovine serum albumin (BSA), heat shock treated, was purchased from Fisher Scientific (Lot no. 43233). Cuprisorb was purchased from Seachem on Amazon.com. Goat anti-mouse IgG HRP conjugate and goat anti-mouse IgM HRP conjugate were both purchased from Abcam, reconstituted, diluted 2x with glycerol, and stored at −80 °C following manufacturer's recommendations. Pierce BCA assay kit and enzyme-linked immunosorbent assay (ELISA) TMB development solution was purchased from ThermoFisher Scientific. Insulin ELISA kit was purchased from Mercodia. Any kD Mini-PROTEAN-TGX™ PAGE gels and SDS-PAGE protein standards (Precision Plus ProteinTM Dual Color) were purchased from Bio-Rad. Amicon Centriprep^{TM} tubes were purchased from Millipore. ^{64}Cu radioisotope was purchased from Washington University School of Medicine. Initiators, methacrylate trehalose monomer (TrMA), and polymers excepting pTrMA-*co*-DOTA were synthesized as previously described and their synthesis is briefly described below.[9, 15, 20]

2.4.2 Analytical Techniques

Nuclear Magnetic Resonance (NMR) spectroscopy were performed on a Bruker AV 400 MHz, DRX 500 MHz, or AV 500 MHz instrument. ^{1}H-NMR spectra were acquired with a relaxation delay of 2 s for small molecules and 30 s for polymers. ^{13}C-NMR spectra were acquired with a relaxation delay of 30 s for polymers. Preparatory reverse phase high performance liquid chromatography (HPLC) purification was performed on a Shimadzu HPLC system equipped with a UV detector using a Luna 5 μm C18 100A column (preparatory: 5 μm, 250 x 21.2 mm) with monitoring at λ = 215 nm and 254 nm. Aqueous gel permeation chromatography (GPC) was conducted on a Malvern Viscotek GPCMax system equipped with a triple detector array (TDA 305-040 Quadruple Detector Array), with two Viscotek A600 M general mixed aq. columns (300x8.0mm). Samples were injected at 5 mg/mL and run with the water and 20% methanol (MeOH) at a flow rate of 1 mL/min. The RI detector used a dn/dc value of 0.15, and calibration was performed with near-monodisperse PEG standards from Polymer Labs. Fast protein liquid chromatography (FPLC) to purify BSA conjugates was performed on a Bio-Rad BioLogic DuoFlow chromatography system equipped with a HiTrap^{TM} Q HP (1 mL) cation exchange column from GE Healthcare with an eluent of 20 mM Tris buffer pH 8.6 from 0 M to 1 M NaCl. Immune ELISA assay results were read on a ELX800 Universal Microplate Reader (Bio-Tek Instrument Inc., Winooski) with λ = 450 and 630 nm for signal and background, respectively. μPET imaging was performed with a Siemens Inveon μPET scanner, and the corresponding μCT was performed on a CrumpCAT scanner (UCLA Crump Institute for Molecular Imaging). Analytical HPLC for insulin detection was conducted on an Agilent 1260 Infinity II LC System equipped with a UV detector and Zorbax 300 SB-C3 column with a gradient of 0 – 100% acetonitrile in water + 0.1% trifluoroacetic acid (TFA) over 17 min unless otherwise noted. ThT fluorescence

assay results were read on a Tecan Infinite M1000 Pro equipped with a Tecan Quad4 Monochromator. Size exclusion chromatography coupled with multi-angle light scattering (SEC-MALS) was performed on insulin samples with a General Electric Healthcare Äkta Pure and Wyatt Technology miniDawn TREOS in tandem with an Optilab T-rEX refractometer with extended range. The SEC-MALS was equipped with a Wyatt WTC-030S5 SN 0830 SEC column with an eluent of 0.25 M PBS pH 7.4.

2.4.3 Animal Usage

All animal experiments were conducted according to protocols approved by the UCLA Animal Research Committee (ARC).

2.4.4 Methods

Synthesis of methacrylate trehalose monomer (TrMA)

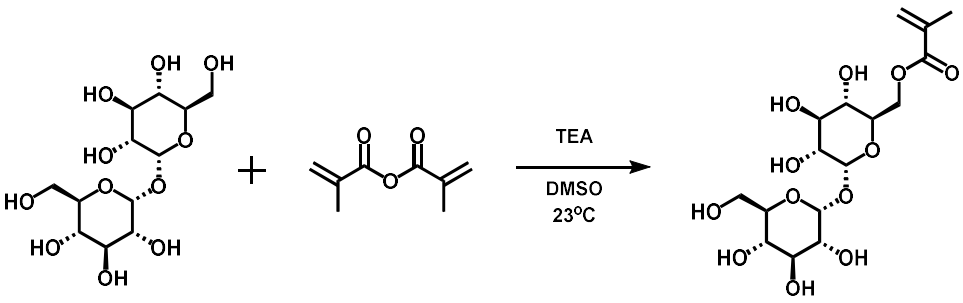

The methacrylate functionalized trehalose monomer was synthesized according to literature procedure.[9] In a flame-dried round bottom flask, trehalose (4.6 g, 13.4 mmol) was dissolved with anhydrous dimethyl sulfoxide (DMSO, 60 mL). Anhydrous trimethylamine (TEA, 5.6 mL, 40.2 mmol) and methacrylic anhydride (400 µL, 2.7 mmol) were added, and the mixture was stirred at 23 °C for 18 h. DMSO was removed by precipitating into 0 °C hexanes and dichloromethane (hex:DCM, 8:2, 1400 mL). The organic layer was decanted and remaining organics were removed from the viscous liquid by rotary evaporation. The crude product was diluted with water before filtering and purifying by preparatory HPLC with a gradient of MeOH

in water (10-50%). To the product containing fractions, mequinol was added to prevent autopolymerization. Solvent was removed by rotary evaporation using a 2-neck flask equipped with a septa and long needle directly into the solution to further prevent autopolymerization by providing a source of oxygen. The product was finally recovered by lyophilization (460.6 mg, 42% yield). ^{1}H NMR (400 MHz in D_2O) δ: 6.03 (s, 1H), 5.62, (s, 1H), 5.07 (d, J = 3.9 Hz, 1H), 5.03 (d, J = 3.9 Hz, 1H), 4.38 (dd, J = 12.2, 2.2 Hz, 1H), 4.24 (dd, J = 12.2, 5.2 Hz, 1H), 3.96 (qd, J = 10.2, 1.8 Hz, 1H), 3.71 (m, 4H), 3.63 (m, 1H), 3.52 (ddd, J = 19.6, 10.2, 3.9 Hz, 1H), 3.42 (dd, J = 10.2, 9.3 Hz, 1H), 3.32 (t, J = 9.3 Hz, 1H), 1.82 (s, 3H). ^{1}H-NMR spectrum agreed with that previously reported.

Synthesis of 2-hydroxyethyl 2-bromoisobutyrate (HEBIB)

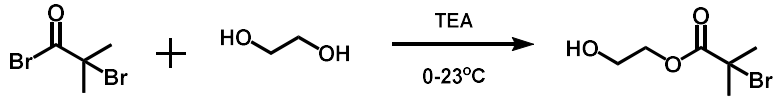

HEBIB was synthesized according to literature procedure.[31] Ethylene glycol (1.33 mL, 23.8 mmol, anhydrous) and anhydrous TEA (0.66 mL, 4.74 mmol) were stirred together and cooled to 0 °C before dropwise adding α-bromoisobutyryl bromide (0.5 mL, 4.8 mmol). The reaction mixture was stirred for 2 h at 0 °C before warming up to 23 °C to stir an additional 12 h. Water (10 mL) was added to the flask and extracted with chloroform three times (10 mL each time). The chloroform layer was washed with dilute hydrochloric acid, saturated sodium bicarbonate ($NaHCO_3$), and water (10 mL each wash). The organic layer was dried over anhydrous magnesium sulfate ($MgSO_4$), filtered, and the product was recovered after rotary evaporation. The product was purified by silica gel flash chromatography with an eluent system of diethyl ether and hexanes (1:1). The product containing fractions were collected and recovered product as a yellow-clear oil by rotary evaporation (658 mg, 65% yield). ^{1}H NMR (400 MHz in $CDCl_3$) δ: 4.32 (t, J = 4.6 Hz,

2H), 3.87 (t, J = 4.6 Hz, 2H), 1.95 (s, 6H), 1.86 (s, 1H). ^{1}H-NMR spectrum agreed with that reported for this compound.

Synthesis of 4-formylphenyl-2-bromoisobutyrylate initiator

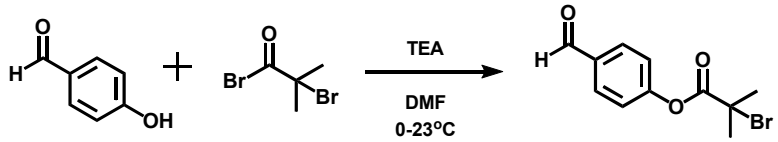

4-Formylphenyl-2-bromoisobutyrylate (benzaldehyde initiator) was synthesized according to literature procedure.[32] 4-Hydroxybenzaldehyde (174 mg, 1.4 mmol) was dissolved in anhydrous dimethylformamide (4 mL) under argon. Anhydrous TEA (0.2 mL, 1.4 mmol) was added and stirred at 0 °C for 10 min before dropwise adding α-bromoisobutyryl bromide (0.1 mL, 1.4 mmol). The reaction mixture was stirred for 30 min at 0 °C before warming up to 23 °C to stir an additional 14 h. The white precipitate that formed was filtered off and the remaining filtrate was concentrated by rotary evaporation. Dissolved crude material in DCM and washed twice with saturated $NaHCO_3$. The organic layer was dried over anhydrous $MgSO_4$, filtered, and the product was recovered after rotary evaporation. The product was purified by silica gel flash chromatography with an eluent system of diethyl ether and ethyl acetate (1:4). The product containing fractions were collected and recovered by rotary evaporation (86 mg, 33% yield). ^{1}H NMR (400 MHz in $CDCl_3$) δ: 10.03 (s, 1H), 7.96 (t, J = 4.6 Hz, 2H), 7.35 (t, J = 4.6 Hz, 2H), 2.08 (s, 6H). ^{1}H-NMR spectrum agreed with that reported for this compound.

AGET ATRP of TrMA with HEBIB initiator for use as an excipient

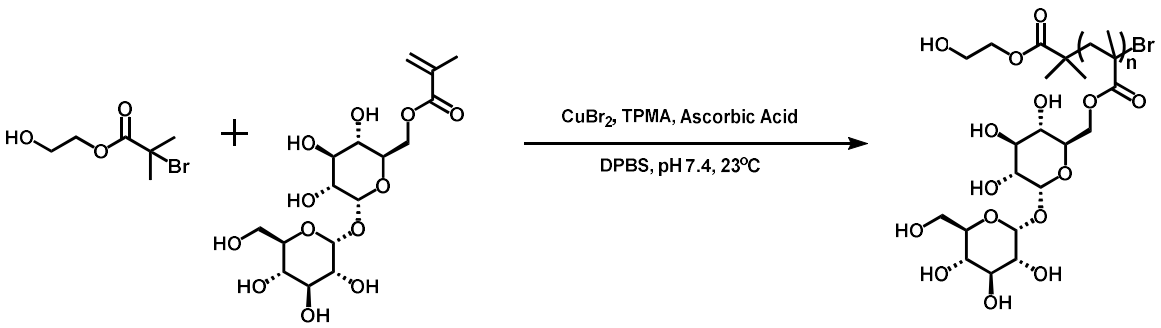

Polymerization was performed according to literature procedure.[15] 0.1 M Dulbecco's phosphate-buffered saline (DPBS) pH 7.4 was degassed by sparging with argon for at least 1 h. Ascorbic acid (AA) was dissolved in DPBS (10 mg/mL) and degassed for > 30 min. TrMA (50 mg, 120 μmol) was added directly to a Schlenk flask equipped with a stir bar, and the flask was evacuated and refilled with argon four times. Stock solutions of copper(II) bromide ($CuBr_2$) and tris(2-pyridylmethyl)amine (TPMA) were prepared using degassed DPBS at 5 mg/mL and 6.75 mg/mL, respectively. HEBIB initiator (0.23 mg, 1.1 μmol) was dissolved with requisite amount of each of the $CuBr_2$ and TPMA solutions (0.24 mg, 1.1 μmol and 0.31 mg, 1.1 μmol), and then transferred to the flask under argon. AA solution (0.1 mg, 0.6 μmol) was added to the flask under argon to initiate the polymerization, with a final TrMA concentration of 0.45 M. The polymerization proceeded under argon at 25 °C for 7.5 h. The polymerization was ended by exposing to air, and the polymer was dialyzed against water (3.5 kDa MWCO) with Curpisorb, a metal-chelating resin, to chelate copper for 2 days (8 L water). Polymer was recovered as fluffy white solid by lyophilization (27.1 mg, 65% yield). ^{1}H NMR (400 MHz in D_2O) δ: 5.10, 5.07, 4.24, 4.02, 3.94, 3.75, 3.53, 3.35, 1.83, 1.51, 0.96, 0.80. Number average molecular weight (M_n) = 10.1 kDa (by GPC with PEG standards), molecular weight dispersity ($Đ$) = 1.25. ^{1}H-NMR spectrum agreed with that previously reported.

AGET ATRP of TrMA with benzaldehyde initiator for conjugation to BSA

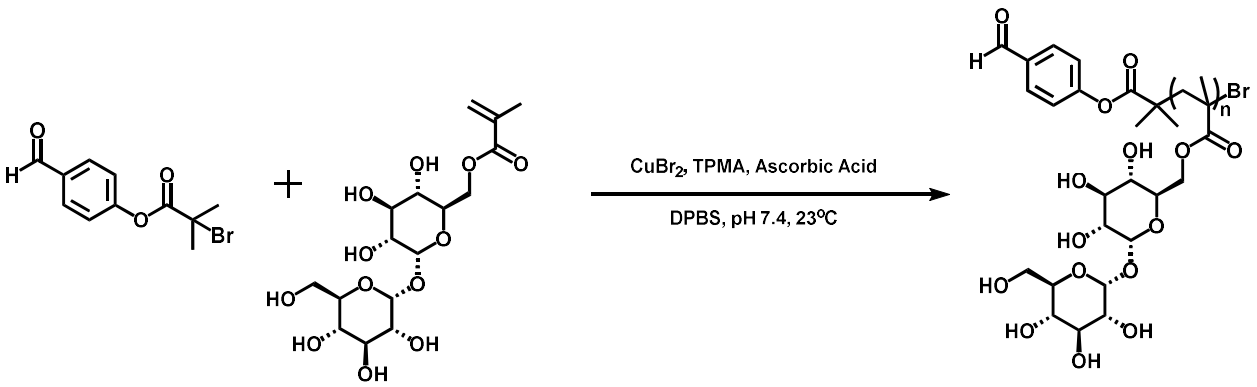

Polymerization was performed according to literature procedure.[15] Water and MeOH (1:1) was degassed by sparging with argon for 40 min. TrMA (150 mg, 0.37 mmol) was added directly to a Schlenk flask equipped with a stir bar and the flask was evacuated and refilled with argon four times. $CuBr_2$ and TPMA were dissolved with degassed water and MeOH as 34.0 mg/mL and 44.2 mg/mL, respectively. Benzaldehyde initiator (4.1 mg, 15 μmol) was dissolved with $CuBr_2$/TPMA solution (3.4 mg, 15 μmol and 4.42 mg, 15 μmol), and then transferred to the flask under argon. AA was dissolved with degassed water and MeOH solution (3 mg/mL), and an aliquot of this solution (1.6 mg, 9 μmol) to flask under argon to initiate the polymerization, with a final concentration of 0.45 M TrMA. The polymerization proceeded under argon at 25 °C for 15 h. Polymerization was ended by exposing to air, and polymer was dialyzed against water and MeOH (1:1, 3.5 kDa MWCO) for 2 days (8 L water, 1 day with Curpisorb). Polymer was recovered via lyophilization (138.1 mg, 92% yield). ^{1}H NMR (400 MHz in D_2O) δ: 9.86, 7.96, 7.26, 5.10, 5.06, 4.24, 4.01, 3.92, 3.75, 3.53, 3.35, 1.82, 1.53, 0.98, 0.80. M_n = 24.9 kDa (by GPC with PEG standards), molecular weight dispersity (~~$Đ$~~) = 1.05. ^{1}H-NMR spectrum agreed with that previously reported.

FRP copolymerization of TrMA and pyridyl disulfide ether methacrylate for studying biodistribution and excretion

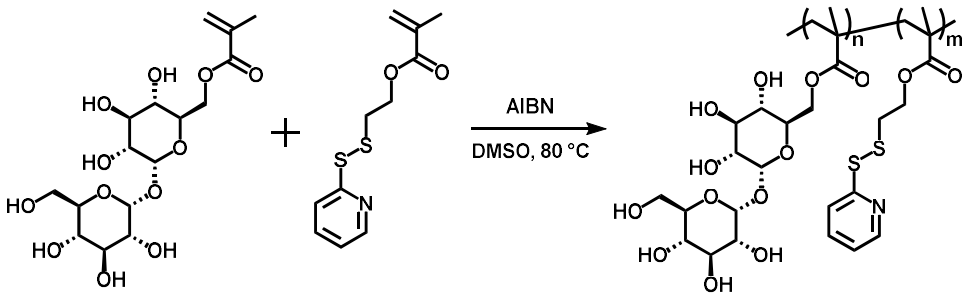

Polymerization was performed according to literature procedure.[20] TrMA (75 mg, 0.18 mmol) and pyridyl disulfide ether methacrylate monomer (PDSMA, 1.9 mg, 7.5 μmol) were dissolved with a solution of AIBN in dry DMSO (10 mg/mL AIBN, 0.25 M TrMA). The solution was freeze-pump-thawed five times, and polymerized at 80 °C for 20 h. Polymer was dialyzed in 3.5 kDa MWCO dialysis tubing against water containing Cuprisorb for 2 days (8 L). Lyophilization yielded a random pTrMA-*co*-PDMSA copolymer with 0.85 PDSMA units per polymer chain as determined by combined ^{1}H NMR and GPC analysis (81.3 mg, 100% yield). ^{1}H NMR (500 MHz in D_2O) δ: 8.37, 7.82, 7.27, 5.10, 5.06, 4.24, 3.95, 3.76, 3.53, 3.36, 1.85, 1.55, 0.97, 0.81. ^{13}C NMR (126 MHz in D_2O) δ: 93.4, 72.7, 72.1, 71.1, 69.7, 64.4, 60.7, 44.9, 38.7. M_n = 8.9 kDa (by GPC with PEG standards), molecular weight dispersity ($Đ$) = 2.19.

Synthesis of pTrMA-co-DOTA via post polymerization modification

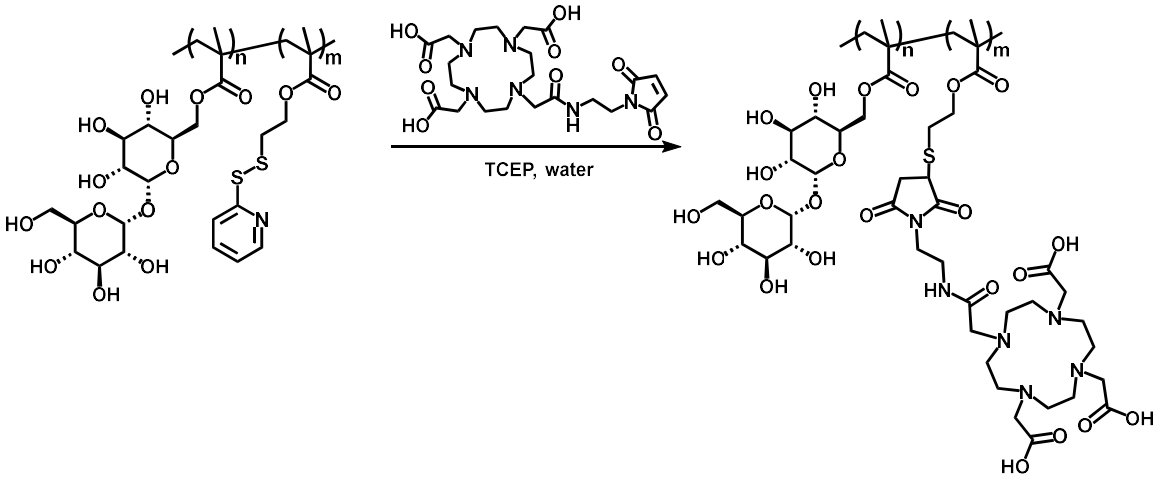

Using metal free water, a stock solution of (tris(2-carboxyethyl)phosphine) (TCEP, 12 mg/mL) was prepared. The polymer pTrMA-*co*-PDMSA (8.9 kDa, $\not{D}$ = 2.19 by GPC, 20.3 mg, 2.3 μmol of polymer, 2.3 μmol of PDMSA) was dissolved with TCEP stock (3.3 mg, 11.4 μmol) and mixed at 25 °C and 350 rpm for 30 min. Small molecules were removed by Centriprep centrifugal filtration (3 kDa MWCO) three times with additional TCEP stock before diluting the polymer with TCEP solution. Maleimide-DOTA (10.0 mg, 18.9 μmol) was dissolved in metal-free MilliQ and added to the reaction for a polymer concentration of 8.4 mM. The reaction was mixed in a ThermoShaker at 25 °C and 350 rpm for 36 h before dialyzing reaction in 3.5 kDa MWCO dialysis tubing against water containing Cuprisorb (16 L, 30 h). Polymer was recovered via lyophilization (18.4 mg, 86% yield). ^{1}H NMR (500 MHz in D_2O) δ: 5.11, 5.07, 4.24, 3.94, 3.75, 3.53, 3.35, 3.04, 2.91, 2.58, 2.48, 1.84, 0.96, 0.80. ^{13}C NMR (126 MHz in D_2O) δ: 178.7, 177.8, 92.4, 71.8, 70.4, 68.9, 63.3, 59.9, 53.1, 51.6, 48.2, 44.0, 17.1, 15.5. M_n = 10.3 kDa (by GPC with PEG standards), molecular weight dispersity ($\not{D}$) = 2.68.

Preparation of BSA conjugate for IgG and IgM ELISA Assay

Bovine serum albumin (BSA, 25 mg, 0.38 μmol) and benzaldehyde pTrMA (24.9 kDa, 55.2 mg, 2.2 μmol) were dissolved with 25 mM borate buffer, pH 8.5. This solution was incubated for 10 min at 23 °C on a rocker. Sodium cyanoborohydride (41.1 mg, 654.3 μmol) was added to the reaction and this was mixed for 4 h at 37 °C with 300 rpm agitation. Small molecules were removed from the crude product by Centriprep centrifugal filtration (30 kDa MWCO) with 25 mM PBS buffer pH 7.4 four times. The conjugate was purified by cation exchange FPLC and product-containing fractions were pooled and buffer exchanged to PBS pH 7.4 using Centriprep centrifugal filtration (MWCO 30 kDa). Some unconjugated BSA was still present along with a majority conjugate product, and the relative amount of unconjugated BSA was measured to be 4.9% using

ImageJ (Figure S1). It was determined that the BSA conjugate could be used as-is, given the majority was BSA conjugate and the subsequent step by ELISA is blocking the wells with unmodified BSA.

Determination of BSA conjugate concentration by BCA assay

BSA-pTrMA conjugate concentration was determined using Pierce BCA assay kit according to manufacturer specifications. Briefly, conjugate was diluted (10 × and 100 ×) and 10 µL of sample and BSA standards (20 – 2,000 µg/mL) were pipetted into a 96-well plate. Working reagent (200 µL, 50-parts A + 1-part B) was added to each well. The plate was incubated at 37 °C for 30 min then cooled to room temperature before measuring absorbance at 562 nm. Diluted BSA-pTrMA conjugate concentration was calculated from the standard curve (R^2 = 0.9954) to be 18.4 mg/mL (final product: 10.0 mg, 40% yield).

Antibody immunogenicity study of OVA and pTrMA in vivo

CD-1 mice (8 weeks, female, n = 5 – 6, Charles River Laboratories) were used to study the immunogenicity of pTrMA (10.1 kDa, $\cancel{Đ}$ = 1.25) alone or with ovalbumin (OVA), a known immunogenic protein. OVA antigen with or without pTrMA was administered via i.p. injection (2 mg/kg OVA, 10 wt% pTrMA in sterile saline buffer); pTrMA (10 wt% pTrMA in sterile saline buffer, 100 mg/mL) was also administered alone via i.p. injection. Mice were challenged again 2 weeks after inoculation with the same dosage for each condition. Blood was collected into serum separator centrifuge tubes (SSTs) via retro-orbital bleeding at 1, 2, and 3 weeks after administration. Blood was centrifuged at 2,000 rcf for 15 min to extract serum. Serum was stored at −80 ºC at least overnight until ELISA could be run. Mice were sacrificed after 4 weeks and a final time point was collected via cardiac puncture. Blood was treated the same as prior time points.

For the ELISA, sterile filtered 0.1 M PBS buffer + 0.3% Tween-20 was used to wash the wells four times between each step, making sure to remove solution by hitting the plates against paper towels after each wash. Antigen solutions of OVA or the BSA-pTrMA conjugate (total 0.02 mg/mL, conjugate only 0.019 mg/mL, 100 µL/well) were plated on 96-well plates. After incubating at 4 °C for 16 h, antigen was removed, the wells washed and blocked with sterile filtered 3% BSA in 0.1 M PBS (300 µL) for 2 h at 37 °C. After washing out the BSA blocking solution, serum from the inoculated mice diluted 100, 500, 2,500, and 12,500-fold with filtered 1% BSA in 0.1 M PBS (100 µL/well) was then incubated with the respective antigen for 2 h at 37 °C (OVA antigen with OVA exposed mice, separately OVA antigen and BSA-pTrMA conjugate with OVA/pTrMA exposed mice, and BSA-pTrMA conjugate with pTrMA exposed mice). After washing the wells, goat anti-rabbit IgG or IgM HRP-conjugate antibody diluted 2,000 × with filtered 1% BSA in 0.1 M PBS (100 µL/well) was incubated for 1 h at 25 °C. The secondary detection antibody HRP conjugate was removed and the wells washed. In the dark, TMB substrate solution was added (100 µL/well), and the plate was incubated at 23 °C. After 5 – 10 min when color had developed in positive control wells, reaction was quenched by adding 2 M H_2SO_4 (50 µL/well) stop solution. Absorbance was measured at 450 nm and background at 570 nm on Tecan plate reader. Controls included the OVA antigen with OVA exposed mouse serum (positive control), OVA antigen with naïve mouse serum (negative control), BSA-pTrMA antigen with naïve mouse serum (negative control), and BSA antigen with naive mouse serum (negative control and check on non-specific BSA binding).

Cytokine immunogenicity of pTrMA

CD-1 mice (6 weeks, female, n = 5, Charles River Laboratories) were used to study the immunogenicity of pTrMA (33.8 kDa, $Đ$ = 1.01, 10 mg/kg in DPBS) relative to the negative

control DPBS administered via i.p. injection. Blood was collected into SSTs via retro-orbital bleeding 1 h and 6 h after administration. Blood was centrifuged at 2,000 rcf for 10 min at 4 °C to extract serum. Mice were sacrificed after 24 h, and a final time point was collected via cardiac puncture. Blood was treated the same as prior time points. IL-1b, IL-2, IL-4, IL-6, KC (IL-8 murine analog), IL-10, IL-12, IFN-γ, and TNF-α were measured using the multiplexed ELISA-type assay (Luminex xMAP®) at the UCLA Immune Assessment Core (Dept. Pathology and Laboratory Medicine directed by Dr. Maura Rossetti).

Radiolabeling of pTrMA-co-DOTA

Dissolved pTrMA-*co*-DOTA (8.9 kDa) in 0.4 M ammonium acetate buffer pH 3.5 (1 mg/mL). Pipetted ^{64}Cu (6 mCi) into a screw-cap polypropylene tube before adding pTrMA-*co*-DOTA solution (300 µL). Solution was mixed gently and set on heat at 50 °C for 30 min. Solution was diluted with PBS (3 mL) for a specific activity of 20 µCi/µg with a purity of > 99%.

µ-Positron Emission Tomography (µPET)/µ-computed tomography (µCT) extended study of ^{64}Cu labeled pTrMA-co-DOTA biodistribution and excretion

C57BL/6 mice (10 weeks, n = 4 female and n = 4 male, from UCLA Radiation Oncology Colony) were anesthetized with 1.5% vaporized isoflurane, and injected with the ^{64}Cu-labeled pTrMA-*co*-DOTA (200 µCi) via i.v. injection (tail vein), immediately followed by a 1 h dynamic µPET scan and a µCT scan. After the 1 h dynamic imaging, mice were then imaged by µPET/µCT at 4 h (static µPET, 10 min), 24 h (static µPET, 15 min), 48 h (static µPET, 20 min), 72 h (static µPET, 30 min), and 120 h (static µPET, 60 min) post-injection. All µPET images were acquired with an energy window of 350 – 650 keV, followed by three-dimensional (3D) histographic analysis and reconstruction using the 3D-ordered subset expectation maximization (OSEM)/maximum a posteriori (MAP) method. Data was decay corrected and scaled by initial

imaging. Co-registered μPET/μCT images were analyzed and maximum-intensity projections (MIPs) were generated using AMIDE software.

μPET/μCT stability study of ^{64}Cu labeled pTrMA-co-DOTA for biodistribution and excretion

^{64}Cu radiolabeled pTrMA-*co*-DOTA was incubated in plasma collected from a female C57BL/6 mouse, at 37 °C for 24 h. Three groups of C57BL/6 mice (8 – 12 weeks, female, n = 4, from UCLA Radiation Oncology Colony) were anesthetized with 1.5% vaporized isoflurane, and injected via i.v. injection (tail vein) with ^{64}Cu-labeled pTrMA-*co*-DOTA (200 μCi), ^{64}Cu-$CuCl_2$ (100 μCi), or the plasma-incubated ^{64}Cu-labeled pTrMA-*co*-DOTA (100 μCi). Each group was scanned immediately after injection for 1 h with a dynamic μPET followed by a μCT scan. Mice were imaged by μPET/μCT again at 4 h (static μPET, 10 min) and 24 h (static μPET, 20 min). All μPET images were acquired with an energy window of 350 – 650 keV, followed by 3D histographic analysis and reconstruction using the 3D-OSEM/MAP method. Data was decay corrected and scaled by initial imaging. Co-registered μPET/μCT images were analyzed and MIPs were generated using AMIDE software.

μPET/μCT study of pTrMA-co-DOTA for tissue-specific local inflammation induction monitored by ^{18}F-fludeoxyglucose (FDG)

C57BL/6 mice (8 – 12 weeks, n = 4 female and n = 4 male, from UCLA Radiation Oncology Colony) were fasted overnight before being anesthetized with 1.5% vaporized isoflurane, and injected ^{18}F-FDG (150 μCi) via i.v. injection (tail vein). After 1 h of anesthetized uptake, took static μPET/μCT baseline scans (10 min). Mice were then injected with either pTrMA-*co*-DOTA or LPS (1 mg/kg) via i.v. and i.p. injection, respectively, before being fasted overnight again. 24 h after injection with polymer or LPS, again anesthetized mice with 1.5%

vaporized isoflurane and injected ^{18}F-FDG (150 μCi) via i.v. injection (tail vein). After 1 h of anesthetized uptake, took static μPET/μCT (10 min). All μPET images were acquired with an energy window of 350 – 650 keV, followed by 3D histographic analysis and reconstruction using the 3D-OSEM/MAP method. Data was decay corrected and scaled by initial imaging. Co-registered μPET/μCT images were analyzed and MIPs were generated using AMIDE software.

Pharmacokinetics study of insulin with or without pTrMA excipient

CD1 mice (5 – 6 weeks, male, n = 4, Charles River Laboratories) were used for the pharmacokinetics studies. A single dose of insulin (120 μg/kg) with or without pTrMA (19.1 kDa, 2 mol. eq. to insulin) was administered by i.v. injection (tail vein). Blood samples were taken from the saphenous vein (30 – 50 μL) at 10, 20, and 40 min and by cardiac puncture after euthanasia by inhalation of CO_2 at 60 min following administration. Blood was collected using a micropipette with ethylenediaminetetraacetic acid (ETDA)-coated tips into LoBind tubes coated with EDTA. Blood was stored on ice until separation of the plasma by centrifugation (2000 × g, 15 min). The amount of insulin in plasma samples was determined by insulin ELISA according to the manufacturer's protocol.

Insulin stability studies with pTrMA excipient

Insulin was dissolved at 2 mg/mL in DPBS pH 7.4. pTrMA (28.1 kDa) was dissolved at 19 mg/mL (2 mol. eq. to insulin). Solutions were added 1:1 to a total volume of 100 μL in a LoBind tube for insulin and insulin + pTrMA (n = 3). Samples were stored at 4 °C or heated to 90 °C for 30 min. Aliquots of each insulin sample were used directly for SDS and native PAGE as well as ThT assay. Samples were filtered (0.22 μm) to remove insulin aggregates and analyzed by RP-HPLC. Thioflavin T (ThT) was prepared at 50 μM (0.0159 mg/mL) in 20 mM DPBS pH 7.4. Into a black 96-well plate, 50 μL of each sample was pipetted. To these was added 250 μL ThT solution

and the plate was incubated at room temperature (21 °C) for 20 min. Fluorescence intensity was measured on a Tecan M1000 plate reader (λ_{ex} = 450 nm, λ_{em} = 482 nm).

SEC-MALS investigation of insulin was performed using pTrMA (26.0 kDa). Insulin was dissolved at 30 mg/mL with minimal metal-free 0.1 M hydrochloric acid followed by 0.1 M PBS pH 7.4. The insulin solution was used to dissolve pTrMA at 30 mg/mL, and samples were either analyzed directly or samples were heated to 90 °C for 30 min and then analyzed by SEC-MALS with an injection volume of 100 µL.

Long term insulin stability studies with pTrMA excipient

Insulin was dissolved at 2 mg/mL in DPBS pH 7.4. pTrMA (10.1 kDa) was dissolved at 2.4 mg/mL (2 molar equivalents to insulin). Added solutions 1:1 for a total volume of 1.4 mL in a LoBind tube for insulin and insulin + pTrMA (n = 3). Samples were stored at 4 °C for 14 weeks followed by regular sampling. Samples were filtered (0.22 µm) to remove insulin aggregates and analyzed by RP-HPLC.

2.4.5 Statistical analysis

All experimental values are reported as the mean ± SEM, and Graph Pad Prism 7 (GraphPad Software, San Diego, USA) was used for the statistical analyses. To assess the statistical significance of differences with the means of two groups, the unpaired, two-tailed Student's t-test was conducted assuming unequal sample variance. For experiments with greater than two groups, one-way analysis of variance (ANOVA) followed by Tukey's test was employed to compare the means and determine the significance of the differences. Results were considered significantly different if $p < 0.05$ (*); results are also reported with $p < 0.01$ (**) and $p < 0.001$ (***).

2.5 Appendix A

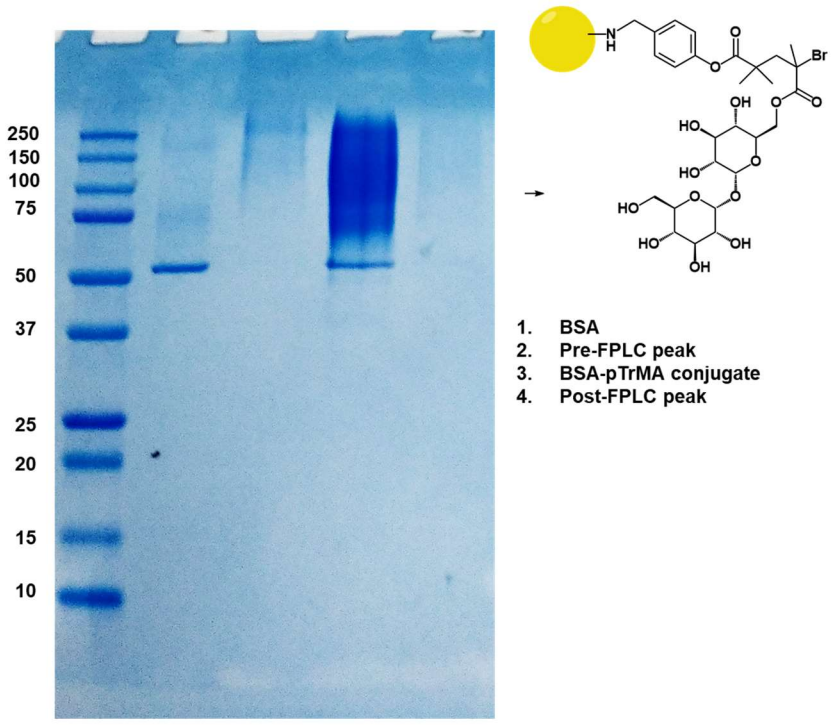

Figure A1 SDS-PAGE gel of BSA-pTrMA conjugate after purifying by FPLC and combining the pre-, post-, and conjugate peak containing fractions.

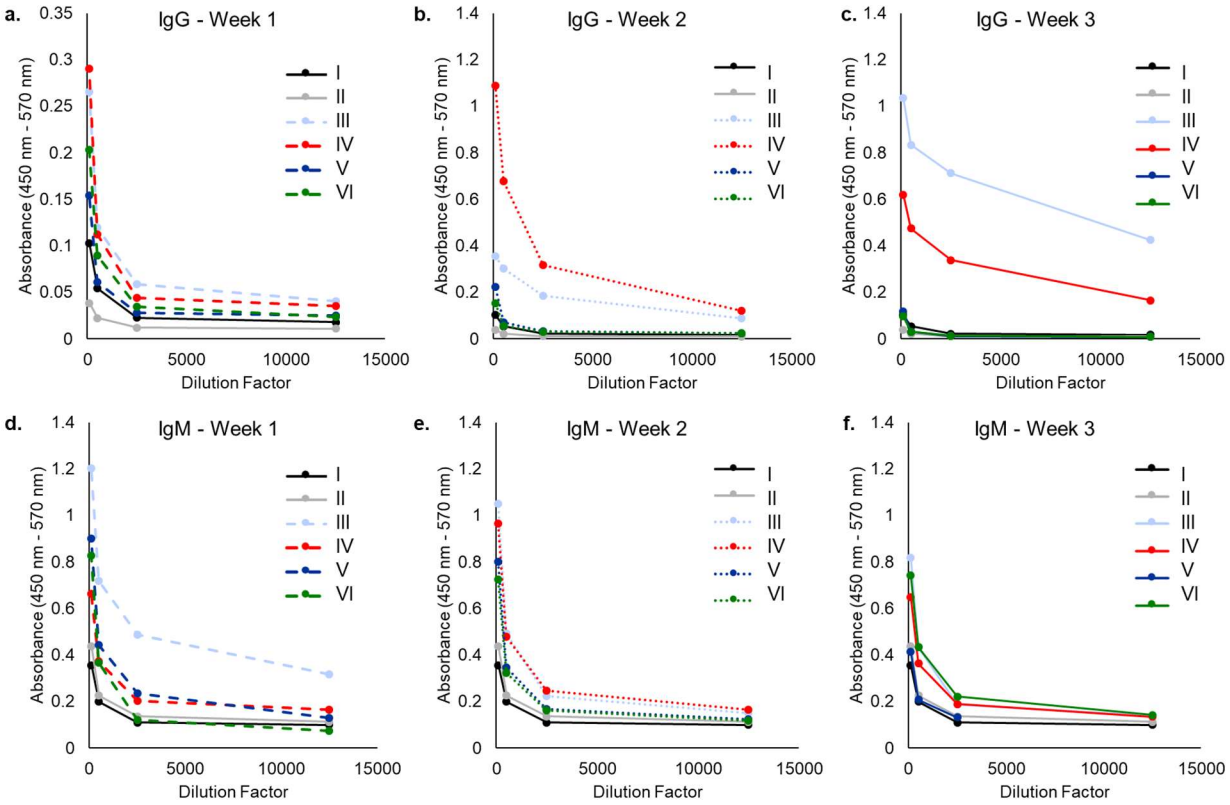

Figure A2 Immunogenicity ELISA serum dilutions of a. IgG week 1, b. IgG week 2, c. IgG week 3, d. IgM week 1, e. IgM week 2, and f. IgM week for I. Naïve OVA [naïve mouse serum with OVA antigen], II. Naïve pTrMA [naïve mouse serum with BSA-pTrMA antigen], III. OVA OVA [mouse serum from mice injected with OVA with OVA antigen], IV. OVA+pTrMA OVA [mouse serum from mice injected with OVA+pTrMA with OVA antigen], V. OVA+pTrMA pTrMA [mouse serum from mice injected with OVA+pTrMA with BSA-pTrMA antigen], VI. pTrMA pTrMA [mouse serum from mice injected with pTrMA with pTrMA antigen].

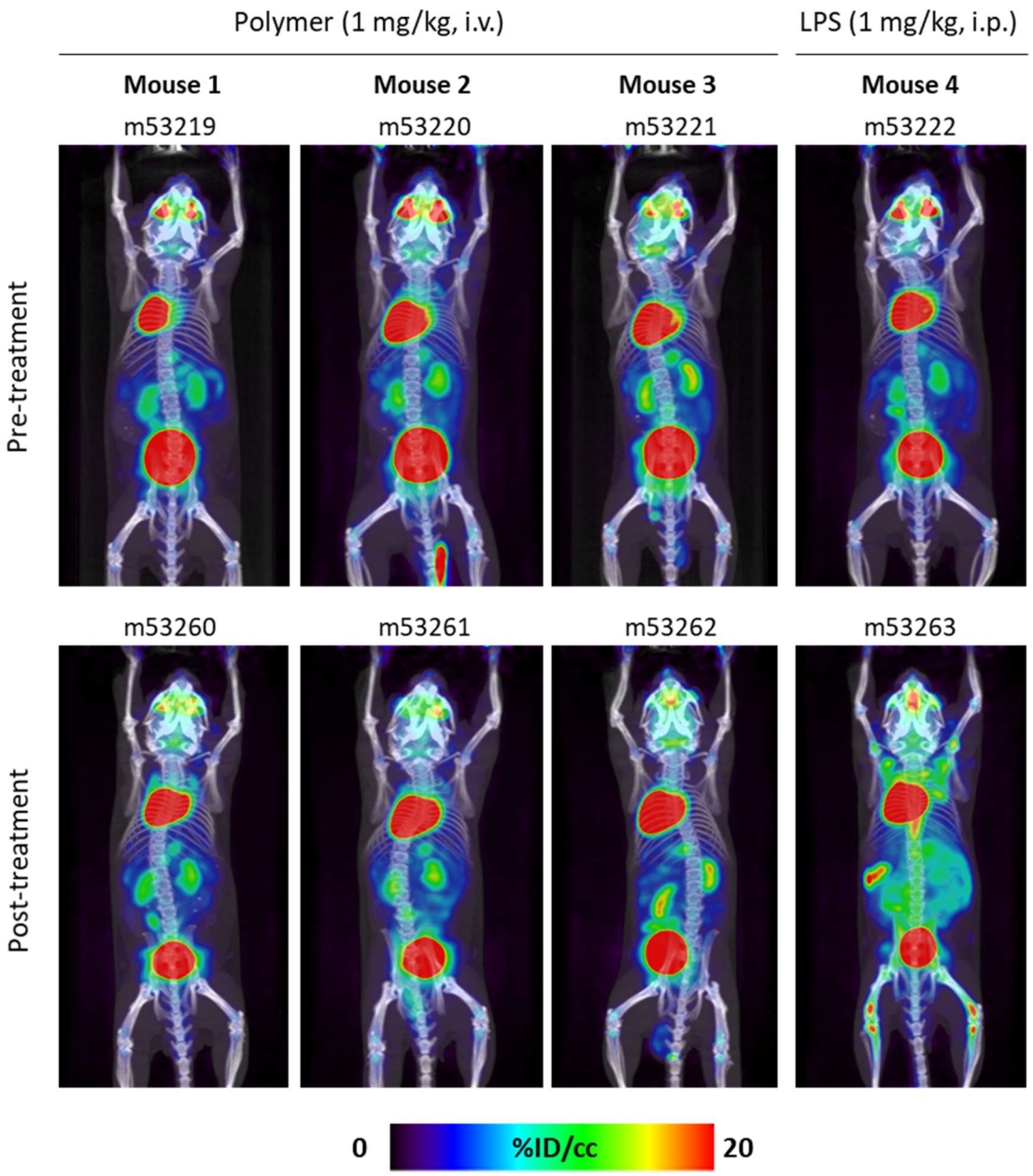

Figure A3 Co-registered μPET and μCT scans of ^{18}F-fludeoxyglucose (FDG) injection to male mice pre- and 24 h post- i.v. injection with pTrMA-*co*-DOTA (1 mg/kg).

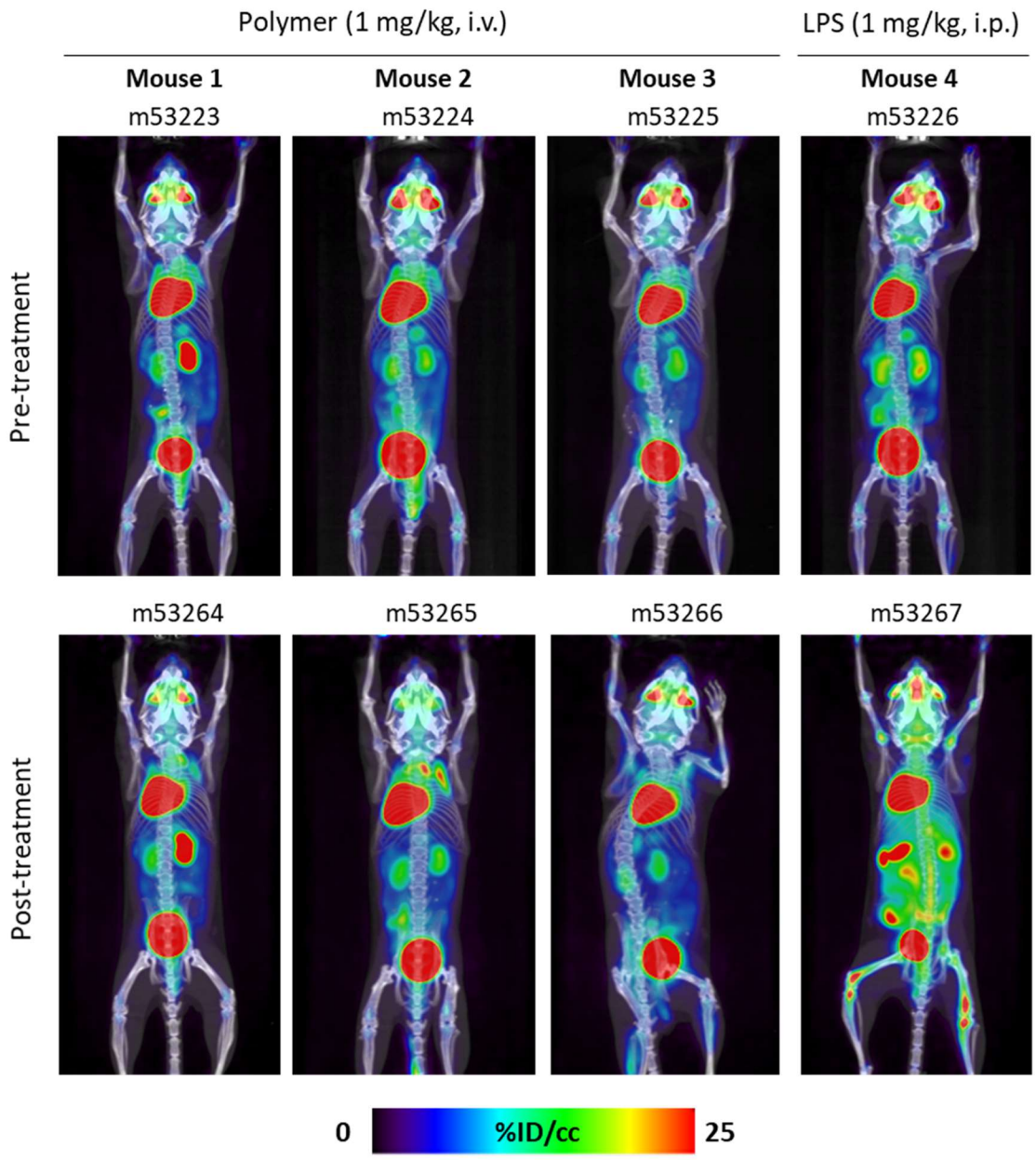

Figure A4 Co-registered μPET and μCT scans of ^{18}F-fludeoxyglucose (FDG) injection to female mice pre- and 24 h post- i.v. injection with pTrMA-*co*-DOTA (1 mg/kg).

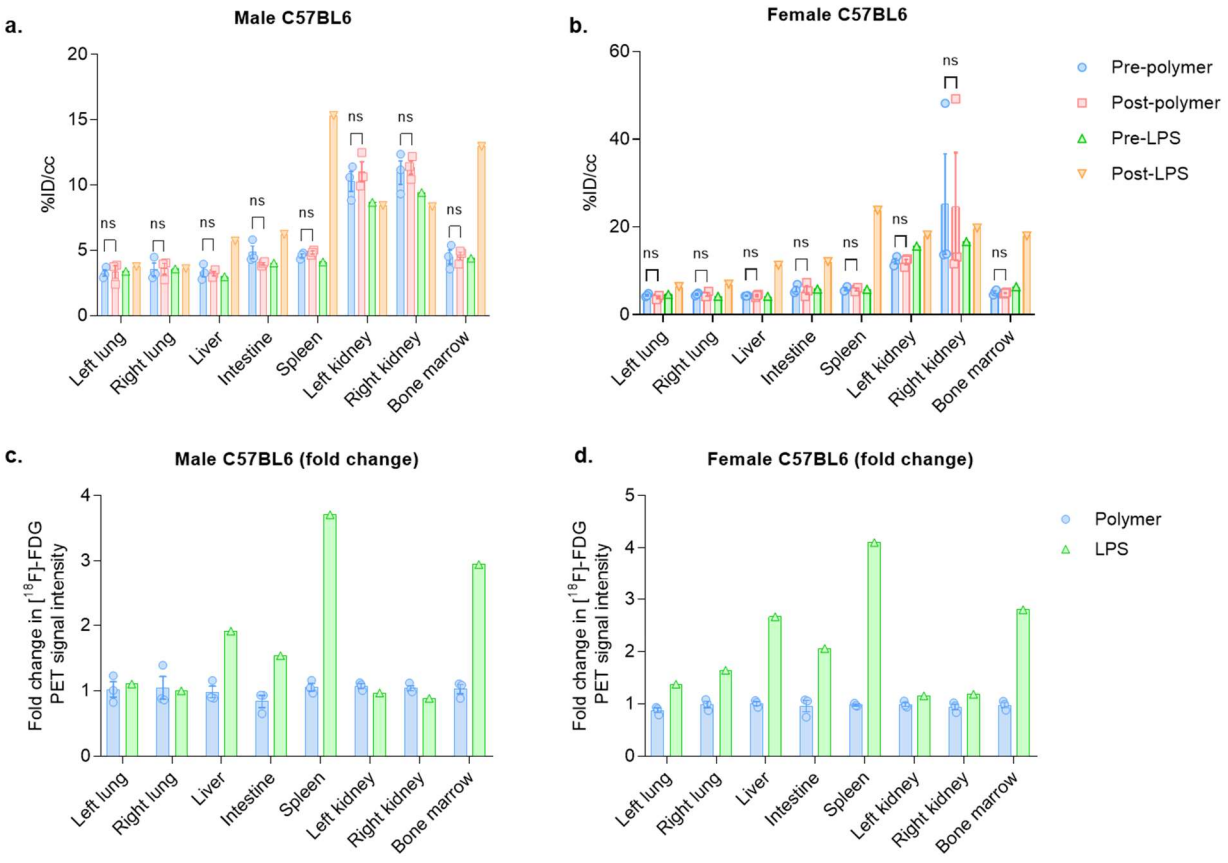

Figure A5 Quantification of µPET scans of ^{18}F-FDG (150 µCi, i.v.) injection to mice pre- and 24 h post- injection of pTrMA-*co*-DOTA or LPS (1 mg/kg, i.v. and i.p., respectively) from the organs with appreciable signal (left lung, right lung, liver, intestine, spleen, left kidney, right kidney, and bone marrow. Fold change from before to after injection with polymer or LPS was calculated and plotted for the c. male and d. female mice.

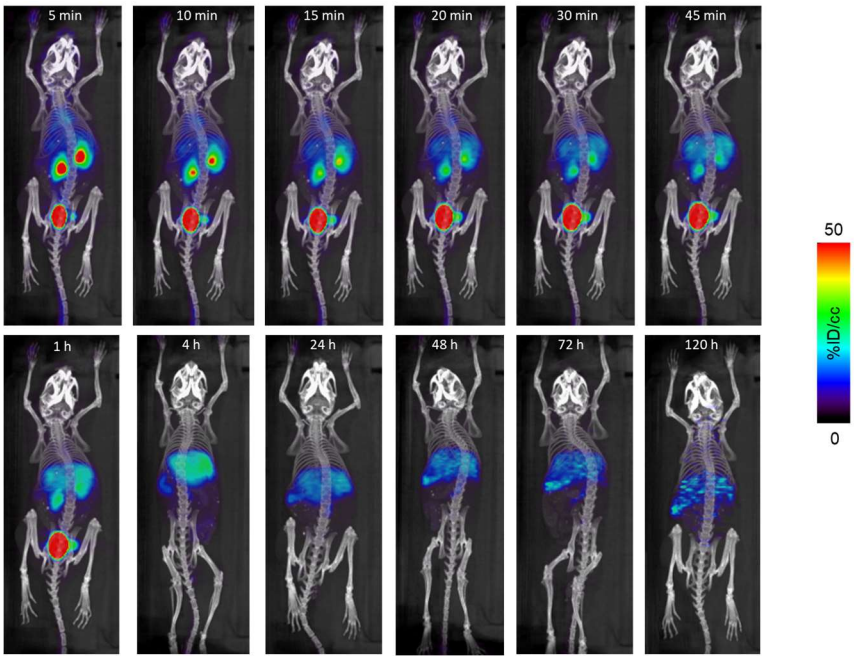

Figure A6 Co-registered μPET and μCT scans post ^{64}Cu-labeled pTrMA-*co*-DOTA injection to female mouse 1.

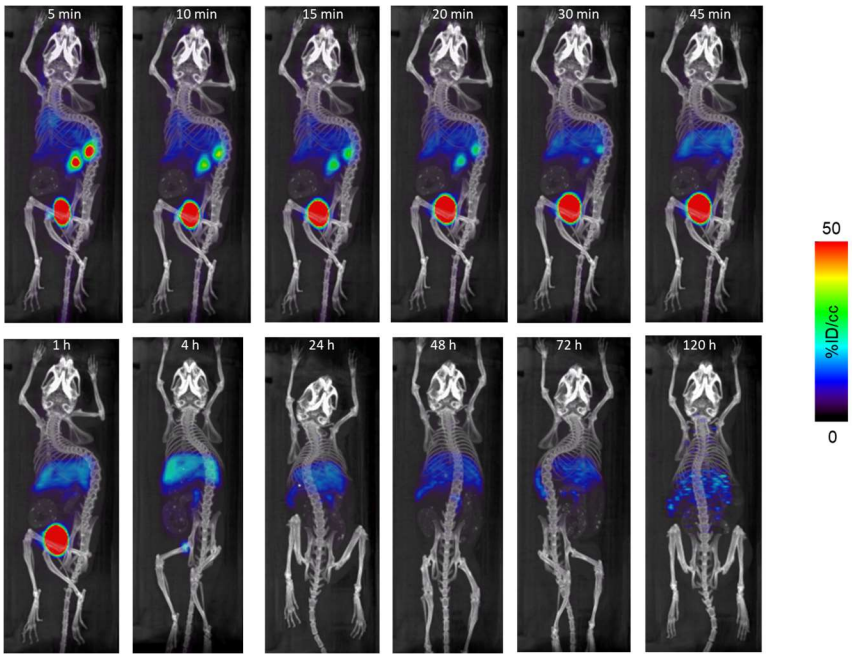

Figure A7 Co-registered μPET and μCT scans post ^{64}Cu-labeled pTrMA-*co*-DOTA injection to female mouse 2.

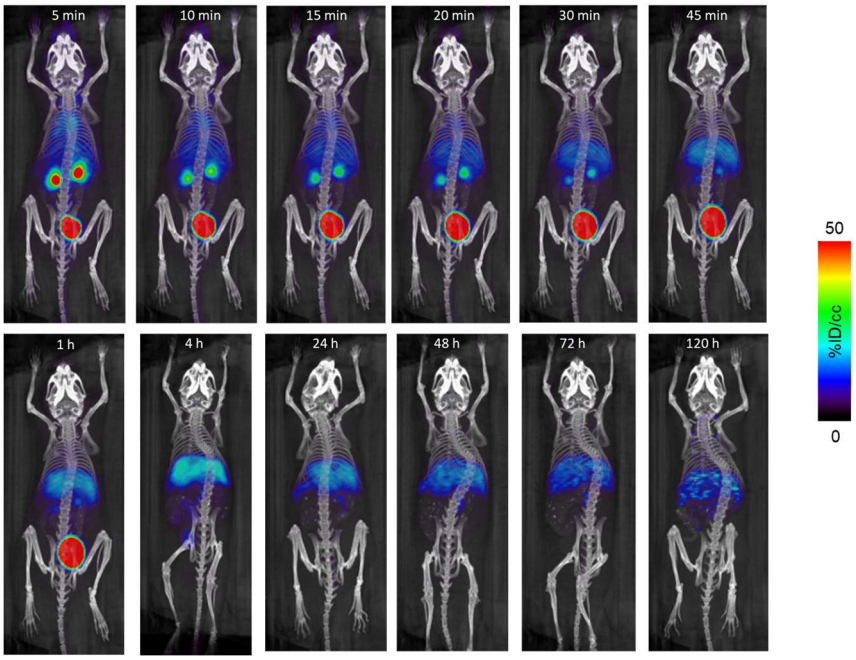

Figure A8 Co-registered μPET and μCT scans post ^{64}Cu-labeled pTrMA-*co*-DOTA injection to female mouse 3.

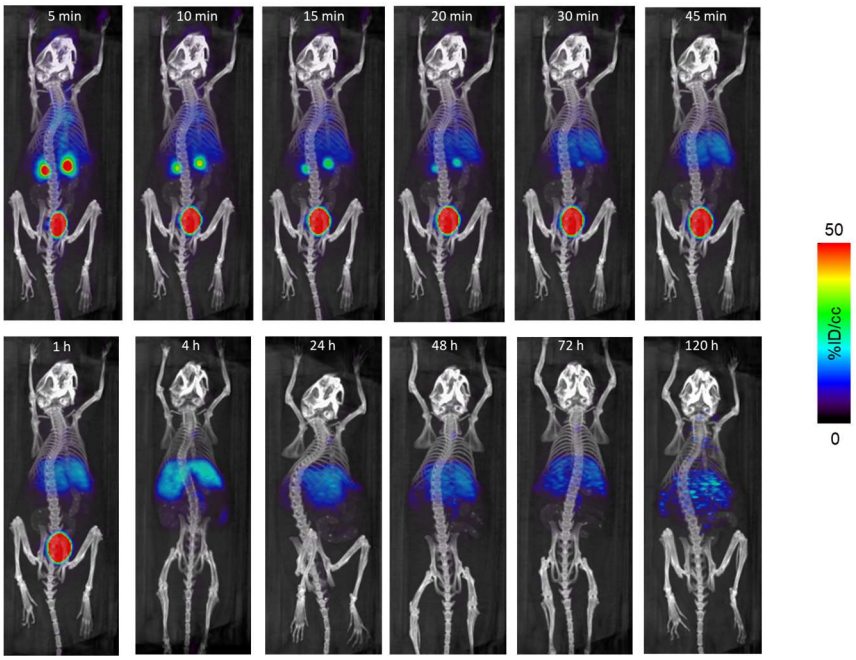

Figure A9 Co-registered μPET and μCT scans post ^{64}Cu-labeled pTrMA-*co*-DOTA injection to female mouse 4.

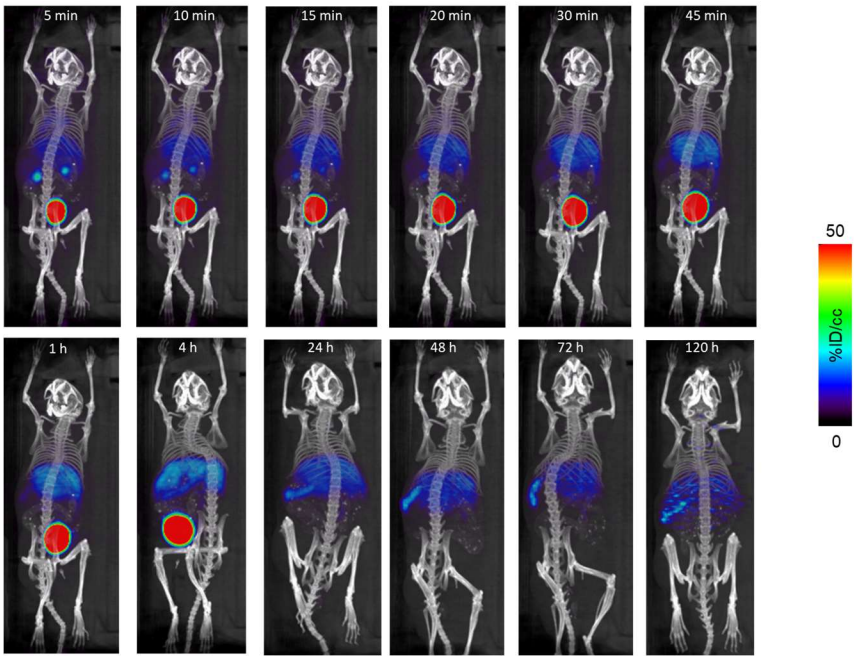

Figure A10 Co-registered μPET and μCT scans post ^{64}Cu-labeled pTrMA-*co*-DOTA injection to male mouse 1.

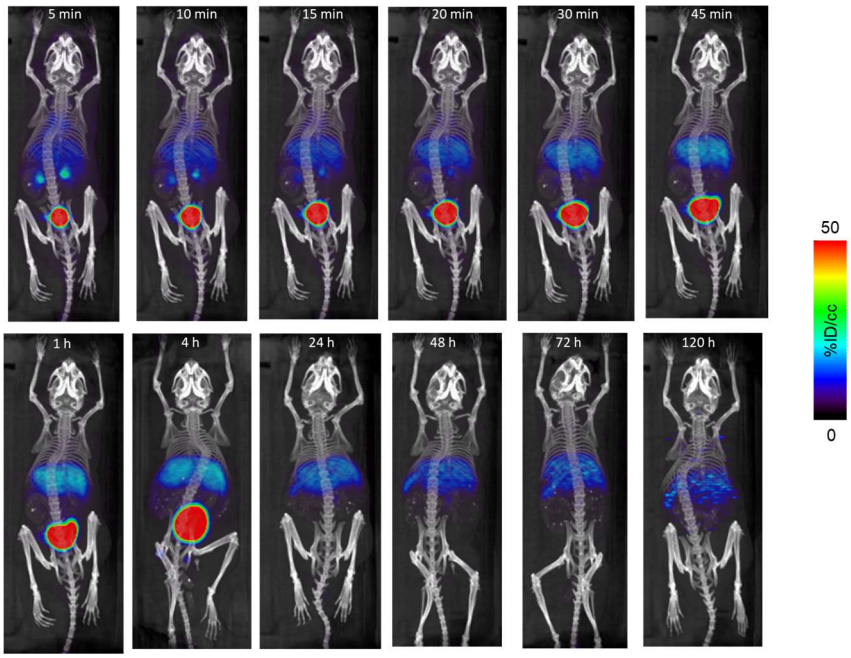

Figure A11 Co-registered μPET and μCT scans post ^{64}Cu-labeled pTrMA-*co*-DOTA injection to male mouse 2.

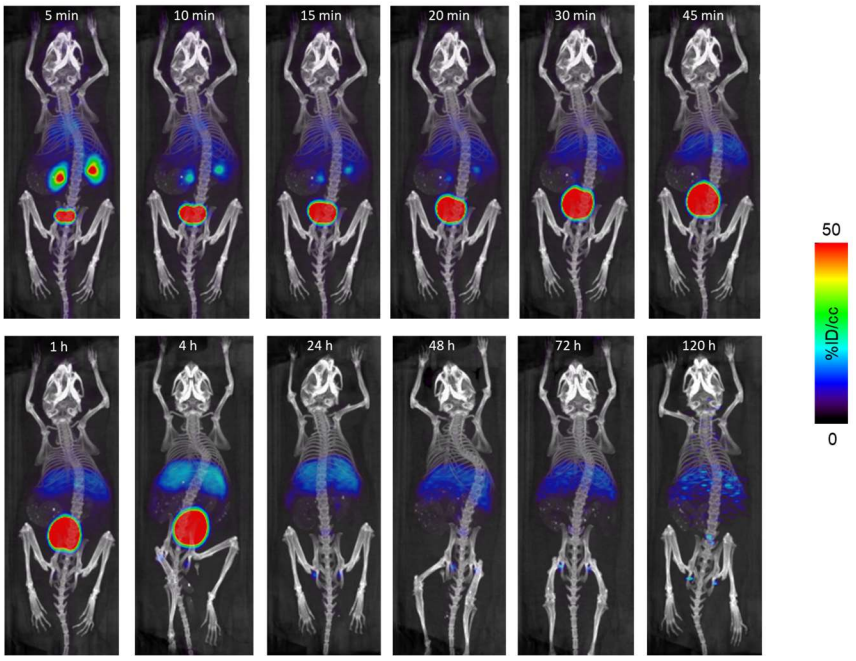

Figure A12 Co-registered μPET and μCT scans post ^{64}Cu-labeled pTrMA-*co*-DOTA injection to male mouse 3.

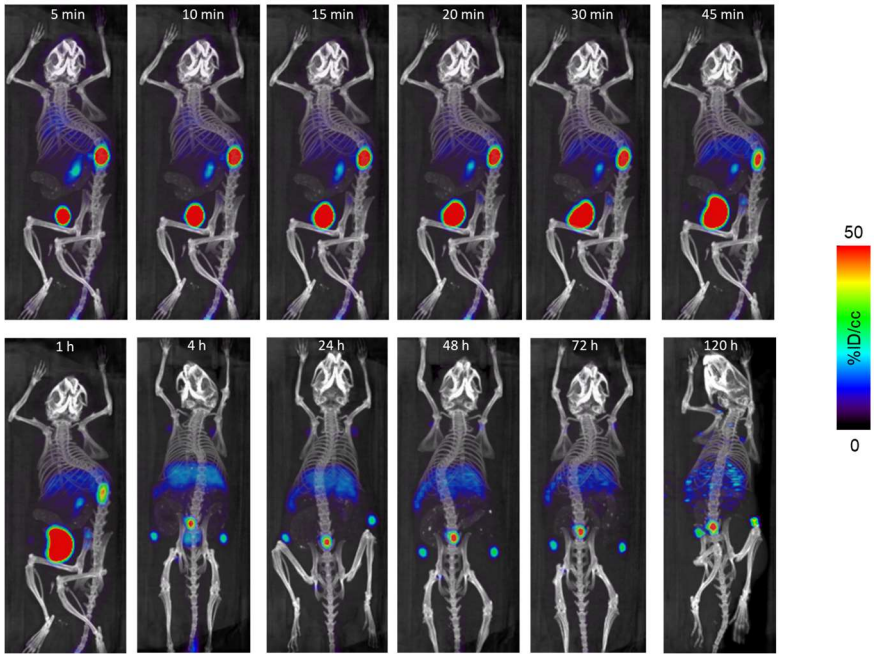

Figure A13 Co-registered μPET and μCT scans post ^{64}Cu-labeled pTrMA-*co*-DOTA injection to male mouse 4.

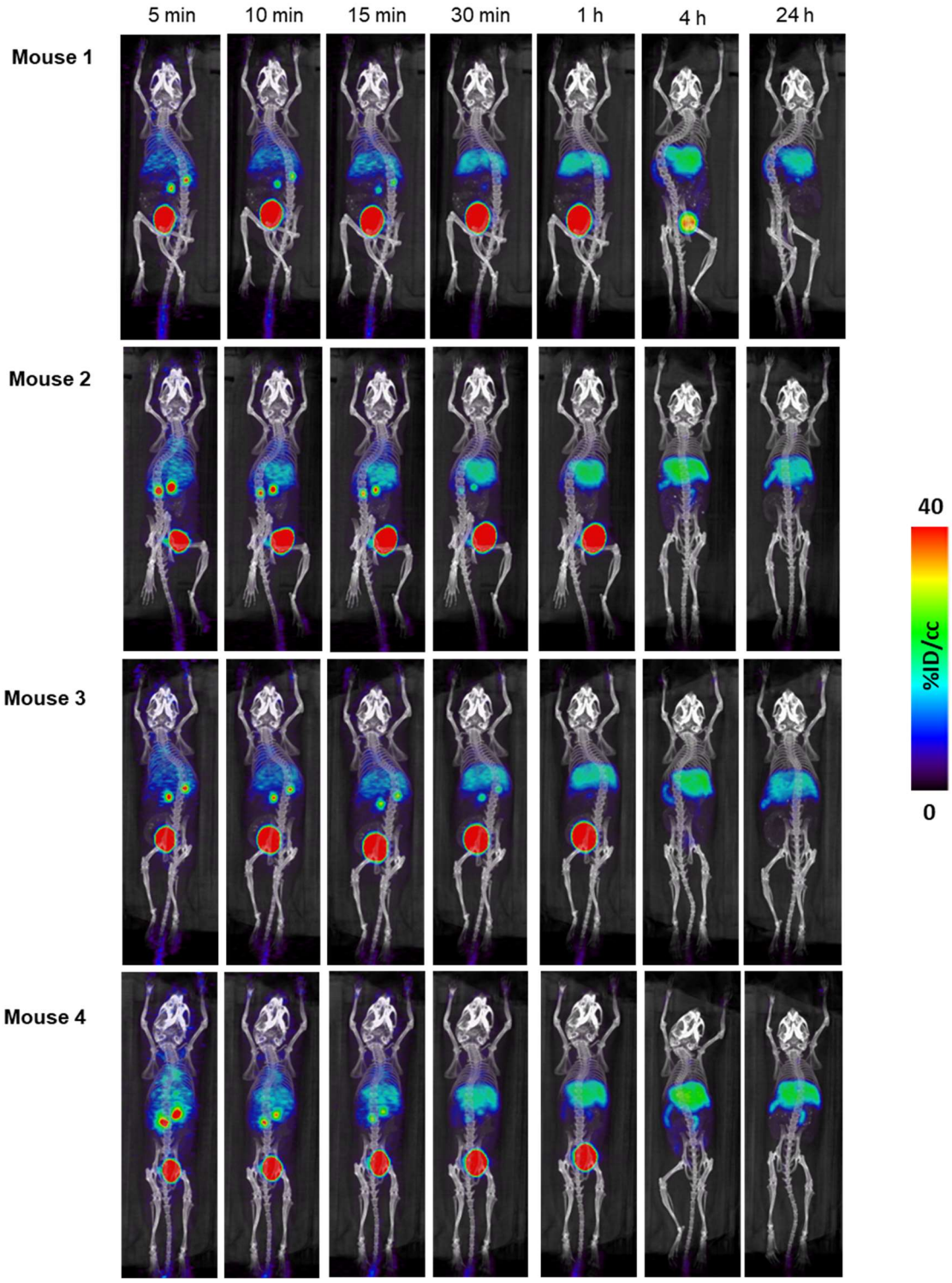

Figure A14 Co-registered μPET and μCT scans post fresh ^{64}Cu-labeled pTrMA-*co*-DOTA injection in mice (n = 4).

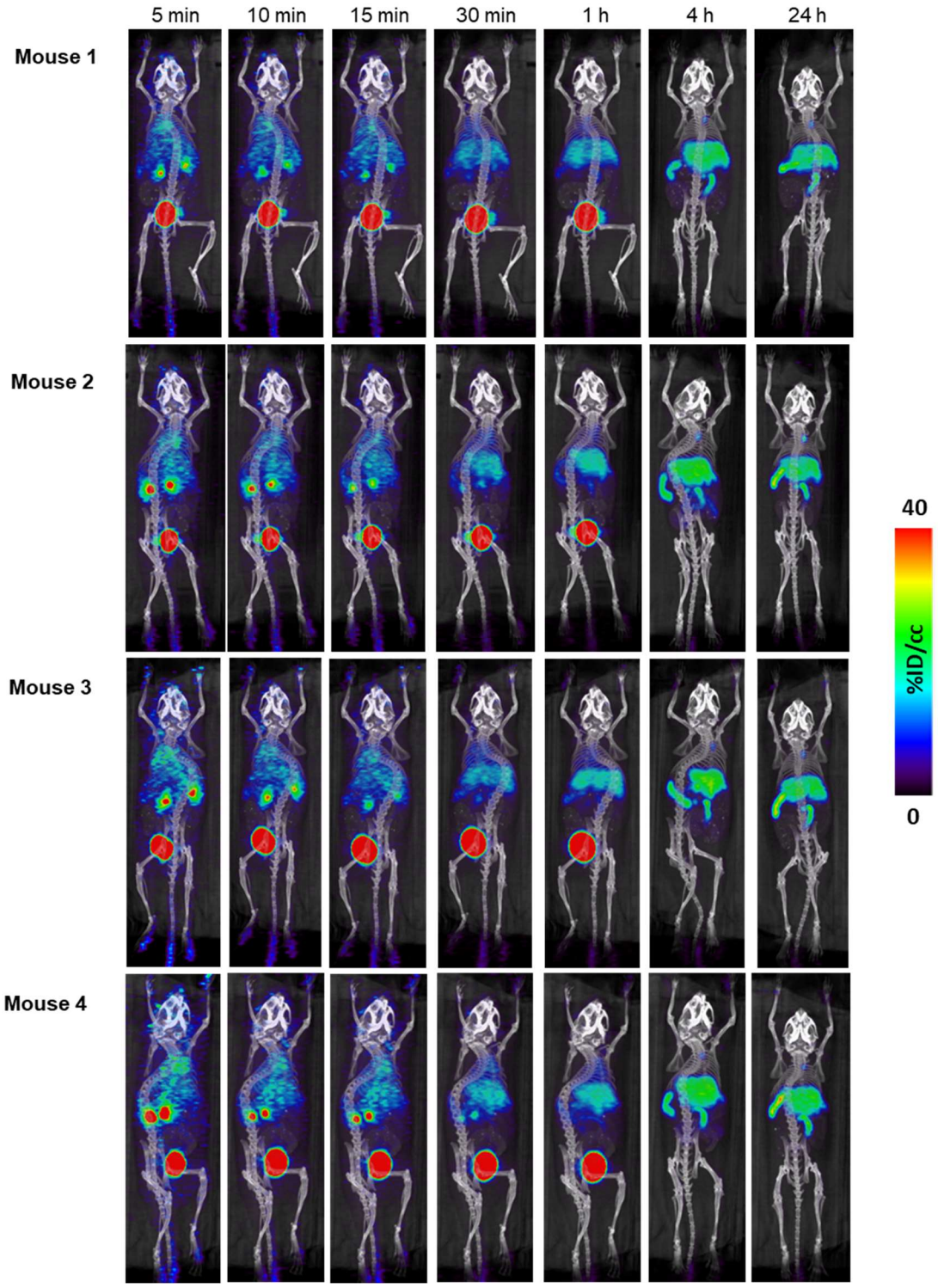

Figure A15 Co-registered μPET and μCT scans post plasma-incubated ^{64}Cu-labeled pTrMA-*co*-DOTA injection in mice (n = 4).

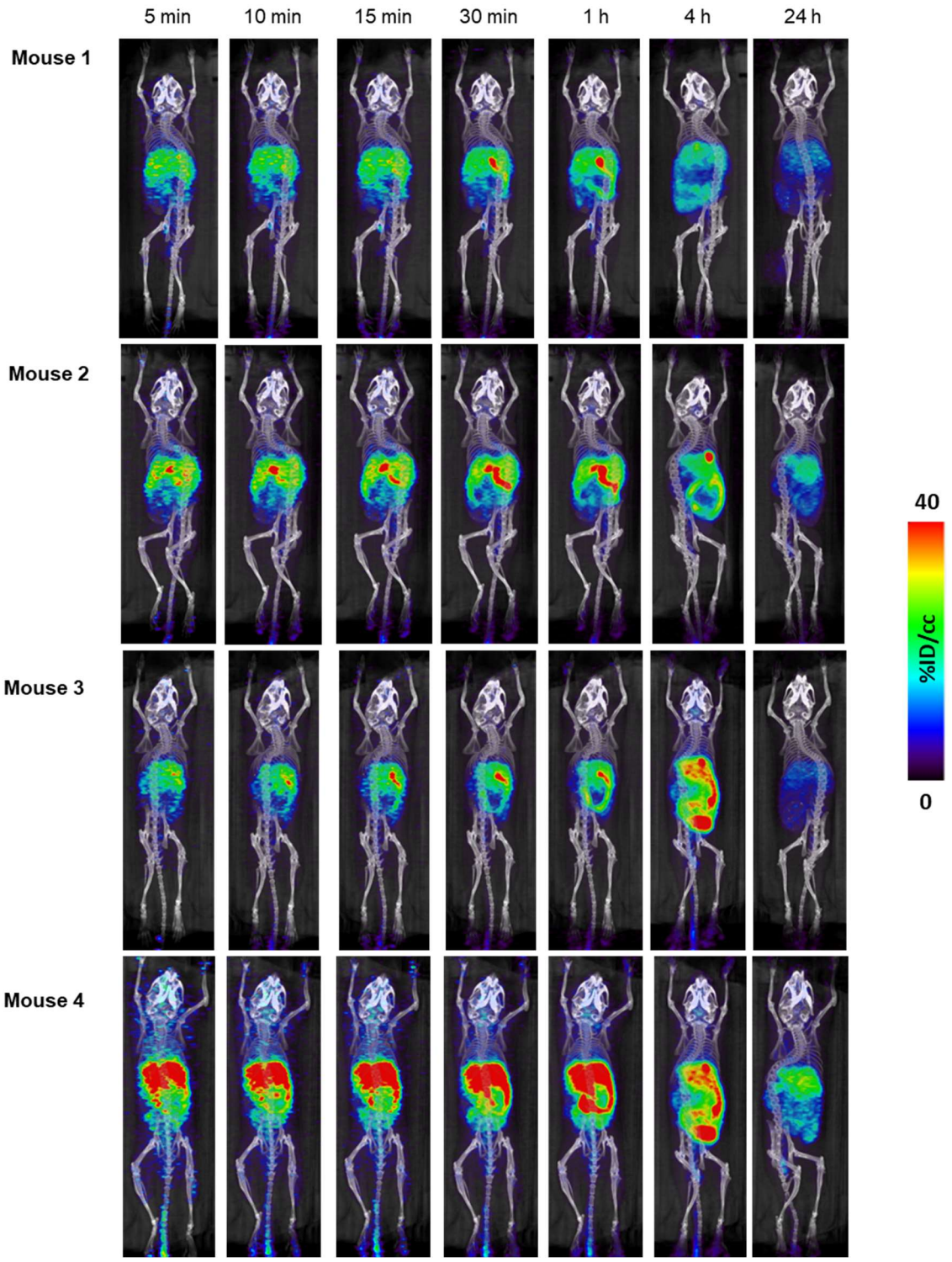

Figure A16 Co-registered μPET and μCT scans post $^{64}CuCl_2$ injection in mice (n = 4).

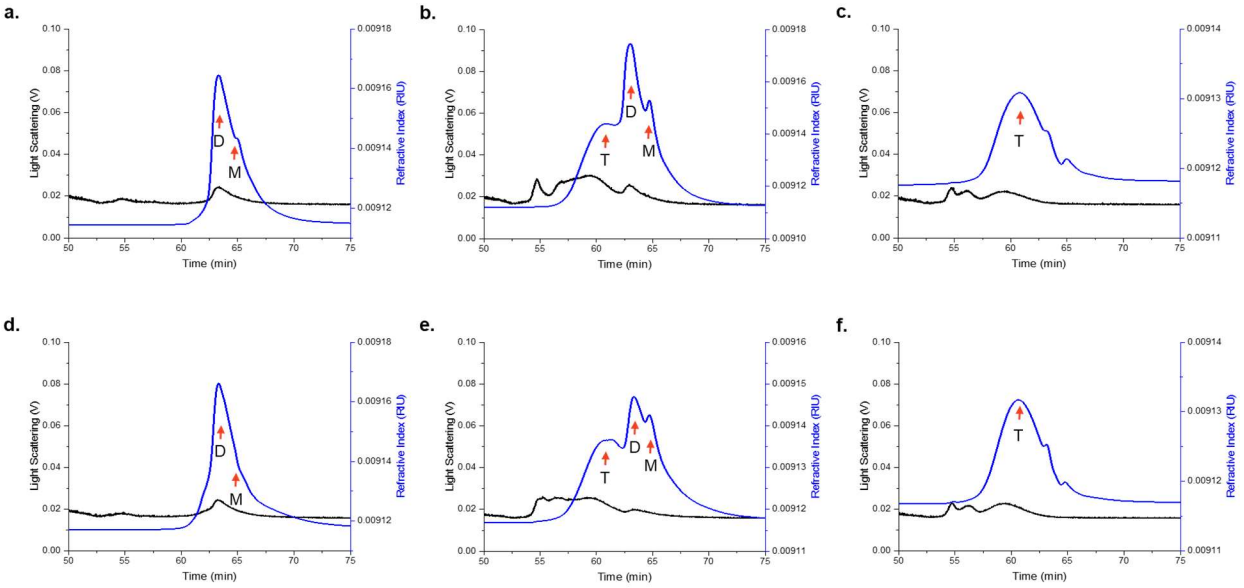

Figure A17 SEC-MALS elution profiles of a. fresh insulin, b. fresh insulin with pTrMA, c. fresh pTrMA, d. heated insulin, e. heated insulin with pTrMA, and f. heated pTrMA. Peaks are labeled as dimer (D), monomer (M), or pTrMA (T).

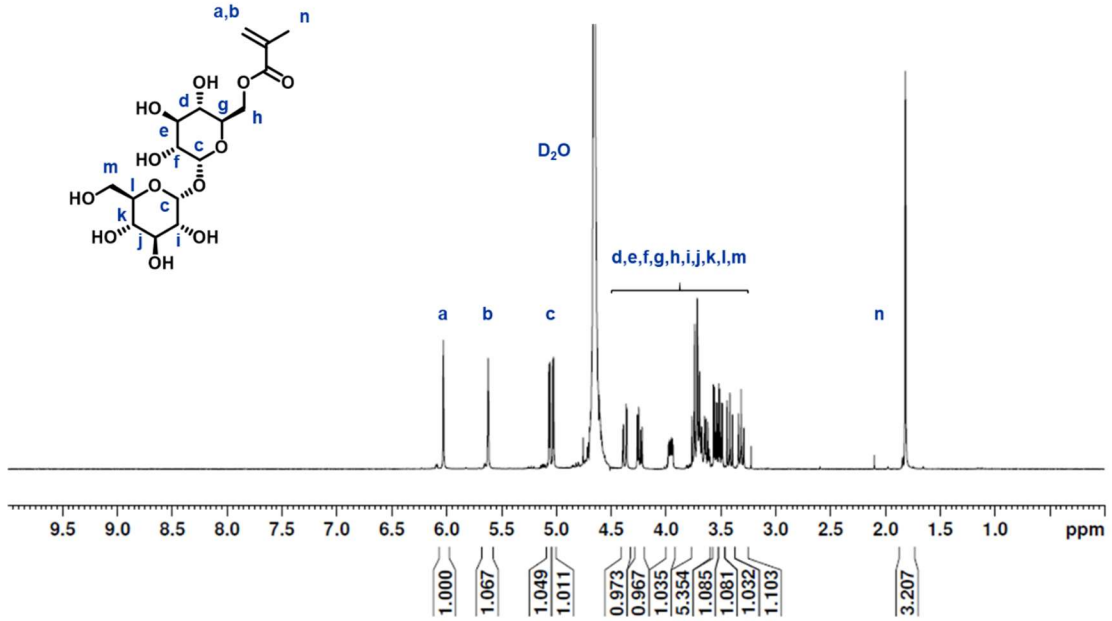

Figure A18 ^{1}H NMR spectrum (400 MHz, D_2O) of trehalose methacrylate (TrMA). ^{1}H-NMR agreed with that reported for this compound.[9]

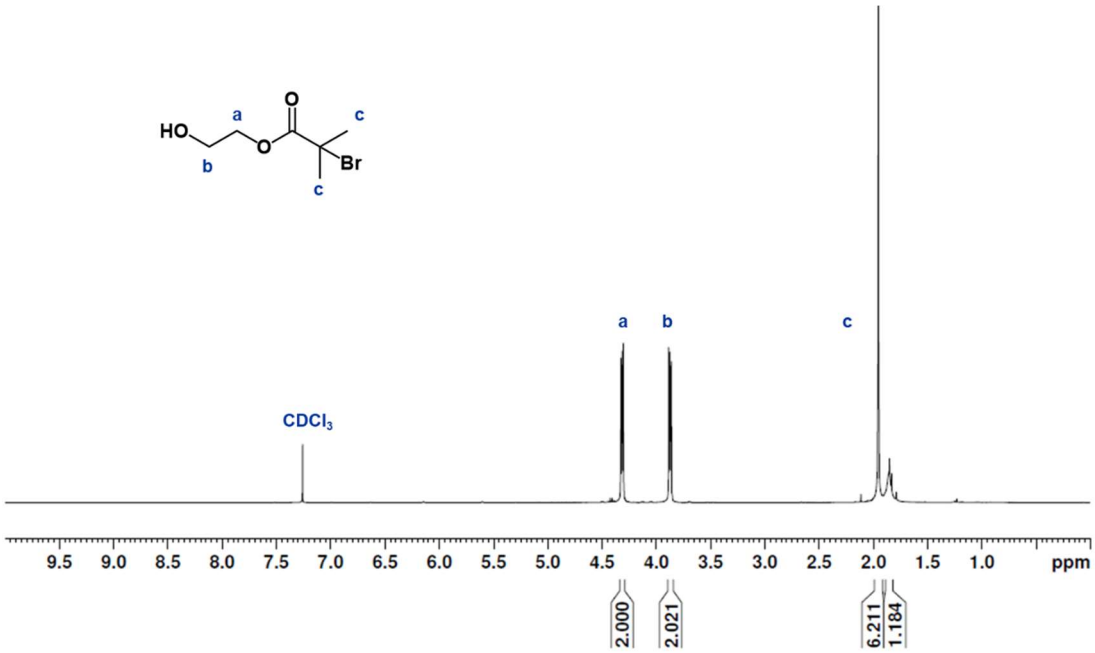

Figure A19 ^{1}H NMR spectrum (400 MHz, $CDCl_3$) of 2-hydroxyethyl 2-bromoisobutyrate (HEBIB) initiator. ^{1}H-NMR agreed with that reported for this compound.[31]

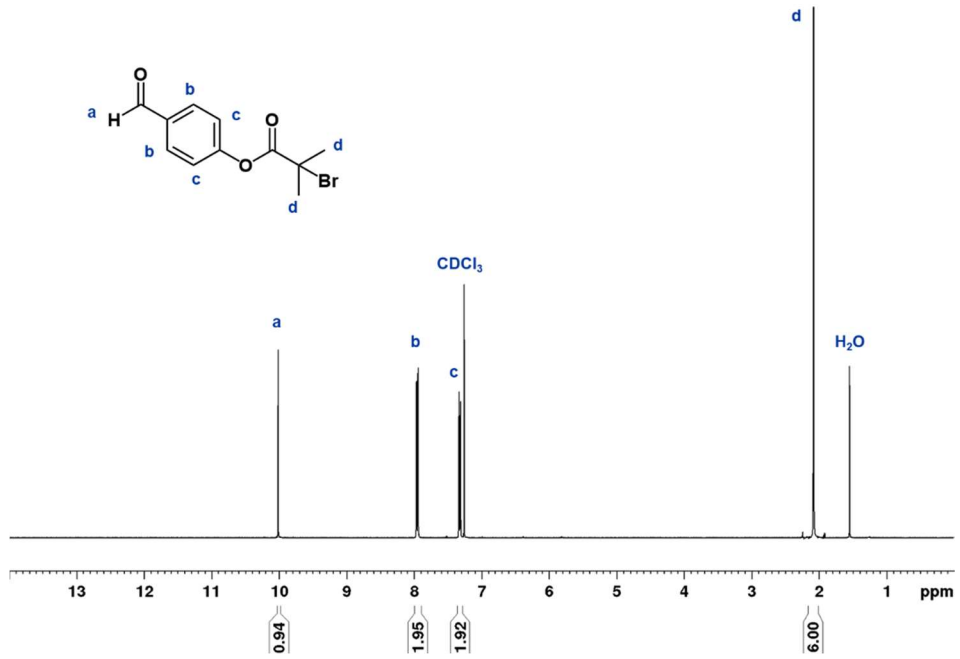

Figure A20 ^{1}H NMR spectrum (400 MHz, $CDCl_3$) of (4-formylphenyl2-bromoisobutyrylate) (benzaldehyde) initiator. ^{1}H-NMR agreed with that reported for this compound.[32]

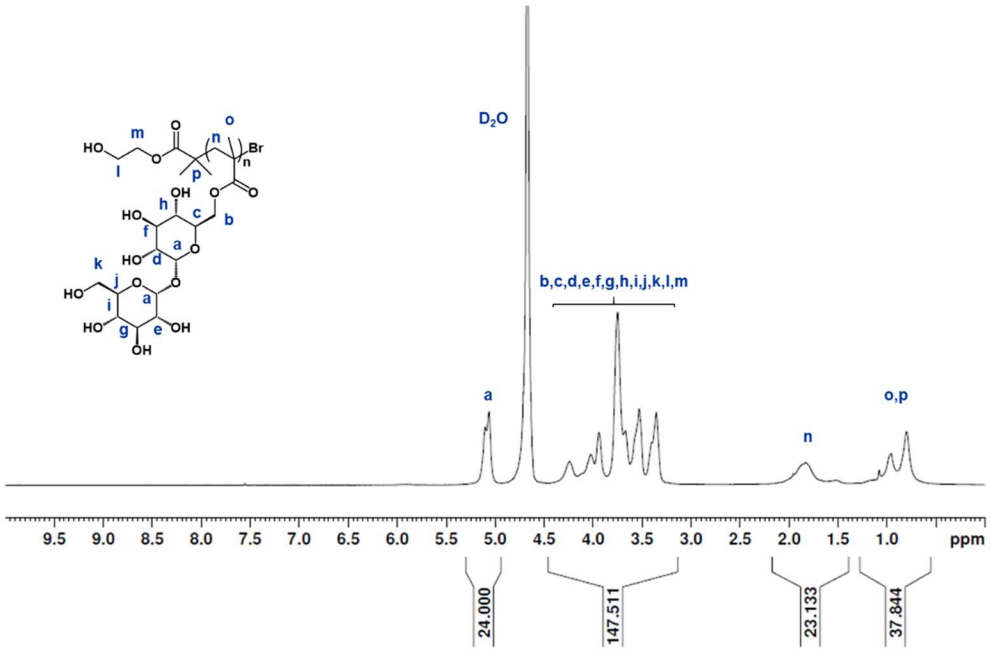

Figure A21 ^{1}H NMR spectrum (400 MHz, D_2O) of pTrMA polymerized with HEBIB initiator. ^{1}H-NMR agreed with that reported for this compound.[31]

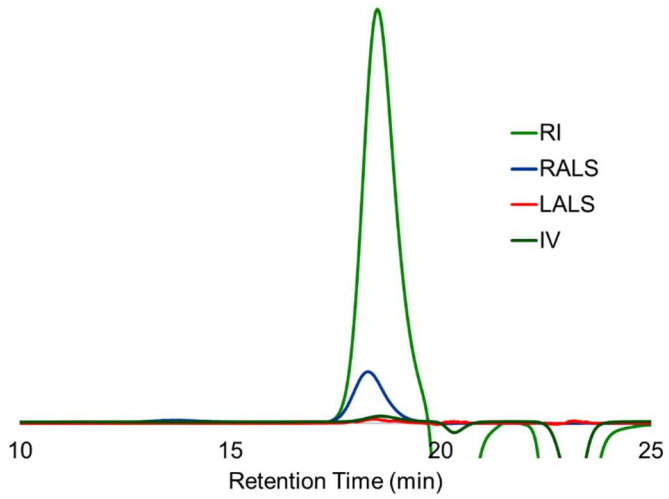

Figure A22 GPC (PEG standards) of pTrMA with HEBIB initiator. Number average molecular weight (M_n) = 10.1 kDa, $Đ$ = 1.25.

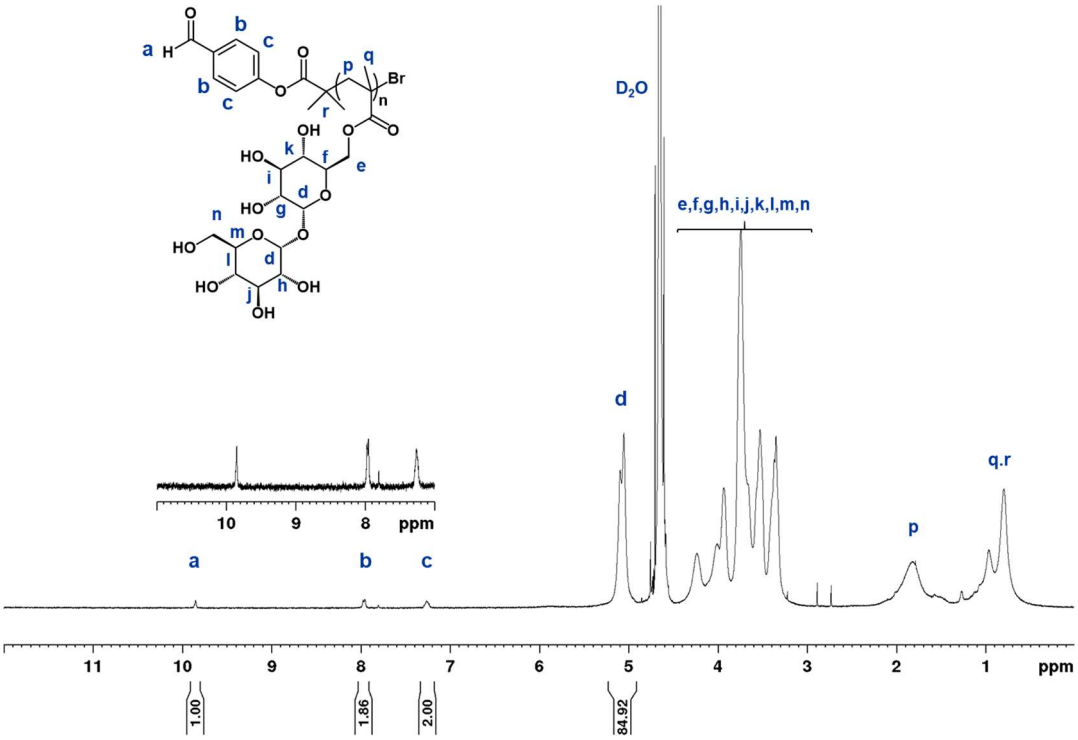

Figure A23 ^{1}H NMR spectrum (400 MHz, D_2O) of pTrMA with benzaldehyde initiator. ^{1}H-NMR agreed with that reported for this compound.[15]

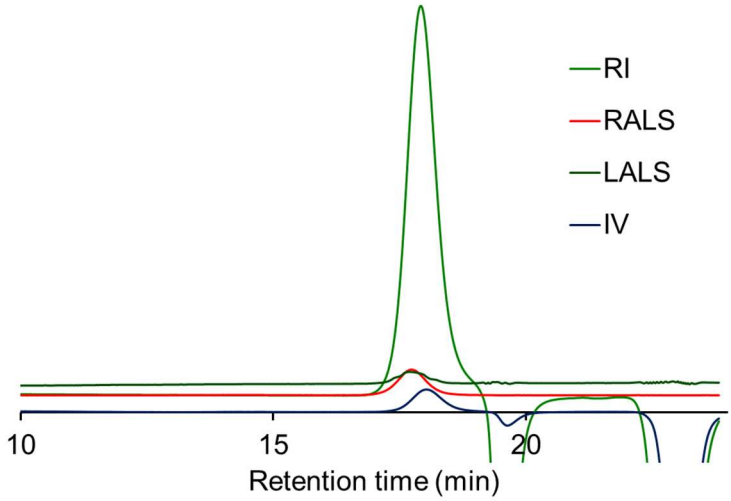

Figure A24 GPC (PEG standards) of pTrMA with benzaldehyde initiator. Number average molecular weight (M_n) = 24.9 kDa, $Đ$ = 1.05.

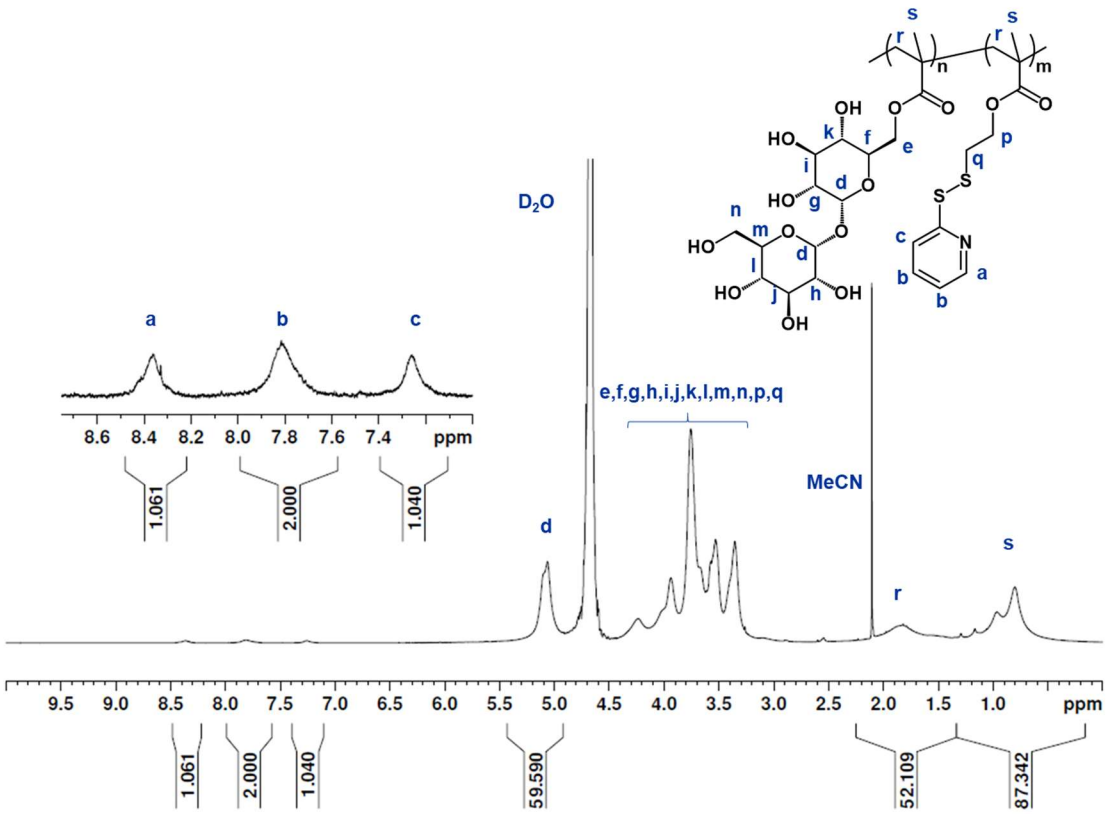

Figure A25 ^{1}H NMR spectrum (500 MHz, D_2O) of pTrMA -*co*-PDSMA polymerized by free radical polymerization. Relative PDSMA incorporation was calculated by integration of the PDSMA peaks a, b, and c in comparison with pTrMA peak d. ^{1}H-NMR agreed with that reported for this compound.[20]

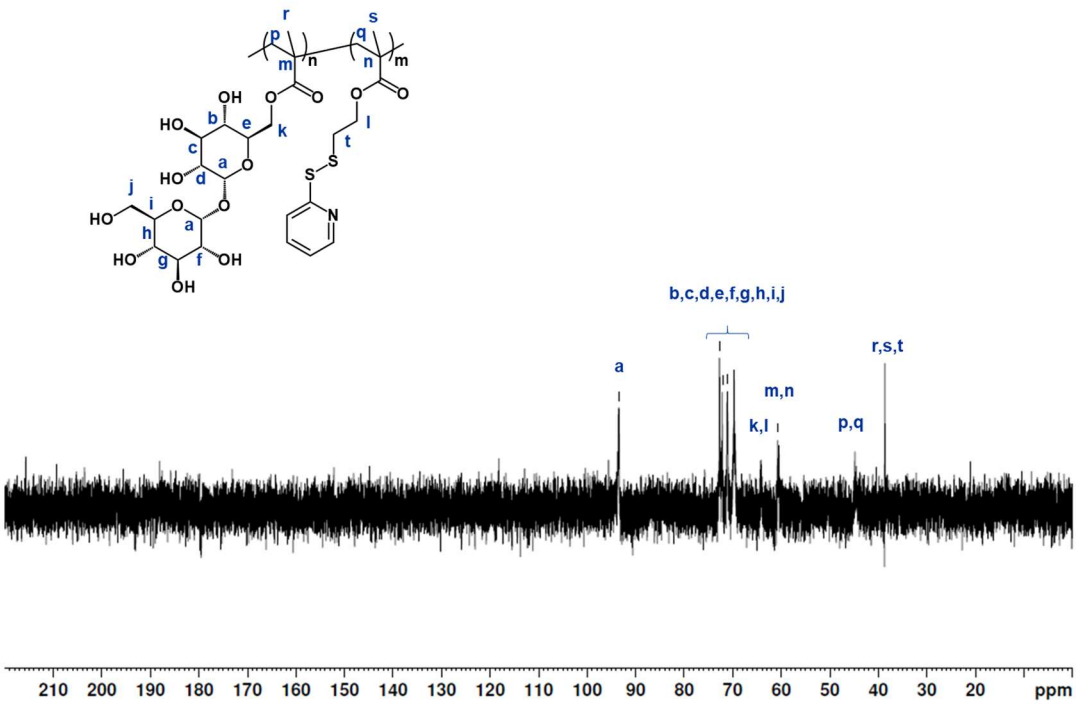

Figure A26 ^{13}C NMR spectrum (500 MHz, D_2O) of pTrMA T-*co*-PDSMA polymerized by free radical polymerization. ^{13}C-NMR agreed with that reported for this compound.[20]

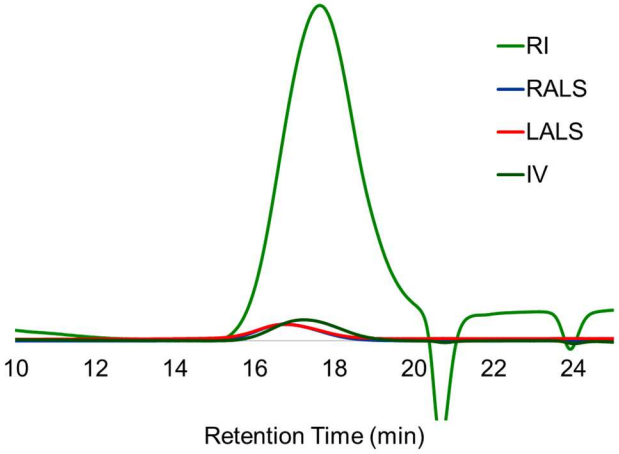

Figure A27 GPC (PEG standards) of pTrMA -*co*-PDSMA. Number average molecular weight (M_n) = 8.9 kDa, $Đ$ = 2.19.

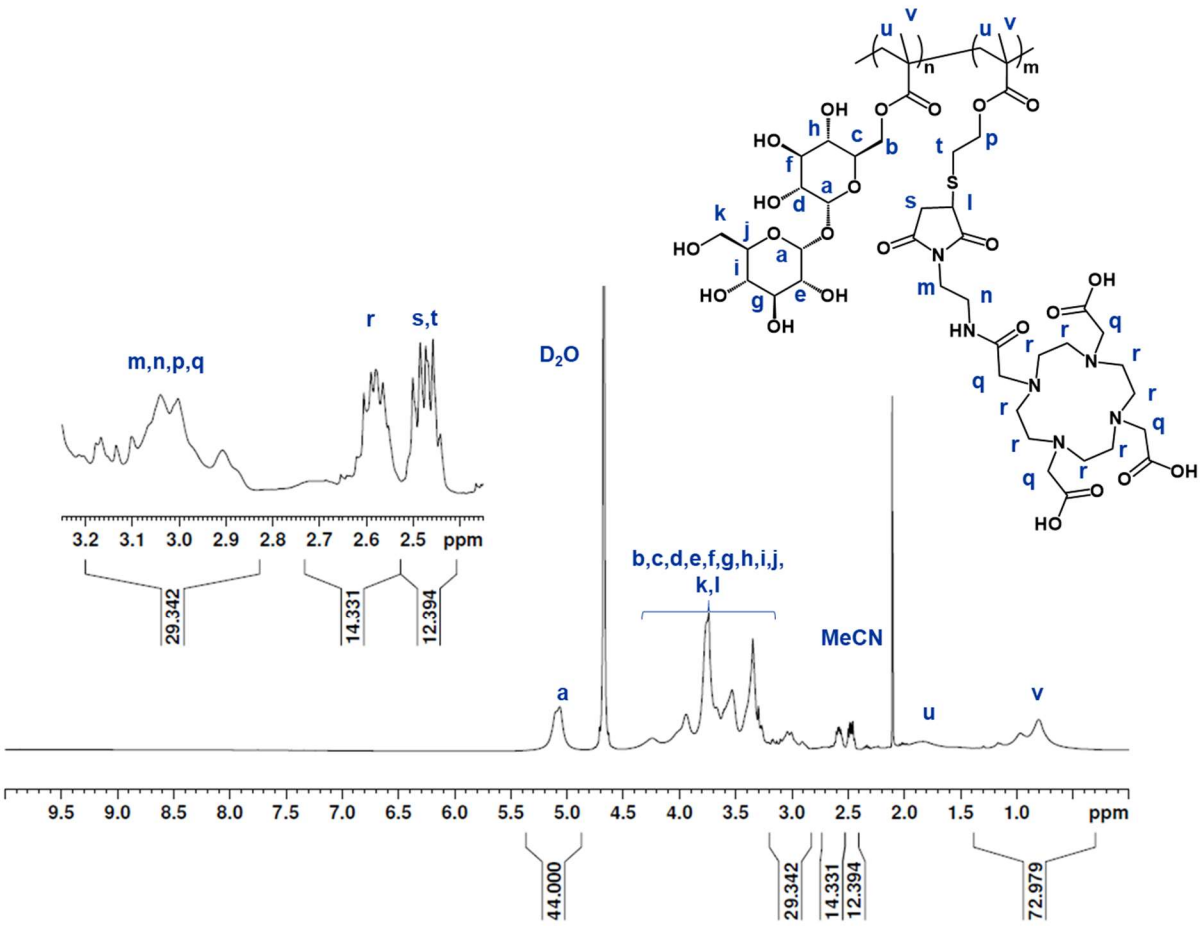

Figure A28 ^{1}H NMR spectrum (500 MHz, D_2O) of pTrMA-*co*-DOTA. Relative DOTA modification was calculated by integration of the DOTA peak r and in comparison with pTrMA peak a.

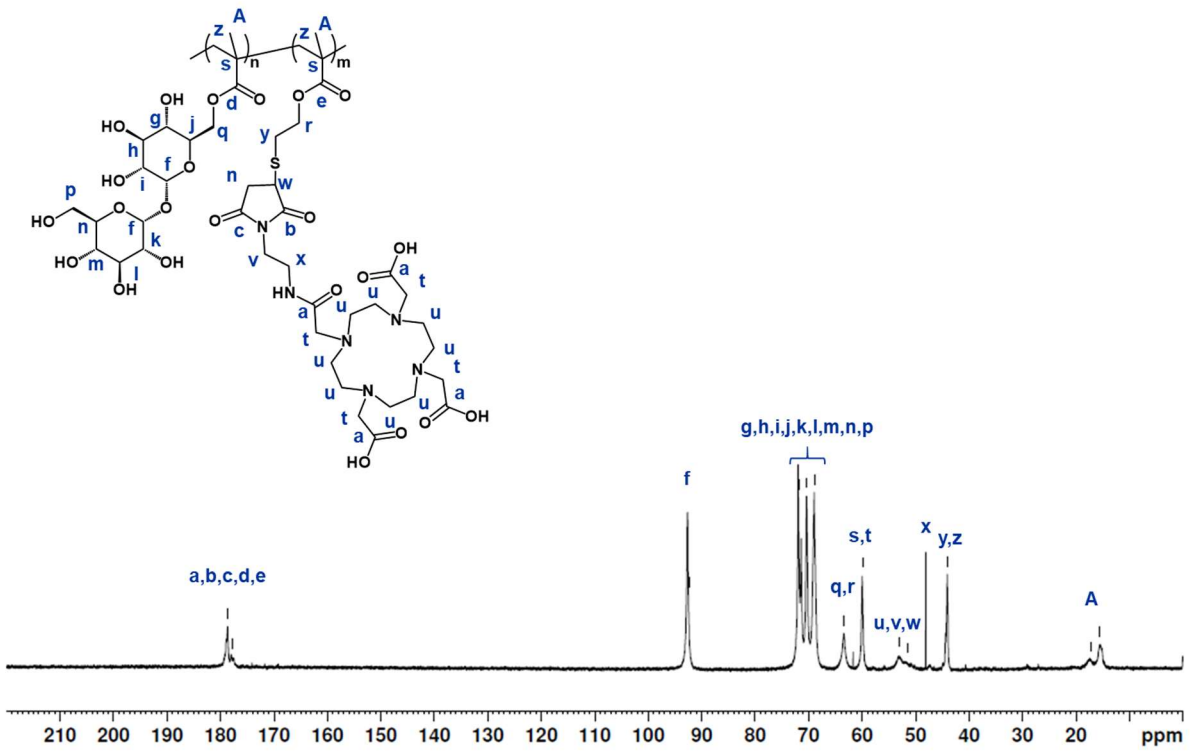

Figure A29 ^{13}C NMR spectrum (500 MHz, D_2O) of pTrMA-*co*-DOTA.

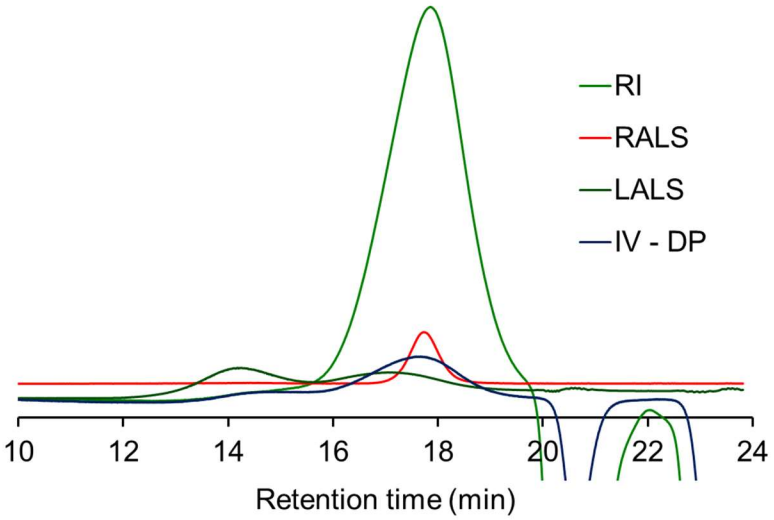

Figure A30 GPC (PEG standards) of pTrMA -*co*-DOTA. Number average molecular weight (M_n) = 10.3 kDa, $Đ$ = 2.68.

References

1. World Health Organization Ten threats to global health in 2019. https://www.who.int/news-room/spotlight/ten-threats-to-global-health-in-2019.

2. Kochanek, K. D.; Xu, J.; Arias, E. *Mortality in the United States, 2019*; U.S. Department of Health and Human Services Centers for Disease Control and Prevention: 2020.

3. *World Health Organization Model List of Essential Medicines, 21st List*; World Health Organization: Geneva, 2019.

4. Lendner, P. Economic Benefits of Improved Insulin Stability In Insulin Pumps. https://www.managedcaremag.com/archives/1105/1105-peer_insulinpump/.

5. Brange, J.; Langkjaer, L.; Havelund, S.; Vølund, A., Chemical Stability of Insulin. 1. Hydrolytic Degradation During Storage of Pharmaceutical Preparations. *Pharm. Res.* **1992,** *9* (6), 715-726.

6. Sluzky, V.; Klibanov, A. M.; Langer, R., Mechanism of insulin aggregation and stabilization in agitated aqueous solutions. *Biotechnol. Bioeng.* **1992,** *40* (8), 895-903.

7. Iannuzzi, C.; Borriello, M.; Portaccio, M.; Irace, G.; Sirangelo, I., Insights into Insulin Fibril Assembly at Physiological and Acidic pH and Related Amyloid Intrinsic Fluorescence. *Int. J. Mol. Sci.* **2017,** *18* (12), 2551.

8. Hermeling, S.; Crommelin, D. J. A.; Schellekens, H.; Jiskoot, W., Structure-Immunogenicity Relationships of Therapeutic Proteins. *Pharm. Res.* **2004,** *21* (6), 897-903.

9. Lee, J.; Lin, E. W.; Lau, U. Y.; Hedrick, J. L.; Bat, E.; Maynard, H. D., Trehalose Glycopolymers as Excipients for Protein Stabilization. *Biomacromolecules* **2013,** *14* (8), 2561-2569.

10. Lee, J.; Ko, J. H.; Lin, E. W.; Wallace, P.; Ruch, F.; Maynard, H. D., Trehalose hydrogels for stabilization of enzymes to heat. *Polym. Chem.* **2015,** *6* (18), 3443-3448.

11. Lau, U. Y.; Saxer, S. S.; Lee, J.; Bat, E.; Maynard, H. D., Direct Write Protein Patterns for Multiplexed Cytokine Detection from Live Cells Using Electron Beam Lithography. *ACS Nano* **2016,** *10* (1), 723-729.

12. Pelegri-O'Day, E. M.; Paluck, S. J.; Maynard, H. D., Substituted Polyesters by Thiol-Ene Modification: Rapid Diversification for Therapeutic Protein Stabilization. *J. Am. Chem. Soc.* **2017,** *139* (3), 1145-1154.

13. Messina, M. S.; Ko, J. H.; Yang, Z. Y.; Strouse, M. J.; Houk, K. N.; Maynard, H. D., Effect of trehalose polymer regioisomers on protein stabilization. *Polym. Chem.* **2017,** *8* (33), 4781-4788.

14. Liu, Y.; Lee, J.; Mansfield, K. M.; Ko, J. H.; Sallam, S.; Wesderniotis, C.; Maynard, H. D., Trehalose Glycopolymer Enhances Both Solution Stability and Pharmacokinetics of a Therapeutic Protein. *Bioconjugate Chem.* **2017,** *28* (3), 836-845.

15. Mansfield, K. M.; Maynard, H. D., Site-Specific Insulin-Trehalose Glycopolymer Conjugate by Grafting from Strategy Improves Bioactivity. *ACS Macro Lett.* **2018**, 324-329.

16. Lee, J.; Ko, J. H.; Mansfield, K. M.; Nauka, P. C.; Bat, E.; Maynard, H. D., Glucose-Responsive Trehalose Hydrogel for Insulin Stabilization and Delivery. *Macromol. Biosci.* **2018,** *18* (5), 1700372.

17. Pelegri-O'Day, E. M.; Bhattacharya, A.; Theopold, N.; Ko, J. H.; Maynard, H. D., Synthesis of Zwitterionic and Trehalose Polymers with Variable Degradation Rates and Stabilization of Insulin. *Biomacromolecules* **2020,** *21* (6), 2147-2154.

18. Gelb, M. B.; Maynard, H. D., Effect of Poly(trehalose methacrylate) Molecular Weight and Concentration on the Stability and Viscosity of Insulin. *Macromol. Mater. Eng.* **2021,** *306* (9), 2100197.

19. Dias, C.; Abosaleem, B.; Crispino, C.; Gao, B.; Shaywitz, A., Tolerability of High-Volume Subcutaneous Injections of a Viscous Placebo Buffer: A Randomized, Crossover Study in Healthy Subjects. *AAPS PharmSciTech* **2015,** *16* (5), 1101-1107.

20. Boehnke, N.; Kammeyer, J. K.; Damoiseaux, R.; Maynard, H. D., Stabilization of Glucagon by Trehalose Glycopolymer Nanogels. *Adv. Funct. Mater.* **2018,** *28* (10), 1705475.

21. Cataldi, M.; Vigliotti, C.; Mosca, T.; Cammarota, M.; Capone, D., Emerging Role of the Spleen in the Pharmacokinetics of Monoclonal Antibodies, Nanoparticles and Exosomes. *Int J Mol Sci* **2017,** *18* (6).

22. Attri, A. K.; Fernández, C.; Minton, A. P., Self-association of Zn-insulin at neutral pH: Investigation by concentration gradient-static and dynamic light scattering. *Biophys. Chem.* **2010,** *148* (1), 23-27.

23. Jonassen, I.; Havelund, S.; Hoeg-Jensen, T.; Steensgaard, D. B.; Wahlund, P.-O.; Ribel, U., Design of the Novel Protraction Mechanism of Insulin Degludec, an Ultra-long-Acting Basal Insulin. *Pharm. Res.* **2012,** *29* (8), 2104-2114.

24. Jiang, L.; Tu, Y.; Hu, X.; Bao, A.; Chen, H.; Ma, X.; Doyle, T.; Shi, H.; Cheng, Z., Pilot Study of 64Cu(I) for PET Imaging of Melanoma. *Sci. Rep.* **2017,** *7* (1), 2574.

25. Sun, X.; Rossin, R.; Turner, J. L.; Becker, M. L.; Joralemon, M. J.; Welch, M. J.; Wooley, K. L., An Assessment of the Effects of Shell Cross-Linked Nanoparticle Size, Core Composition, and Surface PEGylation on in Vivo Biodistribution. *Biomacromolecules* **2005,** *6* (5), 2541-2554.

26. Pressly, E. D.; Rossin, R.; Hagooly, A.; Fukukawa, K.-i.; Messmore, B. W.; Welch, M. J.; Wooley, K. L.; Lamm, M. S.; Hule, R. A.; Pochan, D. J.; Hawker, C. J., Structural Effects on the Biodistribution and Positron Emission Tomography (PET) Imaging of Well-Defined 64Cu-Labeled Nanoparticles Comprised of Amphiphilic Block Graft Copolymers. *Biomacromolecules* **2007,** *8* (10), 3126-3134.

27. Fukukawa, K.-i.; Rossin, R.; Hagooly, A.; Pressly, E. D.; Hunt, J. N.; Messmore, B. W.; Wooley, K. L.; Welch, M. J.; Hawker, C. J., Synthesis and Characterization of Core–Shell Star Copolymers for In Vivo PET Imaging Applications. *Biomacromolecules* **2008,** *9* (4), 1329-1339.

28. Welch, M. J.; Hawker, C. J.; Wooley, K. L., The advantages of nanoparticles for PET. *J. Nucl. Med.* **2009,** *50* (11), 1743-1746.

29. Sun, G.; Hagooly, A.; Xu, J.; Nyström, A. M.; Li, Z.; Rossin, R.; Moore, D. A.; Wooley, K. L.; Welch, M. J., Facile, Efficient Approach to Accomplish Tunable Chemistries and Variable Biodistributions for Shell Cross-Linked Nanoparticles. *Biomacromolecules* **2008,** *9* (7), 1997-2006.

30. Manning, M. C.; Chou, D. K.; Murphy, B. M.; Payne, R. W.; Katayama, D. S., Stability of Protein Pharmaceuticals: An Update. *Pharm. Res.* **2010,** *27* (4), 544-575.

31. Ren, L.; Zhang, J.; Hardy, C. G.; Doxie, D.; Fleming, B.; Tang, C., Preparation of Cobaltocenium-Labeled Polymers by Atom Transfer Radical Polymerization. *Macromolecules* **2012,** *45* (5), 2267-2275.

32. Jin, J.; Liu, J.; Lian, X.; Sun, P.; Zhao, H., Dynamic polymer brushes on the surface of silica particles. *RSC Adv.* **2013,** *3* (19), 7023-7029.

Chapter 3

Effect of Poly(trehalose methacrylate) Molecular Weight and Concentration on the Stability and Viscosity of Insulin

3.1 Introduction

Biopharmaceuticals are increasingly prevalent treatments for both acute and chronic serious diseases, as indicated by a commensurate rise in their market value to nearly $200 billion annually in 2017, with a projection to reach over $500 billion by 2025.[1] As therapeutics, biopharmaceuticals are advantageously intricate, making them highly selective and effective. However, they are limited in their stability with narrow windows of acceptable storage conditions.[2-3] Protein that degrades or aggregates due to inadequate storage prior to injection does not provide patients with the necessary therapeutic action and can elicit immune responses. It is thus important for biopharmaceuticals to maintain stability under a range of environmental conditions.[4-7] This includes stabilizing biopharmaceuticals for storage at physiological pH, room or body temperatures, agitation that may be encountered during shipping or person movement, and at concentrations that reduce the frequency and volume of dosing.

Excipients have been employed extensively to maintain biopharmaceutical activity through the environmental stress caused by manufacturing, transportation, and storage.[8-9] Small molecules such as amino acids,[10-11] osmolytes,[12-13] and carbohydrates[14] all successfully stabilize proteins through buffering, preferentially hydrating, and binding interactions. Macromolecules, both natural and synthetic, have been used to stabilize biopharmaceuticals through various mechanisms including preventing protein adsorption, unfolding, and aggregation.[8] Synthetic polymer side chains have also been designed to incorporate small molecules that have been shown to increase stabilization of biopharmaceuticals as excipients. For example, charged polymers have stabilized protein therapeutics through electrostatic interactions[15-16] and zwitterionic polymers via hydration and protein repulsion.[17-19] Our research has shown that polymers with side chains of the disaccharide trehalose and methacrylate, styrene, caprolactone, valerolactone, carbonate, and

lactide backbones have also stabilized proteins by preventing aggregation, reducing crystallization, and serving as chaperones.[20-24]

Another factor besides stabilization is formulation solution viscosity, as this is important in ensuring patient comfort, convenience, and compliance.[25-28] Therapeutic proteins are often limited to injection routes of administration due to the greater challenges of oral delivery and the benefit of high bioavailability and rapid onset of activity. Inconvenience, difficulty, and pain all reduce the likelihood that patients will properly adhere to a dosing regimen. The results of patient pain studies are mixed, but they agree that the majority of pain from self-administered injections stems from needle insertion.[5, 25-26, 29] However, high viscosity and poor flow complicates self-administration, especially because forcefully depressing the plunger raises the possibility of pushing past the subcutaneous layer and injecting into muscle tissue.[27-30] Issues with self-injection of highly viscous or poor flow solutions are exacerbated when patients must administer them chronically or for patients with dexterity constraints (e.g. rheumatoid arthritis or juvenile patients). Furthermore, high viscosity of solutions can limit administration at all, or require large volumes to dilute the therapeutic, such as in the case of antibodies.[25-27] These biopharmaceutical limitations meaningfully impact the treatment experience of patients with chronic diseases.

Insulin, the first US Food and Drug Administration approved biopharmaceutical and a World Health Organization Essential Medicine, is administered by multiple self-administered injections or pump infusions as the primary treatment for diabetes, a life threatening, chronic disease. As with other biopharmaceuticals, heat, agitation, and other environmental stressors met in manufacturing, transport, and storage can cause insulin to degrade and aggregate.[31-32] Additionally, patients can develop insulin resistance over time due to β-cell failure, and to meet this increased need for externally supplied insulin, higher concentration formulations of insulin

have now emerged ranging from U-100 (3.47 mg mL^{-1}) to U-500 (17.35 mg mL^{-1}).[33-35] Even with concentrated formulations, patients with severe insulin resistance must inject themselves multiple times to meet the required dosage. Again, this is a major disadvantage for patient comfort and compliance as needle insertion is the most painful part of the process, and large volume injections are more likely to produce leakage or discomfort. Additionally, while insulin pumps reduce the frequency of breaking skin and can be more convenient for patients, they are only suitable for patients who need the lowest concentration of insulin available, U-100.[33] Thus, for insulin, it is important that stabilizing excipients are available and do not appreciably increase the viscosity of the solution.

Previous research by our group has shown trehalose based glycopolymers stabilize the protein insulin to stressors such as heat and agitation.[21-24] However, the minimum concentrations and molecular weights (MW) required for the effect are not known. Furthermore, the viscosities of solutions of these polymers have not been investigated. Increasing MW or concentration in solution is generally known to raise solution viscosity due to internal friction between molecules, the degree to which depends on the macromolecule and solvent. Additionally, many macromolecules exhibit non-Newtonian behaviors (e.g. shear thickening or thinning).[27, 36] Thus, the interplay between MW, concentration, stability and viscosity for any excipient must be understood. Herein, we describe a systematic study of pTrMA optimized by MW and concentration to stabilize insulin against agitation and thermal stress, while minimally changing the viscosity and flow properties of the solution.

3.2 Results and Discussion

3.2.1 Polymer Synthesis

Reducing the total excipient used to stabilize biopharmaceuticals is important for both manufacturing/patient finances and minimizing the effect on solution viscosity and flow. We hypothesized that small polymers would be less viscous, but may require higher concentrations to stabilize insulin than larger ones. Thus, a range of MWs relevant for excretion of polymers (2.4-29.2 kDa) was investigated. The polymers were synthesized by activator generated by electron transfer (AGET) atom transfer radical polymerization (ATRP) to target specific MWs of pTrMA, and the initiator 2-hydroxyethyl 2-bromoisobutyrate (HEBIB) was employed.[23] Polymers were all characterized by ^{1}H NMR and GPC and were shown to have the desired range of MWs (2.4 – 29.2 kDa) (**Table 3.1**). While most of the polymers had low MW dispersity (<1.3) as is typical of polymers made from AGET ATRP, two of the higher MW polymers, 12.8 kDa and 29.2 kDa, each had a larger dispersity and the GPC traces were not perfectly symmetrical (**Figures B1-14**). Polymer excipients are not required to be monodisperse, and the polymers were the correct number-average molecular weight (M_n). Thus, this entire library including these two samples was studied further.

Table 3.1 GPC MW data of the AGET ATRP synthesized pTrMA polymers measured in 20% methanol in water using PEG standards.

Target MW (kDa)	Mn (Da)	Mw (Da)	Đ
2.5	2420	3050	1.26
5.0	4650	5830	1.25
10.0	9390	10340	1.10
12.5	12840	20430	1.59
20.0	19770	22070	1.12
30.0	29160	59180	2.03

3.2.2 pTrMA Viscosity and Fluid Behavior

We next tested the fluid behavior of pTrMA using a RheoSense microVisc viscometer. Specifically, the viscosity of each MW of pTrMA was measured across a range of shear rates at decreasing concentrations. Independence of fluid viscosity from the acting force, or shear rate, and a linear relationship between shear stress and shear rate are both fundamental characteristics of Newtonian fluids.[36] Other polymers have been shown to have Newtonian-like behaviors at low concentrations and MWs including polyethylene glycol (PEG), a polymer commonly used with biopharmaceuticals.[37-38] Indeed, the pTrMA each have a linear relationship between shear stress and shear rate, as well as constant viscosity across shear rates (**Figure 3.2** and **Figure 3.3**). From the observed fluid property relationships, we conclude that pTrMA acts with Newtonian-like behavior within the concentration and MW range that we studied. This is important for scaling; as a Newtonian-behaving fluid with simple fluid flow properties, pTrMA solutions would not exhibit either shear thickening or shear thinning during injections.

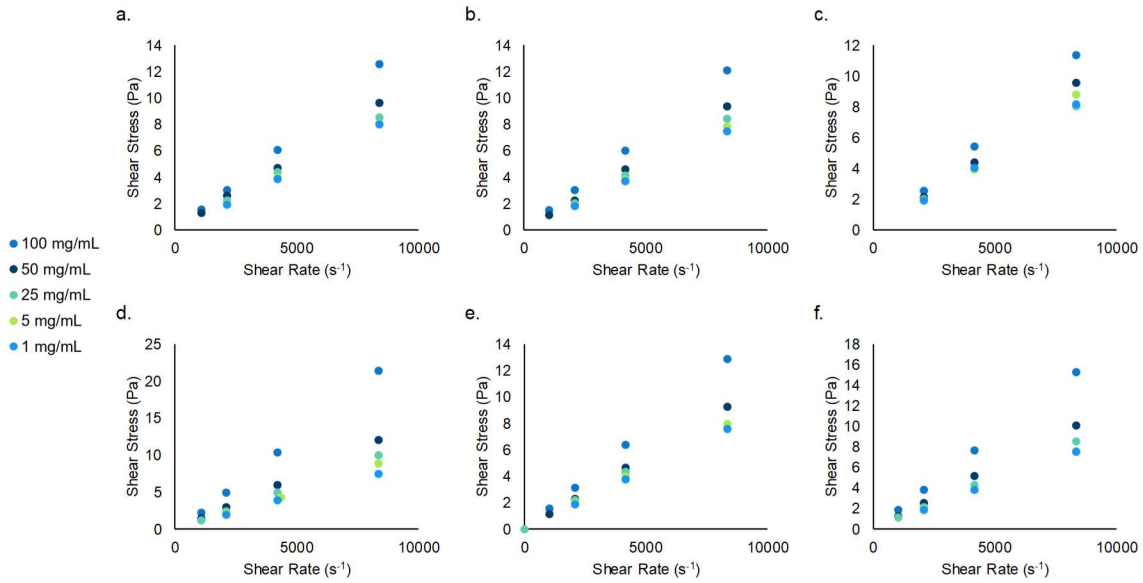

Figure 3.2 Shear stress (Pa) of pTrMA solutions ranging from 1 mg mL^{-1} to 100 mg mL^{-1} (n = 3) over the allowable shear rates (s^{-1}) for pTrMA MWs of a. 2.4 kDa, b. 5.0 kDa, c. 9.4 kDa, d. 12.8 kDa, e. 19.8 kDa, and f. 29.2 kDa.

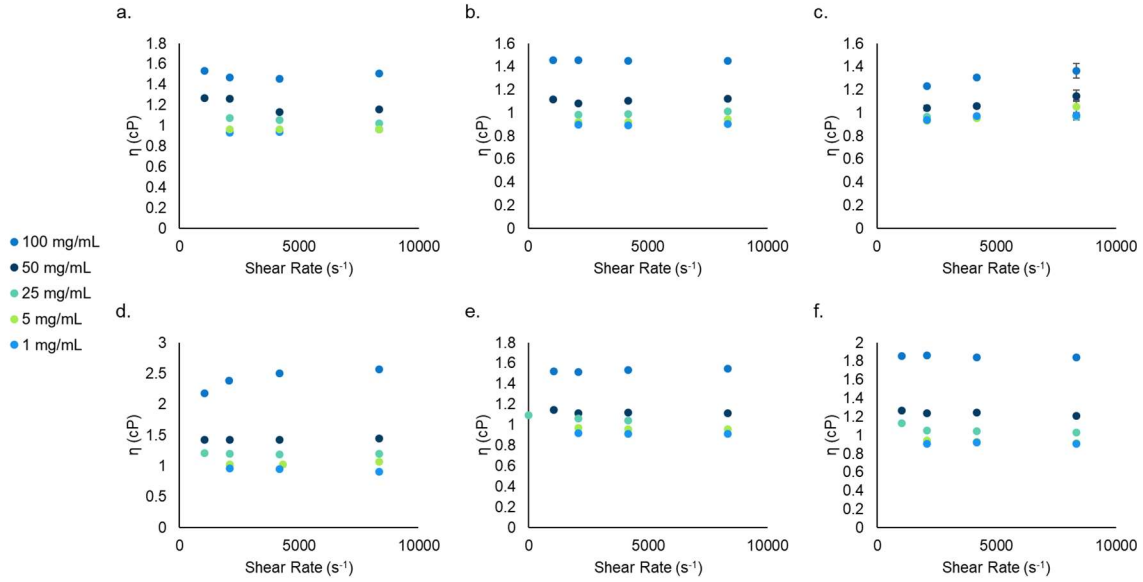

Figure 3.3 Viscosity (η, cP) of pTrMA solutions ranging from 1 mg mL^{-1} to 100 mg mL^{-1} (n = 3) over the allowable shear rates (s^{-1}) for pTrMA MWs a. 2.4 kDa, b. 5.0 kDa, c. 9.4 kDa, d. 12.8 kDa, e. 19.8 kDa, and f. 29.2 kDa.

Interestingly, the viscosities (0.90 - 2.57 cP, shear rate 8342 s^{-1}) we measured for pTrMA for MWs from 2.4-29.2 kDa were much lower than those reported for the commonly used PEG (5.2 - 8.9 cP, shear rates 250 – 1250 s^{-1}) for MWs 1-8 kDa.[37] To directly compare pTrMA to PEG, we studied the viscosities of a range of low-MW PEGs (0.5 – 8.0 kDa) at 8342 s^{-1} from 1-100 mg mL^{-1} and verified that significantly higher viscosities were observed for PEG at 100 mg mL^{-1} (1.5 – 4.2 cP, **Figure B15**). While large macromolecules exhibit increased viscosity as a function of MW, as described by the Mark-Houwink-Sakurada equation it is well understood that this relationship is not necessarily linear. Given the low viscosity of the pTrMA polymers, it is likely that the pTrMA MWs explored herein are below a critical MW threshold and behave more like oligomers of trehalose than entangled polymers.[36] This seems reasonable since the trehalose side chain is large and thus the degree of polymerization of PEG is much higher than pTRMA at the same MW. There is a clear increase in viscosity with pTrMA concentration, but, notably, MW has no discernable impact on viscosity for concentrations below 50 mg mL^{-1} (**Figure 3.4**). Even at 100 mg mL^{-1}, viscosity only appears to be affected at the highest tested MWs (19.8 kDa and 29.2 kDa). The low viscosities measured for the pTrMA polymers are important as they are well below the threshold of solution viscosity known to be tolerable for self-injections in humans (5 cP) and are notably not much higher than water alone (0.89 cP at 25 °C).[7]

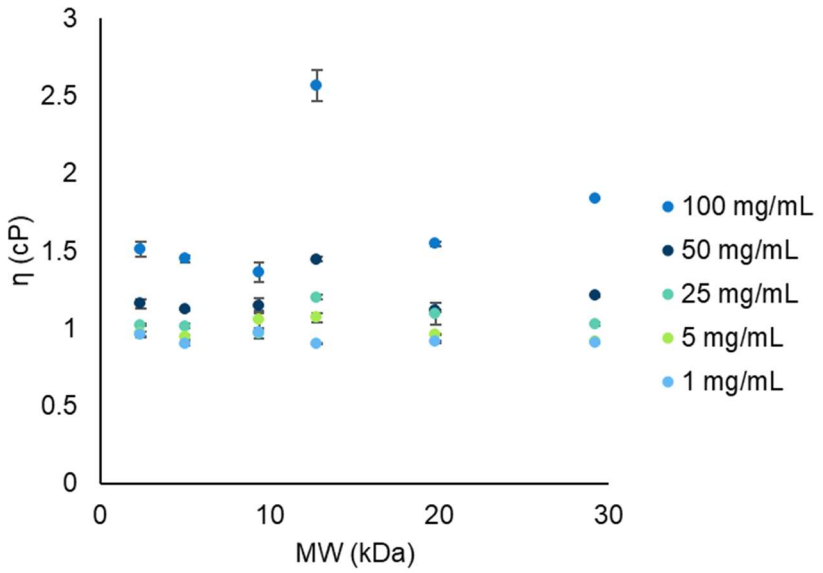

Figure 3.4 Viscosity (η, cP) of pTrMA solutions ranging from 1 mg mL^{-1} to 100 mg mL^{-1} (n = 3) at the shear rate 8342 s^{-1}.

3.2.3 Insulin Stabilization with pTrMA

We next investigated the minimum polymer concentration required to fully stabilize insulin for each MW. pTrMA stabilization of insulin was evaluated with an agitation and heating assay used previously by the group, as insulin is known to be unstable against agitation or heat.[21, 24] This assay is designed to represent insulin carried around by a patient, as there is evidence that severe diabetic ketoacidosis can result after heat exposure of insulin.[31] Polymers 2.4 kDa, 5.0 kDa, 9.4 kDa, and 12.8 kDa were mixed with insulin at 1-10 mol. eq. and 19.8 kDa and 29.2 kDa polymers were mixed with insulin at 0.1-2 mol. eq., since higher MWs should require less polymer. Stock solutions of insulin and TrMA polymers were made by dissolving with DPBS pH 7.4. Samples for each condition were prepared in triplicate by mixing insulin with polymer in a 1:1 manner. As a negative control, an insulin sample was made where DPBS only (no pTrMA) was mixed with the insulin stock. An aliquot was taken from each sample as a control and stored at 4 °C before

transferring each sample to a 1.5 mL glass vial, taping the vial horizontally for greater surface area, and agitating at 250 rpm and 37 °C for 3 h. The percent intact insulin for each MW and concentration was measured by HPLC using the area under the curve (AUC) of the insulin peak relative to a control without heat (example chromatograms see **Figure B16**). We have found that HPLC AUC does relate to *in vivo* bioactivity.[22]

From the data, it can be concluded that the minimum concentrations necessary to maintain over 95% intact insulin are 10 mol. eq. (5.0 kDa), 7.5 mol. eq. (9.4 kDa), 5 mol. eq. (12.8 kDa), 1 mol. eq. (19.8 kDa), and 0.5 mol. eq. (29.2 kDa) (**Figure 3.5** and **Figures B17-20**). For comparison, under these same stress conditions without any additive, only 13.1% insulin was detected. For MW 2.4 kDa polymer, even at 10 mol. eq. polymer the percent intact insulin was only 76.3%. It is possible that, at higher concentrations, this polymer would have reached over 95% intact insulin, although this was not tested. For the other polymers, while some of the lower concentrations stabilized insulin significantly, they did not meet the 95% threshold. It should be noted that the conditions tested were harsh, and may not represent typical storage conditions for insulin. Therefore, it is possible that lower concentrations for each polymer MW could be utilized for normal storage of the therapeutic (for example under refrigeration). It should also be noted that increasing pTrMA MW or molar concentration inevitably causes the mass concentration of pTrMA in the solution to rise. To look at this, the percent intact insulin versus net pTrMA mass concentration were also plotted (**Figure B21)**. The same trend is observed in this plot, but is not as pronounced as when looking at the stability by MW and mol. eq. Specifically, while the higher MW polymers all required low concentrations to reach 100% stabilization, the 5-12.8 kDa polymers required similar mass concentrations.

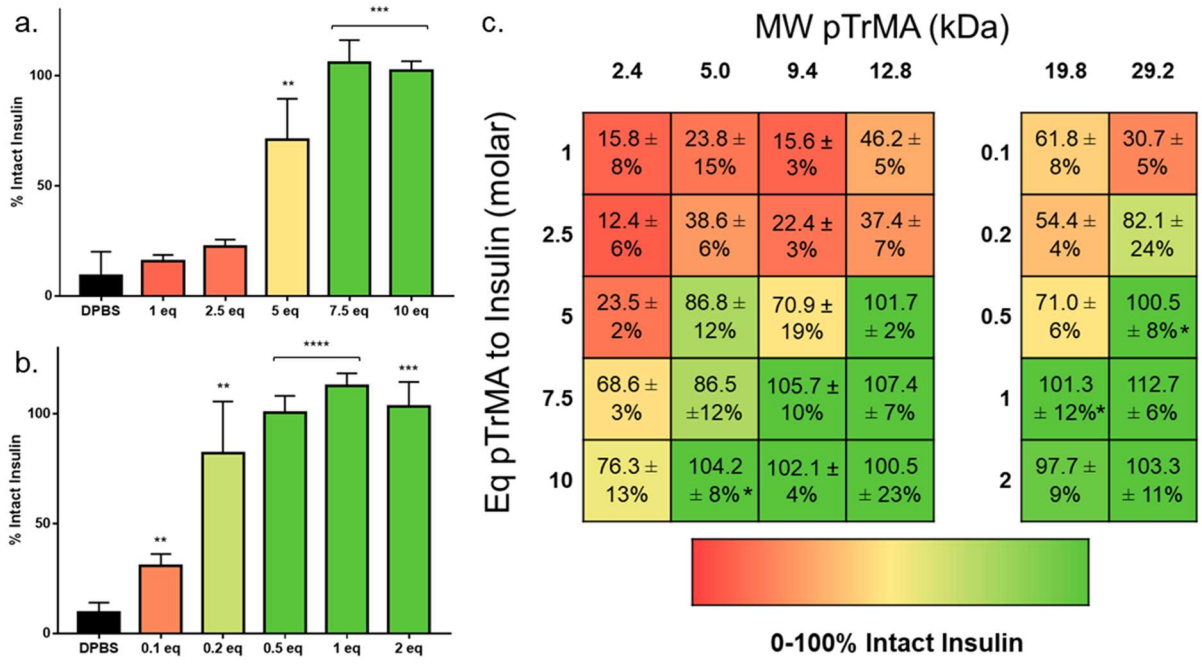

Figure 3.5 Biochemical stability assay of insulin with pTrMA of varying polymer MW and concentration after shaking at 250 rpm at 37 °C for 3 h by HPLC AUC (n = 3, **: $p < 0.01$, ***: $p < 0.001$, ****: $p < 0.0001$). Representative results of exploring an a. pTrMA (9.4 kDa) over 1-10 mol. eq. and b. higher MW pTrMA (29.2 kDa) over 0.1-2 mol. eq. to insulin. DPBS is insulin without any polymer added. c. The full range of pTrMA MWs are summarized with the heat map reporting average and standard deviation of percent intact insulin for each condition. Percent intact insulin is calculated by HPLC AUC of heated sample divided by AUC of insulin without polymer and not stressed.

3.2.4 Viscosity of pTrMA Formulated Insulin

Currently on the market, there are insulin concentrations ranging from U-100 (3.47 mg mL^{-1}) to U-500 (17.35 mg mL^{-1}), but higher concentrated formulations are expected in order to reduce the required injection volumes for those with severe insulin resistance.[33-35] Because this range of insulin concentrations is so wide, we measured viscosity of insulin alone, as well as insulin

formulated with the pTrMA polymers at U-100 (3.47 mg mL^{-1}), U-200 (6.94 mg mL^{-1}), U-400 (13.88 mg mL^{-1}), and U-600 (20.89 mg mL^{-1}) which is not yet on the market. We chose to test three MWs of pTrMA at the minimum concentrations required to provide intact insulin (indicated with an * on **Figure 3.5c**). Specifically, we added 10 mol. eq. of 5.0 kDa, 1 mol. eq. of 19.8 kDa, and 0.5 mol. eq. of 29.2 kDa to insulin. We then measured solution viscosity at both 25 and 37 °C to be relevant to storage and injection, respectively. As we have already demonstrated that pTrMA solutions have Newtonian-like behavior, we only explored viscosity at the maximum shear rate (8342 s^{-1}).

Insulin alone only marginally increased the solution viscosity above that of water (**Figure 3.6**, **Table 3.2**, and **Figure B22**), suggesting that the pTrMA polymers generated the majority effect on formulation viscosity. Viscosities of insulin formulated with these pTrMA MWs were higher than with insulin alone, but the highest viscosity measured (U-600 insulin with 10 mol. eq. of 5 kDa pTrMA) was 1.43 cP at 25 °C and 0.96 cP at 37 °C, which is still well below a tolerable viscosity (5 cP) for up to 3.5 mL injections.[7] As expected, the 0.5 mol. eq. of 29.2 kDa pTrMA produces the lowest viscosity, with the U-600 formulation measuring only 1.18 cP at 25 °C and 0.86 cP at 37 °C (**Table 3.2**).

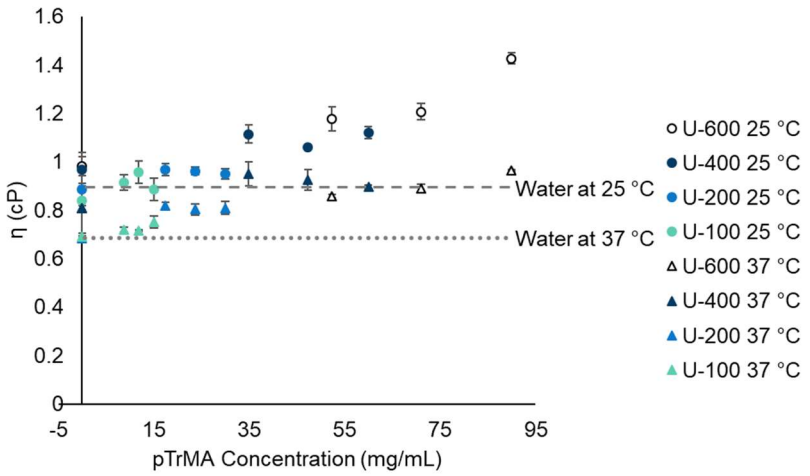

Figure 3.6 Viscosity (η, cP) at the maximum shear rate 8342 s^{-1} of insulin formulated with the requisite equivalents of pTrMA for the explored MWs (5 mol. eq. of 5.0 kDa, 1 mol. eq. of 19.8 kDa, and 0.5 mol. eq. of 29.2 kDa).

These data demonstrate that pTrMA sufficiently stabilizes the biopharmaceutical insulin without raising viscosity to unacceptable levels or creating challenging flow properties such as shear thinning or thickening. All of the polymers could maintain a greater percent intact insulin than insulin alone at the studied pTrMA concentrations, and many formulations maintained >95% intact insulin after heating and mechanical agitation. The stabilizing concentrations were found to have viscosities suitable for self-injection and only minimally increased the viscosity of insulin. Thus, pTrMA should be studied further as an excipient for insulin, and indeed, long term stability, safety and mechanism of stabilization studies were studied in Chapter 2.

Table 3.2 Viscosity (η, cP) at the maximum shear rate 8342 s^{-1} of insulin alone and formulated with the requisite equivalents of pTrMA (5 mol. eq. of 5.0 kDa, 1 mol. eq. of 19.8 kDa, and 0.5 mol. eq. of 29.2 kDa).

pTrMA MW (kDa)	pTrMA *Đ*	pTrMA Conc (mg/mL)	Insulin Conc (mg/mL)	η @ 25 °C (cP)	η @ 37 °C (cP)
0	0	0	20.89 (U-600)	0.98 ± 0.04	0.81 ± 0.01
			13.88 (U-400)	0.97 ± 0.06	0.81 ± 0.08
			6.94 (U-200)	0.89 ± 0.04	0.68 ± 0.01
			3.47 (U-100)	0.84 ± 0.01	0.69 ± 0.003
5.0	1.11	100		1.12 ± 0.01	
		50	0	1.12 ± 0.01	
		25		1.02 ± 0.01	
		5		0.94 ± 0.02	
		89.97	20.89 (U-600)	1.43 ± 0.02	0.96 ± 0.002
		59.98	13.88 (U-400)	1.17 ± 0.06	0.9 ± 0.01
		29.99	6.94 (U-200)	0.95 ± 0.02	0.81 ± 0.02
		15	3.47 (U-100)	0.89 ± 0.04	0.75 ± 0.02
19.8	1.12	100		1.55 ± 0.02	
		50	0	1.11 ± 0.01	
		25		1.09 ± 0.07	
		5		0.96 ± 0.01	
		70.98	20.89 (U-600)	1.21 ± 0.03	0.89 ± 0.02
		47.32	13.88 (U-400)	1.06 ± 0.01	0.93 ± 0.04
		23.66	6.94 (U-200)	0.96 ± 0.01	0.8 ± 0.02
		11.83	3.47 (U-100)	0.96 ± 0.04	0.72 ± 0.003
29.2	2.03	100		1.84 ± 0.005	
		50	0	1.21 ± 0.01	
		25		1.03 ± 0.01	
		5		0.91 ± 0.01	
		52.34	20.89 (U-600)	1.18 ± 0.05	0.86 ± 0.01
		34.89	13.88 (U-400)	1.11 ± 0.03	0.95 ± 0.04
		17.45	6.94 (U-200)	0.96 ± 0.02	0.82 ± 0.01
		8.72	3.47 (U-100)	0.92 ± 0.03	0.72 ± 0.01

3.3 Conclusions

Major challenges in treating chronic conditions with biopharmaceuticals are injection administration and stability against environmental stress. Injection is often the best administrative route for therapeutic proteins due to bioavailability, onset of activity, and difficulties with oral delivery. However, the inconvenience and pain associated with biopharmaceuticals and self-injection negatively impact the treatment experience for patients and can result in poor compliance and dosing adherence. We showed that the MW and concentration of pTrMA can be successfully optimized to stabilize insulin using minimal polymer, advantageous for financial and fluid viscosity reasons. The polymer itself exhibits Newtonian behavior and viscosity below a known threshold of tolerability, which is a favorable attribute for patient self-administration. Moreover, formulations of the 5.0 kDa, 19.8 kDa, and 29.2 kDa pTrMA polymers maintained intact insulin after extreme heating and agitation and have relatively low insulin formulation viscosities which offers the possibility of improved manufacturing, transportation, and storage options for insulin and potentially for other biopharmaceuticals. To verify the efficacy of pTrMA more broadly as a protein stabilizer, the polymer's stabilization efficacy for other antibodies is further explored in Chapter 4.

3.4 Experimental Section

3.4.1 Materials

Chemicals were all purchased from Sigma Aldrich or Fisher Scientific and used without further purification unless otherwise mentioned. Trehalose was purchased from BulkSupplements.com (Henderson, NV) and repeatedly azeotropically dried from ethanol and stored under vacuum. Spectra/Por3® regenerated cellulose membrane (MWCO 1.0 kDa or 3.5

kDa) was purchased from Spectrum Chemical (New Brunswick, NJ) for polymer dialysis. Recombinant human insulin was purchased from Sigma-Aldrich (Lot no. 17N331). Cuprisorb was purchased from Amazon.com. Initiator, trehalose methacrylate monomer (TrMA), and pTrMA polymers were synthesized according to literature and described below.[20, 23]

3.4.2 Analytical Techniques

NMR spectroscopy were performed on a Bruker AV 400 MHz or AV 500 MHz instrument. ^{1}H-NMR spectra were acquired with a relaxation delay of 2 s for small molecules and 30 s for polymers. Preparatory HPLC purification was performed on a Shimadzu HPLC system equipped with a UV detector using a Luna 5 µm C18 100 Å column (preparatory: 5 µm, 250 x 21.2 mm) with monitoring at λ = 215 nm and 254 nm. Aqueous GPC was conducted on a Malvern Viscotek GPCMax system equipped with a triple detector array (TDA 305-040 Quadruple Detector Array), with two Viscotek A600 M general mixed aq. Columns (300x8.0mm). The eluent was 20% methanol in water at a flow rate of 1 mL/min. Near-monodisperse PEG standards from Polymer Labs were used for calibration. Viscosity was measured using a RheoSense microVisc (San Ramon, CA). Analytical HPLC for insulin detection was conducted on an Agilent 1260 Infinity II LC System equipped with a UV detector and Poroshell 2.7 µm Bonus-RP C18 120 Å column (4.6 x 100mm) with a gradient of 25-90% acetonitrile/water + 0.1% trifluoroacetic acid over 6 min with insulin eluting at 4.3 min.

3.4.3 Methods

Synthesis of methacrylate trehalose monomer (TrMA)

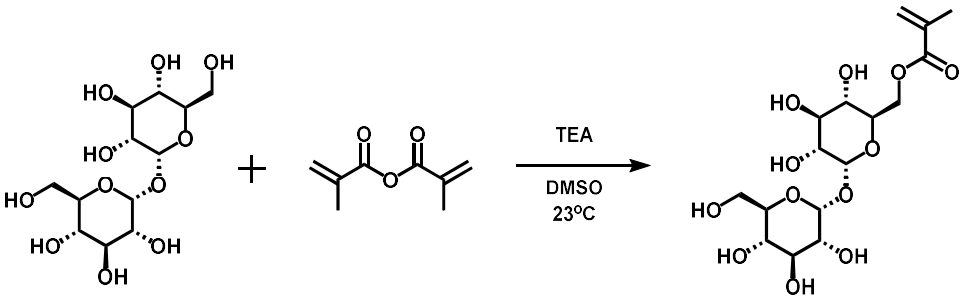

The methacrylate functionalized trehalose monomer (TrMA) was synthesized from literature procedure.[20] In a flame-dried round bottom flask was added trehalose (4.6 g, 13.4 mmol) with anhydrous dimethyl sulfoxide (DMSO, 60 mL). Next anhydrous trimethylamine (TEA, 5.6 mL, 40.2 mmol) and methacrylic anhydride (400 µL, 2.7 mmol) were added, and the mixture was stirred at 23 °C for 18 h. DMSO was removed by precipitating into 0 °C hexanes and dichloromethane (8:2, 1400 mL). The organic layer was decanted and remaining organics were removed from the viscous liquid by rotary evaporation. The crude product was diluted with water before filtering and purifying by preparatory HPLC with a gradient of methanol in water (10-50%, TrMA elutes at 14 min, 25% methanol). To the product containing fractions, mequinol was added to prevent autopolymerization. Solvents were removed by rotary evaporation using a 2-neck flask equipped with a septa and long needle directly into the solution to further prevent autopolymerization by providing a source of oxygen. The product was finally recovered by lyophilization (418.4 mg, 30.1% yield). ^{1}H-NMR agreed with that previously reported: ^{1}H NMR (400 MHz, D_2O) δ: 6.01 (s, 1H), 5.60 (s, 1H), 5.04 (d, J = 3.5 Hz, 1H), 5.01 (d, J = 3.5 Hz, 1H), 4.35 (d, J = 12.5 Hz, 1H), 4.24 (dd, J = 12.5, 5.2 Hz, 1H), 3.94 (dd, J = 10.0, 5.2 Hz, 1H), 3.69 (m, 4H), 3.62 (m, 1H), 3.50 (ddd, J = 19.4, 13.5, 6.1 Hz, 1H), 3.40 (t, J = 9.5 Hz, 1H), 3.29 (t, J = 9.5 Hz, 1H), 1.79 (s, 3H).

Synthesis of 2-hydroxyethyl 2-bromoisobutyrate (HEBIB)

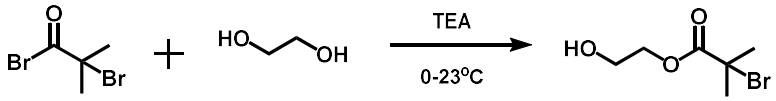

HEBIB was synthesized according to literature procedure.[39] Ethylene glycol (1.33 mL, 23.8 mmol, anhydrous) and anhydrous TEA (0.66 mL, 4.7 mmol) were stirred together and cooled to 0 °C before dropwise adding α-bromoisobutyryl bromide (0.59 mL, 4.7 mmol). The reaction mixture was stirred for 2 h at 0 °C before warming up to 23 °C to stir an additional 12 h. Water (10 mL) was added to the flask and extracted with chloroform three times (10 mL each time). The chloroform layer was washed with dilute hydrochloric acid, saturated sodium bicarbonate ($NaHCO_3$), and water (10 mL each wash). The organic layer was dried over anhydrous magnesium sulfate ($MgSO_4$), filtered, and the product was recovered after rotary evaporation. The product was purified by silica gel flash chromatography with an eluent system of diethyl ether and hexanes (1:1). The product containing fractions were collected and recovered product as a yellow-clear oil by rotary evaporation (658 mg, 65% yield). ^{1}H-NMR agreed with that reported for this compound: ^{1}H NMR (400 MHz, $CDCl_3$) δ: 4.32 (t, J = 4.6 Hz, 2H), 3.87 (t, J = 4.6 Hz, 2H), 1.95 (s, 6H).

Representative AGET ATRP of methacrylate trehalose monomer (TrMA) with HEBIB initiator

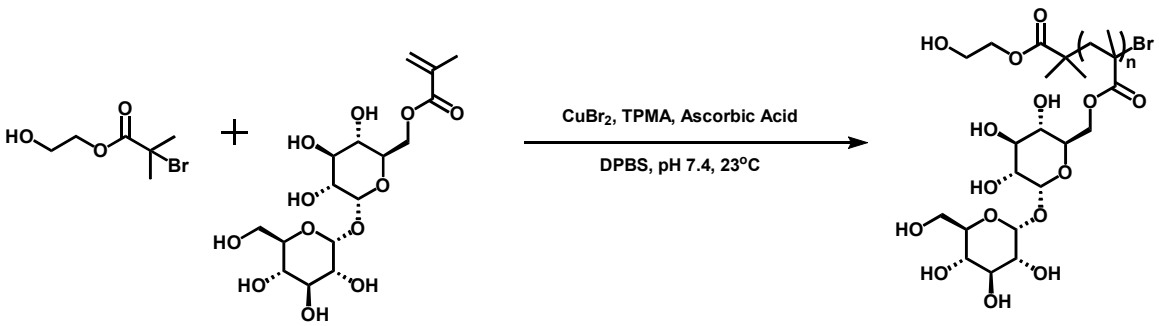

Polymerization was performed according to literature procedure.[23] 0.1 M Dulbecco's phosphate-buffered saline (DPBS) pH 7.4 was degassed by sparging with argon for at least 1 h. Ascorbic acid (AA) was dissolved in DPBS (10 mg mL^{-1}) and degassed for >30 minutes. TrMA (400 mg, 0.97 mmol) was added to an oven-dried Schlenk flask equipped with a stir bar, and the flask was evacuated and refilled with argon four times. A stock solution of copper(II) bromide ($CuBr_2$) and tris(2-pyridylmethyl)amine (TPMA) were prepared using degassed DPBS at 5 mg mL^{-1} and 6.75 mg mL^{-1}, respectively. Dissolved HEBIB initiator (7.6 mg, 34.8 µmol) with the $CuBr_2$ and TPMA solution (7.8 mg, 34.8 µmol and 10.1 mg, 34.8 µmol), and then transferred to the flask under argon. AA solution (3.7 mg, 20.9 µmol) was added to the flask under argon to initiate the polymerization for a final TrMA concentration of 0.45 M. The polymerization proceeded under argon in a water bath at 25 °C for 15 h. The polymerization was ended by exposing to air, and the polymer was dialyzed against water (3.5 kDa MWCO) with Curpisorb, a metal-chelating resin, to chelate copper for 2 days (8 L water). Recovered polymer was a fluffy white solid after lyophilization (261.2 mg, 75% yield). ^{1}H-NMR agreed with that previously reported: ^{1}H NMR (400 MHz, D_2O) δ: 5.07, 4.23, 4.03, 3.92, 3.72, 3.51, 3.33, 1.83, 1.48, 1.04, 0.93, 0.77. Target MW of 10 kDa, experimental *Mn* of 12.8 kDa (by SEC with PEG standards, 5 mg mL^{-1}, dn/dc = 0.15), MW dispersity (*Đ*) = 1.59.

Viscosity Measurements

The microVisc is a microfluidics based slit-viscometer that measures the pressure drop from fluid flowing through the microchannel as a function of flow rate to calculate fluid viscosity. Samples are injected into the microfluidics chip with a 50 µm flow channel (A05) at programmed rates using the built-in syringe pump. Each MW of pTrMA was dissolved at 100 mg $mL^{-1}$and solutions were diluted to reach 50 mg mL^{-1}, 25 mg mL^{-1}, 10 mg mL^{-1}, 5 mg mL^{-1}, and 1 mg mL^{-1}.

Insulin formulations were made by dissolving insulin in the minimum necessary 0.1 M HCl to dissolve insulin and then diluting with 0.1 M PBS pH 7.4 to reach insulin concentrations of U-100 (3.47 mg mL^{-1}), U-200 (6.94 mg mL^{-1}), U-400 (13.88 mg mL^{-1}), and U-600 (20.89 mg mL^{-1}). The insulin solution was then used to dissolve the desired pTrMA for their respective concentrations. All pTrMA measurements were performed in triplicate at 25 °C with shear rates starting at 8342 s^{-1} and decreasing by half (4071 s^{-1}, 2085.5 s^{-1}, 1042.8 s^{-1}, and 521.4 s^{-1}) until the pressure drop was below the instrument's measurable threshold (pressure-scale <5%). Selected insulin formulations were also measured in triplicate and at both 25 and 37 °C but only at the maximum shear (8342 s^{-1}). Summarized results are reported only for the maximum shear rate with all formulations (**Table 3.2**).

Stabilization of insulin with pTrMA

Insulin stabilization was measured according to literature procedure.[21, 24] Briefly, insulin was dissolved at 2 mg mL^{-1} in 0.1 M DPBS pH 7.4. pTrMA was dissolved at 100 mg mL^{-1} in 0.1 M DPBS pH 7.4 and then diluted to the requisite mol. eq. to insulin (0.1, 0.2, 0.5, 1, 2.5, 5, 7.5, or 10 mol. eq.). Insulin solution 1:1 with pTrMA solutions (n =3) were mixed and a reference time-point taken from each sample prior to heat and shaking, followed by storing at 4 °C until analysis. Mixed solutions (200 µL) were added to 1.5 mL clear glass screw-top vials, samples were taped horizontally for maximum surface area, and shaken at 250 rpm for 3 h in the incubating shaker set to 37 °C. Samples were filtered (0.22 µm) to remove insulin aggregates and analyzed by RP-HPLC, and the 4 °C reference was used to quantify percent intact insulin.

3.4.4 Statistical Analysis

All experimental values are reported as the average ± SEM. Graph Pad Prism 7 (GraphPad Software, San Diego, USA) was used for the statistical analyses. To assess the statistical

significance of differences between control and stressed insulin samples, the paired, two-tailed Student's t-test was conducted assuming unequal sample variance. For experiments with greater than two groups, one-way analysis of variance (ANOVA) followed by Tukey's test was employed to compare the means and determine the significance of the differences. Results were considered significantly different if $p < 0.05$ (*); results are also reported with $p < 0.01$ (**), $p < 0.001$ (***), and $p < 0.0001$ (****).

3.5 Appendix B

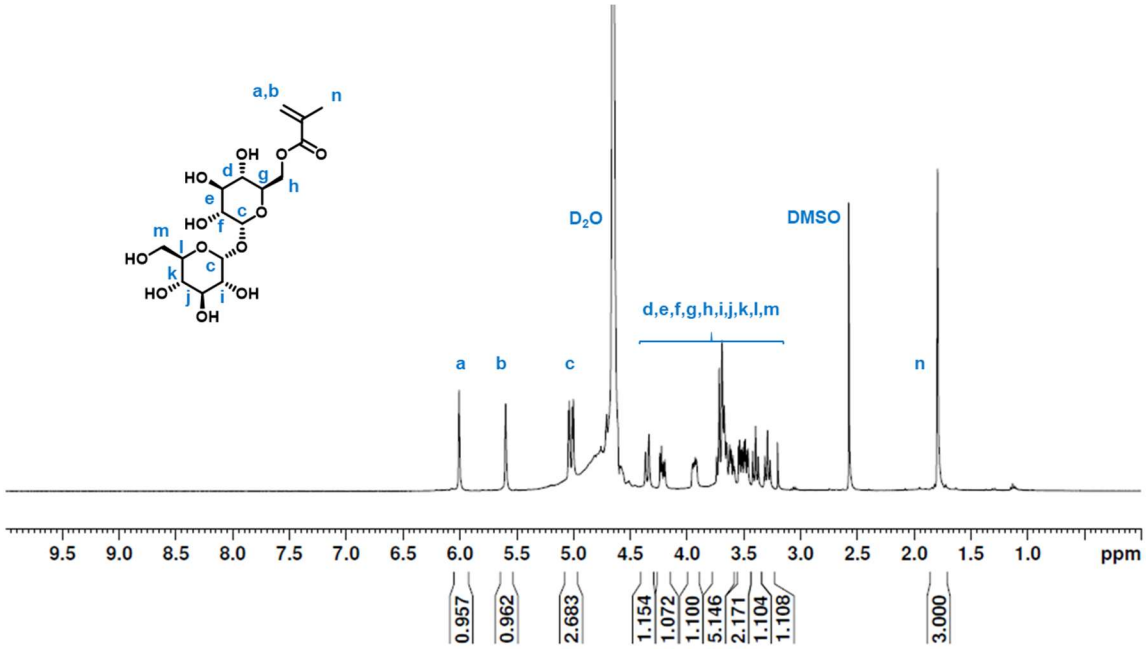

Figure B1 ^{1}H NMR spectrum (400 MHz, D_2O) of methacrylate trehalose (MA-T). ^{1}H-NMR agreed with that reported for this compound.[20]

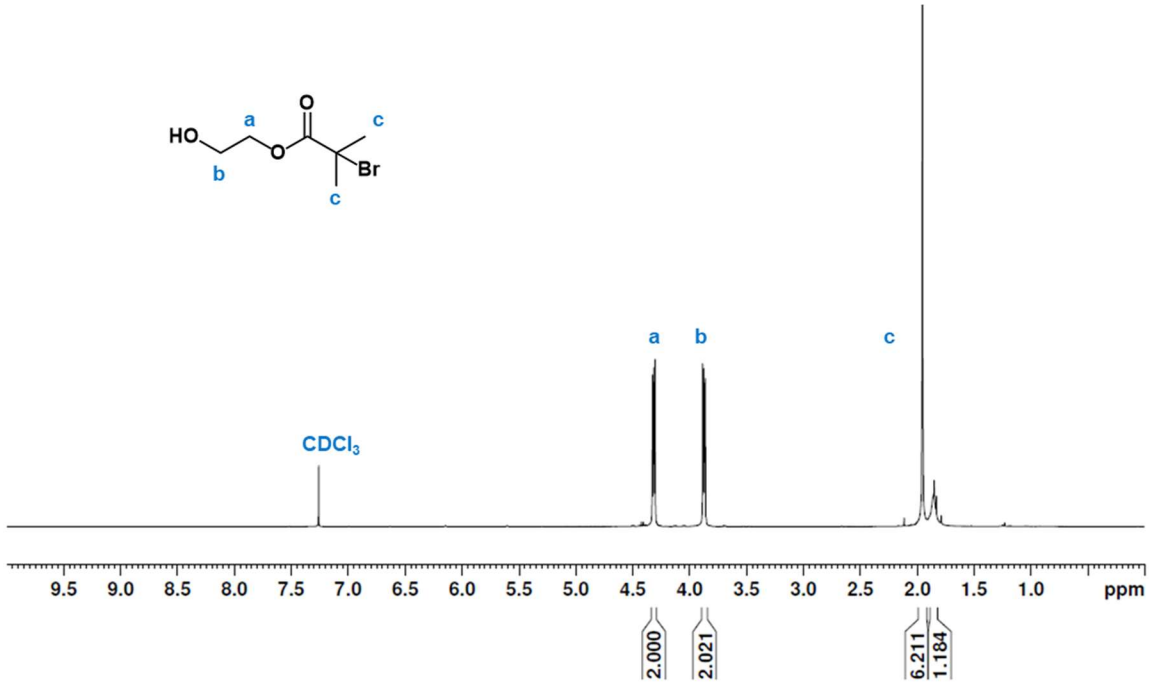

Figure B2 ^{1}H NMR spectrum (400 MHz, $CDCl_3$) of 2-hydroxyethyl 2-bromoisobutyrate (HEBIB) initiator. ^{1}H-NMR agreed with that reported for this compound.[39]

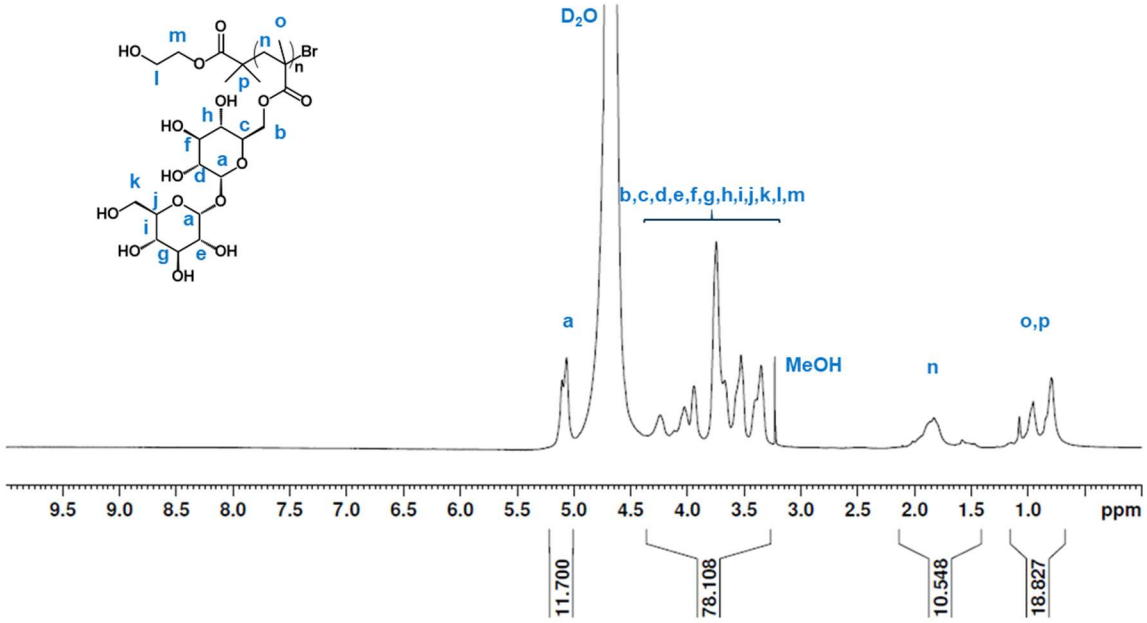

Figure B3 ^{1}H NMR spectrum (400 MHz, D_2O) of pTrMA 2.4 kDa polymerized with HEBIB initiator. ^{1}H-NMR agreed with that reported for this compound.[23]

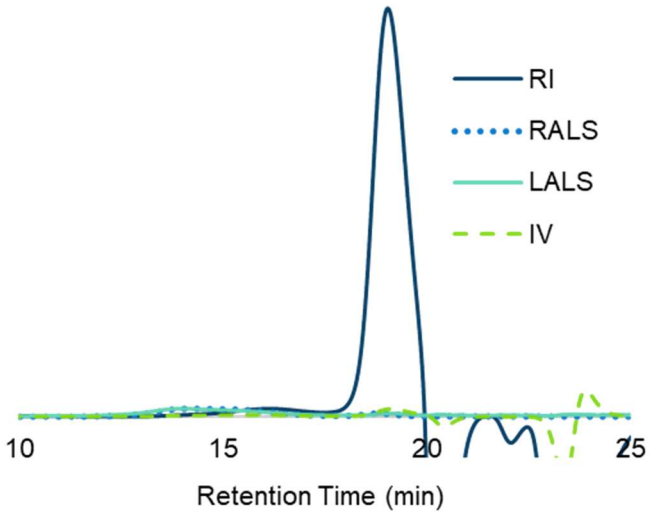

Figure B4 GPC (PEG standards) of pTrMA with HEBIB initiator. M_n = 2.4 kDa, $\cancel{D}$ = 1.26.

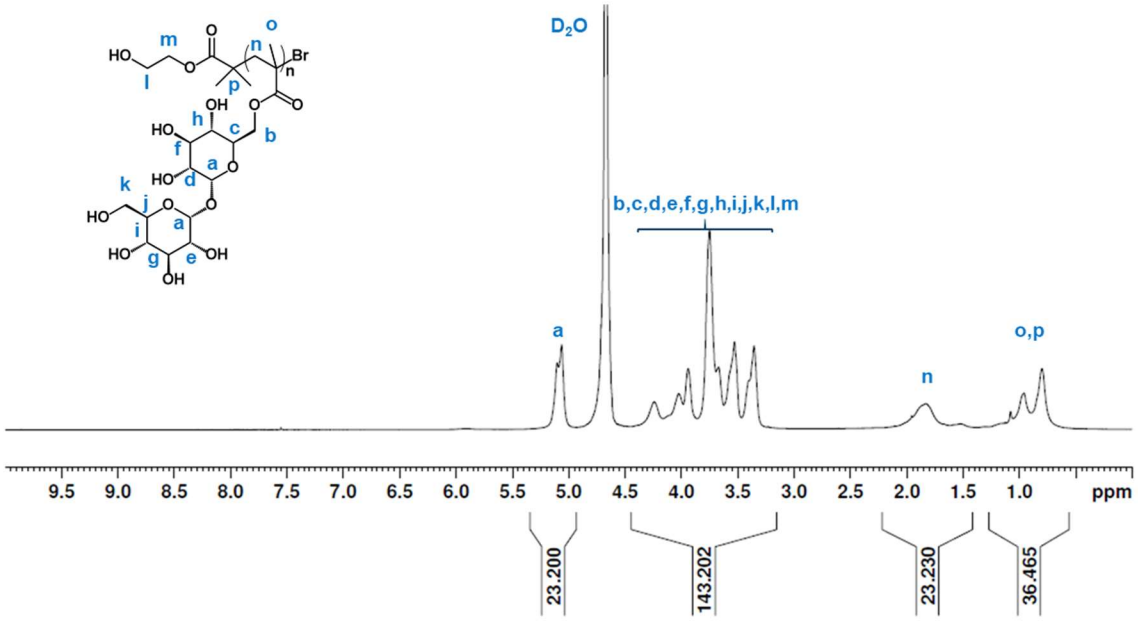

Figure B5 ^{1}H NMR spectrum (400 MHz, D_2O) of pTrMA 5.0 kDa polymerized with HEBIB initiator. ^{1}H-NMR agreed with that reported for this compound.

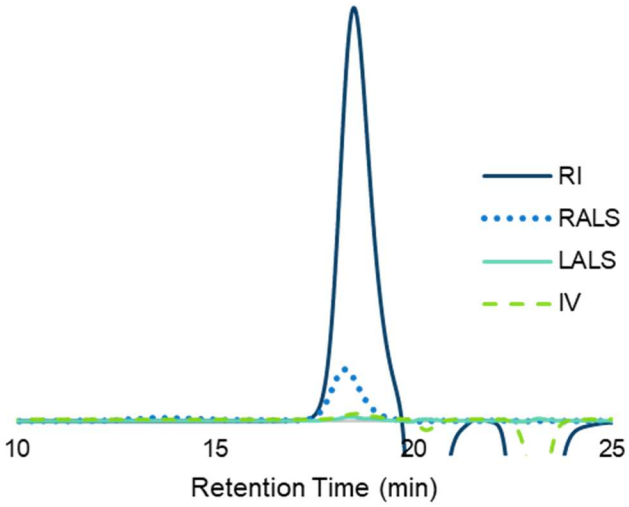

Figure B6 GPC (PEG standards) of pTrMA with HEBIB initiator. M_n = 5.0 kDa, $\cancel{D}$ = 1.25.

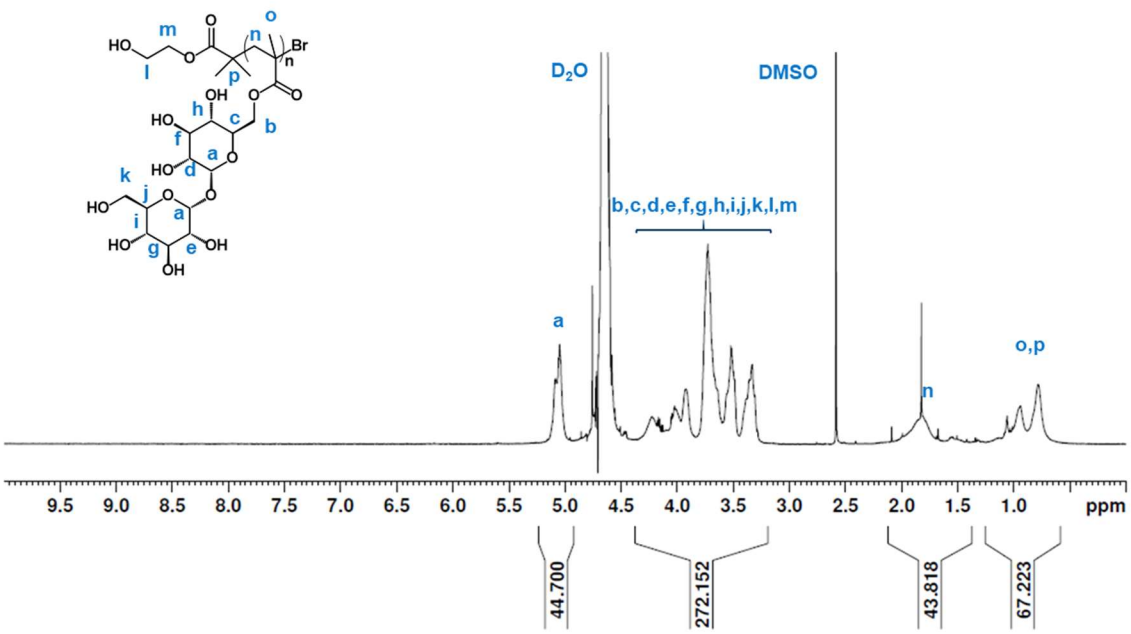

Figure B7 ^{1}H NMR spectrum (400 MHz, D_2O) of pTrMA 9.4 kDa polymerized with HEBIB initiator. ^{1}H-NMR agreed with that reported for this compound.

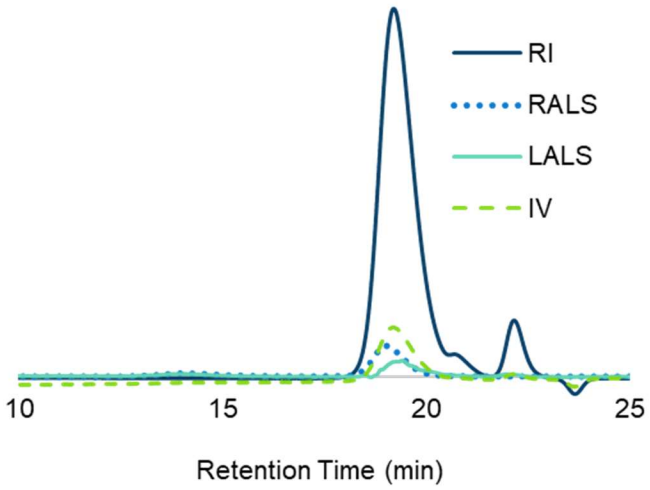

Figure B8 GPC (PEG standards) of pTrMA with HEBIB initiator. M_n = 9.4 kDa, $\cancel{D}$ = 1.10.

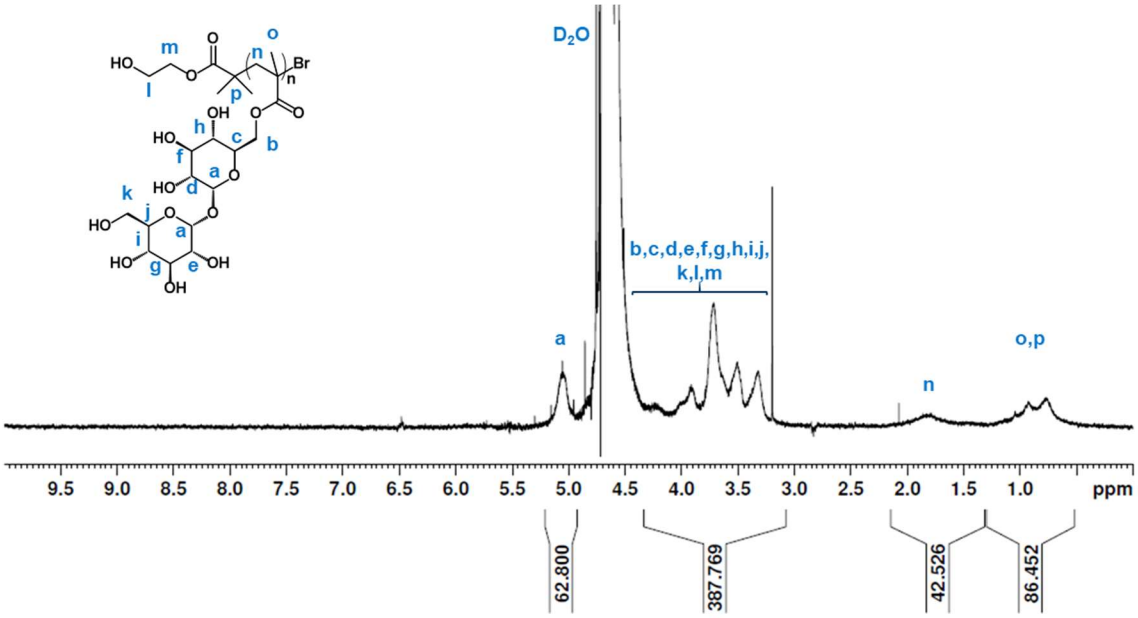

Figure B9 ^{1}H NMR spectrum (400 MHz, D_2O) of pTrMA 12.8 kDa polymerized with HEBIB initiator. ^{1}H-NMR agreed with that reported for this compound.

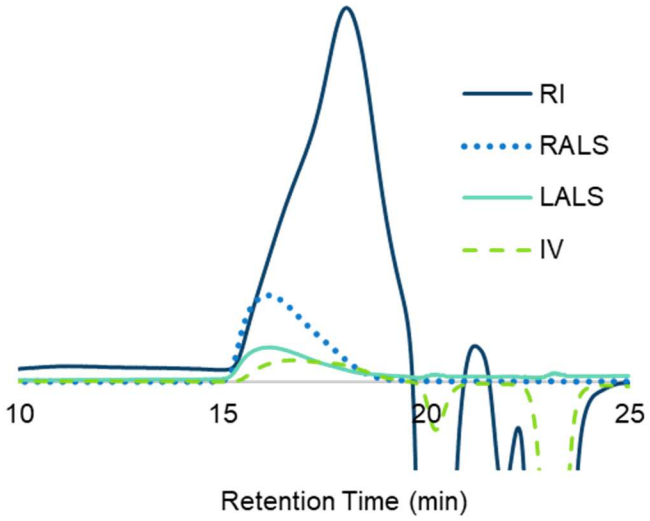

Figure B10 GPC (PEG standards) of pTrMA with HEBIB initiator. M_n = 12.8 kDa, $\cancel{D}$ = 1.59.

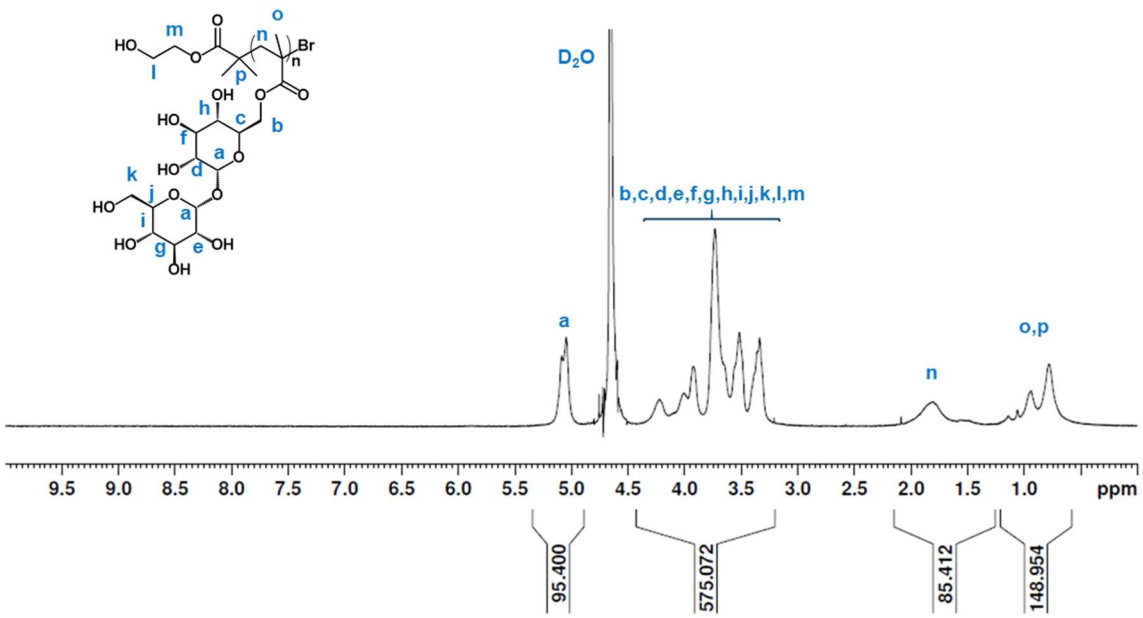

Figure B11 ^{1}H NMR spectrum (400 MHz, D_2O) of pTrMA 19.8 kDa polymerized with HEBIB initiator. ^{1}H-NMR agreed with that reported for this compound.

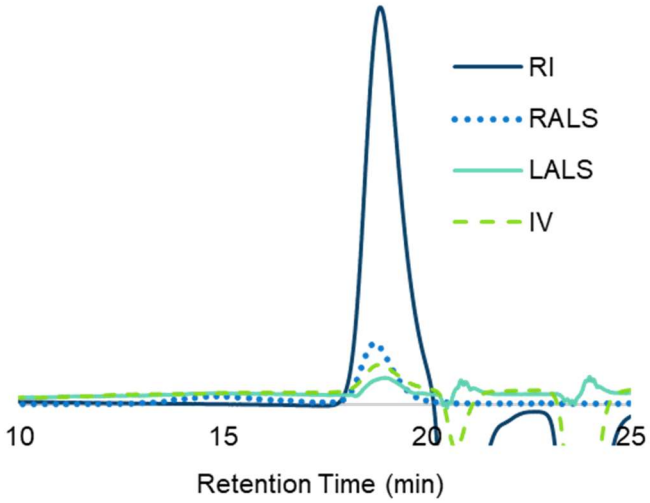

Figure B12 GPC (PEG standards) of pTrMA with HEBIB initiator. M_n = 19.8 kDa, $\cancel{D}$ = 1.12.

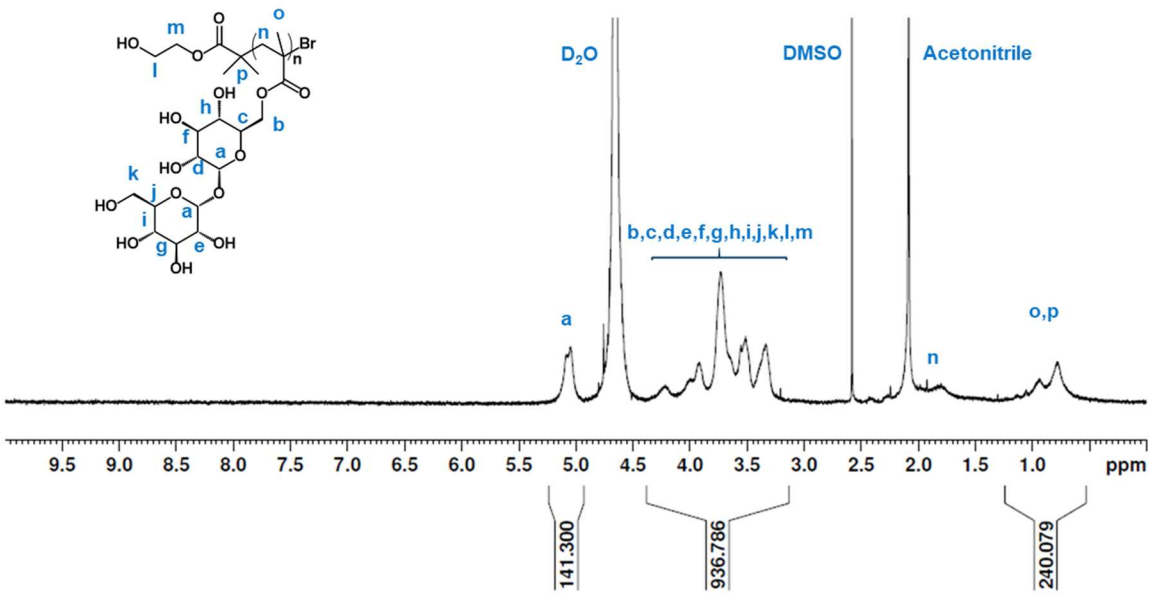

Figure B13 ^{1}H NMR spectrum (400 MHz, D_2O) of pTrMA 29.2 kDa polymerized with HEBIB initiator. ^{1}H-NMR agreed with that reported for this compound.

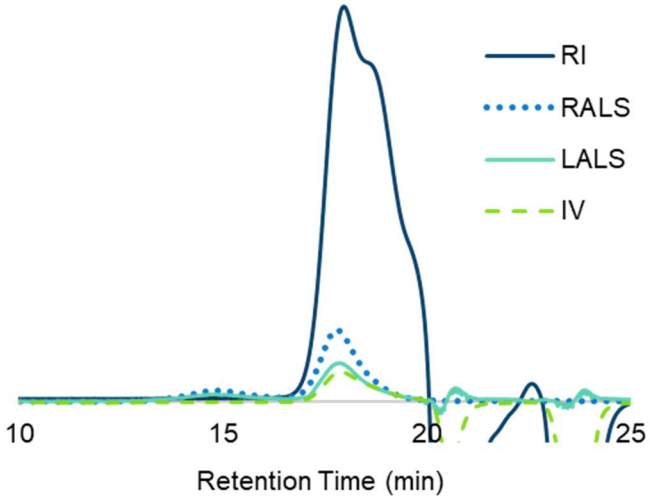

Figure B14 GPC (PEG standards) of pTrMA with HEBIB initiator. M_n = 29.2 kDa, $\cancel{D}$ = 2.03.

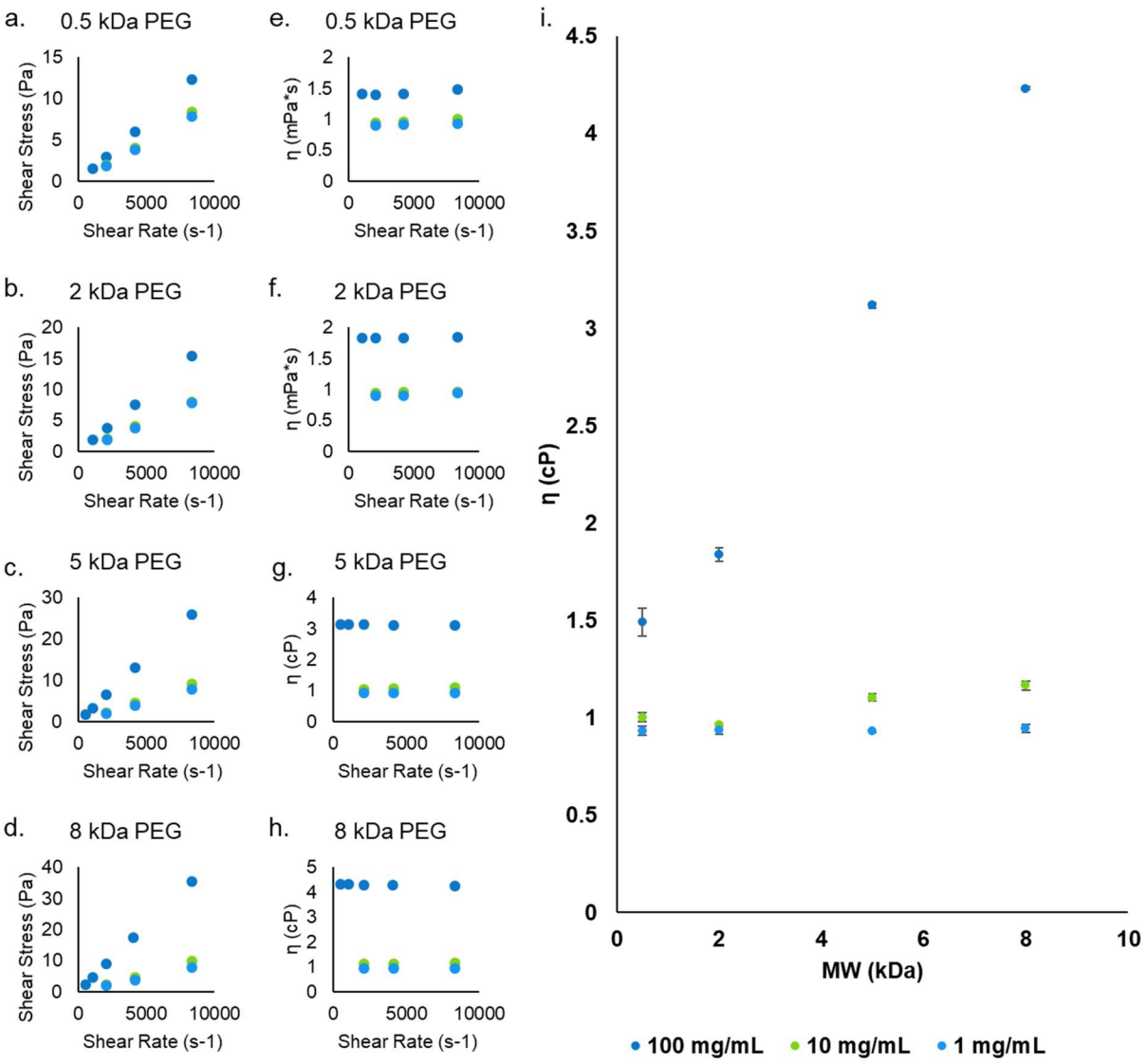

Figure B15 Shear stress (Pa) (a.-d.) and viscosity (η, cP) (e.-h.) measurements of PEG solutions of 1 mg mL^{-1} to 100 mg mL^{-1} (n = 3) over the allowable shear rates (s^{-1}) for PEG MW's of 0.5 kDa (a., e.), 2.0 kDa (b., f.), 5.0 kDa (c., g.), and 8.0 kDa (d., h.). The PEG solutions were clearly Newtonian across the MWs and concentrations, but the i. viscosity measurements (shear rate 8342 s^{-1}) at the highest concentration showed a clear linear dependence on MW.

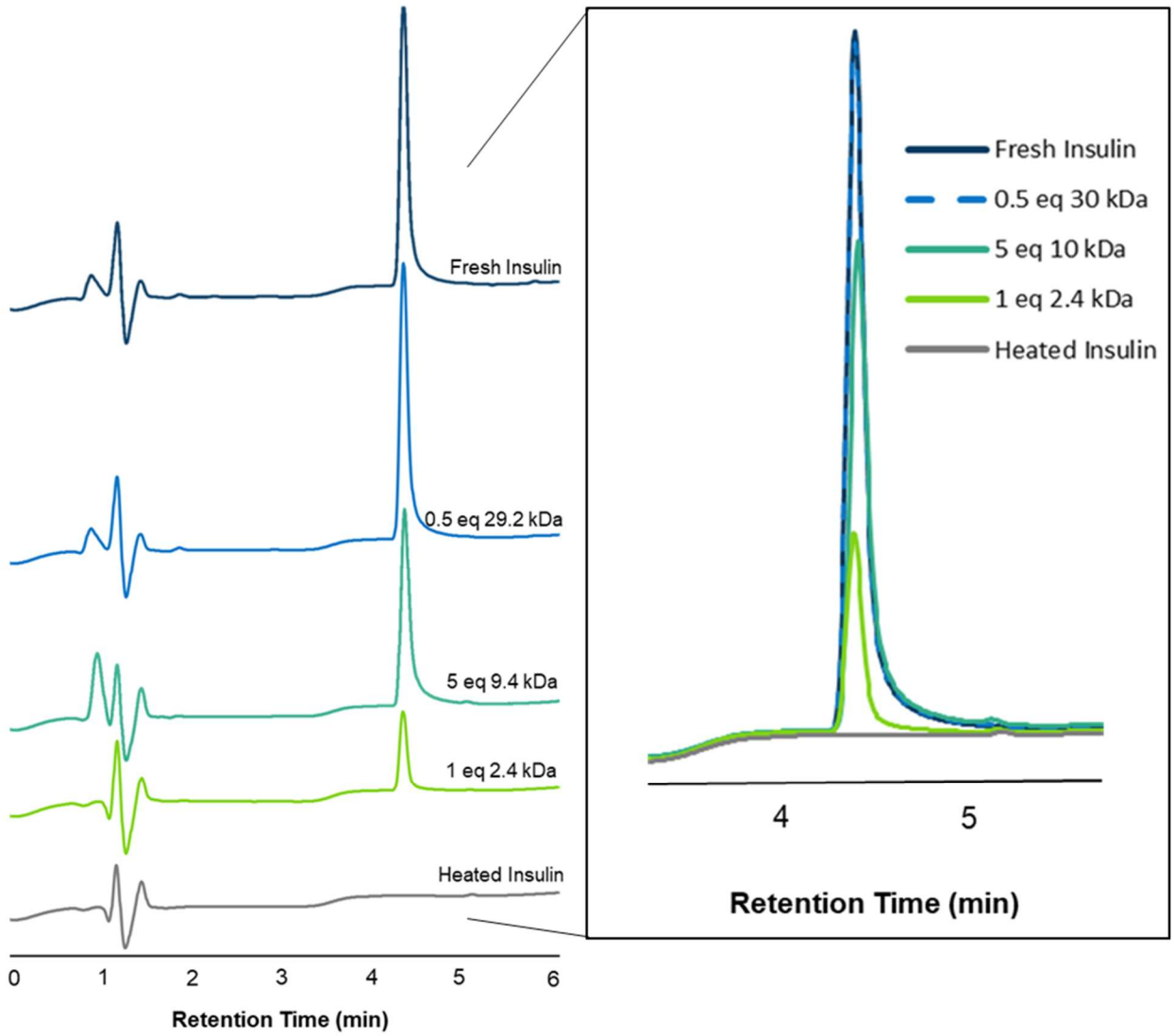

Figure B16 HPLC (220 nm) chromatograms of insulin from the biochemical stability assay stressed by shaking at 250 rpm and heating to 37 °C for 3 h. Left side from top to bottom: Unstressed insulin, stressed insulin with 1 mol. eq. of 2.4 kDa pTrMA, 5 mol. eq. of 9.4 kDa pTrMA, and 0.5 mol. eq. of 29.2 kDa pTrMA added, and insulin stressed without polymer. Right: Insulin peak at 4.3 min overlaid from chromatograms on the left.

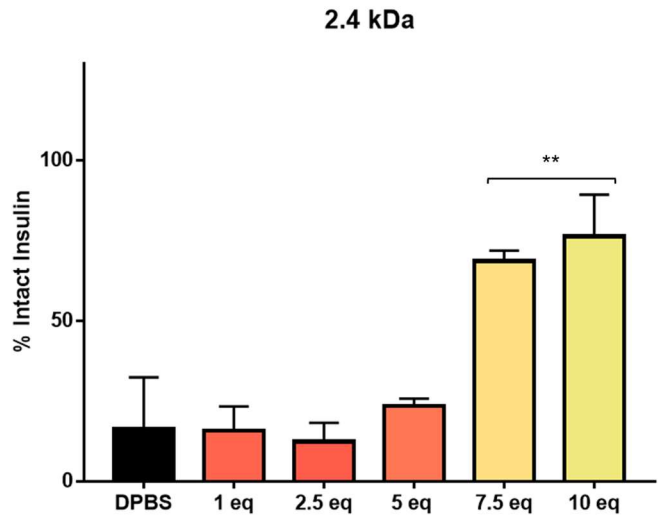

Figure B17 Percent intact insulin without polymer (DPBS) and with 1-10 eq of 2.4 kDa pTrMA after shaking at 250 rpm and heating to 37 °C for 3 h. The percent intact insulin for each sample was determined by HPLC AUC (n = 3, **: $p < 0.01$) compared to the same sample not stressed.

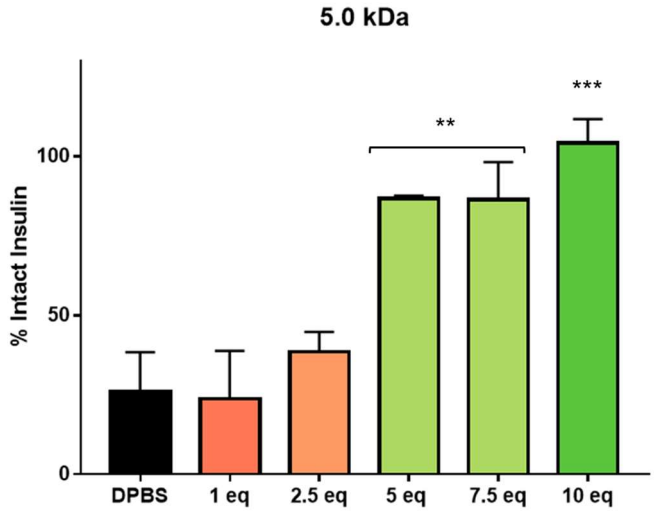

Figure B18 Percent intact insulin without polymer (DPBS) and with 1-10 eq of 5.0 kDa pTrMA after shaking at 250 rpm and heating to 37 °C for 3 h. The percent intact insulin for each sample was determined by HPLC AUC (n = 3, **: $p < 0.01$, ***: $p < 0.001$) compared to the same sample not stressed.

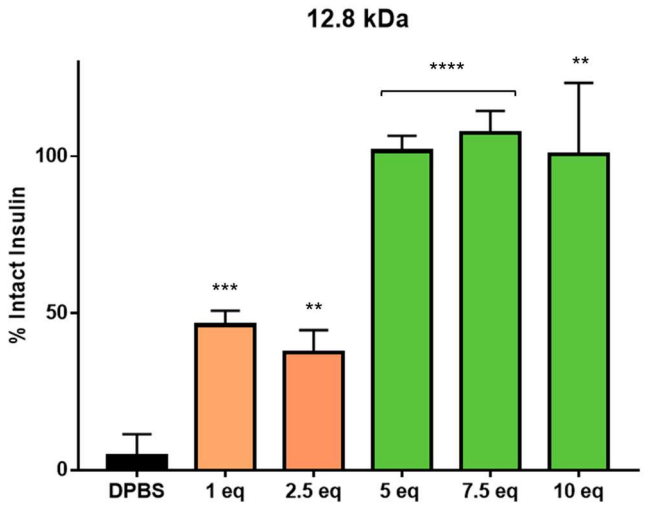

Figure B19 Percent intact insulin without polymer (DPBS) and with 1-10 eq of 12.8 kDa pTrMA after shaking at 250 rpm and heating to 37 °C for 3 h. The percent intact insulin for each sample was determined by HPLC AUC (n = 3, **: $p < 0.01$, ***: $p < 0.001$, ****: $p < 0.0001$) compared to the same sample not stressed.

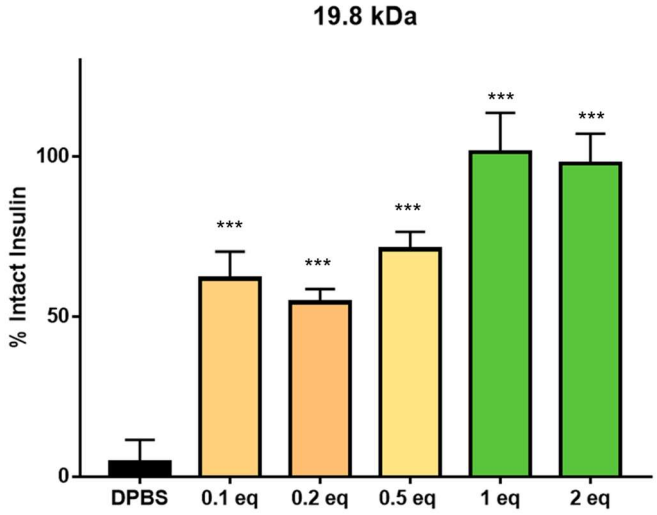

Figure B20 Percent intact insulin without polymer (DPBS) and with 0.1-2 eq of 19.8 kDa pTrMA after shaking at 250 rpm and heating to 37 °C for 3 h. The percent intact insulin for each sample was determined by by HPLC AUC (n = 3, ***: $p < 0.001$) compared to the same sample not stressed.

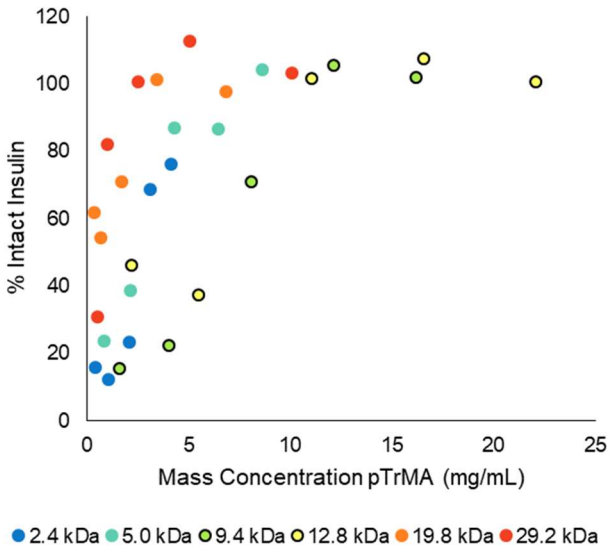

Figure B21 Biochemical stability assay (3 h of agitation at 250 rpm at 37 °C) of insulin as a function of mass concentration of pTrMA. Percent intact insulin is measured by comparing the AUC of the intact insulin peak to the fresh control sample.

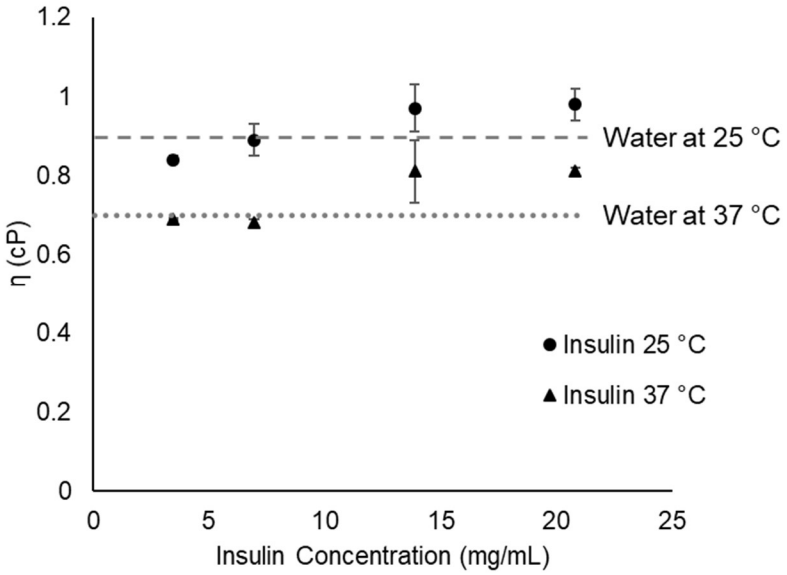

Figure B22 Viscosity (η, cP) at the maximum shear rate 8342 s^{-1} of insulin at U-100 (3.47 mg/mL), U-200 (6.94 mg/mL), U-400 (13.88 mg/mL), and U-600 (20.89 mg/mL).

References

1. Walsh, G., Biopharmaceutical benchmarks 2018. *Nat. Biotechnol.* **2018,** *36* (12), 1136-1145.

2. Leader, B.; Baca, Q. J.; Golan, D. E., Protein therapeutics: A summary and pharmacological classification. *Nat. Rev. Drug Discov.* **2008,** *7* (1), 21-39.

3. Moncalvo, F.; Martinez Espinoza, M. I.; Cellesi, F., Nanosized Delivery Systems for Therapeutic Proteins: Clinically Validated Technologies and Advanced Development Strategies. *Front. Bioeng. Biotechnol.* **2020,** *8*, 89-89.

4. Usach, I.; Martinez, R.; Festini, T.; Peris, J.-E., Subcutaneous Injection of Drugs: Literature Review of Factors Influencing Pain Sensation at the Injection Site. *Adv. Ther.* **2019,** *36* (11), 2986-2996.

5. Fernandez, J. M.; Madsen, S.; Krase, J. M.; Shi, V. Y., Classification and mitigation of negative injection experiences with biologic medications. *Dermatol. Ther.* **2020,** *33* (2), e13240.

6. Bolge, S. C.; Goren, A.; Tandon, N., Reasons for discontinuation of subcutaneous biologic therapy in the treatment of rheumatoid arthritis: a patient perspective. *Patient Prefer. Adherence* **2015,** *9*, 121-131.

7. Dias, C.; Abosaleem, B.; Crispino, C.; Gao, B.; Shaywitz, A., Tolerability of High-Volume Subcutaneous Injections of a Viscous Placebo Buffer: A Randomized, Crossover Study in Healthy Subjects. *AAPS PharmSciTech* **2015,** *16* (5), 1101-1107.

8. Kamerzell, T. J.; Esfandiary, R.; Joshi, S. B.; Middaugh, C. R.; Volkin, D. B., Protein–excipient interactions: Mechanisms and biophysical characterization applied to protein formulation development. *Adv. Drug Delivery Rev.* **2011,** *63* (13), 1118-1159.

9. Rao, V. A.; Kim, J. J.; Patel, D. S.; Rains, K.; Estoll, C. R., A Comprehensive Scientific Survey of Excipients Used in Currently Marketed, Therapeutic Biological Drug Products. *Pharm. Res.* **2020,** *37* (10), 200.

10. Chen, B.; Bautista, R.; Yu, K.; Zapata, G. A.; Mulkerrin, M. G.; Chamow, S. M., Influence of histidine on the stability and physical properties of a fully human antibody in aqueous and solid forms. *Pharm. Res.* **2003,** *20* (12), 1952-60.

11. Arakawa, T.; Tsumoto, K.; Kita, Y.; Chang, B.; Ejima, D., Biotechnology applications of amino acids in protein purification and formulations. *Amino Acids* **2007,** *33* (4), 587-605.

12. Arakawa, T.; Timasheff, S. N., The stabilization of proteins by osmolytes. *Biophys. J.* **1985,** *47* (3), 411-414.

13. Auton, M.; Bolen, D. W.; Rösgen, J., Structural thermodynamics of protein preferential solvation: Osmolyte solvation of proteins, aminoacids, and peptides. *Proteins: Struct., Funct., Bioinf.* **2008,** *73* (4), 802-813.

14. Arsiccio, A.; Giorsello, P.; Marenco, L.; Pisano, R., Considerations on Protein Stability During Freezing and Its Impact on the Freeze-Drying Cycle: A Design Space Approach. *J. Pharm. Sci.* **2020,** *109* (1), 464-475.

15. Nguyen, T. H.; Kim, S.-H.; Decker, C. G.; Wong, D. Y.; Loo, J. A.; Maynard, H. D., A heparin-mimicking polymer conjugate stabilizes basic fibroblast growth factor. *Nat. Chem.* **2013,** *5*, 221.

16. Mazzaferro, L.; Breccia, J. D.; Andersson, M. M.; Hitzmann, B.; Hatti-Kaul, R., Polyethyleneimine–protein interactions and implications on protein stability. *Int. J. Biol. Macromol.* **2010,** *47* (1), 15-20.

17. Keefe, A. J.; Jiang, S. Y., Poly(zwitterionic)protein conjugates offer increased stability without sacrificing binding affinity or bioactivity. *Nat. Chem.* **2012,** *4* (1), 60-64.

18. Lin, X.; Boit, M. O. K.; Wu, K.; Jain, P.; Liu, E. J.; Hsieh, Y.-F.; Zhou, Q.; Li, B.; Hung, H.-C.; Jiang, S., Zwitterionic Carboxybetaine Polymers Extend the Shelf-Life of Human Platelets. *Acta Biomater.* **2020**.

19. Zhang, P.; Sun, F.; Tsao, C.; Liu, S.; Jain, P.; Sinclair, A.; Hung, H.-C.; Bai, T.; Wu, K.; Jiang, S., Zwitterionic gel encapsulation promotes protein stability, enhances pharmacokinetics, and reduces immunogenicity. *Proc. Natl. Acad. Sci. U. S. A.* **2015,** *112* (39), 12046-12051.

20. Lee, J.; Lin, E. W.; Lau, U. Y.; Hedrick, J. L.; Bat, E.; Maynard, H. D., Trehalose Glycopolymers as Excipients for Protein Stabilization. *Biomacromolecules* **2013,** *14* (8), 2561-2569.

21. Messina, M. S.; Ko, J. H.; Yang, Z. Y.; Strouse, M. J.; Houk, K. N.; Maynard, H. D., Effect of trehalose polymer regioisomers on protein stabilization. *Polym. Chem.* **2017,** *8* (33), 4781-4788.

22. Liu, Y.; Lee, J.; Mansfield, K. M.; Ko, J. H.; Sallam, S.; Wesderniotis, C.; Maynard, H. D., Trehalose Glycopolymer Enhances Both Solution Stability and Pharmacokinetics of a Therapeutic Protein. *Bioconjugate Chem.* **2017,** *28* (3), 836-845.

23. Mansfield, K. M.; Maynard, H. D., Site-Specific Insulin-Trehalose Glycopolymer Conjugate by Grafting from Strategy Improves Bioactivity. *ACS Macro Lett.* **2018**, 324-329.

24. Pelegri-O'Day, E. M.; Bhattacharya, A.; Theopold, N.; Ko, J. H.; Maynard, H. D., Synthesis of Zwitterionic and Trehalose Polymers with Variable Degradation Rates and Stabilization of Insulin. *Biomacromolecules* **2020,** *21* (6), 2147-2154.

25. Shire, S. J.; Shahrokh, Z.; Liu, J., Challenges in the development of high protein concentration formulations. *J. Pharm. Sci.* **2004,** *93* (6), 1390-1402.

26. Shire, S. J., Formulation and manufacturability of biologics. *Curr. Opin. Biotechnol.* **2009,** *20* (6), 708-714.

27. Jezek, J.; Rides, M.; Derham, B.; Moore, J.; Cerasoli, E.; Simler, R.; Perez-Ramirez, B., Viscosity of concentrated therapeutic protein compositions. *Adv. Drug Delivery Rev.* **2011,** *63* (13), 1107-1117.

28. Zhang, Z.; Liu, Y., Recent progresses of understanding the viscosity of concentrated protein solutions. *Curr. Opin. Chem. Eng.* **2017,** *16*, 48-55.

29. Gonçalves, A. D.; Alexander, C.; Roberts, C. J.; Spain, S. G.; Uddin, S.; Allen, S., The effect of protein concentration on the viscosity of a recombinant albumin solution formulation. *RSC Adv.* **2016,** *6* (18), 15143-15154.

30. Saluja, A.; Kalonia, D. S., Nature and consequences of protein–protein interactions in high protein concentration solutions. *Int. J. Pharm.* **2008,** *358* (1), 1-15.

31. Pryce, R., Diabetic ketoacidosis caused by exposure of insulin pump to heat and sunlight. *BMJ* **2009,** *338*, a2218.

32. Oliva, A.; Fariña, J.; Llabrés, M., Influence of temperature and shaking on stability of insulin preparations: Degradation kinetics. *Int. J. Pharm.* **1996,** *143* (2), 163-170.

33. Painter, N. A.; Sisson, E., An Overview of Concentrated Insulin Products. *Diabetes Spectrum* **2016,** *29* (3), 136.

34. Segal, A. R.; El Sayed, N., Are you ready for more insulin concentrations? *J. Diabetes Sci. Technol.* **2015,** *9* (2), 331-338.

35. McAdams, B. H.; Rizvi, A. A., An Overview of Insulin Pumps and Glucose Sensors for the Generalist. *J. Clin. Med.* **2016,** *5* (1), 5.

36. Su, W.-F., Polymer Size and Polymer Solutions. In *Principles of Polymer Design and Synthesis*, Su, W.-F., Ed. Springer Berlin Heidelberg: Berlin, Heidelberg, 2013; pp 9-26.

37. Gonzalez-Tello, P.; Camacho, F.; Blazquez, G., Density and Viscosity of Concentrated Aqueous Solutions of Polyethylene Glycol. *Journal of Chemical & Engineering Data* **1994,** *39* (3), 611-614.

38. Debasmita, D.; Mallika, C.; Mudali, U. K., Temperature and Concentration Dependence of Viscosity of Binary Mixtures of PEG-1000 + water. *Chemical Product and Process Modeling* **2017,** *12* (2), 20160037.

39. Ren, L.; Zhang, J.; Hardy, C. G.; Doxie, D.; Fleming, B.; Tang, C., Preparation of Cobaltocenium-Labeled Polymers by Atom Transfer Radical Polymerization. *Macromolecules* **2012,** *45* (5), 2267-2275.

Chapter 4

Antibody Stabilizing Trehalose Glycopolymer and its Effect on Viscosity

4.1 Introduction

Therapeutic antibodies have become the fastest growing segment of the biopharmaceuticals market as their highly specific recognition and binding of specific antigens gains awareness and usage.[1-2] The therapeutic applications of antibodies currently range from inhibiting or stimulating the immune system, imaging, and treating diseases like cancer using antibody-drug conjugates. Just as with other biologics, however, antibodies are susceptible to activity loss when exposed to stressful environments in storage and transportation.[1] Another major limitation with antibody therapeutics is their relatively low potency that requires high doses of the protein.[3-4] To allow for self-administered, subcutaneous (s.c.) injections, formulations must fit within a lower volume (1.5-2.5 mL).[4] Antibodies intended for s.c. injection need to be formulated at high and ultra-high concentrations (>100 mg mL^{-1} or >150 mg mL^{-1}) which dramatically increases formulation viscosity.[4-5] The high solution viscosity of antibodies is caused at least in part by intermolecular protein-protein interactions (PPI) as well as aggregation, both adversely impacted by increasing antibody concentration.[4, 6] The increased concentration makes every variation of PPI a more common occurrence as there is less solute space between antibodies; non-native aggregation, unfolding, and other non-native protein conformations are more likely to have undesirable PPI that will also cause higher viscosity. Additionally, highly concentrating antibody and other protein solutions can increase protein instability resulting in solutions that more easily undergo unfolding, aggregation and loss of intact or active protein that can further increase the solution viscosity.[3-4, 7-10]

In considering using antibodies as drugs, many small molecule excipients have been explored for their use as stabilizers or viscosity reducing agents (VRA). In particular salts, amino acids, and even nucleotide analogs like caffeine have been found to reduce viscosity by preventing

antibody-antibody PPI.[5] Unfortunately, some of these VRA also destabilize the antibody, necessitating the addition of stabilizing excipients such as sugars or amino acids.[5] While trehalose has been repeatedly shown to be one of the best sugars for stabilizing biologics, it is not typically studied for antibodies with viscosity challenges because it has a much higher viscosity than other sugars including maltose, glucose, fructose, and even sucrose, another disaccharide, at the same molar concentrations (**Figure 4.1**).[11]

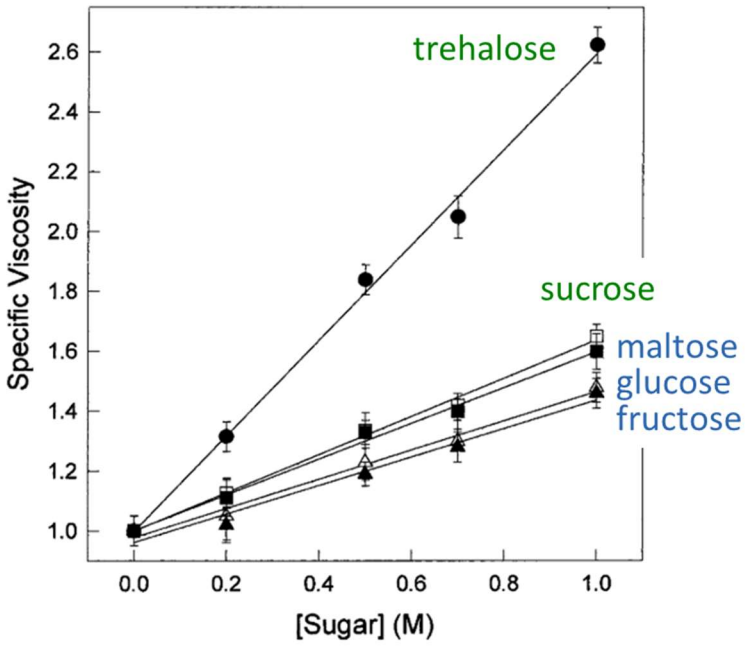

Figure 4.1 Relative viscosities of disaccarides (● trehalose, □ sucrose) and monosaccharides (■ maltose, Δ glucose, ▲ fructose) at 25 °C reproduced with permission from Sola-Penna, M. and Meyer-Fernandes, J. R., **1998**, Figure 1.[11]

In the Maynard lab we have already explored the utility of trehalose methacrylate polymer as both an excipient and protein-polymer conjugate to stabilize a range of therapeutic proteins.[12-14] As part of this body of work, pTrMA was "grafted to" the therapeutic antibody trastuzumab (trade name Herceptin) and its Fab fragment in an effort to provide greater stability and potentially increase the half-life *in vivo*.[15] Trastuzumab is currently used to treat Human Epidermal growth

factor Receptor 2 (HER2) positive breast cancer.[16-17] Further, its formulation is comprised of 11:10 weight ratio of antibody:trehalose small molecule and administered as an intravenous (i.v.) infusion at 21 mg mL^{-1} with a pH ~6.0. This is a relatively high amount of trehalose by weight and corresponds to ~386 mol. eq. of trehalose relative to antibody. As with other therapeutic antibodies, the low potency of trastuzumab requires high protein doses currently administered by i.v. at a relatively low antibody concentration. This route of administration is less desired by both patients and clinicians because i.v. infusion is a clinical procedure while s.c. or intramuscular (i.m.) injections can be at-home and self-administered.[1, 10] However, Herceptin is formulated to be administered by i.v. for multiple reasons including injecting larger volumes than is allowable with s.c. and i.m. injections. Because trastuzumab requires a large amount of trehalose for stability, increasing antibody concentrations to reduce injection volume would likely increase the viscosity dramatically due to both the antibody PPIs and trehalose viscosity. A more concentrated version of Herceptin could be uncomfortable and even difficult for patients to self-administer if the resulting viscosity is too high.[18]

While small molecule trehalose has issues with high viscosity, in the most recently published iteration of pTrMA excipient work (see **Chapter 3**), we found that pTrMA up to 29.2 kDa and 100 mg mL^{-1} has relatively low solution viscosity (<2.6 cP) and Newtonian like fluid behavior.[14] We had also already shown that pTrMA prevents both aggregation and chemical degradation of insulin without causing insulin to form larger quaternary structure complexes (**Chapter 2**). Additionally, the trastuzumab and Fab site-specific conjugates synthesized with pTrMA were found to have far better stability against heat (constant and ramped) than the unmodified proteins.[15] Both conjugates were able to withstand aggregation up to 75 °C in a heat ramp. Holding constant at 75 °C, the antibody and Fab conjugate lost significantly less intact

protein than their unmodified species; both conjugates maintained >50% protein after 30 min at 75 °C, as compared to the unmodified species at ~0% antibody and <25% Fab.[15]

We hypothesized that exploring trastuzumab formulated with excipient pTrMA would result in improved antibody stability without dramatically increasing the viscosity. This in turn would allow the use of pTrMA as an excipient potentially for other therapeutic IgGs. As with other antibodies, the viscosity of the antibody stabilizing formulation can affect patient compliance,[18] so we studied the viscosity at a range of highly concentrated conditions (100, 200 and 400 mg mL^{-1}).

4.2 Results and Discussion

4.2.1 Polymer Synthesis

Due the viscosity challenges presented by highly concentrated antibody formulations and the low viscosity of pTrMA seen in Chapter 2,[14] we hypothesized that we could improve the stability of an antibody without adversely increasing the viscosity of even highly concentrated samples. As in the previous chapters, pTrMA was synthesized by AGET ATRP using the initiator HEBIB. The polymer was then characterized by ^{1}H NMR and GPC. pTrMA was shown to have a M_n of 22.9 g/mol and a low $Đ$ of 1.04 (see experimental section for full characterization).

4.2.2 Trastuzumab Stabilization with pTrMA

We investigated the efficacy of pTrMA to stabilize the antibody trastuzumab against mild heat conditions that could be encountered during shipping and storage. Antibody solutions were prepared with the addition of MilliQ water to the lyophilized Herceptin overnight without any unnecessary shaking or other agitation. Formulated Herceptin was taken from this dissolved solution and diluted to reach 20 mg mL^{-1} of antibody. The deformulated antibody formulations were made by removing the Herceptin excipients (trehalose, L-histidine HCl, L-histidine, and polysorbate-20) via centrifugal preparation before diluting the deformulated antibody with 0.1 M

PBS pH 7.4 with and without pTrMA (22.9 kDa, $Đ$ 1.04) to reach 20 mg mL^{-1} of antibody with 2 and 0 mol. eq. of polymer and filtering (0.22 μm).

We first explored these solutions by DLS to study aggregation calculated as a percent of the original non-aggregated antibody solution (Figure 4.2). Each condition was transferred to low-volume polystyrene cuvettes (n = 3) before taking DLS measurements of the samples as a control time point. Samples were then heated inside of the capped cuvettes in a water bath at 40 °C for 2 h, 24 h, 48 h, 72 h, 120 h, 168 h and 228 h, returning the samples back to the water bath in between time points. The size of the particles or aggregates in solution at each time point were averaged until the point when the DLS was unable to obtain good quality measurements from each sample. Alone, trastuzumab begins to lose a significant amount of non-aggregated antibody at 72 h. The amount of aggregation in the Herceptin formulated and pTrMA formulated samples is only significantly different at 168 h at which point the Herceptin formulation out-performs pTrMA (***: $p < 0.001$). However, this difference is not apparent at the final time point of 228 h when both are aggregating approximately 20% and when none of the Herceptin formulated samples measurements were of good quality according to the standard criteria set by the DLS.

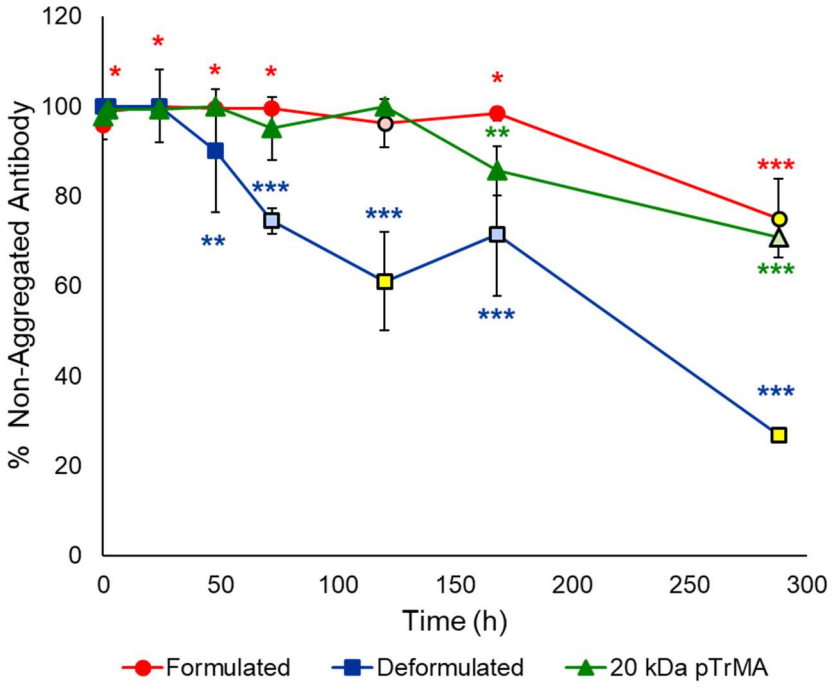

Figure 4.2 Antibody formulation stability against heating (40 °C) as measured by DLS particle size (n = 3). Solution formulations include Herceptin (red), deformulated trastuzumab alone (blue), and deformulated trastuzumab with 2 mol. eq. of 22.9 kDa pTrMA (green) (*: $p < 0.05$, **: $p < 0.01$, ***: $p < 0.001$). Noted time point measurements that include data of not good quality with black outlined marker and lighter fill (Formulated 120 h, Deformulated 72 h and 168 h, 20 mol. eq. pTrMA 288 h); time points with no good DLS measurements are outlined in black and filled in with yellow (Formulated 288 h, Deformulated 120 h and 288 h).

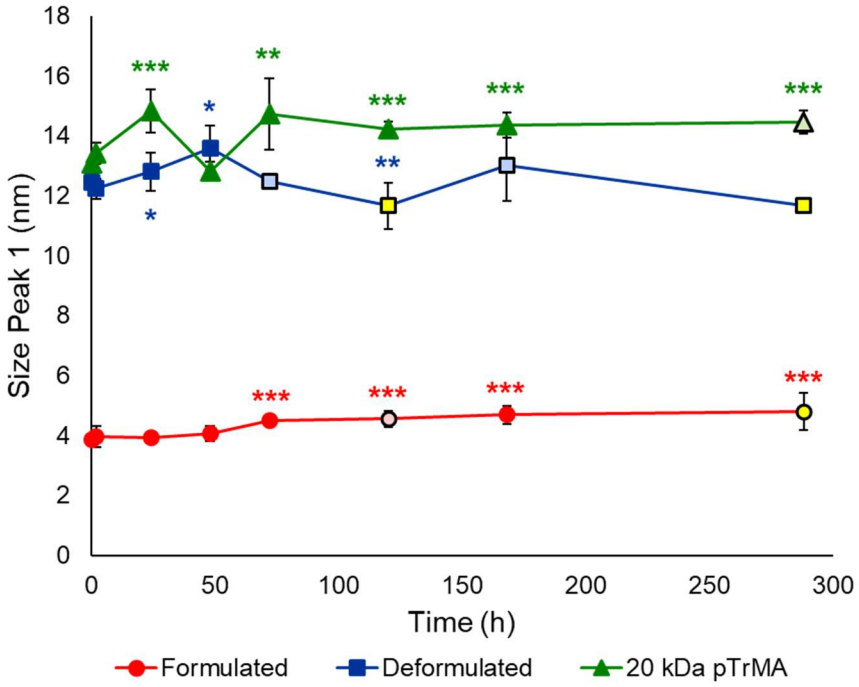

Figure 4.3 DLS size distribution by intensity of peak 1 (non-aggregated antibody) for Herceptin formulated, deformulated trastuzumab, and trastuzumab with 2 mol. eq. of 22.9 kDa pTrMA (n = 3) over 288 h with heating (40 °C) (*: $p < 0.05$, **: $p < 0.01$, ***: $p < 0.001$).

Table 4.1 DLS size distribution by intensity of antibody formulation exposed to 40 °C (n = 3). Non-aggregated sample peaks were clearly defined by the system, and peaks 2 and 3 were defined as aggregated species >2000 nm or <2000 nm, respectively.

Sample	Time (h)	Peak 1 (nm)	Peak 1 (%)	Peak 2 (nm)	Peak 2 (%)	Peak 3 (nm)	Peak 3 (%)
Herceptin	0	3.9 ± 0.1	95.8 ± 3.3	3190 ± 495	2.5 ± 3.0	1520 ± 388	1.7 ± 3.3
	2	4.0 ± 0.3	98.8 ± 1.2	3690 ± 196	1.2 ± 1.2		
	24	3.9 ± 0.2	100				
	48	4.1 ± 0.2	99.5 ± 0.9	4200 ± 221	0.5 ± 0.9		
	72	4.5 ± 0.1	99.5 ± 1.0	4150 ± 273	0.5 ± 0.9		
	120	4.6 ± 0.3	96.2 ± 5.3	4070 ± 702	1.6 ± 1.7	504 ± 80.2	2.3 ± 4.5
	168	4.7 ± 0.3	98.3 ± 1.6	4330 ± 445	1.7 ± 1.6		
	288	4.8 ± 0.62	75.1 ± 8.8	4930 ± 234	4.2 ± 2.9	859 ± 364	20.8 ± 7.0
Deformulated	0	12.5 ± 0.6	100				
	2	12.2 ± 0.2	100				
	24	12.8 ± 0.3	100				
	48	13.6 ± 0.6	90.0 ± 8.1	3160 ± 1060	2.4 ± 4.3	1110 ± 390	7.6 ± 9.4
	72	12.5 ± 0.7	74.5 ± 13.6	4540 ± 103	0.4 ± 0.8	1100 ± 42.6	25.1 ± 14.4
	120	11.6 ± 0.1	61.1 ± 2.8			0.81 ± 0.08	38.9 ± 2.8
	168	13.0 ± 0.8	71.4 ± 11.0	4950 ± 404	1.2 ± 1.7	878 ± 265	27.4 ± 11.1
	288	11.7 ± 1.2	26.7 ± 13.5	5320 ± 109	1.7 ± 2.9	731 ± 238	71.6 ± 15.1
2 mol. eq. 22.9 kDa pTrMA	0	13.1 ± 0.3	97.7 ± 3.5	2750 ± 849	1.4 ± 2.9	1294 ± 0	0.8 ± 2.5
	2	13.4 ± 0.3	99.3 ± 1.1	4100 ± 123	0.7 ± 1.2		
	24	14.8 ± 0.7	99.3 ± 1.0	4050 ± 178	0.7 ± 1.0		
	48	12.8 ± 0.3	100				
	72	14.7 ± 0.2	95.1 ± 7.0	4390	0.3 ± 0.7	1430 ± 286	4.6 ± 7.0
	120	14.2 ± 0.3	99.9 ± 0.4	4610	0.1 ± 0.4		
	168	14.4 ± 0.4	85.6 ± 5.5	3830 ± 695	4.1 ± 3.9	1360 ± 325	10.2 ± 6.2
	288	14.4 ± 0.4	70.8 ± 4.5	4900 ± 294	3.3 ± 2.4	943 ± 205	25.9 ± 5.7

We next investigated the stability of the formulations by HPLC for each condition to confirm that aggregation would indeed lead to loss of soluble antibody. Samples were diluted to 0.25 mg mL^{-1} with MilliQ or 0.1 M PBS pH 7.4 for the formulated Herceptin or deformulated antibody, respectively, and split the samples up into LoBind tubes (n = 3). A t0 aliquot was taken from each sample as a control and stored at 4 °C before transferring the remaining material to a water bath at 40 °C. Additional time points for each condition were taken at 2 h, 4 h, 24 h, 48 h, 72 h, 120 h, 168 h, 288 h, and 432 h and stored at 4 °C until HPLC analysis could be run. The percent intact and soluble antibody for each condition was measured by HPLC calculated by the area under the curve (AUC) of the antibody peak relative to the t0 control without heat as seen with loss of soluble, intact, insulin in Chapter 3 (**Figure B12**).

Similar to the DLS study, there was a significant loss of antibody first from the deformulated samples and beginning at 120 h (*: $p < 0.05$, Figure 4.4). There was no significant aggregation that would result in detecting a loss of soluble antibody for Herceptin formulated or pTrMA formulated samples except at 168 h when Herceptin formulation dipped below the allowable error and became significantly different (*: $p < 0.05$). All samples had less than 20% of the original soluble antibody by 432 h at 40 °C, and the study was thus ended.

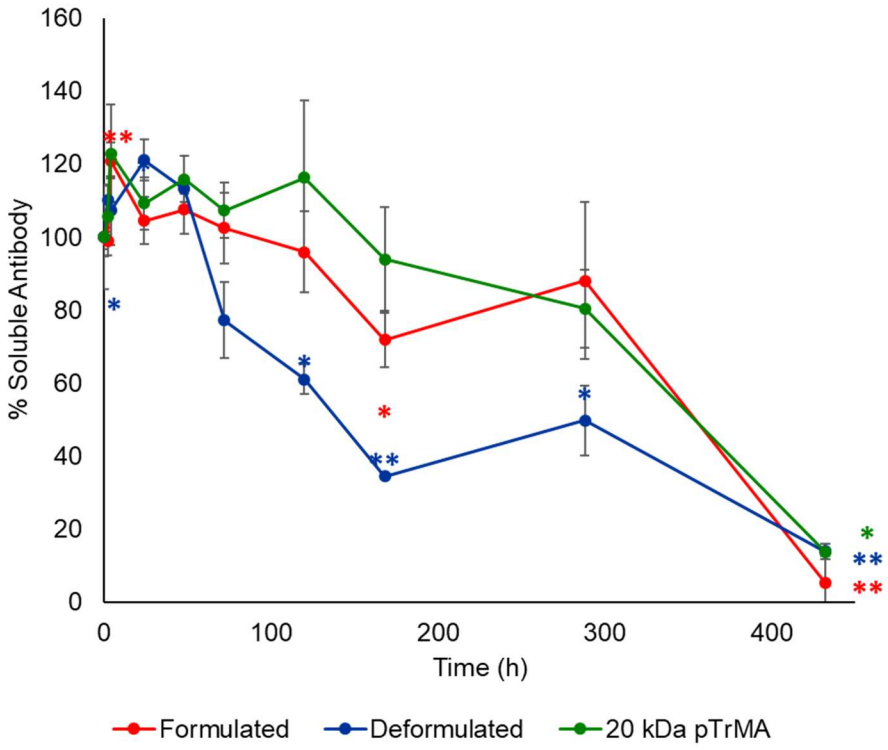

Figure 4.4 Antibody formulation stability against heating (40 °C) as measured by HPLC (n = 3). Solution formulations include Herceptin (red), deformulated trastuzumab alone (blue), and deformulated trastuzumab with 2 mol. eq. of 22.9 kDa pTrMA (green) (*: $p < 0.05$, **: $p < 0.01$, ***: $p < 0.001$).

4.2.3 Viscosity of pTrMA Formulated Trastuzumab

We finally measured the fluid behavior of pTrMA using a RheoSense microVisc viscometer to study how deformulating trastuzumab and adding pTrMA to the antibody would affect solution viscosity and patient experience. Samples were prepared following the same method as performed with DLS and HPLC studies but targeting concentrations of 100 mg mL^{-1}, 200 mg mL^{-1}, and 400 mg mL^{-1} and without a filtration step after making the solution. The standard Herceptin formulation was also prepared at the label concentration of 20 mg mL^{-1} for comparison. Samples were loaded into the microVisc syringes and the viscosity was measured in triplicate at 25 °C (**Figure 4.5**).

While below 400 mg mL^{-1} the formulations do have significantly different viscosities (**Figure 4.5**) with the pTrMA formulation always the highest, the change in viscosity was not dramatic enough to cause difficulties or discomfort for the patient.[18] At 400 mg mL^{-1}, however, the viscosity of both the deformulated and pTrMA formulated trastuzumab are significantly and noticeably higher than the viscosity of Herceptin formulated trastuzumab. Although this increase was certainly due to the higher viscosity of the deformulated and pTrMA formulated solutions, the difference is likely exacerbated due to differences in applied shear rates for these later two solutions. Because the solutions were measured starting at the lowest concentrations, the shear rate was originally set to 8432 s^{-1} until the force required to perform measurements at that rate were above the instrument's abilities with the deformulated and pTrMA formulated samples (**Figure 4.5**). These two formulations alone were measured according to the instrument's automatic settings with the deformulated and pTrMA formulated solutions measured at 2035 s^{-1} and 962 s^{-1}, respectively. Antibody and protein containing solutions are well known to have fluid behavior not characteristic of Newtonian fluids including shear thinning properties.[3, 19] As a result, while the viscosity measurements for these two samples are significantly higher than the Herceptin formulated solution at 400 mg mL^{-1}, this is not an exact comparison to make. However, with excess solution from the label Herceptin formulation (20 mg mL^{-1}), it is clear that, at lower concentrations, the formulated Herceptin behaves with Newtonian characteristics as the relationship between shear stress and shear rate is linear (**Figure C11**) and the viscosity is constant across a range of shear rates (**Figure C12**).

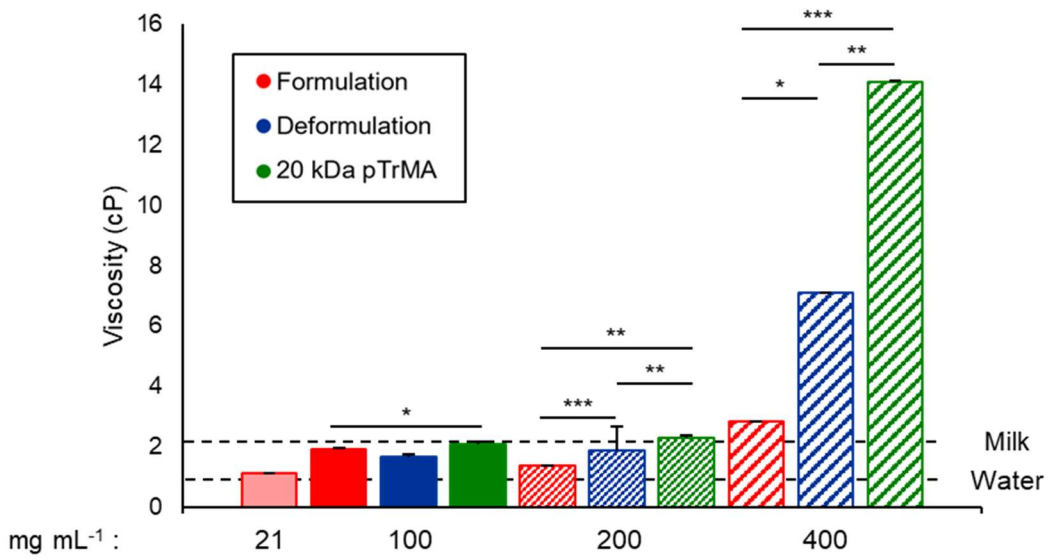

Figure 4.5 Viscosity of trastuzumab antibody formulations at increasingly concentrated antibody levels taken at 25 °C and 8434 s^{-1} except for 400 mg mL^{-1} of deformulated (2035 s^{-1}) and pTrMA formulated (962 s^{-1}) trastuzumab where the solution viscosity was too high for the microVisc to run at the maximum shear rate. Solution formulations include Herceptin (red), deformulated trastuzumab alone (blue), and deformulated trastuzumab with 2 mol. eq. of 22.9 kDa pTrMA (green) (*: $p < 0.05$, **: $p < 0.01$, ***: $p < 0.001$). Overlaid on the plot are lines indicated the viscosity of water (0.89 cP) and whole milk (2.0 cP).

Together these experiments demonstrate that pTrMA sufficiently stabilizes the biopharmaceutical trastuzumab, and only raises viscosity to unacceptable levels at the highest of highly concentrated formulations (400 mg mL^{-1} antibody). The 2 mol. eq. of pTrMA (22.9 kDa, DP 55.3, 110.5 mol. eq. of trehalose) prevented aggregation at a similar rate as the Herceptin formulation (Figures 4.2, 4.3, and 4.4) with 386 mol. eq. of small molecule trehalose (~3.5x the amount of trehalose) and viscosities up to 200 mg mL^{-1} were within a range tolerated by patients for self-injection. Both the polymer and the formulated Herceptin maintained a greater amount of soluble and non-aggregated antibody compared to trastuzumab alone, and the pTrMA formulated

antibody was 99.9 ± 0.3% stable in the 40 °C heating conditions for 120 h by DLS. However, at 400 mg mL^{-1} the pTrMA formulated trastuzumab had a significantly higher viscosity (14.1 cP) that brought it above an established viscosity threshold of 5 cP.[18] While the viscosity results at the highest concentration were not in favor of using pTrMA as a stabilizing excipient, it is possible that the addition of VRA excipients would sufficiently reduce the viscosity to acceptable levels. However, further studies would be needed to explore VRAs, so, at this point in time, the pTrMA polymer does not appear suitable for ultra high concentration antibody formulations.

4.3 Conclusions

Having already shown the pTrMA polymers to behave with Newtonian characteristics and have surprisingly low viscosity for a trehalose-based molecule, we chose to explore the effect of stabilization and viscosity as an excipient for an antibody solution. We found that pTrMA stabilizes the therapeutic antibody trastuzumab (trade name Herceptin) by preventing aggregation at a similar rate as the ~3.5x fold higher concentration of small molecule trehalose found in the Herceptin formulation. Measuring the viscosity of the pTrMA formulated antibody at high concentrations (>100 mg mL^{-1}) indicated that, up to a point, the polymer does not increase viscosity to unmanageable levels for patients self-administering injections. However, the highest antibody concentration measured is significantly higher in viscosity than even deformulated trastuzumab antibody, indicating that the polymer is having a negative effect above a certain concentration. Further studies would be required to elucidate if the dramatic increase in viscosity is primarily due to an increase in PPIs as the dissolved polymer further crowds antibodies together or if polymer-polymer or polymer-antibody interactions are driving the increase.

4.4 Experimental Section

4.4.1 Materials

Chemicals were all purchased from Sigma Aldrich or Fisher Scientific and used without further purification unless otherwise mentioned. Trehalose was purchased from BulkSupplements.com (Henderson, NV) and repeatedly azeotropically dried from ethanol and stored under vacuum. Spectra/Por3® regenerated cellulose membrane (MWCO 3.5 kDa) was purchased from Spectrum Chemical (New Brunswick, NJ) for polymer dialysis. Herceptin was purchased from the UCLA Ronald Reagan Pharmacy (Lot no. 3407392). Cuprisorb was purchased from Amazon.com. TrMA was gifted by Haillie C. Lower, and HEBIB by Daniele Vinciguerra. Both reagents and pTrMA were synthesized according to literature and Chapters 2 and 3.[12, 14, 20] ^{1}H-NMR agreed with that reported for all compounds.

4.4.2 Analytical Techniques

NMR spectroscopy were performed on a Bruker AV 400 MHz or AV 500 MHz instrument and spectra were acquired with a relaxation delay of 2 s for initiator or monomer and 30 s for polymer. Aqueous GPC of pTrMA was conducted on a Malvern Viscotek GPCMax system equipped with a triple detector array (TDA 305-040 Quadruple Detector Array), with two Viscotek A600 M general mixed aq. Columns (300x8.0mm) with an eluent system of 20% methanol in water 1 mL min^{-1}. A RheoSense microVisc (San Ramon, CA) viscometer was used to measure viscosity. Analytical HPLC for antibody detection was conducted on an Agilent Q-TOF 6530 and Zorbax 300SB-C3 3.5 μm column (3.0 x 150 mm) with a gradient of 10-95% acetonitrile+ 0.1% TFA with an isocratic 5% IPA + 0.1% TFA, over 30 min at 70 °C with trastuzumab eluting at 15 min.

4.4.3 Methods

Stabilization of antibody with pTrMA

Trastuzumab stabilization was measured by DLS and HPLC to calculate loss of soluble antibody and formation of small and large aggregates. Briefly, as with the viscosity studies, lyophilized Herceptin was dissolved in MilliQ water overnight. Formulated Herceptin was prepared by either diluted to 20 mg mL^{-1} or 0.25 mg mL^{-1} with MilliQ water. The deformulated antibody conditions were centriprepped before diluting to 20 mg mL^{-1} or 0.25 mg mL^{-1} with 0.1 M PBS pH = 7.4 alone and with pTrMA to reach 0 or 2 mol. eq. of pTrMA. Samples were filtered (0.22 μm) and analyzed by DLS (20 mg mL^{-1}) and RP-HPLC (0.25 mg mL^{-1}) before and after heating in a water bath at 40 °C.

Viscosity Measurements

As in Chapter 2, solution viscosity was measured using the microVisc, a microfluidics based slit-viscometer. Samples are injected into the microfluidics chip with a 50 μm flow channel (A05) at programmed rates using the built-in syringe pump. The Herceptin formulated trastuzumab formulations were made by dissolving the lyophilized Herceptin in sterile MilliQ overnight at the desired concentration. The deformulated conditions were made by first dissolving the lyophilized Herceptin in MilliQ overnight before removing the Herceptin small molecule excipients by centrifugal filtration preparation (6.6 krpm, 5 min) using a 50 kDa MW cut off centriprep filter and excess 0.1 M PBS pH 7.4 (4x). All formulation measurements were performed in triplicate at 25 °C with the maximum allowable shear rates (8342 s^{-1} up to 200 mg mL^{-1} and 8342 s^{-1}, 2035 s^{-1}, and 962 s^{-1} at 400 mg mL^{-1} when formulations became more viscous).

3.4.4 Statistical Analysis

All experimental values are reported as the average ± SEM. Graph Pad Prism 7 (GraphPad Software, San Diego, USA) was used for the statistical analyses. To assess the statistical

significance of differences between control and stressed antibody samples, the one-tailed Student's t-test was conducted assuming unequal sample variance. Results were considered significantly different if $p < 0.05$ (*); results are also reported with $p < 0.01$ (**), and $p < 0.001$ (***).

3.5 Appendix C

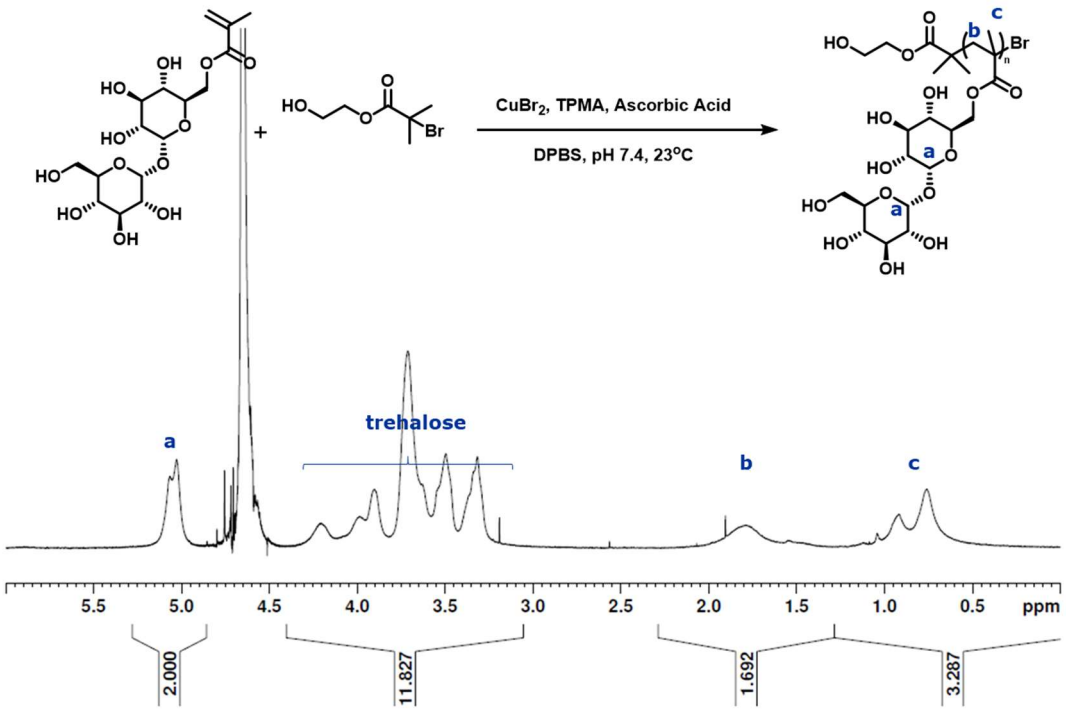

Figure C1 ^{1}H NMR spectrum (400 MHz, D_2O) of pTrMA 22.9 kDa polymerized with HEBIB initiator. ^{1}H-NMR agreed with that reported for this compound.[20]

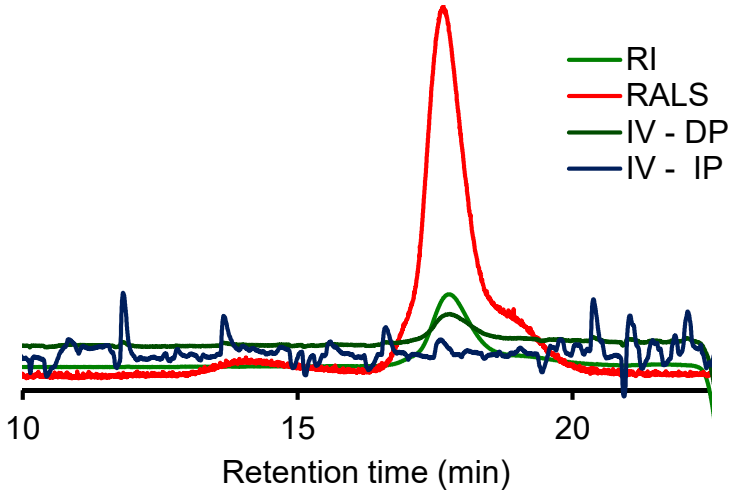

Figure C2 GPC (PEG standards) of pTrMA with HEBIB initiator. M_n = 22.9 kDa, $\cancel{D}$ = 1.04.

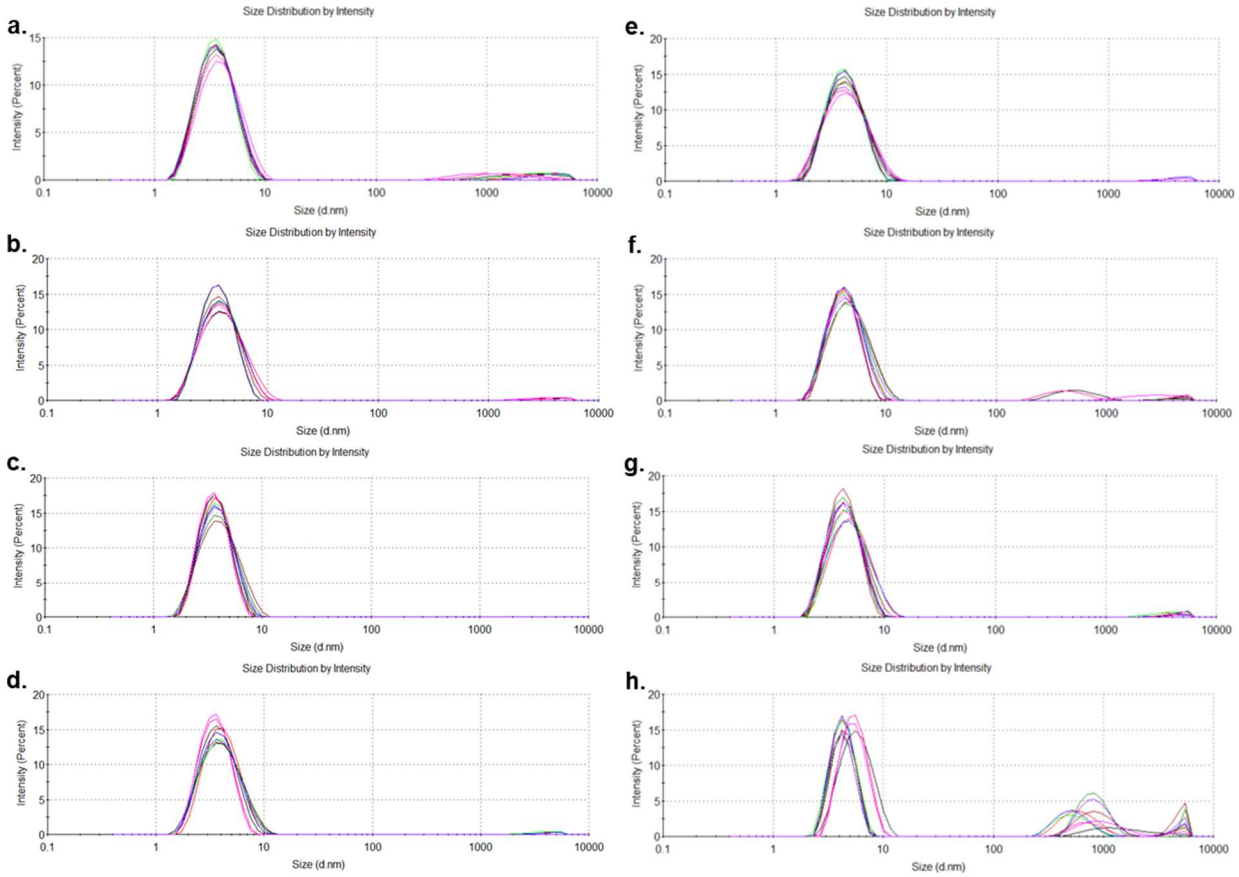

Figure C3 DLS size distribution by intensity of Herceptin formulated antibody (n = 3) over a. 0 h, b. 2 h, c. 24 h, d. 48 h, e. 72 h, f. 120 h, g. 168 h, and h. 288 h.

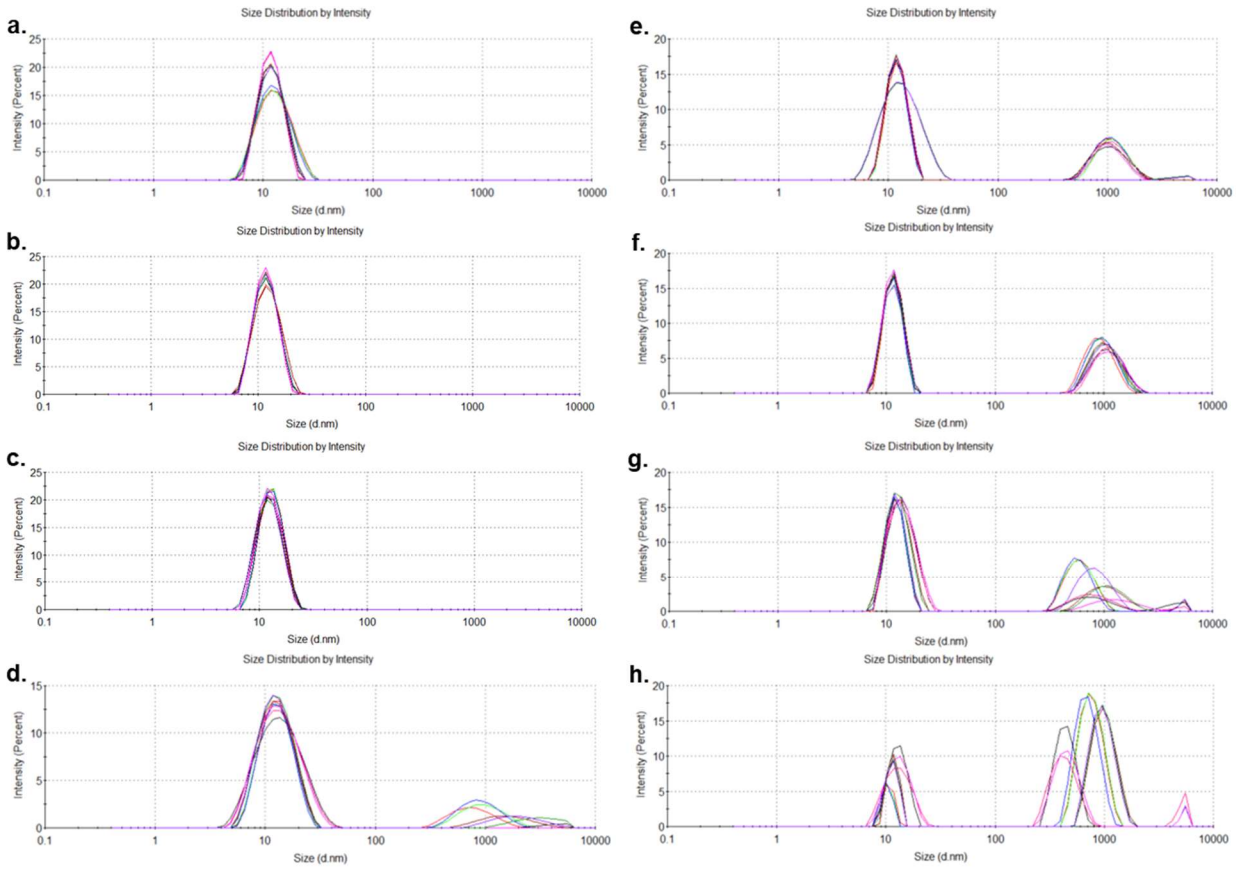

Figure C4 DLS size distribution by intensity of deformulated trastuzumab (n = 3) over a. 0 h, b. 2 h, c. 24 h, d. 48 h, e. 72 h, f. 120 h, g. 168 h, and h. 288 h.

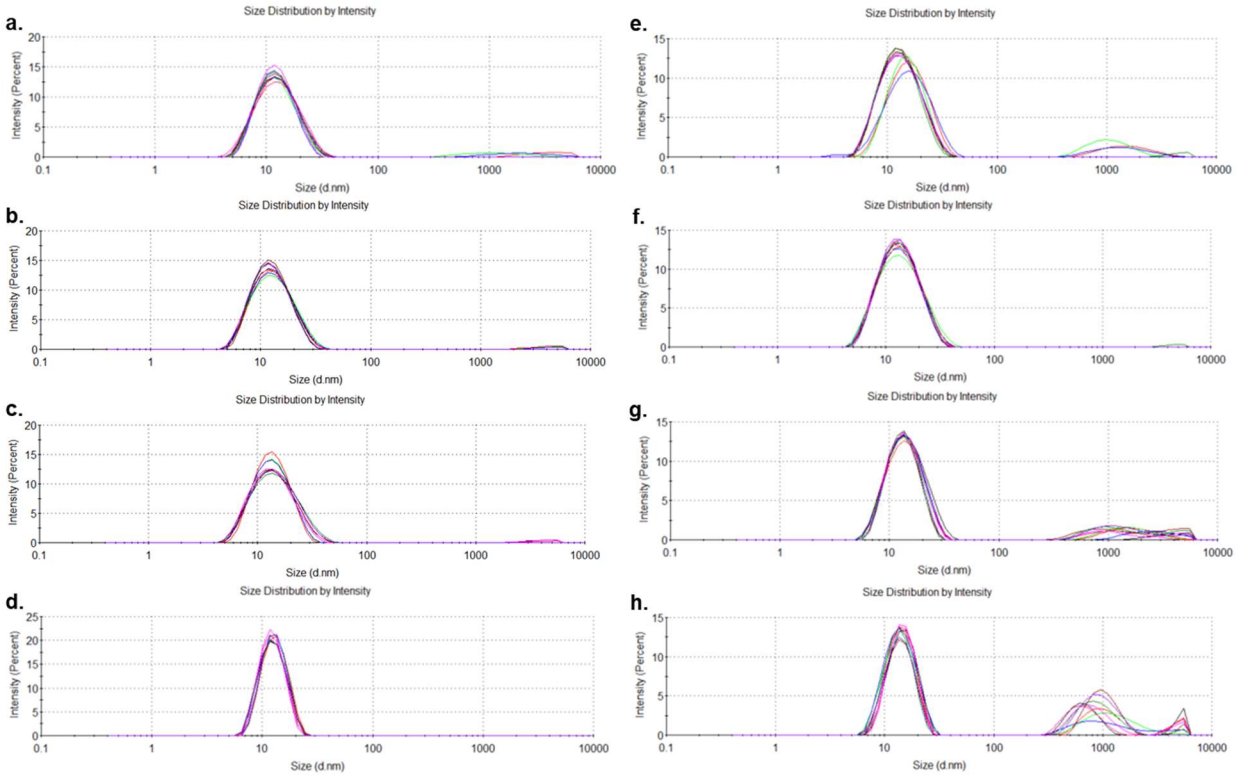

Figure C5 DLS size distribution by intensity of trastuzumab formulated with 2 mol. eq. of 22.9 kDa pTrMA (n = 3) over a. 0 h, b. 2 h, c. 24 h, d. 48 h, e. 72 h, f. 120 h, g. 168 h, and h. 288 h.

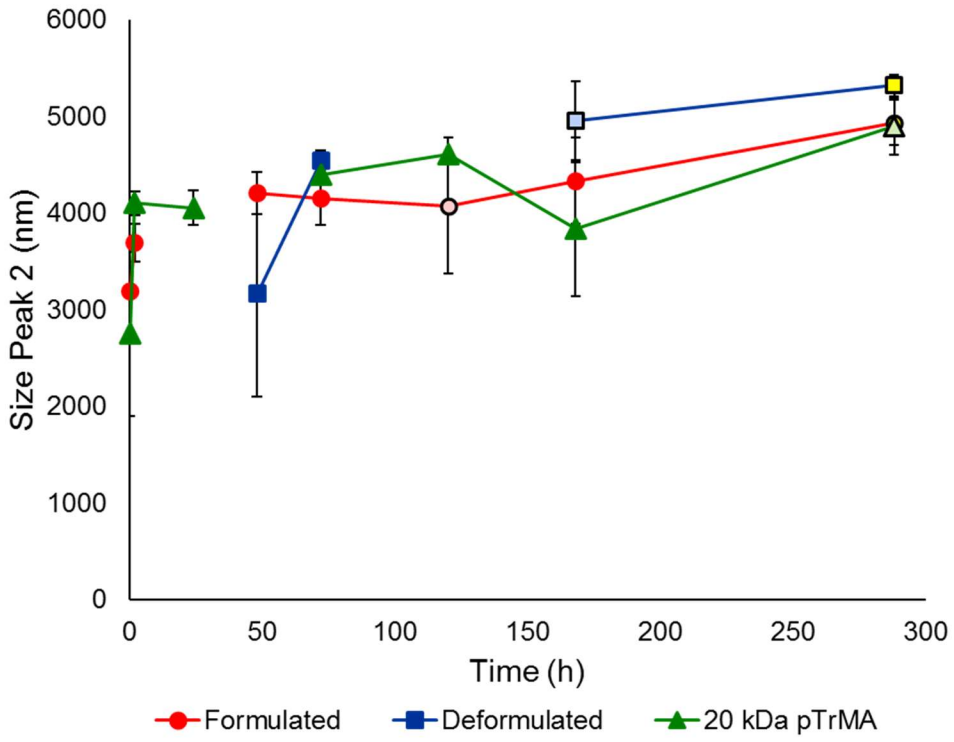

Figure C6 DLS size distribution by intensity of peak 2 (>2000 nm) for Herceptin formulated, deformulated trastuzumab, and trastuzumab with 2 mol. eq. of 22.9 kDa pTrMA (n = 3) over 288 h with heating (40 °C). Time points could not be statistically compared as the number measurements >2000 nm for all conditions was inconsistent.

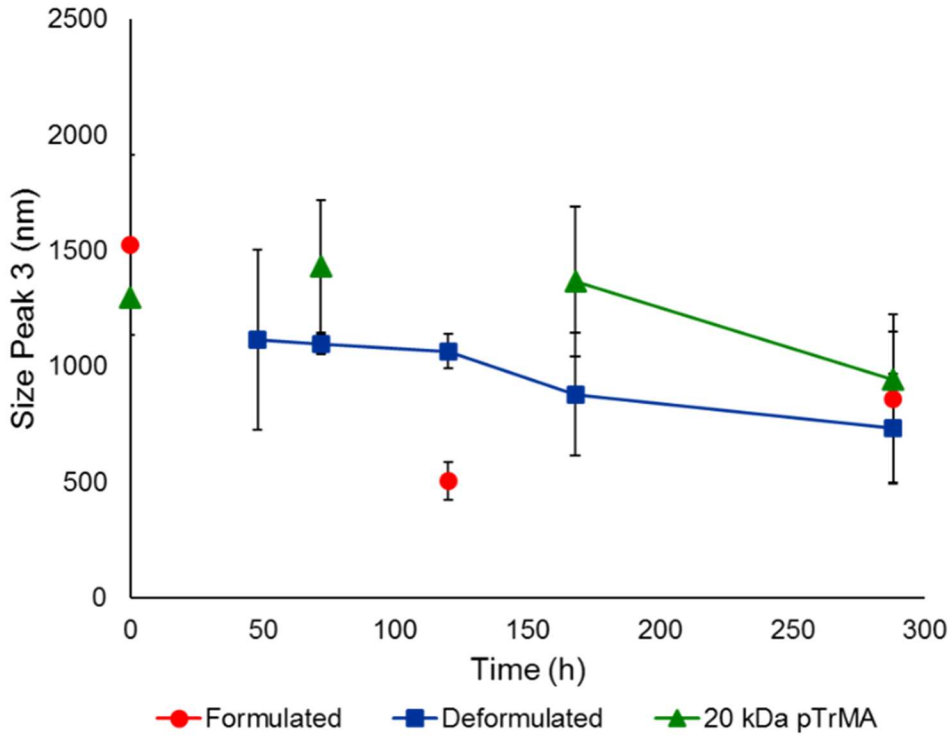

Figure C7 DLS size distribution by intensity of peak 3 for Herceptin formulated, deformulated trastuzumab, and trastuzumab with 2 mol. eq. of 22.9 kDa pTrMA (n = 3) over 288 h with heating (40 °C) (*: $p < 0.05$, **: $p < 0.01$, ***: $p < 0.001$). Time points could not be statistically compared as the number measurements <2000 nm for all conditions was inconsistent.

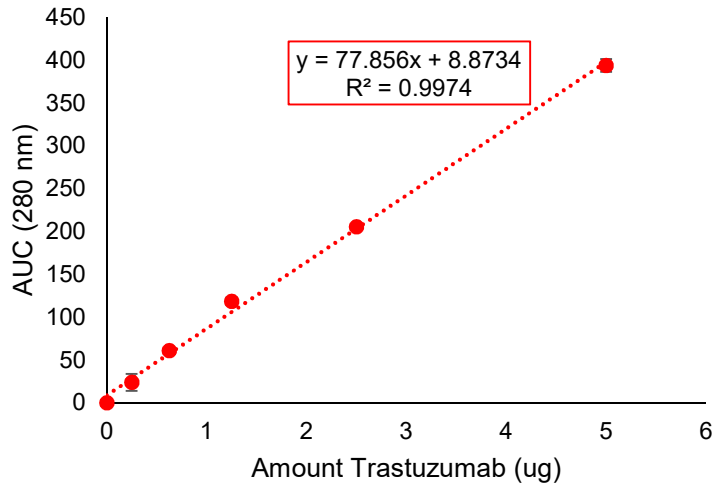

Figure C8 Trastuzumab antibody standard curve by HPLC. Three standards were sampled in between the samples from each time point to detect any loss of signal due to overnight HPLC methods. No loss of soluble antibody was detected from the standards, and the final standard curve is a very good fit with an R^2 of 0.9974.

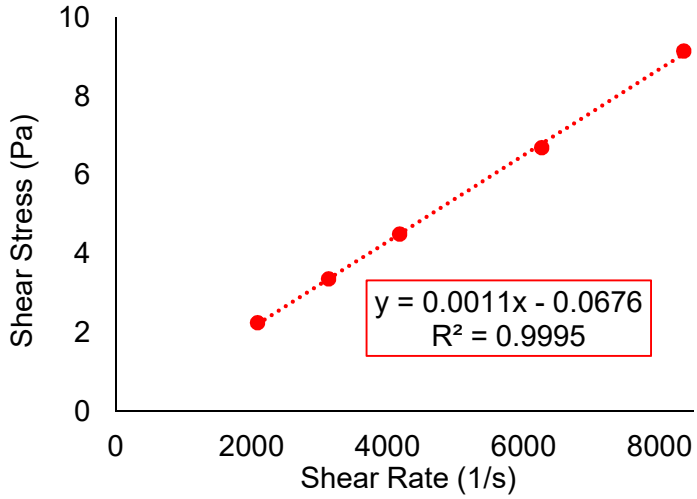

Figure C9 Shear stress (Pa) of Herceptin label formulated solution (20 mg mL^{-1}) over the allowable shear rates (s^{-1}) with the RheoSense microVisc (n = 3). The standard curve is a very good fit with an R^2 of 0.9995.

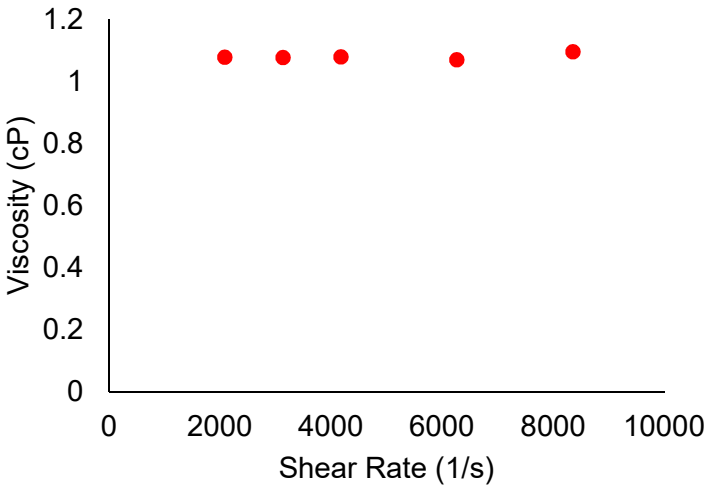

Figure C10 Viscosity (η, cP) of Herceptin label formulated solution (20 mg mL^{-1}) over the allowable shear rates (s^{-1}) with the RheoSense microVisc (n = 3). Further emphasizing the Newtonian characteristic of this formulation, the highest and lowest measured viscosities, 1.095 cP and 1.070, corresponded to the highest and second highest shear rates, 8342 s^{-1} and 6256 s^{-1}, respectively.

References

1. Shire, S. J., Formulation and manufacturability of biologics. *Curr. Opin. Biotechnol.* **2009,** *20* (6), 708-714.

2. Mullard, A., Maturing antibody–drug conjugate pipeline hits 30. *Nat. Rev. Drug Discov.* **2013,** *12*, 329.

3. Jezek, J.; Rides, M.; Derham, B.; Moore, J.; Cerasoli, E.; Simler, R.; Perez-Ramirez, B., Viscosity of concentrated therapeutic protein compositions. *Adv. Drug Delivery Rev.* **2011,** *63* (13), 1107-1117.

4. Whitaker, N.; Xiong, J.; Pace, S. E.; Kumar, V.; Middaugh, C. R.; Joshi, S. B.; Volkin, D. B., A Formulation Development Approach to Identify and Select Stable Ultra–High-Concentration Monoclonal Antibody Formulations With Reduced Viscosities. *J. Pharm. Sci.* **2017,** *106* (11), 3230-3241.

5. Zidar, M.; Rozman, P.; Belko-Parkel, K.; Ravnik, M., Control of viscosity in biopharmaceutical protein formulations. *J. Colloid Interface Sci.* **2020,** *580*, 308-317.

6. Tomar, D. S.; Kumar, S.; Singh, S. K.; Goswami, S.; Li, L., Molecular basis of high viscosity in concentrated antibody solutions: Strategies for high concentration drug product development. *mAbs* **2016,** *8* (2), 216-228.

7. O'Shea, T. M.; Webber, M. J.; Aimetti, A. A.; Langer, R., Covalent Incorporation of Trehalose within Hydrogels for Enhanced Long-Term Functional Stability and Controlled Release of Biomacromolecules. *Adv. Healthc. Mater.* **2015,** *4* (12), 1802-1812.

8. Schön, A.; Clarkson, B. R.; Siles, R.; Ross, P.; Brown, R. K.; Freire, E., Denatured state aggregation parameters derived from concentration dependence of protein stability. *Anal. Biochem.* **2015,** *488*, 45-50.

9. Saluja, A.; Badkar, A. V.; Zeng, D. L.; Kalonia, D. S., Ultrasonic rheology of a monoclonal antibody (IgG2) solution: Implications for physical stability of proteins in high concentration formulations. *J. Pharm. Sci.* **2007,** *96* (12), 3181-3195.

10. Shire, S. J.; Shahrokh, Z.; Liu, J., Challenges in the development of high protein concentration formulations. *J. Pharm. Sci.* **2004,** *93* (6), 1390-1402.

11. Sola-Penna, M.; Meyer-Fernandes, J. R., Stabilization against thermal inactivation promoted by sugars on enzyme structure and function: why is trehalose more effective than other sugars? *Arch Biochem Biophys* **1998,** *360* (1), 10-4.

12. Lee, J.; Lin, E. W.; Lau, U. Y.; Hedrick, J. L.; Bat, E.; Maynard, H. D., Trehalose Glycopolymers as Excipients for Protein Stabilization. *Biomacromolecules* **2013,** *14* (8), 2561-2569.

13. Mancini, R. J.; Lee, J.; Maynard, H. D., Trehalose Glycopolymers for Stabilization of Protein Conjugates to Environmental Stressors. *J. Am. Chem. Soc.* **2012,** *134* (20), 8474-8479.

14. Gelb, M. B.; Maynard, H. D., Effect of Poly(trehalose methacrylate) Molecular Weight and Concentration on the Stability and Viscosity of Insulin. *Macromol. Mater. Eng.* **2021,** *306* (9), 2100197.

15. Forsythe, N. L.; Maynard, H. D., Synthesis of disulfide-bridging trehalose polymers for antibody and Fab conjugation using a bis-sulfone ATRP initiator. *Polym. Chem.* **2021,** *12* (9), 1217-1223.

16. Romond, E. H.; Perez, E. A.; Bryant, J.; Suman, V. J.; Geyer, C. E.; Davidson, N. E.; Tan-Chiu, E.; Martino, S.; Paik, S.; Kaufman, P. A.; Swain, S. M.; Pisansky, T. M.; Fehrenbacher, L.; Kutteh, L. A.; Vogel, V. G.; Visscher, D. W.; Yothers, G.; Jenkins, R. B.; Brown, A. M.; Dakhil, S. R.; Mamounas, E. P.; Lingle, W. L.; Klein, P. M.; Ingle, J. N.; Wolmark, N., Trastuzumab plus

Adjuvant Chemotherapy for Operable HER2-Positive Breast Cancer. *New Engl. J. Med.* **2005,** *353* (16), 1673-1684.

17. Slamon, D.; Eiermann, W.; Robert, N.; Pienkowski, T.; Martin, M.; Press, M.; Mackey, J.; Glaspy, J.; Chan, A.; Pawlicki, M.; Pinter, T.; Valero, V.; Liu, M.-C.; Sauter, G.; von Minckwitz, G.; Visco, F.; Bee, V.; Buyse, M.; Bendahmane, B.; Tabah-Fisch, I.; Lindsay, M.-A.; Riva, A.; Crown, J., Adjuvant Trastuzumab in HER2-Positive Breast Cancer. *New Engl. J. Med.* **2011,** *365* (14), 1273-1283.

18. Dias, C.; Abosaleem, B.; Crispino, C.; Gao, B.; Shaywitz, A., Tolerability of High-Volume Subcutaneous Injections of a Viscous Placebo Buffer: A Randomized, Crossover Study in Healthy Subjects. *AAPS PharmSciTech* **2015,** *16* (5), 1101-1107.

19. Su, W.-F., Polymer Size and Polymer Solutions. In *Principles of Polymer Design and Synthesis*, Su, W.-F., Ed. Springer Berlin Heidelberg: Berlin, Heidelberg, 2013; pp 9-26.

20. Mansfield, K. M.; Maynard, H. D., Site-Specific Insulin-Trehalose Glycopolymer Conjugate by Grafting from Strategy Improves Bioactivity. *ACS Macro Lett.* **2018**, 324-329.

Chapter 5

Degradable Poly(Caprolactone-Carboxybetaine) Conjugated to a Growth Hormone Receptor Antagonist

5.1 Introduction

Over the last thirty years, human growth hormone (hGH) and growth hormone receptor antagonists (GHRA) have been used to treat an increasing number of diseases. Just as hGH was identified as a treatment for deficient or insufficient endogenous hGH levels due to pituitary disorders and tumors,[1-2] GHRAs were first explored to treat diseases characterized by excessive hGH levels such as acromegaly.[3-8] hGH is a peptide hormone comprised of 191 amino acids (approximately 22 kDa) that is excreted from the pituitary gland to bind with growth hormone receptor (GHR) dimer on the surface of cell membranes to promote growth and regulate metabolism.[7] hGH stimulates the production of molecules such as insulin-like growth factor (IGF-1) which, along with hGH, has been tied to numerous cancers, leading to the exploration of GHRAs as antineoplastic agents in addition to a treatment for acromegaly.[3-4, 9-10] GHRAs were first derived from hGH by selectively modifying amino acids to retain the affinity for GHR-binding while concomitantly suppressing signal transduction.[2, 7] Modification of just the residue 120 from glycine in hGH to lysine (G120K) creates an effective GHRA, and the addition of eight further modifications (H18D, H21N, R167N, K168A, D171S, K172R, E174S, and I179T) improves binding to GHR yielding the highly effective GHRA, B2036, used clinically as somatropin (Norditropin) and in a PEGylated form pegvisomant (Somavert).[5, 7]

A key challenge in using hGH therapeutically is its short half-life reported to be 21.1 ± 5.1 min in the FDA label for somatropin and 13.0-28.1 min under certain conditions of dosage and disease state.[1, 5, 11-13] Because the GHRA B2036 is so structurally similar to hGH, the pharmacokinetics (PK) are also a challenge which is exacerbated by the high plasma concentration required for the receptor antagonist to be effective in preventing the excessive hGH from binding to the receptor. Currently, the primary way of increasing the *in vivo* pharmacokinetics of clinically

utilized biologics is via PEGylation, the covalent attachment of polyethylene glycol (PEG) to the therapeutic.[14-15] The half-life of PEGylated proteins and peptides is extended by protecting the biomolecule from enzymatic degradation and immunogenic recognition, while the increased size also prevents filtration by the renal clearance pathway.[15-17] However, PEGylation suffers from drawbacks including findings that PEG does not increase protein stability for storage or transportation; additionally patients have experienced immunogenic responses, some previously naïve to PEGylated therapeutics. To increase the half-life of B2036 from ~30 min, , 4-5 5kDa amine reactive PEG chains were non-specifically conjugated to B2036 at lysine residues and the N-terminus to form pegvisomant.[5-8, 12, 18-20] While the resulting PEGylated GHRA does have an increased half-life of nearly 74 h,[7] as with other non-specifically PEGylated proteins, masking of the lysine residues results in pegvisomant having a reduced activity, and the PEGylation could elicit immunogenic responses in patients.[6-7, 12, 18-19] In fact, early studies with pegvisomant reported antibody production to occur in 16.9% of patients in a long-term clinical study.[6, 12]

To solve this first challenge, our group designed a modification to the GHRA B2036 wherein the tyrosine at the residue site 35 is replaced with the unnatural amino acid (UAA) propargyl tyrosine (pgIY, T35pgIY) to function as a site-specific handle for orthogonal bioconjugation.[21] UAA incorporation into hGH was originally performed by researchers interested in scanning a range of residues to determine which sites could be modified without interfering with GHR binding[2, 22-24] and later which could be used to site-specifically PEGylate hGH for increased peptide half-life without significantly reducing the bioactivity.[25-26] These initial researchers scanned a range of residues in hGH for sites that could be modified with UAAs without interfering with GHR binding and found three key sites (Y35, G131, and K145). In a direct comparison of these three sites, researchers chose to replace each individual residue with Nε-2-

azideoethyloxycarbonyl-L-lysine to enable copper-free alkyne azide click chemistry with 4-dibenzocyclooctynol-PEG chains of 5, 10, 20, or 40 kDa.[26] Based on the best performing site in this paper, Y35, our group with Perry and Jamieson, directed the insertion of pgIY into site 35 of B2036 and PEGylated the resulting GHRA-yne with 5, 10, and 20 kDa azide end-group PEG chains.[21] Similar to PEGylated hGH,[26] while the bioactivity of PEGylated B2036-yne was much closer to free B2036 and B2036-yne, PEG size was inversely related to bioactivity, with the largest chain, 20 kDa, performing 12.5x better than pegvisomant despite the comparable PEG weight (20-25 kDa with pegvisomant). However, PEGylation has been repeatedly tied to increased immunogenicity, and researchers have detected induced IgG production increasing with PEG chain length for site-specifically PEGylated hGH.[26]

Our group has long been interested in moving beyond PEG both for improving the stabilization of therapeutic proteins and for increasing the safety and biocompatibility of the polymers being used.[27-28] Recent efforts by our group have included designing degradable caprolactone-based polymers with stabilizing side chain moieties including trehalose and the zwitterion carboxybetaine to be used as stabilizing excipients for therapeutic proteins.[27] In particular, the poly(caprolactone-zwitterion) (pCLZ) was effective at stabilizing granulocyte-colony stimulating factor, a comparably sized (174 or 177 residues and19.6 kDa) protein to B2036 and which is similarly comprised of multiple helix coils.

We hypothesized that site-specific protein-polymer conjugation of pCLZ to B2036-yne would improve the pharmacokinetics without decreasing the bioactivity or increasing the immunogenicity of the GHRA. To conjugate pCLZ to B2036-yne, we first tried directly polymerizing caprolactone from an azide-containing initiator (1-Azido-3,6,9-trioxaundecane-11-ol) followed by light-activated thiol-ene click chemistry with dimethylaminoethanethiol

hydrochloride, the first component of the carboxybetaine zwitterion. Two subsequent steps, quaternizing the amine and deprotecting the carboxyl group, yielded pCLZ, but, after inconsistencies in protein-polymer conjugation efforts, we found that the thiol-ene click step was inconsistently eliminating the azide end group of the polymer rendering it unable to perform conjugation to the alkyne. At this point, the synthesis was redesigned using a tert-butyl carbamate protected-amine initiator (tert-butyl (4-((6-hydroxyhexyl)oxy)phenethyl)carbamate) and addition of the carboxybetaine group through a one-step addition of the thiol-based precursor and single deprotection of both the amine end-group and carboxyl side end group. The pCLZ end group could then be converted to an azide using azidoacetic acid NHS ester in preparation for copper-catalyzed alkyne azide click (CuAAC) chemistry with the propargyl tyrosine of B2036-yne. B2036-yne was obtained by Kyle Tamshen (KT) as described in the paper where he designed the 35pgIY insertion.[21] Synthesis of second generation pCLZ and the B2036-pCLZ conjugate was conducted by Jane Yang (JY) and will be described in a not-yet-submitted paper. In this chapter, the safety of pCLZ alone and conjugated as B2036-pCLZ is investigated for safety, activity, and PK.

5.2 Results and Discussion

5.2.1 Original polycaprolactone zwitterion polymer synthesis

Scheme 5.1 Original synthetic strategy for polycaprolactone zwitterion polymer.

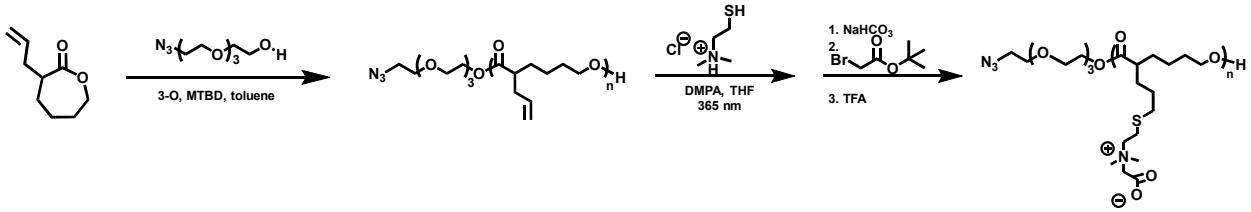

The initial polymer synthesis was developed in our lab as a highly-flexible platform for synthesizing polymers that could be used as excipients to stabilize therapeutic proteins.[27] In an effort to expand one of our best-performing polymers, pCLZ, from its use as an excipient to a

component of a protein-polymer conjugate, an extensive literature search was conducted. From this search, we chose to use an azide-functionalized initiator as a polymerization and post-polymerization modification reaction-compatible end group that could be later used to conjugate to an alkyne-functionalized protein. Following improvements upon the original synthetic route,[28] 1-azido-3,6,9-trioxaundecane-11-ol was employed as the azide-functionalized initiator for allyl-caprolactone with MTBD and 3-O as co-catalysts for the reaction. Post-polymerization, the azide group was verified to be present by both FT-IR and MALDI ToF, allowing for the subsequent functionalization of pCL-allyl in two steps, first via thiol-ene click chemistry using a hand-held UV lamp to add the dimethylaminoethanethiol hydrochloride. A subsequent addition of t-butyl bromoacetate and TFA deprotection formed the carboxybetaine side chain. After the addition of side chain it became more difficult to characterize the polymer end group, but, in pCL-allyl up to at least 20 kDa in size, a small peak corresponding to an azide-group does appear by FT-IR. The azide end-group pCLZ was conjugated to GHRA-yne via CuAAC by KT and JY, as will be discussed in the not-yet-submitted paper with JY.

Despite initial success in synthesizing each step in the route and subsequent CuAAC conjugation with GHRA-yne, over time the conjugations were not consistently successful. Following investigations by KT, JY, and myself, it was determined that the strength of UV irradiation that the polymer was exposed to during the thiol-ene reaction was inconsistent, and, at higher strengths, the azide functional end group was being ablated. Thus, a new synthetic route was designed and implemented by JY and KT which will not be discussed here.

5.2.2 Conjugate immunogenicity *in vivo*

The adaptive immune response can produce antibodies in response to perceived antigens that, in addition to the immune reaction, will remove foreign material. As GHRA-yne shares 182

of its 191 residues in common with hGH, we did not expect the alkyne modifications to elicit antibody production, and utilized an immunogenicity study to confirm this hypothesis. The immunogenicity study was performed early on with GHRA-pCLZ synthesized through the first route before the UV irradiation issue was discovered. It was decided that the later change in synthetic strategy was not so different as to warrant the sacrifice of additional animals. The GRHA-yne, GHRA-pCLZ, and original pCLZ were all studied for their potential to trigger the immune system to produce IgG and IgM antibodies, two of the most abundant types of antibody isotypes accounting for 75-95% of all antibodies. Mice were challenged with intraperitoneal (i.p.) injections of GHRA-yne, GHRA-pCLZ, and pCLZ (2 mg/kg) at weeks 0 and 2. Enzyme-linked immunosorbent assay (ELISA), the most widely used technique for anti-polymer and anti-conjugate antibody detection, was used to measure IgGs and IgMs in serum specific to each potential antigen for each week.[29] As a negative control, naïve mouse serum was added to the GHRA-yne and GHRA-pCLZ coated microplate. None of the possible antigens, modified protein, conjugate, or polymer elicited any measurable IgG or IgM response as compared to the naïve controls (**Figure 5.1**). Therefore, we concluded that the GHRA-yne does not instigate an immune reaction, and both pCLZ alone and conjugated to GHRA-yne are similarly benign with respect to the adaptive immune system, aligning with our original hypothesis. We would therefore expect that, without the production of antibodies in response to polymer, conjugate, or protein, the half-life in circulation would not be affected by antibody clearance mechanisms.

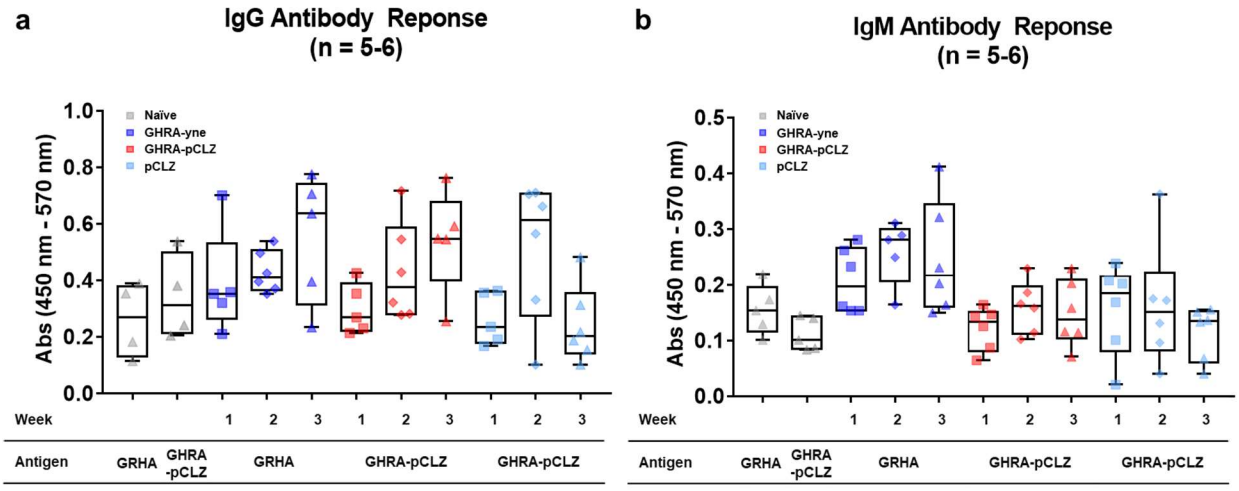

Figure 5.1 Antibody levels in mice specific to GHRA-yne or GHRA-pCLZ antigens over 3 weeks after i.p. injection of GHRA, GHRA-pCLZ, or azide-pCLZ at weeks 0 and 2 (n = 5 – 6). Levels measured by immune indirect ELISA for a. IgG and b. IgM specific antibody responses and compared to non-specific baseline antibody recognition in naïve mice.

5.2.3 Conjugate activity *in vitro* as a function of pCLZ molecular weight

As previously described in the literature by our group and others, the efficacy of GHRA-yne and the different conjugates was assessed by a cell viability assay with Ba/F3 cells engineered to stably express GHR and depend on hGH for proper growth.[21] For this assay, cells were incubated with different GHRAs and hGH for a period of time (48 h) before the cells were measured for viability with resazurin blue and the resulting GHRA response was calculated from these varying levels of observed viability. As the efficacy of GHRA-yne had already been found comparable to B2036 without the 35pgIY insertion and the conjugation of mPEG polymers was clearly shown to reduce bioactivity as a function of polymer size,[21] it was decided to study GHRA-pCLZ and GHRA-mPEG at a range of sizes compared against GHRA-yne. Despite increasing polymer size having a detrimental effect on conjugate bioactivity, it was reported that pegvisomant, the non-site-specifically conjugated GHRA-mPEG (totalling 20-25 kDa in mPEG), had an IC_{50} an order

of magnitude larger (1289 nM) than the site-specific GHRA-mPEG (20 kDa) (103.3 nM).[21] The pCLZ used for these conjugates was prepared by JY using the second-generation synthetic route. Following polymer synthesis, JY also prepared and purified the GHRA-pCLZ and GHRA-mPEG conjugates. By measuring the bioactivity of Ba/F3-GHR cells incubated with GHRA-yne, GHRA-pCLZ (60 kDa), GHRA-pCLZ (20 kDa), GHRA-pCLZ (5 kDa), GHRA-mPEG (20 kDa), GHRA-mPEG (10 kDa), and GHRA-mPEG (5 kDa), the inhibitory effect of the different polymers as well as the polymer chain lengths could be compared to determine the relationship between polymer type and size, and bioactivity (**Figure 5.2**).

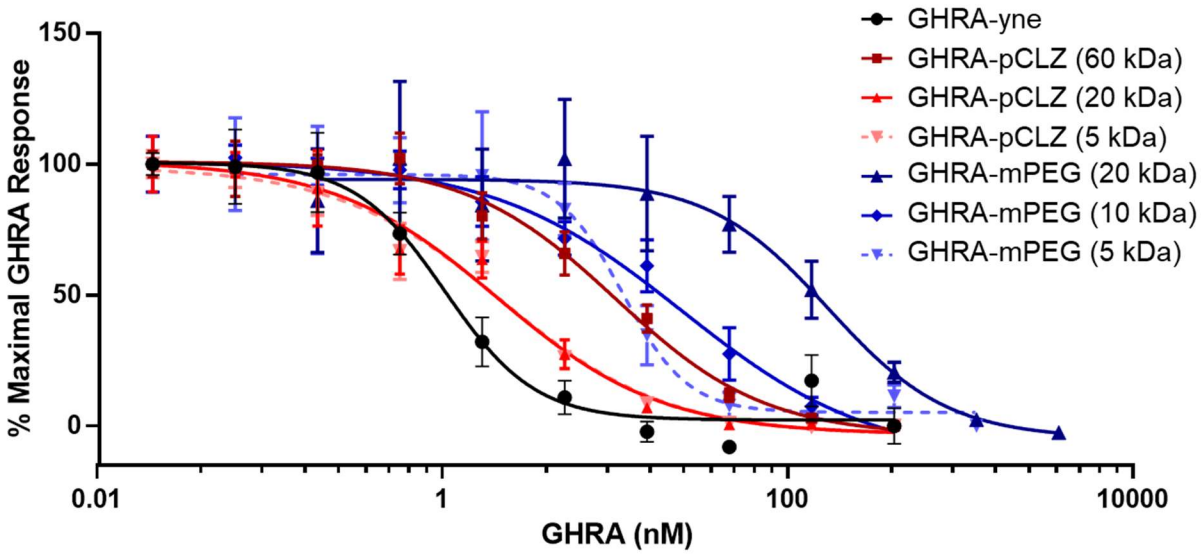

Figure 5.2 GHRA efficacy of GHRA-yne, GHRA-pCLZ conjugates (5-60 kDa), and GHRA-mPEG conjugates (5-20 kDa) measured by inhibitory bioactivity dose response in Ba/F3-GHR cells. Exact IC_{50} values are reported in **Table 5.1**. Note that GHRA-pCLZ 5 kDa and 20 kDa are mostly overlapping.

In comparing the two different polymer types, it is clear that conjugation of either polymer decreases the bioactivity of the conjugates, but the decrease in bioactivity with pCLZ conjugates is less when compared with mPEG (**Figure 5.2**, **Table 5.1**). All of these conjugates have IC_{50}

values at or an order of magnitude below the GHRA-mPEG (20 kDa) reported here (92.9 nM) underlining the earlier finding that site-specifically conjugated polymers do not reduce the bioactivity of GHRA-yne too much.[21] This new data further expands our knowledge regarding the effect of different polymers as conjugates. The bioactivity of the mPEG conjugates, ranging in size from 5-20 kDa, were all lower than the bioactivity of the even larger pCLZ conjugates which ranged from 5-60 kDa (**Table 5.1**). In fact, the two smaller pCLZ conjugates (5 kDa and 20 kDa) were not statistically different from each other (3.3 nM), and very close to the inhibitory activity of GHRA-yne (2.7 nM). Further, the largest GHRA-pCLZ conjugate (60 kDa) (11.9 nM) had a bioactivity similar to GHRA-mPEG (10 kDa) (12.1 nM). Altogether, this bioactivity data clearly indicates that the site-specific conjugation of pCLZ is less disruptive to the GHRA bioactivity as the addition of mPEG and could allow for the addition of larger polymer sizes without causing dramatic decreases in bioactivity.

Table 5.1 Averaged IC_{50} and 95% confidence interval (CI) results from three individual Ba/F3-GHR cell inhibitory experiments. All IC_{50} values are statistically different from each other ($p < 0.05$) except for the two smallest GHRA-pCLZ conjugates (5 and 20 kDa, $p < 0.05$) according to ANOVA with subsequent Students' t-Test.

GHRA	IC_{50} (nM)	95% CI (nM)
GHRA-yne	2.7	1.3 – 4.2
GHRA-pCLZ (60 kDa)	11.9	7.6 – 21.0
GHRA-pCLZ (20 kDa)	3.3	2.3 – 4.9
GHRA-pCLZ (5 kDa)	3.3	2.4 – 4.7
GHRA-mPEG (20 kDa)	92.9	39.5 – 215.9
GHRA-mPEG (10 kDa)	33.0	17.9 – 293.4
GHRA-mPEG (5 kDa)	12.1	9.2 – 15.8

5.2.4 Pharmacokinetics of GHRA-pCLZ 60 kDa conjugate *in vivo*

Finally, plasma levels in mice injected with GRHA-pCLZ (60 kDa) and GHRA-yne were measured by ELISA over time to measure the half-life of the GHRA-yne and conjugate. For these measurements, mice were injected by i.v. with GHRA-yne (2 mg/kg) or the largest size of GHRA-pCLZ (60 kDa) (0.75 mg/kg). It is noted here that the concentration of conjugate was reduced from the planned 2 mg/kg due to insufficient materials. Subsequently, time points were taken at 0.5, 2, 4, and 8 h by saphenous vein collection and a final time point at 24 h was taken post-mortem. Plasma from each time point was diluted four times, requiring samples be split over three and two plates for GRHA-pCLZ (60 kDa) and GHRA-yne, respectively. For each plate, the corresponding GRHA-pCLZ or GHRA-yne standard was used to make a standard curve.

Due to limitations in how quickly the first time point (0.5 h) could be taken after

administration, the measurements of GHRA-yne are best used as a baseline for the conjugate as the literature reports a half-life for hGH of 15-30 min.[1, 7-8, 13] The half-life of GRHA-pCLZ (60 kDa) was calculated to be 2.28 ± 0.5 h, and clearly has extended the circulation time *in vivo* as compared to the GHRA-yne (**Figure 5.3**). This increase in half-life resulted in measurable levels of GHRA in blood circulation as far out as 8 h, although nowhere near as long as the reported half-life of pegvisomant (~74 h). Due to the limitations in measuring GHRA blood content by this method, further exploration of the GHRA-pCLZ (60 kDa) will be performed by radiolabeling the conjugate and measuring biodistribution and excretion by μPET/μCT.

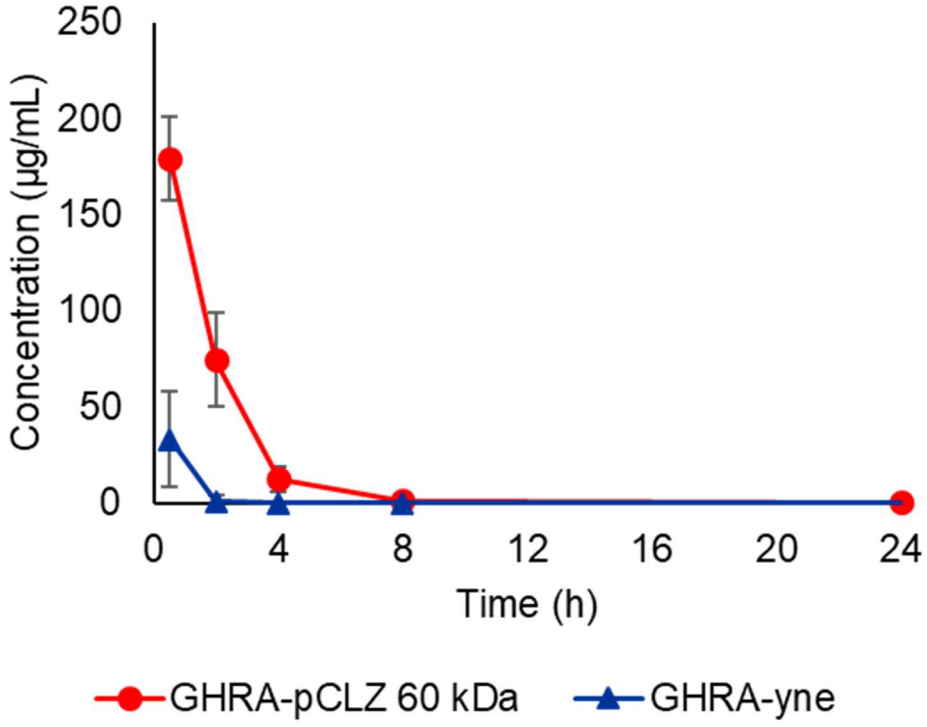

Figure 5.3 GHRA levels in mice over 24 h after i.v. injection of GHRA-yne or GHRA-pCLZ (60 kDa) (n = 5 – 6). GHRA levels were\ measured by sandwich ELISA compared to GHRA-yne or GHRA-pCLZ (60 kDa) standard curves.

Altogether GHRA-yne, GHRA-pCLZ, and pCLZ were all found to not elicit antibody production, the site-selective addition of pCLZ via CuAAC significantly but minimally decreased

the bioactivity of the GHRA *in vitro*, and there was a measurable increase in *in vivo* circulation time. As PEG is a potential antigen with many reports of it eliciting an immune response,[26] the immunocompatibility reported herein is promising. Although 40 kDa is generally accepted as the limit of renal clearance, the degradability of the pCLZ polymer should prevent conjugation of polymers over 40 kDa from posing safety or *in vivo* attenuation risks, as we expect any polymer not excreted in the form of conjugate would degrade over time. Despite this, the increase in half-life was found to be significantly less compared to that reported for pegvisomant ($t_{1/2}$ ~74 h).[7] This result was particularly surprising as the net increase in MW with the GHRA-pCLZ is 60 kDa, and the combined 4-5 mPEG chains (5 kDa each) increase the MW of pegvisomant only ~20 kDa. Since the activity of site-selective GHRA-pCLZ (60 kDa) is much better than any of the site-selective GHRA-mPEG conjugates, we would need to next study bioactivity *in vivo* to determine the efficacy of increased activity with concomitant loss of circulation time. Finally, although not included in this chapter, during polymer synthesis and conjugation JY, KT, and I found that pCLZ and GHRA-pCLZ have a smaller hydrodynamic radius (Rh) than mPEG and GHRA-mPEG by GPC and SDS-PAGE gels, respectively. We have hypothesized that the hydrodynamic radius is actually what affects both bioactivity and PK, and, if true, this would explain why conjugation of larger pCLZ polymers has less of an impact on bioactivity or PK than the mPEG polymers. This could be further studied using other non-immunogenic polymers with different Rh conjugated to GHRA-yne and by studying the addition of pCLZ at more sites through the introduction of additional pgIY sites in B2036.

5.3 Conclusions

In this chapter, pCLZ alone and as the GHRA-pCLZ conjugate were investigated for safety, activity, and PK. Through ELISA, antibody production in response to GHRA-yne, pCLZ, and

GHRA-pCLZ were measured, and no significant immunogenic response was detected. The activity of GHRA-pCLZ at a range of polymer sizes was measured *in vitro* and compared with GHRA-mPEG it was found that the GHRA-pCLZ conjugates provided better lower IC_{50} values than the GHRA-mPEG conjugates. Finally, plasma levels in mice injected with the largest GHRA-pCLZ conjugate (60kDa) and unmodified GHRA-yne were measured by ELISA over time, and it was found that the GHRA-pCLZ conjugate did increase the half-life of the GHRA by approximately 2 h compared to what is reported in literature, although this result is preliminary and needs to be repeated.

5.4 Experimental Section

5.4.1 Materials

Chemicals were all purchased from Sigma Aldrich or Fisher Scientific and used without further purification unless otherwise mentioned. Anhydrous toluene was distilled from CaH_2 and stored under argon prior to use. Anhydrous tetrahydrofuran (THF) was distilled from sodium benzophenone and stored under argon prior to use. 1-Azido-3,6,9-trioxaundecane-11-ol was purchased from Toronto Research Chemicals and purified via HPLC prior to use. Allyl-caprolactone was synthesized as previously described and purified by distillation under reduced pressure before use.[27-28, 30] Bistristhiourea (3-O) was synthesized and purified according to literature precedent.[28, 31] Spectra/Por3® regenerated cellulose membrane (MWCO 1.0 kDa or 3.5 kDa) used for polymer dialysis was purchased from Spectrum Chemical (New Brunswick, NJ). Amicon Centriprep™ tubes were purchased from Millipore. Any kD Mini-PROTEAN-TGX™ PAGE gels and SDS-PAGE protein standards (Precision Plus Protein™ Dual Color) were purchased from Bio-Rad. Murine Ba/F3 cells stably expressing human GHR (Ba/F3-GHR) were obtained from Professor Michael Waters (University of Queensland, Australia). RPMI 1640 media

with L-glutamine and 25 mM HEPES buffer was purchased from Gibco, and recombinant hGH (rhGH) purchased from Dr. A.F. Parlow at the National Hormone and Peptide Program (Harbor-UCLA Medical Center, Torrance, CA) was resuspended at 0.5 mg/mL in 0.1 M PBS before being stored at -80 °C, following storage instructions. Goat anti-mouse IgG HRP conjugate and goat anti-mouse IgM HRP conjugate were both purchased from Abcam, reconstituted, diluted 2x with glycerol, and stored at -80 °C following manufacturer's recommendations. Pierce BCA assay kit and enzyme-linked immunosorbent assay (ELISA) TMB development solution was purchased from ThermoFisher Scientific. DuoSet hGH ELISA kit was purchased from R&D Systems (catalog #DY1067).

5.4.2 Analytical Techniques

NMR spectroscopy were performed on a Bruker AV 400 MHz or AV 500 MHz instrument and spectra were acquired with a relaxation delay of 2 s for small molecules and 30 s for polymers. Organic GPC (DMF) of the allyl-caprolactone polymers was conducted on a Shimadzu high performance liquid chromatography (HPLC) system with a refractive index detector RID-10A, one Polymer Laboratories PLgel guard column, and two Polymer Laboratories PLgel 5 μm mixed D columns. Eluent was DMF with LiBr (0.1 M) at 40 °C (flow rate: 0.80 mL/ min). Calibration was performed using near-monodisperse pMMA standards from Polymer Laboratories. Aqueous GPC of the polymers was conducted on a Malvern Viscotek GPCMax system equipped with a triple detector array (TDA 305-040 Quadruple Detector Array), with two Viscotek A600 M general mixed aq. Columns (300x8.0mm) with an eluent system of 20% methanol in water 1 mL min^{-1}.

5.4.3 Animal Usage

All animal experiments were conducted according to protocols approved by the UCLA

Animal Research Committee (ARC).

5.4.4 Methods

Polymerization of allyl-caprolactone with 1-azido-3,6,9-trioxaundecane-11-ol

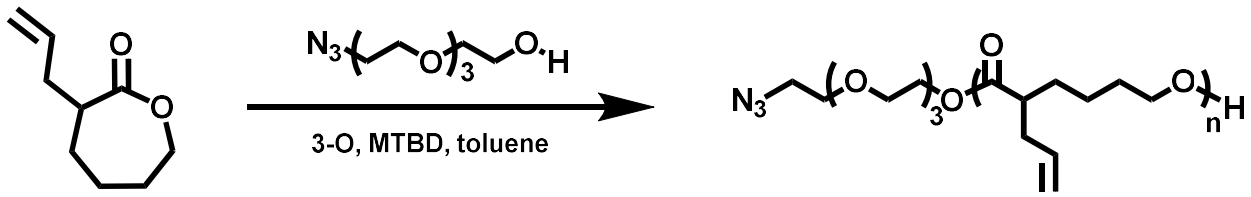

In the inert atmosphere of a nitrogen glovebox, weighed out allyl-caprolactone (250 mg, 1.62 mmol) into a glass dram vial with a stir bar. In a separate vial, measured out the catalyst 3-O (18.5 mg, 0.02 mmol). Added to the 3-O, the co-catalyst MTBD stock (10% in toluene, 29 µL, 0.02 mmol) and 1-azido-3,6,9-trioxaundecane-11-ol initiator (21.1 mg, 96.2 µmol). Added initiator, catalyst, and co-catalyst solution to monomer solution and immediately began monitoring conversion by ^{1}H NMR. After the desired conversion was achieved, the reaction was removed from inert atmosphere and quenched with AcOH (20 µL). Product was purified via column chromatography (eluent 20-50% EtOAc in hexanes) yielding pCL-allyl. *Mn* (GPC) = 2990 Da, *Đ* = 1.04. ^{1}H-NMR agreed with that reported for this compound.[27]

Original post-polymerization thiol-ene and amine quaternization of pCL to pCLZ

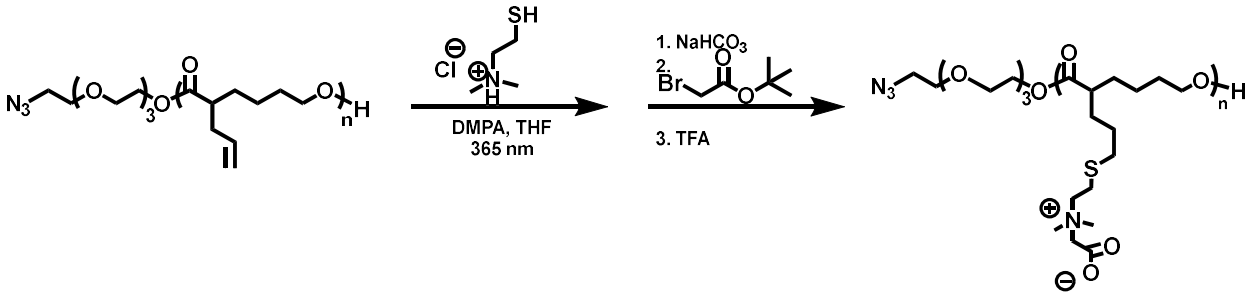

In a glass dram vial, pCL-allyl (60 mg, 20 µmol) was dissolved in MeOH:DCM 1:1. To pCL-allyl, added dimethylaminoethanethiol hydrochloride (204.4 mg, 1.4 mmol) and 2,2-dimethoxy-2-phenylacetophenone (DMPA) (46.2 mg, 180 µmol). The vial was degassed by

sparging with argon for ten minutes and then exposed to a handheld UV lamp (λ = 365 nm) for 3 h. The crude solution was concentrated *in vacuo* before adding sodium bicarbonate (3 mL). Extracted aqueous layer with DCM (3 x 10 mL). Organic layer was dried over $MgSO_4$ and concentrated *in vacuo*. Dissolved oil in acetonitrile (2 mL) and added *t*-butyl bromoacetate (267 µL, 1.8 mmol) and let stir at 50 °C for 12 h. The reaction solution was allowed to cool to room temperature and ACN was removed *in vacuo*. To the reaction, trifluoroacetic acid (TFA, 1.67 mL) was added in excess, and the reaction was stirred for 3.5 h at room temperature. TFA was removed *in vacuo*, and material was dissolved in water and dialyzed against 3.5 kDa MWCO in MeOH:water 1:1 for 24 h and then pure water for 24 h. The dialyzed solution was dried *in vacuo* yielding pCLZ as a fluffy white solid (73.9 mg, 58% yield). GPC prior to TFA deprotection M_n = 7.71 kDa, $Đ$ = 1.04 corresponding to pCLZ of M_n = 6.56 kDa. ^{1}H-NMR agreed with that reported for this compound.[27]

Antibody immunogenicity of GHRA-yne, GHRA-pCLZ, and pCLZ in Mice

CD-1 mice (8 weeks, female, n = 5 – 6, Charles River Laboratories) were used to study the immunogenicity of GHRA-yne, GHRA-pCLZ (6.56 kDa), and pCLZ (6.56 kDa). Protein, conjugate, and polymer were each administered via i.p. injection (2 mg/kg in sterile saline buffer). Mice were challenged again 2 weeks after inoculation with the same dosage for each condition. Blood was collected into serum separator centrifuge tubes (SSTs) via retro-orbital bleeding at 1, 2, and 3 weeks after administration. Blood was centrifuged at 2,000 rcf for 15 min to extract serum. Serum was stored at −80 ºC until ELISA could be run. Mice were sacrificed after 4 weeks and a final time point was collected via cardiac puncture. Blood was treated the same as prior time points.

Antibody IgG and IgM immunogenicity ELISA

For the ELISA, sterile filtered 0.1 M PBS buffer + 0.3% n-dodecyl-β-D-maltoside was

used to wash the wells four times between each step, making sure to remove solution by hitting the plates against paper towels after each wash. Antigen solutions of GHRA-yne or GHRA-pCLZ conjugate (total 0.02 mg/mL, 100 µL/well) were plated on 96-well plates. After incubating at room temperature (21 °C) for 13 h, antigen was removed, the wells washed and blocked with sterile filtered 3% BSA in 0.1 M PBS (300 µL) for 2 h at 37 °C. After washing out the BSA blocking solution, serum from the mice was diluted 100, 500, 2,500, and 12,500-fold with filtered 3% BSA in 0.1 M PBS (100 µL/well) was then incubated with the respective antigen for 2 h at 37 °C (GHRA-yne antigen with GHRA-yne exposed mice, GHRA-pCLZ antigen GHRA-pCLZ exposed mice, and GHRA-pCLZ antigen with pCLZ exposed mice). After washing the wells, goat anti-rabbit IgG or IgM HRP-conjugate antibody diluted 2,000 × with filtered 1% BSA in 0.1 M PBS (100 µL/well) was incubated for 1 h at 37 °C. The secondary detection antibody HRP conjugate was removed and the wells washed. In the dark, TMB substrate solution was added (100 µL/well), and the plate was incubated at room temperature (21 °C). After 5 – 10 min when color had developed in positive control wells, reaction was quenched by adding 2 M H_2SO_4 (50 µL/well) stop solution. Absorbance was measured at 450 nm and background at 570 nm. Controls included OVA antigen with OVA exposed mouse serum (positive control), OVA antigen with naïve mouse serum (negative control), GHRA-yne antigen with naïve mouse serum (negative control), and GHRA-pCLZ antigen with naïve mouse serum (negative control and check on non-specific binding).

Cell viability assay measure of second generation GHRA-pCLZ conjugate activity

Ba/F3-GHR cells were cultured at 37 ºC and 5% CO_2 in RPMI 1640 media completed with 100 U/mL penicillin, 100 U/mL streptomycin, 1% Glutamax, 5% fetal bovine serum (FBS), and 25 ng/mL rhGH (added fresh at least every 7 days). After thaw, Ba/F3-GHR cells were cultured

every 2-4 days with fresh media to stay within a cell concentration of 10-200,000 cells/mL; a common splitting ratio was 1:10 to maintain the appropriate concentrations of cells.

After the cells had grown to sufficient density for the assay, cells were serum starved overnight for up to 16 h. To replace the serum with complete media sans 25 ng/mL rhGH, cells were spun down, media was removed, and cells were resuspended in the incomplete serum media two times. Cells were then diluted and plated at 20,000 cells/well (80 µL) in the interior wells of a standard, clear, 96-well plate. The outer wells were filled with media to prevent edge effects, and plates were incubated for 20 min at room temperature before being returned to the incubator (37 ºC and 5% CO_2) while serial dilutions of the GHRA-yne and conjugates were made. The dilutions ranged from 0 to 36,000 nM depending on the antagonist, and, upon completion, they were added to the wells (10 µL) (n = 4 replicates per dilution). Finally, rhGH was added to the wells (10 µL) for a concentration of 20 ng/mL and the cells were incubated for 48 h (37 ºC and 5% CO_2). Final cell viability after incubation with GHRA-yne or a conjugate was measured by adding resazurin sodium salt (0.25 mg/mL) to each well (10 µL), incubating for 2 h (37 ºC and 5% CO_2), and taking fluorescence measurements (λ_{excite} = 530 nm, λ_{emit} = 585 nm). In vitro assays were repeated at least two times on cells of different generations, and a representative figure of these is shown in the text. The half-maximal inhibitory concentration (IC_{50}) for GHRA-yne and each GHRA conjugate was calculated by fitting a sigmoidal dose-response model.

Pharmacokinetics of GHRA-yne and GHRA-pCLZ conjugate in mice

CD-1 mice (8 weeks, female, n = 5 – 6, Charles River Laboratories) were used to study the blood clearance rate of GHRA-yne and GHRA-pCLZ (60 kDa). Protein and conjugate were each administered via i.v. tail injection (2 mg/kg of GHRA-yne and 0.75 mg/kg of GHRA-pCLZ in sterile saline buffer). Blood was collected by saphenous vein bleeding at 0.5, 2, 4, and 8 h using

EDTA-coated pipette tips and LoBind tubes and tubes were rotated to prevent clotting. A time point was taken after the mice were sacrificed at 24 h, and the final time point was collected via cardiac puncture and the blood was treated the same as the earlier time points. After each time point was taken, blood was centrifuged at 2,000 rcf for 15 min to extract plasma. Plasma was transferred to a fresh LoBind tube (not EDTA coated) and stored at -80 ºC until the pharmacokinetics ELISA could be run.

Pharmacokinetics ELISA of GHRA-yne and GHRA-pCLZ conjugate

Plasma collected as part of the pharmacokinetic study of GHRA-yne and GHRA-pCLZ was analyzed by hGH DuoSet ELISA. To accommodate the many time points and dilutions, the samples were split up over five different 96-well plates with space dedicated to the necessary standard curve on each plate. The same sterile filtered 0.1 M PBS buffer + 0.05% Tween-20 was used to wash the wells four times between each step, making sure to remove solution by hitting the plates against paper towels after each wash. First, hGH capture antibody was diluted 180 fold with 0.1 M PBS (2 μg/mL) and added to each well (100 μL) and incubated at room temperature (21 °C) for 18 h. Afterwards, capture antibody was removed, the wells washed, and finally cells were blocked with sterile filtered 3% BSA in 0.1 M PBS (300 μL) for 1 h at room temperature. After washing out the BSA blocking solution, standards of GHRA-yne or GHRA-pCLZ conjugate (60 kDa) were plated on 96-well plates (100 μL/well) at nine concentrations (8,000, 4,000, 2,000, 1,000, 500, 250, 125, 62.5, 31.25, 15.63, and 0 pg/mL). The collected plasma was diluted 20, 200, 2,000, and 20,000 fold before being plated (100 μL/well) and incubating both the plasma and standards at room temperature (21 °C) for 18 h. Samples were removed, the wells washed and blocked with sterile filtered 3% BSA in 0.1 M PBS (300 μL) for 1 h at room temperature. Diluted the hGH detection antibody 360x with sterile filtered 1% BSA in 0.1 M PBS (100 ng/mL), and,

after washing out the BSA blocking solution, added the detection antibody (100 µL/well). Incubated the plates again at room temperature but for 2 h. After washing the wells, streptavidin-HRP conjugate was diluted 2,000× with filtered 1% BSA in 0.1 M PBS and, in the dark, added to the wells (100 µL/well) before incubating the plates in the dark for 20 min at room temperature. Still in the near-complete dark, the HRP conjugate was washed from the wells and TMB substrate solution was added (100 µL/well) and the wells were allowed to develop for approximately 30 min. When color had developed appropriately according to the standard curve wells, the reaction was quenched by adding 2 M H_2SO_4 (50 µL/well). The absorbance was measured at 450 nm and background at 570 nm.

5.4.4 Statistical Analysis

All experimental values are reported as the average ± SEM. Graph Pad Prism 7 (GraphPad Software, San Diego, USA) was used for the statistical analyses. Results were considered significantly different if $p < 0.05$ (*); results are also reported with $p < 0.01$ (**), and $p < 0.001$ (***). Cell viability assay was analyzed with a nonlinear regression analysis also in GraphPad Prism 7 with data expressed as means with 95% CI and compared using Student's t-tests or one-way ANOVA as necessary. Outliers were determined using the interquartile range (IQR) of 1.5 times less than the 1st quartile or 1.5 times more than the 3rd quartile whenever possible; this IQR range covers the middle 50% spread of data. For data with less than 6 points in a group, outliers were confirmed or found using a score fit of 1.5 times standard deviation greater or lower than the average. No more than one outlier was removed from each time point for each condition.

5.5 Appendix D

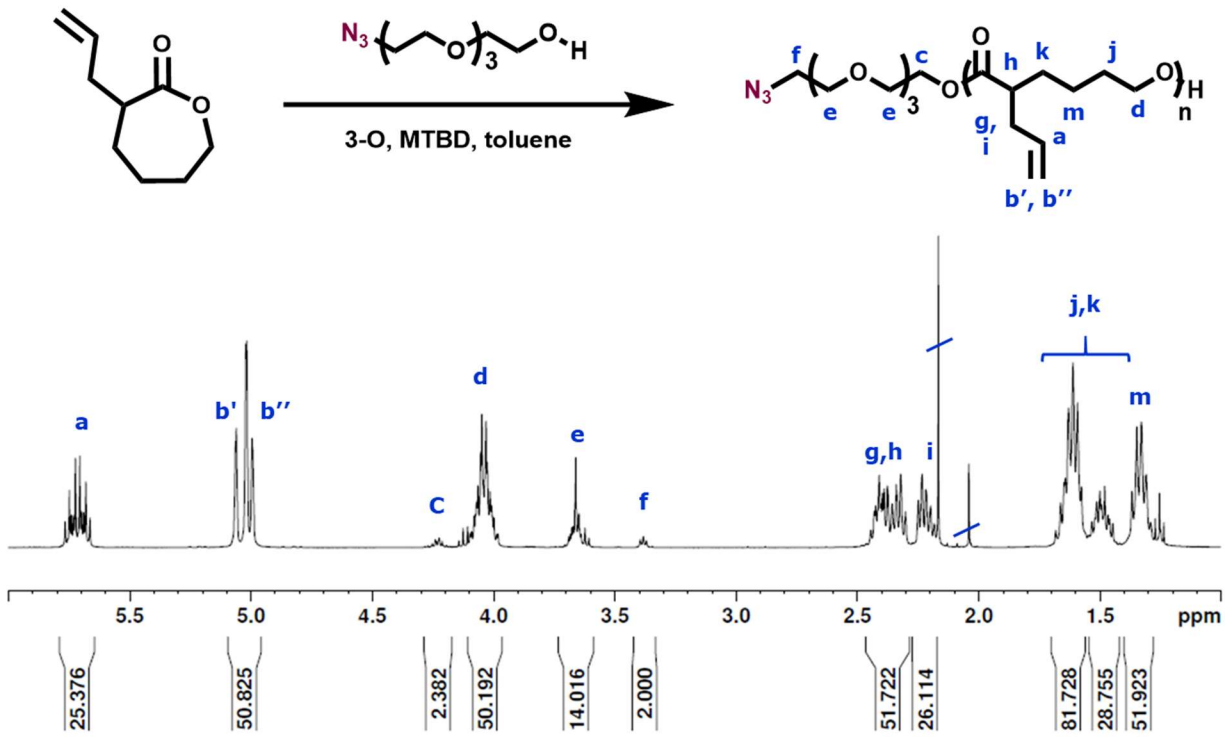

Figure D1 Representative ^{1}H NMR spectrum (400 MHz, $CDCl_3$) of pCL polymerized with 1-azido-3,6,9-trioxaundecane-11-ol initiator. ^{1}H-NMR agreed with that reported for this pCL-allyl.[27]

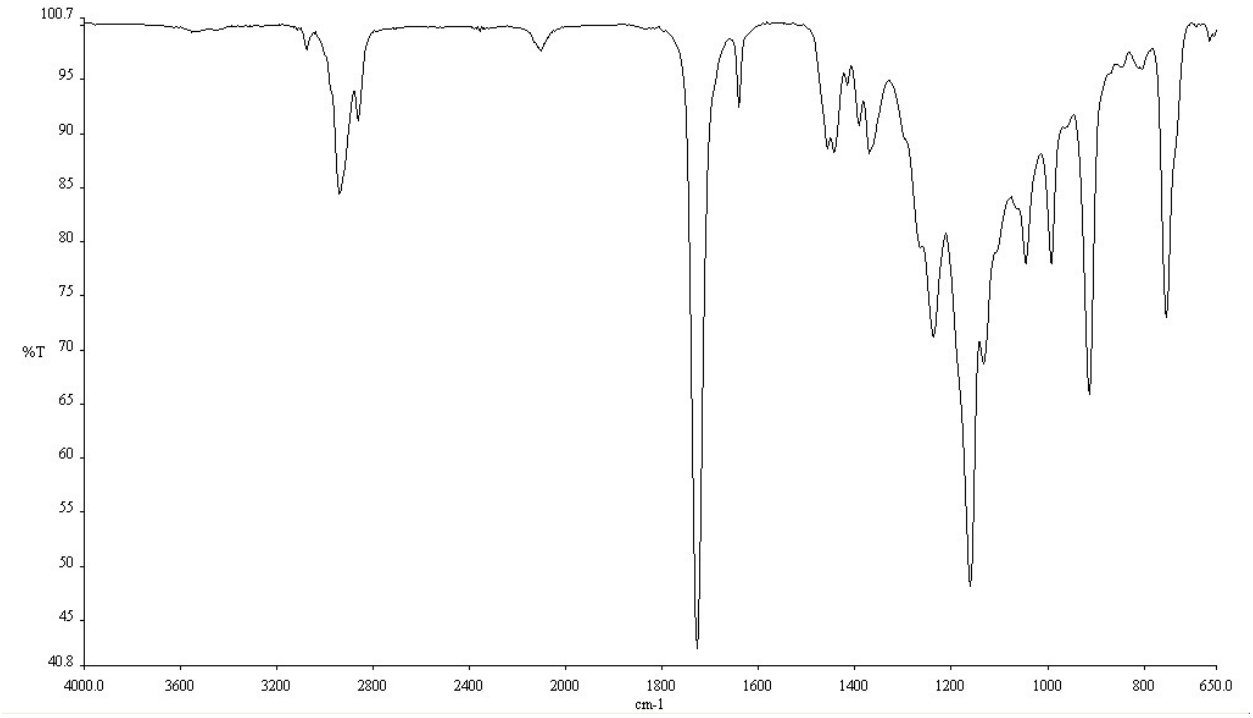

Figure D2 Representative FT-IR of pCL-allyl polymerized with 1-Azido-3,6,9-trioxaundecane-11-ol initiator. Clear azide stretch with peak at ~2100 cm^{-1} along with peak at 1250 cm^{-1}.

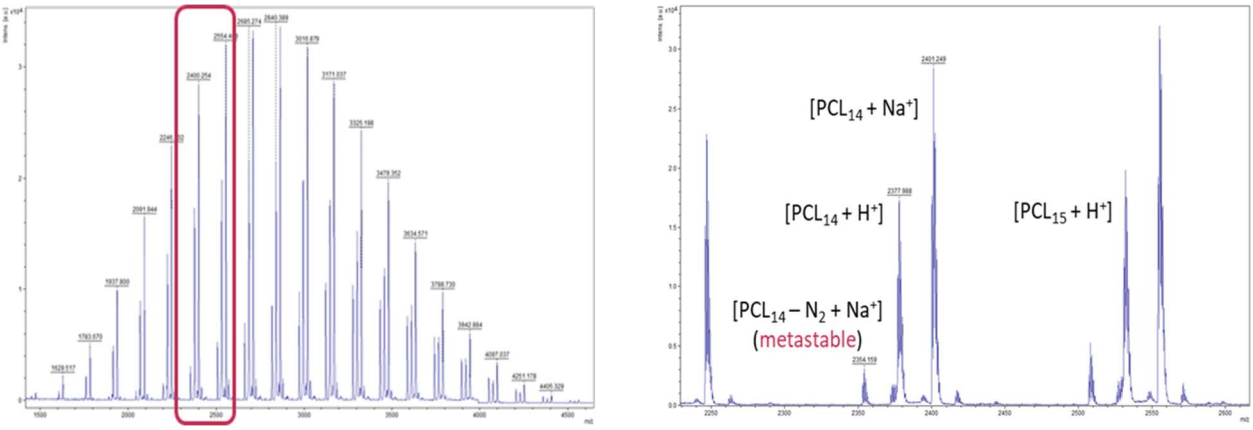

Figure D3 MALDI-ToF of pCL-allyl polymerized with 1-azido-3,6,9-trioxaundecane-11-ol initiator taken with DCTB matrix with azido end group creating characteristic metastable peaks.[32]

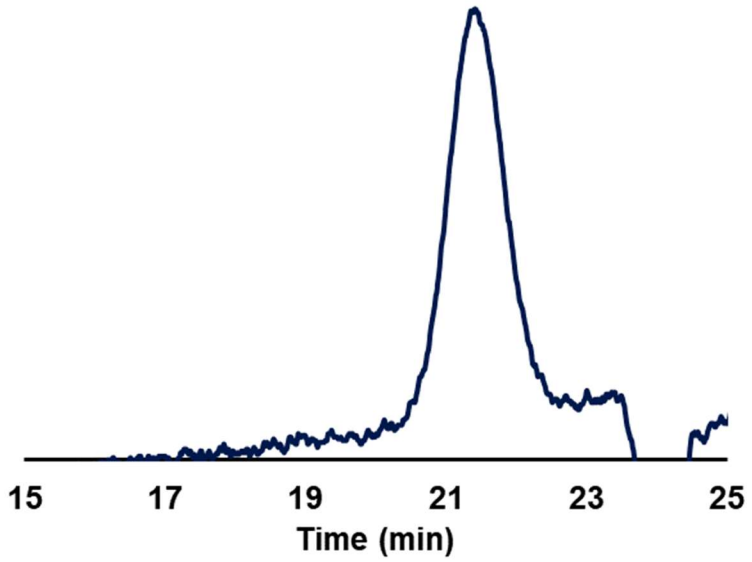

Figure D4 DMF GPC trace of pCL-allyl polymerized with 1-azido-3,6,9-trioxaundecane-11-ol initiator. M_n = 2990 Da, $Đ$ = 1.04.

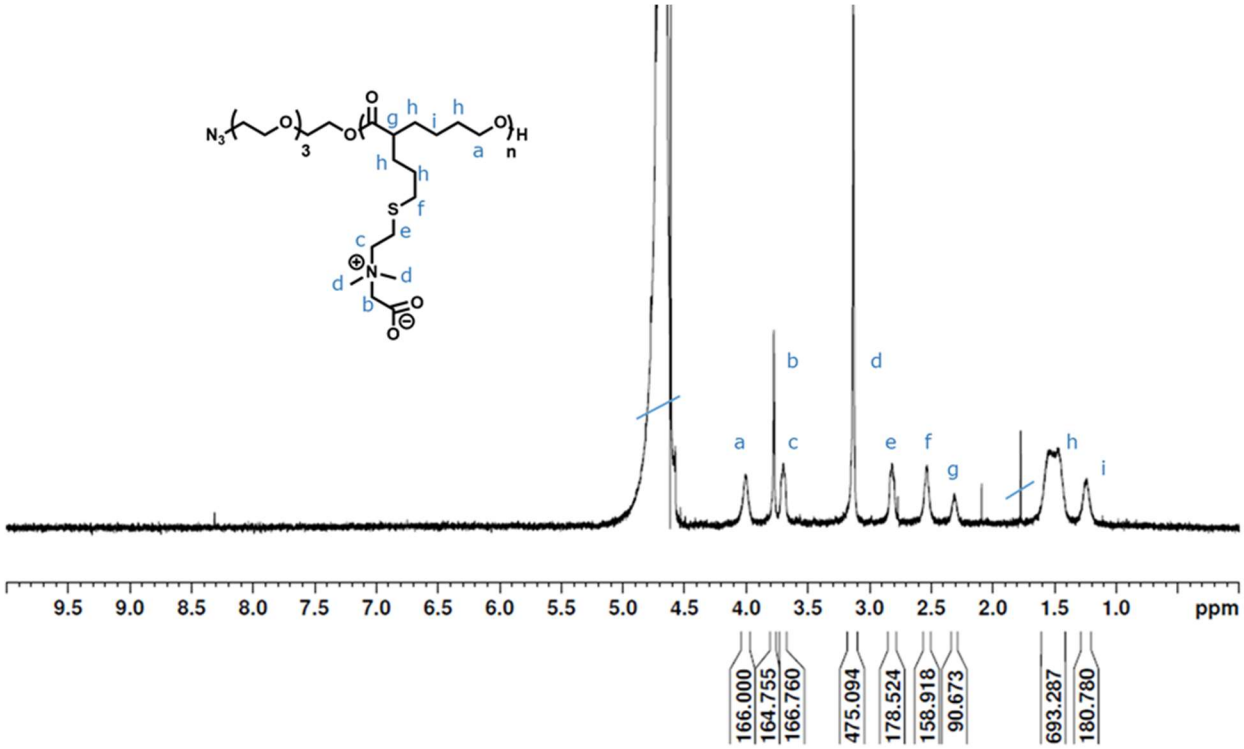

Figure D5 Representative ^{1}H NMR spectrum (400 MHz, D_2O) of pCLZ polymerized with 1-azido-3,6,9-trioxaundecane-11-ol initiator. ^{1}H-NMR agreed with that reported for this compound.[27]

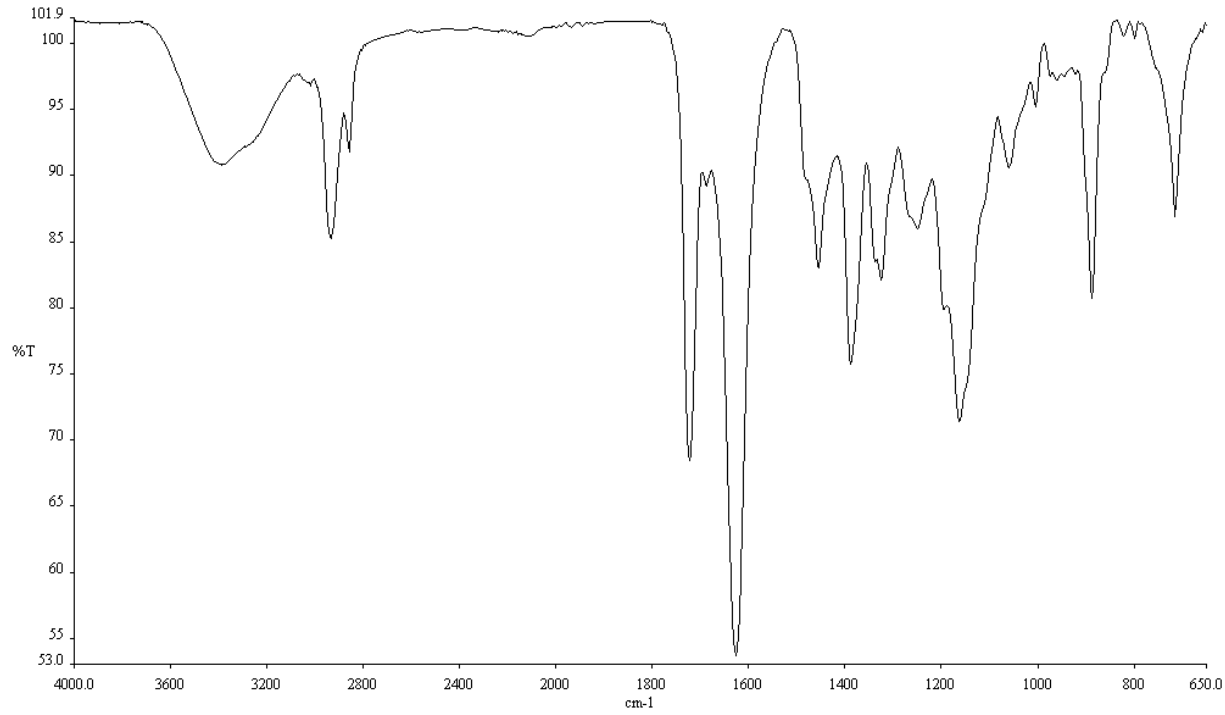

Figure D6 Representative FT-IR of pCLZ polymerized with 1-azido-3,6,9-trioxaundecane-11-ol initiator. Slight peak at ~2100 cm^{-1} along with peak at 1250 cm^{-1} that is overlaid by the 1150 cm^{-1} peak, indicate azide is retained, but the loss in clarity could be due to the relative concentration of azide after the addition of carboxybetaine side chain or due to loss of azide during the post-polymerization reactions.

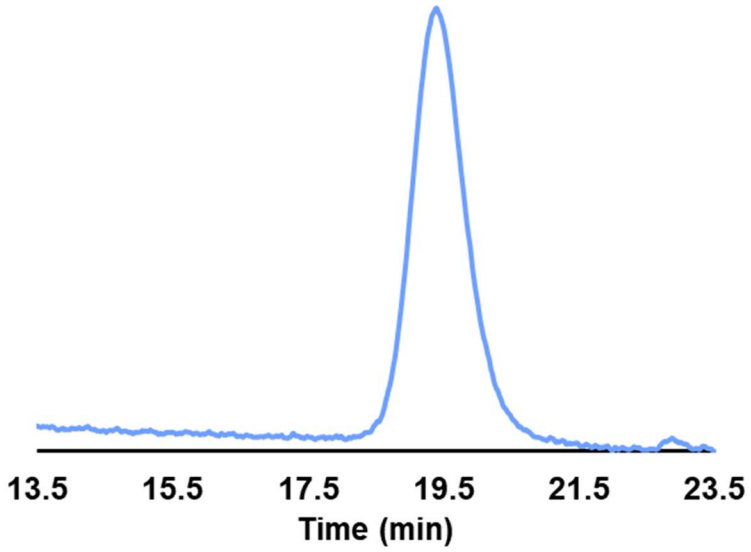

Figure D7 DMF GPC trace of t-butyl protected pCLZ polymerized with 1-azido-3,6,9-trioxaundecane-11-ol initiator. M_n = 7.71 kDa, $\cancel{D}$ = 1.04, corresponds to M_n = 6.56 kDa of deprotected pCLZ.

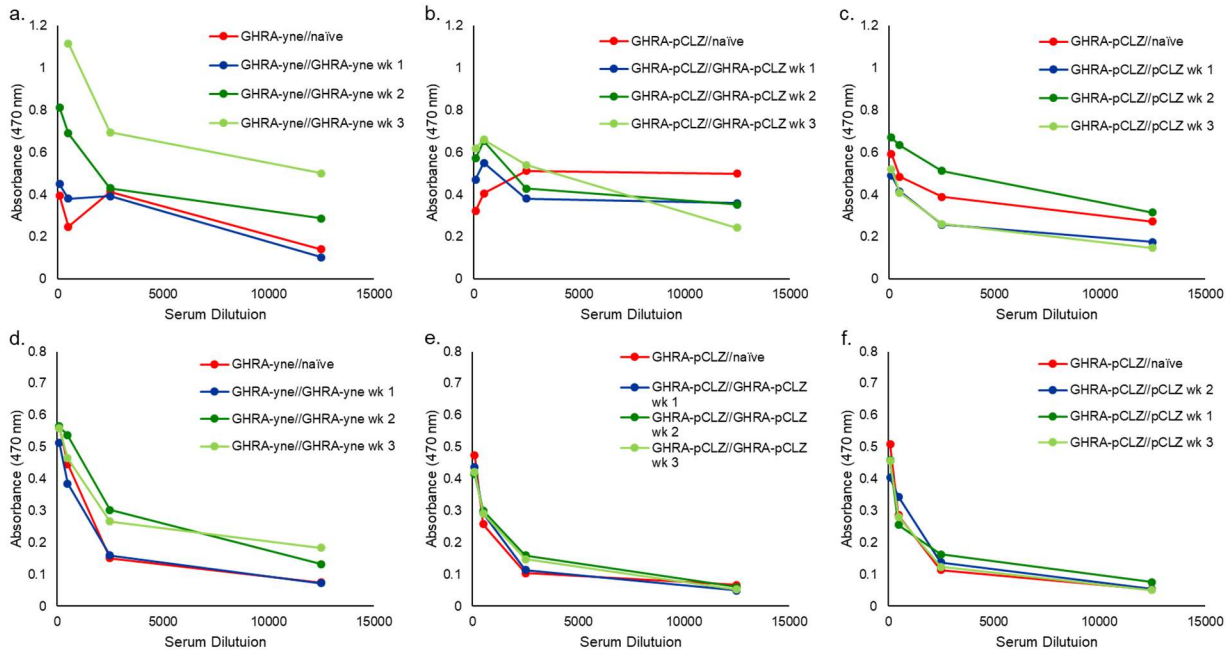

Figure D8. Immunogenicity ELISA serum dilutions of a. IgG week 1, b. IgG week 2, c. IgG week 3, d. IgM week 1, e. IgM week 2, and f. IgM week for I. Naïve GHRA-yne [naïve mouse serum with GHRA-yne antigen], II. Naïve GHRA-pCLZ [naïve mouse serum with GHRA-pCLZ antigen], III. GHRA-yne GHRA-yne [mouse serum from mice injected with GHRA-yne with GHRA-yne antigen], IV. GHRA-pCLZ GHRA-pCLZ [mouse serum from mice injected with GHRA-pCLZ with GHRA-pCLZ antigen], and V. pCLZ GHRA-pCLZ [mouse serum from mice injected with pCLZ with GHRA-pCLZ antigen].

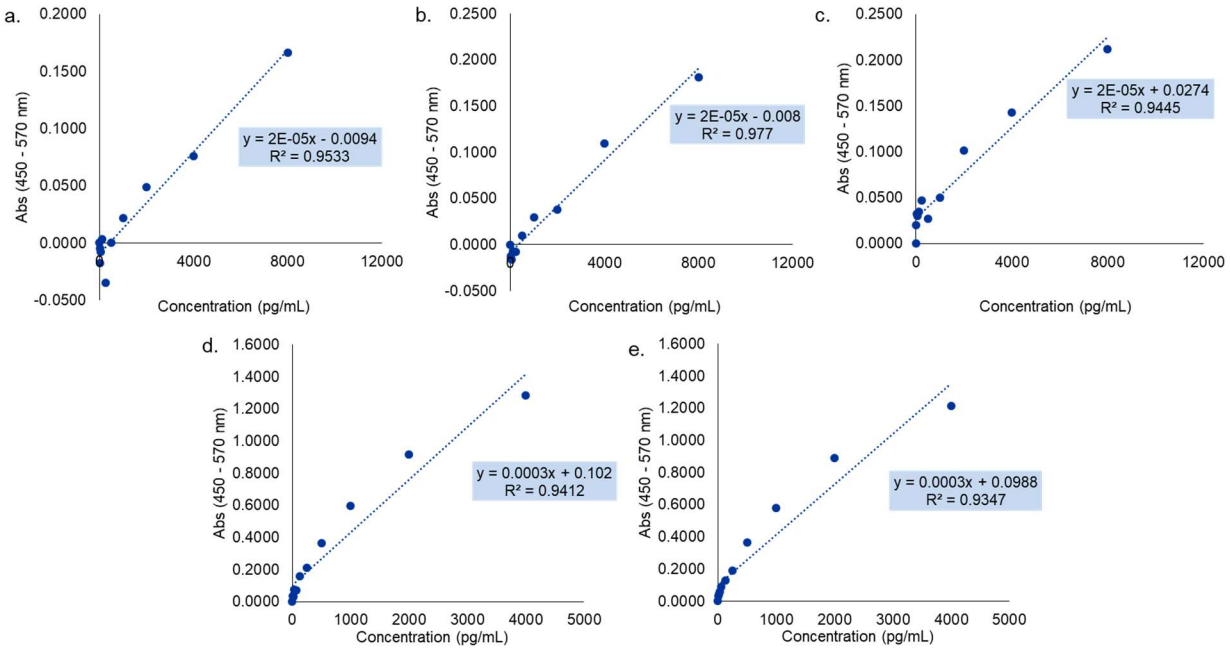

Figure D9 ELISA standard curves of a-c. GHRA-pCLZ and d-e. GHRA-yne used in the calculation of plasma concentration for the corresponding conjugate or protein at the time points at a. 0.5 h and 1 h, b. 2 h and 4 h, c. 8 h and 24 h, d. 0.5 h,1 h, and 2 h, and e. 4 h, 8 h, and 24 h.

References

1. Haffner, D.; Schaefer, F.; Girard, J.; Ritz, E.; Mehls, O., Metabolic clearance of recombinant human growth hormone in health and chronic renal failure. *J Clin Invest* **1994,** *93* (3), 1163-1171.

2. Cunningham, B. C.; Wells, J. A., Rational design of receptor-specific variants of human growth hormone. *Proc Natl Acad Sci U S A* **1991,** *88* (8), 3407-11.

3. Trainer, P. J.; Drake, W. M.; Katznelson, L.; Freda, P. U.; Herman-Bonert, V.; van der Lely, A. J.; Dimaraki, E. V.; Stewart, P. M.; Friend, K. E.; Vance, M. L.; Besser, G. M.; Thorner, M. O.; Parkinson, C.; Klibanski, A.; Powell, J. S.; Barkan, A. L.; Sheppard, M. C.; Maldonado, M.; Rose, D. R.; Clemmons, D. R.; Johannsson, G.; Bengt-Åke Bengtsson, B.-Å.; Stavrou, S.; Kleinberg, D. L.; Cook, D. M.; Phillips, L. S.; Bidlingmaier, M.; Strasburger, C. J.; Hackett, S.; Zib, K.; Bennett, W. F.; Davis, R. J.; Scarlett, J. A., Treatment of Acromegaly with the Growth Hormone–Receptor Antagonist Pegvisomant. *New Engl. J. Med.* **2000,** *342* (16), 1171-1177.

4. Drake, W. M.; Parkinson, C.; Besser, G. M.; Trainer, P. J., Clinical use of a growth hormone receptor antagonist in the treatment of acromegaly. *Trends in Endocrinology & Metabolism* **2001,** *12* (9), 408-413.

5. Kopchick, J. J.; Parkinson, C.; Stevens, E. C.; Trainer, P. J., Growth Hormone Receptor Antagonists: Discovery, Development, and Use in Patients with Acromegaly. *Endocrine Reviews* **2002,** *23* (5), 623-646.

6. Kopchick, J. J., Discovery and mechanism of action of pegvisomant. **2003,** *148* (Suppl_2), S21.

7. Muller, A. F.; Kopchick, J. J.; Flyvbjerg, A.; van der Lely, A. J., Growth Hormone Receptor Antagonists. *The Journal of Clinical Endocrinology & Metabolism* **2004,** *89* (4), 1503-

1511.

8. van der Lely, A. J.; Kopchick, J. J., Growth Hormone Receptor Antagonists. *Neuroendocrinology* **2006,** *83* (3-4), 264-268.

9. Friend, K. E., Cancer and the potential place for growth hormone receptor antagonist therapy. *Growth Hormone & IGF Research* **2001,** *11*, S121-S123.

10. Jenkins, P. J.; Mukherjee, A.; Shalet, S. M., Does growth hormone cause cancer? *Clinical Endocrinology* **2006,** *64* (2), 115-121.

11. Novo Nordisk, I., Norditropin (Somatropin) [Package Insert]. U.S. Food and Drug Administration website, June 2000.

12. van der Lely, A. J.; Hutson, R. K.; Trainer, P. J.; Besser, G. M.; Barkan, A. L.; Katznelson, L.; Klibanski, A.; Herman-Bonert, V.; Melmed, S.; Vance, M. L.; Freda, P. U.; Stewart, P. M.; Friend, K. E.; Clemmons, D. R.; Johannsson, G.; Stavrou, S.; Cook, D. M.; Phillips, L. S.; Strasburger, C. J.; Hacker, S.; Zib, K. A.; Davis, R. J.; Scarlett, J. A.; Thorner, M. O., Long-term treatment of acromegaly with pegvisomant, a growth hormone receptor antagonist. *The Lancet* **2001,** *358* (9295), 1754-1759.

13. Clark, R.; Olson, K.; Fuh, G.; Marian, M.; Mortensen, D.; Teshima, F.; Chang, S.; Chu, H.; Mukku, V.; CanovaDavis, E.; Somer, T.; Cronin, M.; Winkler, M.; Wells, J. A., Long-acting growth hormones produced by conjugation with polyethylene glycol. *J. Biol. Chem.* **1996,** *271* (36), 21969-21977.

14. Leader, B.; Baca, Q. J.; Golan, D. E., Protein therapeutics: A summary and pharmacological classification. *Nat. Rev. Drug Discov.* **2008,** *7* (1), 21-39.

15. Alconcel, S. N. S.; Baas, A. S.; Maynard, H. D., FDA-approved poly(ethylene glycol)-protein conjugate drugs. *Polym. Chem.* **2011,** *2* (7), 1442-1448.

16. Ganson, N. J.; Kelly, S. J.; Scarlett, E.; Sundy, J. S.; Hershfield, M. S., Control of hyperuricemia in subjects with refractory gout, and induction of antibody against poly(ethylene glycol) (PEG), in a phase I trial of subcutaneous PEGylated urate oxidase. *Arthritis Res Ther* **2006,** *8* (1).

17. Hershfield, M. S.; Ganson, N. J.; Kelly, S. J.; Scarlett, E. L.; Jaggers, D. A.; Sundy, J. S., Induced and pre-existing anti-polyethylene glycol antibody in a trial of every 3-week dosing of pegloticase for refractory gout, including in organ transplant recipients. *Arthritis Res Ther* **2014,** *16* (2).

18. Pradhananga, S.; Wilkinson, I.; Ross, R., Pegvisomant: structure and function. *Journal of Molecular Endocrinology* **2002,** *29* (1), 11-14.

19. Ross, R. J. M.; Leung, K. C.; Maamra, M.; Bennett, W.; Doyle, N.; Waters, M. J.; Ho, K. K. Y., Binding and Functional Studies with the Growth Hormone Receptor Antagonist, B2036-PEG (Pegvisomant), Reveal Effects of Pegylation and Evidence That It Binds to a Receptor Dimer1. *The Journal of Clinical Endocrinology & Metabolism* **2001,** *86* (4), 1716-1723.

20. Pfizer, I., Somavert (Pegvisomant) [Package Insert]. U.S. Food and Drug Administration website, December 2013.

21. Tamshen, K.; Wang, Y.; Jamieson, S. M. F.; Perry, J. K.; Maynard, H. D., Genetic Code Expansion Enables Site-Specific PEGylation of a Human Growth Hormone Receptor Antagonist through Click Chemistry. *Bioconjugate Chem.* **2020,** *31* (9), 2179–2190.

22. Cunningham, B. C.; Wells, J. A., High-Resolution Epitope Mapping of hGH-Receptor Interactions by Alanine-Scanning Mutagenesis. *Science* **1989,** *244* (4908), 1081-1085.

23. Cunningham, B. C.; Wells, J. A., Comparison of a Structural and a Functional Epitope. *J Mol Biol* **1993,** *234* (3), 554-563.

24. Vos, A. M. d.; Ultsch, M.; Kossiakoff, A. A., Human Growth Hormone and Extracellular Domain of Its Receptor: Crystal Structure of the Complex. *Science* **1992,** *255* (5042), 306-312.

25. Cho, H.; Daniel, T.; Buechler, Y. J.; Litzinger, D. C.; Maio, Z.; Putnam, A.-M. H.; Kraynov, V. S.; Sim, B.-C.; Bussell, S.; Javahishvili, T.; Kaphle, S.; Viramontes, G.; Ong, M.; Chu, S.; GC, B.; Lieu, R.; Knudsen, N.; Castiglioni, P.; Norman, T. C.; Axelrod, D. W.; Hoffman, A. R.; Schultz, P. G.; DiMarchi, R. D.; Kimmel, B. E., Optimized clinical performance of growth hormone with an expanded genetic code. *Proc. Natl. Acad. Sci. U. S. A.* **2011,** *108* (22), 9060-9065.

26. Wu, L.; Chen, J.; Wu, Y.; Zhang, B.; Cai, X.; Zhang, Z.; Wang, Y.; Si, L.; Xu, H.; Zheng, Y.; Zhang, C.; Liang, C.; Li, J.; Zhang, L.; Zhang, Q.; Zhou, D., Precise and combinatorial PEGylation generates a low-immunogenic and stable form of human growth hormone. *J Control Release* **2017,** *249*, 84-93.

27. Pelegri-O'Day, E. M.; Paluck, S. J.; Maynard, H. D., Substituted Polyesters by Thiol-Ene Modification: Rapid Diversification for Therapeutic Protein Stabilization. *J. Am. Chem. Soc.* **2017,** *139* (3), 1145-1154.

28. Pelegri-O'Day, E. M.; Bhattacharya, A.; Theopold, N.; Ko, J. H.; Maynard, H. D., Synthesis of Zwitterionic and Trehalose Polymers with Variable Degradation Rates and Stabilization of Insulin. *Biomacromolecules* **2020,** *21* (6), 2147-2154.

29. Kozma, G. T.; Shimizu, T.; Ishida, T.; Szebeni, J., Anti-PEG antibodies: Properties, formation, testing and role in adverse immune reactions to PEGylated nano-biopharmaceuticals. *Adv. Drug Del. Rev.* **2020,** *154-155*, 163-175.

30. Parrish, B.; Quansah, J. K.; Emrick, T., Functional polyesters prepared by polymerization of alpha-allyl(valerolactone) and its copolymerization with epsilon-caprolactone and delta-

valerolactone. *Journal of Polymer Science Part a-Polymer Chemistry* **2002,** *40* (12), 1983-1990.

31. Fastnacht, K. V.; Spink, S. S.; Dharmaratne, N. U.; Pothupitiya, J. U.; Datta, P. P.; Kiesewetter, E. T.; Kiesewetter, M. K., Bis- and Tris-Urea H-Bond Donors for Ring-Opening Polymerization: Unprecedented Activity and Control from an Organocatalyst. *ACS Macro Lett.* **2016,** *5* (8), 982-986.

32. Tibbitt, M. W.; Langer, R., Living Biomaterials. *Acc. Chem. Res.* **2017,** *50* (3), 508-513.